


AN ABSTRACT OF THE DISSERTATION OF

Young Kim for the degree of Doctor of Philosophy in Civil Engineering presented on February 22, 2000. Title: Aerobic Cometabolism of Chlorinated Aliphatic Hydrocarbons by a Butane-Grown Mixed Culture: Transformation Abilities, Kinetics and Inhibition

Redacted for privacy

Abstract approved:

 Lewis Semprini

This study evaluated the potential of an aerobic butane-grown mixed culture to cometabolize a broad range of chlorinated aliphatic hydrocarbons (CAHs). A systematic method for batch kinetic and inhibition studies was developed and applied to evaluate inhibition types and coefficients among the CAHs and butane. The butane-grown mixed culture transformed chlorinated methanes, chloroethanes and chlorinated ethylenes, such as vinyl chloride (VC), 1,1-dichloroethylene (1,1-DCE), cis-1,2-dichloroethene (c-DCE) and trichloroethylene. Greater amounts of 1,1-DCE and 1,1,1-trichloroethane (1,1,1-TCA) per cell mass were transformed than had been previously achieved with methanotrophs. Thus, the butane-grown culture has potential for treating mixtures of 1,1,1-TCA, 1,1-DCE, and 1,1-dichloroethane (1,1-DCA) that are commonly found together as problematic groundwater contaminants to treat via aerobic cometabolism. Chloride release studies showed nearly complete oxidative dechlorination of chloromethane (CM), dichloromethane (DCM),

chloroform (CF), chloroethane (CA), VC, and c-DCE (86% ~ 100%), but not of di- or tri-chloroethanes and 1,1-DCE. Transformation of CF, 1,1,2-trichloroethane, and 1,1-DCE resulted in the highest cell inactivation, based on the butane utilization rate.

Batch inhibition studies were performed focusing on 1,1,1-TCA, 1,1-DCE, 1,1-DCA, and butane. The developed method, that combined both direct linear plots to identify the inhibition type and nonlinear regression analysis to estimate the kinetic parameters (using graphically estimated kinetic parameters as initial guesses), proved to be very effective. Two different inhibition types were observed: 1) competitive inhibition of a CAH on other CAHs and on butane degradation and 2) mixed inhibition of butane on CAH transformation. The ratio of half-saturation coefficient (K_s) values was a good indicator of competitive inhibition among the CAHs. However, the ratio of K_s values of CAH and butane was not a good indicator of the competitive inhibition of the CAHs on butane degradation. Butane was a strong inhibitor of CAH transformation; however, the CAHs were weak inhibitors of butane degradation.

The acetylene cell inactivation results indicate that a kinetically similar butane-oxidizer was responsible for the degradation of butane and the CAHs. Thus, mixed inhibition of butane on CAH transformation likely indicates multiple binding sites on the enzyme for butane and a single binding site for the CAHs.

Aerobic Cometabolism of Chlorinated Aliphatic Hydrocarbons

by a Butane-Grown Mixed Culture:

Transformation Abilities, Kinetics and Inhibition

by

Young Kim

A DISSERTATION

submitted to

Oregon State University

in partial fulfillment of

the requirements for the

degree of

Doctor of Philosophy

Completed February 22, 2000

Commencement June 2000

Doctor of Philosophy dissertation of Young Kim presented on February 22, 2000

APPROVED:

Redacted for privacy

Major Professor, representing Civil Engineering

Redacted for privacy

Chair of Department of Civil, Construction, and Environmental Engineering

Redacted for privacy

Dean of Graduate School

I understand that my dissertation will become part of the permanent collection of Oregon State University libraries. My signature below authorizes release of my dissertation to any reader upon request.

Redacted for privacy

Young Kim, Author

ACKNOWLEDGMENTS

I would first like to thank my Ph.D. advisor, Dr. Lewis Semprini for his never-ending support and guidance throughout this project. I would also like to acknowledge and thank Dr. Daniel Arp, my project co-advisor. His interest and insightful comments contributed immeasurably to the value of the final product. I would also like to extend my gratitude to committee members, Dr Kenneth J. Williamson and Dr. Gregory Rorrer for their helpful input. I would also like to thank Dr. Mark Dolan for his interest and helpful discussions. I would also like to thank George Pon, Adisorn (Merf) Tovanabootr, and the rest of my Merryfield Lab peers for not only tolerating me, but also for their assistance and encouragement. I would specially like to thank to Brian Davis for all of his proofreading help. I would like to thank God for helping me finish this thesis. I would also like to thank my father, who lives on in my heart and whose memory will always encourage me. I am most grateful to my wife, Myung Jung, and my son, Yul Kim, who have sacrificed for the sake of my thesis completion. I will not forget my wife's loving support and thoughtfulness. I appreciate very much the encouragement and assistance provided in countless ways by my mother, mother-in-law, father-in-law, and brother.

CONTRIBUTION OF AUTHORS

Dr. Semprini assisted in the conception and writing this dissertation. Dr. Arp provided helpful consultation for the biochemistry and microbiology aspects of the work as well as helpful comments on this dissertation.

TABLE OF CONTENTS

CHAPTER	<u>Page</u>
1: Introduction.....	1
OBJECTIVES.....	3
REFERENCES.....	4
CHAPTER 2: Literature Review.....	6
AEROBIC MICROORGANISMS THAT GROW ON CAHs.....	7
AEROBIC COMETABOLISM OF CAHs.....	9
Supply of Endogenous Reductant.....	9
Enzyme Inhibition.....	11
Transformation Product Toxicity.....	11
ACETYLENE AS A MECHANISM-BASED INACTIVATOR OF OXYGENASE.....	14
Mechanism-Based Inactivation.....	15
Kinetics for Mechanism-Based Enzyme Inactivation.....	16
SURVEY THE POTENTIAL OF AEROBIC MICROORGANISMS TO COMETABOLIZE CAHs.....	19
Biotransformation.....	20
Transformation capacity (T_c) and cell inactivation.....	23
Oxidative Dechlorination.....	24
CAH Transformation Products Detected.....	25
AEROBIC COMETABOLISM OF CAHs BY PROPANE- AND BUTANE-OXIDIZING MICROORGANISMS.....	26
Propane-Oxidizers.....	26
Butane-Oxidizers.....	28
KINETICS OF AEROBIC COMETABOLISM.....	34
Estimation of Kinetic Parameters (k_{max} and K_s).....	35

TABLE OF CONTENTS (Continued)

	<u>Page</u>
Linearized forms of Michaelis-Menten equation (Lineweaver Burk plot).....	36
Direct linear Plot.....	38
NLSR Analysis Using the Differential Form of Michaelis- Menten/Monod Equation.....	40
NLSR Analysis using the Integrated Form of Michaelis -Menten/Monod Equation.....	40
Inhibition.....	43
Determination of Inhibition Types.....	47
Determination of Inhibition Coefficients.....	48
Review Inhibition Studies in Aerobic CAH Cometabolism.....	50
Inhibition type.....	51
Determination of inhibition coefficients.....	54
METHOD USED IN THIS RESEARCH.....	56
REFERENCES.....	59
CHAPTER 3: Aerobic Cometabolism of Chlorinated Methanes, Ethanes, and Ethenes by a Butane-Grown Mixed Culture: Survey.....	66
SUMMARY.....	66
INTRODUCTION.....	67
MATERIALS AND METHODS.....	69
A Butane-Utilizing Mixed Culture.....	69
Chemicals.....	70
Analysis.....	71
Transformation of CAHs.....	72
Cell Inactivation after Exposure to Compounds.....	73
Chloride Release Study.....	74
c-DCE or 1,1-DCE Transformation and Cell Inactivation.....	74
RESULTS AND DISCUSSION.....	75

TABLE OF CONTENTS (Continued)

	<u>Page</u>
Cell Activities for Different Cell Preparation Batches.....	75
Transformations of 1,1-DCE and c-DCE and the Effects of Their Transformation on Cell Inactivation.....	76
Transformation of Chlorinated Methanes, Ethanes, and Ethylenes.....	79
CAHs Transformation Effects on Cell Inactivation.....	84
Class I ($\approx 0 \mu\text{mol}$ transformed/mg TSS and more than 70% of activity remaining).....	85
Class II (less than $1 \mu\text{mol}$ transformed/mg TSS and more than 5% of cell activity remaining).....	86
Class III (more than $1 \mu\text{mol}$ transformed/mg TSS and more than 5% of activity remaining).....	87
Class IV (less than $1 \mu\text{mol}$ transformed/mg TSS and less than 5% of activity remaining).....	88
Class V (more than $1 \mu\text{mol}$ transformed/mg TSS and less than 5% of activity remaining).....	89
Chloride Release.....	90
CONCLUSIONS.....	93
ACKNOWLEDGMENTS.....	96
REFERENCES.....	96
CHAPTER 4: Kinetic and Inhibition Studies for Aerobic Cometabolism of 1,1,1-Trichloroethane, 1,1-Dichloroethylene, 1,1-Dichloroethane by a Butane-Grown Mixed Culture.....	101
SUMMARY.....	101
INTRODUCTION.....	102
MATERIALS AND METHODS.....	106
A Butane-Utilizing Mixed Culture.....	106
Chemicals.....	109
Analysis.....	109
Batch Experiments.....	111
Mass Transfer Experiments.....	112
Acetylene Inactivation Experiment.....	114

TABLE OF CONTENTS (Continued)

	<u>Page</u>
Determination of Inhibition Types.....	115
Determination of k_{\max} , K_s , and K_I	118
RESULTS.....	119
Liquid and Gas Mass Transfer Coefficients.....	119
Acetylene Blocking Experiment.....	122
k_{\max} and K_s for Butane, 1,1-DCE, 1,1-DCA, and 1,1,1-TCA.....	123
Inhibition Types and Inhibition Coefficients.....	125
Inhibition among CAHs.....	125
CAH inhibition on butane.....	128
Butane inhibition on CAH.....	130
Comparison of Kinetic Parameters Determined with Different Methods.....	135
Comparison of K_s with K_{ic}	137
Effects of k_{\max} and/or K_s on Inhibition Coefficients in NLSR Analysis.....	138
NLSR Analysis with Different Inhibition Models.....	141
DISCUSSION.....	147
ACKNOWLEDGEMENTS.....	153
NOMENCLATURE.....	153
REFERENCES.....	154
CHAPTER 5: Engineering Significance and Conclusions.....	159
ENGINEERING SIGNIFICANCE.....	159
CONCLUSIONS.....	162
FUTURE WORK.....	163
REFERENCES.....	165
BIBLIOGRAPHY.....	166
APPENDICES.....	175

LIST OF FIGURES

<u>Figure</u>	<u>Page</u>
2.1 Different pathways of 1,2-DCA degradation by <i>Pseudomonas</i> sp. Strain DCA1 (proposed) (Hage and Hartmans, 1999), <i>Xanthobacter autotrophicus</i> GJ10 (Janssen et al. 1985) and <i>Ancylobacter aquaticus</i> AD25 (van den Wijngaard et al., 1992).....	8
2.2 Transformation capacity versus methane uptake activity after 4 hours of exposure. Values in Class V box (no transformation) indicate percentage of methane uptake activity remaining after exposure to each compound.....	14
2.3 Nonpseudo first-order loss of enzyme activity (Silverman 1988).....	19
2.4 Propane degradation and transformation of mixtures of chlorinated ethylenes (A) and chlorinated ethanes (B) in propane microcosms. The total mass of propane was 0.09 μ mole for each incubation, representing aqueous concentration of 51 μ M. Initial average aqueous concentrations of chlorinated ethanes and chlorinated ethylenes were 0.6 (Standard deviation [SD] \pm 0.12) μ M and 0.8 (SD \pm 0.14) μ M, respectively, representing total masses addition ranging from 0.03 to 0.09 μ mole (Unpublished data).....	29
2.5 Proposed degradation pathway of butane in <i>Nocardia</i> TB1 (Van Ginkel et al. 1987).....	32
2.6 Butane degradation and transformation of mixtures of 1,1,1-TCA and 1,1-DCE before and after the addition of yeast extract (25 mg/L) in a butane microcosm (Kim et al., 1997).....	34
2.7 Lineweaver-Burk plot of $1/k_{\max}$ vs. $1/S_L$, with ± 0.05 v (Cornish-Bowden, 1994).....	37
2.8 Direct linear plot of k_{\max} against K_s	39
2.9 TCE disappearance in formate-amended batch bottles at seven initial TCE concentrations. Experiment data (symbols) are plotted along with predictions (lines) by use of the cometabolic transformation model and k (k_{\max}) and K_s determined from NLSR analysis of curve D (Alvarez-Cohen and McCarty, 1991a).....	42
2.10 General model scheme for competitive, uncompetitive and mixed inhibition (Adapted from Cornish-Bowden, 1994).....	44

LIST OF FIGURES (Continued)

<u>Figure</u>	<u>Page</u>
2.11 Lineweaver-Burk plots for different inhibitions (Adapted from Dixon and Webb, 1979).....	48
2.12 Lineweaver-Burk plot for various concentrations of C_2H_5Cl as an inhibitor of NH_4^+ -dependent NO_2^- production in <i>N. europaea</i> . Inset shows that y intercepts (■) and slopes (○) were replotted against the inhibitor concentrations to obtain K_{IE} (K_{ic}) and K_{IES} (K_{iu}), respectively (Keener and Arp, 1993).....	50
2.13 Schematic diagram for kinetic and inhibition studies.....	57
2.14 Direct linear plots showing the shifting directions of best estimate point (k_{max}^{app} , K_s^{app}) at various levels of I_L providing visual evidence of inhibition type (Adapted from Cornish-Bowden, 1994).....	58
3.1 Resting cell transformation of (a) 1,1-DCE and (b) c-DCE in the presence or absence of O_2 , butane, butyrate, or formate. 3.4 mg TSS and 4.5 mg TSS were used for 1,1-DCE and c-DCE transformation experiments, respectively.....	77
3.2 Resting cell transformation of (a) chlorinated methanes, (b) chlorinated ethanes, and (c) chlorinated ethylenes. CM, DCM, CA, and 1,1-DCA values (scale on the right Y-axis) are cumulative amounts following multiple additions of CAH. The addition times in hours are as follows: CM (9.8, 22), DCM (4.6, 11, and 17), CA (1.2 and 3.4), and 1,1-DCA (2.7, 9.8, and 17).....	81
3.3 The mass of CAHs transformed per mg TSS after 30 hours of incubation versus butane uptake activity after the exposure. Values in Class I box (no transformation) indicate percentage of butane uptake activity remaining after exposure to each compound.....	85
3.4 Average percent dechlorination of the CAHs after 30 hours of incubation.....	92
4.1 A butane-grown mixed culture viewed under a fluorescence microscope....	107
4.2 Determination of K_{LaL} (A) and K_{GaG} (B) for 1,1-DCE. The aqueous stock solution of 1,1-DCE was injected in the liquid phase (A), and gaseous 1,1-DCE was added in the headspace (B). The data were fit to equations 3 and 4. Input parameters: $H_{cc} = 0.86$; $V_L = 0.005$ L; $V_G = 0.021$ L; $C_{G,0} = C_{L,0} = 0$ μ M; and $M_{tot} = 0.13$ μ mol (A) and 0.56 μ mol (B).....	120

LIST OF FIGURES (Continued)

<u>Figure</u>	<u>Page</u>
4.3 Decay of butane degradation rates as a function of time after acetylene exposure. Data were fit to first order decay model. r/r_0 indicates the ratio of the rate at time t to that at time zero.....	122
4.4 Initial degradation rates at various initial concentrations of butane (A), 1,1-DCE (B), 1,1-DCA (C), and 1,1,1-TCA (D). The curve represents the best fit of data to equation 4.5 using NLSR.....	124
4.5 Direct linear plot showing competitive inhibition of 1,1-DCA on 1,1-DCE transformation. Aqueous 1,1-DCA concentrations were 0 (\blacktriangle), 153 (\blacklozenge), 387 (\bullet), 608 (\blacksquare), and 887 (X) μM	125
4.6 Direct linear plot showing competitive inhibition of 1,1,1-TCA on 1,1-DCA transformation (A), linearized plot of K_s^{app} vs. I_L to graphically evaluate K_s and K_{ic} (B), and the NLSR best fit of the data to the competitive inhibition equation (C).....	127
4.7 Direct linear plot showing competitive inhibition of 1,1,1-TCA on butane degradation (A), plot of K_s^{app} versus I_L to graphically evaluate K_s and K_{ic} (B), and the NLSR best fit of the data to the competitive inhibition equation (C).....	129
4.8 Direct linear plot showing mixed inhibition of butane on 1,1-DCA transformation (A), plot of $1/k_{max}^{app}$ or K_s^{app}/k_{max}^{app} versus I_L to graphically evaluate k_{max} , K_s , K_{ic} , and K_{iu} (B), and the NLSR best fit of the data to the mixed inhibition equation (C).....	131
4.9 Direct linear plot showing mixed inhibition of butane on 1,1,1-TCA transformation (A), plot of $1/k_{max}^{app}$ or K_s^{app}/k_{max}^{app} versus I_L to graphically evaluate k_{max} , K_s , K_{ic} , and K_{iu} (B) and the NLSR best fit of the data to the mixed inhibition equation (C).....	132
4.10 Direct linear plot showing mixed inhibition of butane on 1,1-DCE transformation (A), plot of $1/k_{max}^{app}$ or K_s^{app}/k_{max}^{app} versus I_L to graphically evaluate k_{max} , K_s , K_{ic} , and K_{iu} (B) and the NLSR best fit of the data to the mixed inhibition equation (C).....	133

LIST OF FIGURES (Continued)

<u>Figure</u>	<u>Page</u>
4.11 Comparison of k_{\max} and K_s that are separately estimated from single-compound batch kinetic studies, linear plots, and NLSR analysis using rate data in the presence of inhibitors. The error bars represent the 95% confidence intervals.....	136
4.12 Comparison of the ratio of K_s of the substrate over K_s of the inhibitor and the K_s of substrate over estimated K_i of the inhibitor. The data obtained from competitive inhibition among the CAHs (◆) and the data obtained from competitive inhibition of CAHs on butane degradation (□) are separately fit by linear least squares regression.....	138
4.13 Comparison of butane inhibition coefficients, K_{ic} (A) and K_{iu} (B), determined by four different NLSR analyses along with values from the linearized plot. Linearized indicates linear plot; NLSR indicates NLSR with all 4 kinetic parameters varying (k_{\max} , K_s , K_{ic} , and/or K_{iu}); NLSR GkmaxKs indicates NLSR with constant k_{\max} and K_s and with 2 inhibition coefficients varying; NLSR Gkmax indicates NLSR with constant k_{\max} and with K_s and inhibition coefficients varying; and NLSR GKs indicates NLSR with constant K_s , and with k_{\max} and inhibition coefficients varying.....	140
4.14 Kinetic coefficients determined by NLSR analysis using mixed, noncompetitive, and competitive inhibition models for the case of butane inhibition on 1,1-DCA transformation (A), the best fit of the data to the noncompetitive inhibition model (B), and the competitive inhibition model (C). The k_{\max} values in panel (A) are presented by multiplying the estimated values by a factor of 10.....	142
4.15 Kinetic coefficients determined by NLSR analysis using mixed, noncompetitive and competitive inhibition models for the case of butane inhibition on 1,1-DCE transformation (A), the best fit of the data to the noncompetitive inhibition model (B), and the competitive inhibition model (C).....	144
4.16 Kinetic coefficients determined by NLSR analysis using mixed, noncompetitive, and competitive inhibition models for the case of 1,1-DCA inhibition on 1,1-DCE inhibition (A), the best fit of the data to mixed inhibition model (B), and the noncompetitive inhibition model (C). The values for k_{\max} , K_s and K_{ic} in panel (A) are presented by multiplying the estimated values by a factor of 100, 100 and 10, respectively.....	146

LIST OF TABLES

<u>Table</u>	<u>Page</u>
2.1 T _c values, cell activity remaining after exposure to each compound, and the amount of chloride released, and products detected by a methane-grown mixed culture (Chang and Alvarez-Cohen, 1996), <i>Methylosinus trichosporium</i> OB 3b (Bartnicki and Castro, 1994; Oldenhuis et al., 1991; van Hylckama Vlieg et al., 1996), or <i>Nitrosomonas europaea</i> (Rasche et al., 1991).....	21
2.2 The effects of inhibitors on the parameters of the Michaelis-Menten equation (Adapted from Cornish-Bowden, 1994).....	46
2.3 Intercepts and slopes of Lineweaver-Burk plot in the presence of inhibitor and graphical determination of inhibition coefficients (Adapted from Dixon and Webb, 1979).....	49
2.4 Summary of methods for determination of K _s , inhibition types, and inhibition coefficients.....	52
3.1 Average initial transformation rates of chlorinated methanes, ethanes, and ethylenes.....	83
4.1 The effects of inhibitors on the parameters of the Michaelis-Menten equation and linearized equations of the parameters.....	117
4.2 Overall mass transfer coefficients (K _{La} and K _{Ga}) for 1,1-DCE, 1,1-DCA, 1,1,1-TCA, and butane.....	121
4.3 k _{max} and K _s with their 95% confidence intervals for butane, 1,1-DCE, 1,1-DCA, and 1,1,1-TCA.....	124
4.4 Summary of determined inhibition types.....	128
4.5 Inhibition coefficients estimated from linearized equation and NLSR analysis.....	135

LIST OF APPENDICES

	<u>Page</u>
APPENDIX A: Derivation of the Analytical Solutions for the Mass Transfer of Volatile Compounds in a Batch Reactor and Tests of the Validity of Equilibrium Assumption in the Batch Kinetic Studies.....	176
A1. DERIVATION OF ANALYTICAL SOLUTIONS FOR MASS TRANSFER.....	177
A2. VALIDITY OF EQUILIBRIUM ASSUMPTION.....	185
APPENDIX B: Derivation of Inhibition Equations and Linearized Inhibition Equations.....	187
B1. DERIVATION OF INHIBITION MODEL EQUATIONS.....	188
B2. DERIVATION OF LINEARIZED EQUATIONS USED TO EVALUATE THE INITIAL GUESS OF KINETIC PARAMETERS FOR NLSR ANALYSIS.....	193
APPENDIX C: Estimation Methods Combining the Direct Linear Plot to Determine Inhibition Type and Values of K_s^{app} and k_{max}^{app} , Linearized Equations to Obtain the Initial Guesses of Kinetic Parameters, and NLSR Analysis to Determine the Kinetic Parameters.....	197
C1. MIXED INHIBITION ON 1,1-DCE TRANSFORMATION BY BUTANE.....	198
C2. MIXED INHIBITION ON 1,1-DCA TRANSFORMATION BY BUTANE.....	204
C3. MIXED INHIBITION ON 1,1,1-TCA TRANSFORMATION BY BUTANE.....	210
C4. COMPETITIVE INHIBITION ON BUTANE DEGRADATION BY 1,1-DCE.....	219
C5. COMPETITIVE INHIBITION ON 1,1-DCA TRANSFORMATION BY 1,1-DCE.....	225
C6. COMPETITIVE INHIBITION ON 1,1,1-TCA TRANSFORMATION BY 1,1-DCE.....	231

LIST OF APPENDICES (Continued)

	<u>Page</u>
C7. COMPETITIVE INHIBITION ON BUTANE DEGRADATION BY 1,1-DCA.....	237
C8. COMPETITIVE INHIBITION ON 1,1-DCE TRANSFORMATION BY 1,1-DCA.....	243
C9. COMPETITIVE INHIBITION ON 1,1,1-TCA TRANSFORMATION BY 1,1-DCA.....	249
C10. COMPETITIVE INHIBITION ON BUTANE DEGRADATION BY 1,1,1-TCA.....	255
C11. COMPETITIVE INHIBITION ON 1,1-DCE TRANSFORMATION BY 1,1,1-TCA.....	261
C12. COMPETITIVE INHIBITION ON 1,1-DCA TRANSFORMATION BY 1,1,1-TCA.....	267
C13. SUMMARY OF KINETIC PARAMETERS AND COMPARISON OF THOSE OBTAINED FROM DIFFERENT METHODS.....	273
APPENDIX D: Kinetic Parameters Obtained by Performing NLSR Analysis Using the Different Inhibition Models and Fit of Data to the Models.....	279
D1. BUTANE INHIBITION ON 1,1-DCE TRANSFORMATION.....	280
D2. BUTANE INHIBITION ON 1,1-DCA TRANSFORMATION.....	282
D3. BUTANE INHIBITION ON 1,1,1-TCA TRANSFORMATION.....	284
D4. 1,1-DCE INHIBITION ON BUTANE DEGRADATION.....	286
D5. 1,1-DCE INHIBITION ON 1,1-DCA TRANSFORMATION.....	288
D6. 1,1-DCE INHIBITION ON 1,1,1-TCA TRANSFORMATION.....	290
D7. 1,1-DCA INHIBITION ON BUTANE DEGRADATION.....	292

LIST OF APPENDICES (Continued)

	<u>Page</u>
D8. 1,1-DCA INHIBITION ON 1,1-DCE TRANSFORMATION.....	294
D9. 1,1-DCA INHIBITION ON 1,1,1-TCA TRANSFORMATION.....	296
D10. 1,1,1-TCA INHIBITION ON BUTANE DEGRADATION.....	298
D11. 1,1,1-TCA INHIBITION ON 1,1-DCE TRANSFORMATION.....	300
D12. 1,1,1-TCA INHIBITION ON 1,1-DCA TRANSFORMATION.....	302
APPENDIX E: Kinetic Parameters Obtained from Linear Plots Using the Linearized Equations for Different Inhibition Models.....	304
E1. COMPETITIVE INHIBITION LINEAR PLOTS USING THE DATA SHOWING MIXED INHIBITION OF BUTANE ON THE CAHs...	305
E2. MIXED INHIBITION LINEAR PLOTS USING THE DATA SHOWING COMPETITIVE INHIBITION.....	306
APPENDIX F: Criteria to be Classified as Mechanism-Based Inactivator	311

LIST OF APPENDIX FIGURES

<u>Figure</u>	<u>Page</u>
A2.1 Simulation results of butane degradation at different levels of TSS.....	185
A2.2. The k_{\max} calculated versus TSS.....	186
C1.1 Direct linear plot showing mixed inhibition on 1,1-DCE transformation by butane.....	202
C1.2 Linearized plot in the case of mixed inhibition of 1,1-DCE transformation by butane.....	203
C1.3 Best fit obtained from NLSR analysis using mixed inhibition model (Residual Standard Error = 0.018, $k_{\max} = 1.2 \pm 0.04 \mu\text{mol/mg TSS/hr}$, $K_s = 1.05 \pm 0.18 \mu\text{M}$, $K_{ic} = 0.33 \pm 0.07 \mu\text{M}$ and $K_{iu} = 6.9 \pm 1.6 \mu\text{M}$).....	203
C2.1 Direct linear plot showing mixed inhibition on 1,1-DCA transformation by butane.....	208
C2.2 Linearized plot in the case of mixed inhibition of 1,1-DCA transformation by butane.....	209
C2.3 Best fit obtained from NLSR analysis using mixed inhibition model. (Residual Standard Error = 0.01, $k_{\max} = 0.45 \pm 0.026 \mu\text{mol/mg TSS/hr}$, $K_s = 17.8 \pm 4.08 \mu\text{M}$, $K_{ic} = 2.8 \pm 1.6$, $K_{iu} = 3.8 \pm 0.88 \mu\text{M}$).....	209
C3.1 Direct linear plot showing mixed inhibition on 1,1,1-TCA transformation by butane.....	217
C3.2 Linearized plot in the case of mixed inhibition of 1,1,1-TCA transformation by butane.....	218
C3.3 Best fit obtained from NLSR analysis using mixed inhibition model. (Residual Standard Error = 0.005, $k_{\max} = 0.20 \pm 0.007 \mu\text{mol/mg TSS/hr}$, $K_s = 12.7 \pm 2.07 \mu\text{M}$, $K_{ic} = 0.28 \pm 0.13 \mu\text{M}$ and $K_{iu} = 0.51 \pm 0.094 \mu\text{M}$).....	218
C4.1 Direct linear plot showing competitive inhibition on butane degradation by 1,1-DCE.....	223
C4.2 Linearized plot in the case of competitive inhibition of butane degradation by 1,1-DCE.....	224

LIST OF APPENDIX FIGURES (Continued)

<u>Figure</u>	<u>Page</u>
C4.3 Best fit obtained from NLSR analysis using competitive inhibition model. (Residual Standard Error = 0.054, $k_{\max} = 2.09 \pm 0.17$ $\mu\text{mol/mg TSS/hr}$, $K_s = 8.5 \pm 2.14$ μM , and $K_{ic} = 8.7 \pm 2.26$ μM).....	224
C5.1 Direct linear plot showing competitive inhibition on 1,1-DCA transformation by 1,1-DCE.....	229
C5.2 Linearized plot in the case of competitive inhibition of 1,1-DCA transformation by 1,1-DCE.....	230
C5.3 Best fit obtained from NLSR analysis using competitive inhibition model. (Residual Standard Error = 0.028, $k_{\max} = 0.56 \pm 0.06$ $\mu\text{mol/mg TSS/hr}$, $K_s = 18.4 \pm 8.5$ μM , and $K_{ic} = 3.64 \pm 1.46$ μM).....	230
C6.1 Direct linear plot showing competitive inhibition on 1,1,1-TCA transformation by 1,1-DCE.....	235
C6.2 Linearized plot in the case of competitive inhibition of 1,1,1-TCA transformation by 1,1-DCE.....	236
C6.3 Best fit obtained from NLSR analysis using competitive inhibition model. (Residual Standard Error = 0.01, $k_{\max} = 0.20 \pm 0.015$ $\mu\text{mol/mg TSS/hr}$, $K_s = 14.3 \pm 4.8$ μM , and $K_{ic} = 1.02 \pm 0.304$ μM).....	236
C7.1 Direct linear plot showing competitive inhibition on butane degradation by 1,1-DCA.....	241
C7.2 Linearized plot in the case of competitive inhibition of butane degradation by 1,1-DCA.....	242
C7.3 Best fit obtained from NLSR analysis using competitive inhibition model. (Residual Standard Error = 0.020, $k_{\max} = 2.12 \pm 0.23$ $\mu\text{mol/mg TSS/hr}$, $K_s = 10.9 \pm 2.22$ μM , and $K_{ic} = 403 \pm 51$ μM).....	242
C8.1 Direct linear plot showing competitive inhibition on 1,1-DCE transformation by 1,1-DCA.....	247
C8.2 Linearized plot in the case of competitive inhibition of 1,1-DCE transformation by 1,1-DCA.....	248

LIST OF APPENDIX FIGURES (Continued)

<u>Figure</u>	<u>Page</u>
C8.3 Best fit obtained from NLSR analysis using competitive inhibition model. (Residual Standard Error = 0.035, $k_{\max} = 1.16 \pm 0.07$ $\mu\text{mol/mg TSS/hr}$, $K_s = 1.67 \pm 0.51$ μM , and $K_{ic} = 17.8 \pm 4.87$ μM).....	248
C9.1 Direct linear plot showing competitive inhibition on 1,1,1-TCA transformation by 1,1-DCA.....	253
C9.2 Linearized plot in the case of competitive inhibition of 1,1,1-TCA transformation by 1,1-DCA.....	254
C9.3 Best fit obtained from NLSR analysis using competitive inhibition model. (Residual Standard Error = 0.006, $k_{\max} = 0.20 \pm 0.016$ $\mu\text{mol/mg TSS/hr}$, $K_s = 14.3 \pm 3.69$ μM , and $K_{ic} = 16.24 \pm 4.77$ μM).....	254
C10.1 Direct linear plot showing competitive inhibition on butane degradation by 1,1,1-TCA.....	259
C10.2 Linearized plot in the case of competitive inhibition of butane degradation by 1,1,1-TCA.....	260
C10.3 Best fit obtained from NLSR analysis using competitive inhibition model. (Residual Standard Error = 0.073, $k_{\max} = 2.53 \pm 0.312$ $\mu\text{mol/mg TSS/hr}$, $K_s = 13.1 \pm 4.4$ μM , and $K_{ic} = 313 \pm 88$ μM).....	260
C11.1 Direct linear plot showing competitive inhibition on 1,1-DCE transformation by 1,1,1-TCA.....	265
C11.2 Linearized plot in the case of competitive inhibition of 1,1-DCE transformation by 1,1,1-TCA.....	266
C11.3 Best fit obtained from NLSR analysis using competitive inhibition model. (Residual Standard Error = 0.029, $k_{\max} = 1.18 \pm 0.068$ $\mu\text{mol/mg TSS/hr}$, $K_s = 2.11 \pm 0.542$ μM , and $K_{ic} = 17.3 \pm 3.91$ μM).....	266
C12.1 Direct linear plot showing competitive inhibition on 1,1-DCA transformation by 1,1,1-TCA.....	271
C12.2 Linearized plot in the case of competitive inhibition of 1,1-DCA transformation by 1,1,1-TCA.....	272

LIST OF APPENDIX FIGURES (Continued)

<u>Figure</u>	<u>Page</u>
C12.3 Best fit obtained from NLSR analysis using competitive inhibition model. (Residual Standard Error = 0.012, $k_{\max} = 0.47 \pm 0.023$ $\mu\text{mol/mg TSS/hr}$, $K_s = 13.7 \pm 3.2 \mu\text{M}$, and $K_{ic} = 9.8 \pm 2.21 \mu\text{M}$).....	272
C13.1 Comparison of K_{ic} values for butane determined different methods.....	276
C13.2 Comparison of K_{iu} values for butane determined different methods.....	276
C13.3 Comparison of K_{ic} values for 1,1-DCE determined different methods.....	277
C13.4 Comparison of K_{ic} values for 1,1-DCA determined different methods.....	277
C13.5 Comparison of K_{ic} values for 1,1,1-TCA determined different methods.....	278
D1.1 Comparison of parameters obtained from NLSR analysis fitting all inhibition models to data identified as mixed inhibition on 1,1-DCE transformation by butane.....	280
D1.2 Noncompetitive inhibition model fit to data identified as mixed inhibition of butane on 1,1-DCE transformation.....	281
D1.3 Competitive inhibition model fit to data identified as mixed inhibition of butane on 1,1-DCE transformation.....	281
D2.1 Comparison of parameters obtained from NLSR analysis fitting all inhibition models to data identified as mixed inhibition of butane on 1,1-DCA transformation.....	282
D2.2 Noncompetitive inhibition model fit to data identified as mixed inhibition of butane on 1,1-DCA transformation.....	283
D2.3 Competitive inhibition model fit to data identified as mixed inhibition of butane on 1,1-DCA transformation.....	283
D3.1 Comparison of parameters obtained from NLSR analysis fitting all inhibition models to data identified as mixed inhibition of butane on 1,1,1-TCA transformation. The values for k_{\max} , K_{ic} and K_{iu} were multiplied by a factor of 10.....	284

LIST OF APPENDIX FIGURES (Continued)

<u>Figure</u>	<u>Page</u>
D3.2 Noncompetitive inhibition model fit to data identified as mixed inhibition of butane on 1,1,1-TCA transformation.....	285
D3.3 Competitive inhibition model fit to data identified as mixed inhibition of butane on 1,1,1-TCA transformation.....	285
D4.1 Comparison of parameters obtained from NLSR analysis fitting all inhibition models to data identified as competitive inhibition of 1,1-DCE on butane degradation. The values for k_{\max} , and K_s were multiplied by a factor of 10.....	286
D4.2 Mixed inhibition model fit to data identified as competitive inhibition of 1,1-DCE on butane degradation.....	287
D4.3 Noncompetitive inhibition model fit to data identified as competitive inhibition of 1,1-DCE on butane degradation.....	287
D5.1 Comparison of parameters obtained from NLSR analysis fitting all inhibition models to data identified as competitive inhibition of 1,1-DCE on 1,1-DCA transformation. The k_{\max} , and K_{ic} values were multiplied by a factor of 10 and 20, respectively.....	288
D5.2 Mixed inhibition model fit to data identified as competitive inhibition of 1,1-DCE on 1,1-DCA transformation.....	289
D5.3 Noncompetitive inhibition model fit to data identified as competitive inhibition of 1,1-DCE on 1,1-DCA transformation.....	289
D6.1 Comparison of parameters obtained from NLSR analysis fitting all inhibition models to data identified as competitive inhibition of 1,1-DCE on 1,1,1-TCA transformation. The k_{\max} , and K_{ic} values were multiplied by a factor of 200 and 50, respectively.....	290
D6.2 Mixed inhibition model fit to data identified as competitive inhibition of 1,1-DCE on 1,1,1-TCA transformation.....	291
D6.3 Noncompetitive inhibition model fit to data identified as competitive inhibition of 1,1-DCE on 1,1,1-TCA transformation.....	291

LIST OF APPENDIX FIGURES (Continued)

<u>Figure</u>	<u>Page</u>
D7.1 Comparison of parameters obtained from NLSR analysis fitting all inhibition models to data identified as competitive inhibition of 1,1-DCA on butane degradation. The k_{\max} , and K_s values were multiplied by a factor of 200 and 40, respectively. Inset shows k_{\max} values in logarithmic scale.....	292
D7.2 Noncompetitive inhibition model fit to data identified as competitive inhibition of 1,1-DCA on butane degradation.....	293
D8.1 Comparison of parameters obtained from NLSR analysis fitting all inhibition models to data identified as competitive inhibition of 1,1-DCA on 1,1-DCE transformation. The k_{\max} , K_s and K_{ic} values were multiplied by a factor of 100, 100 and 10, respectively.....	294
D8.2 Mixed inhibition model fit to data identified as competitive inhibition of 1,1-DCA on 1,1-DCE transformation.....	295
D8.3 Noncompetitive inhibition model fit to data identified as competitive inhibition of 1,1-DCA on 1,1-DCE transformation.....	295
D9.1 Comparison of parameters obtained from NLSR analysis fitting all inhibition models to data identified as competitive inhibition of 1,1-DCA on 1,1,1-TCA transformation. The k_{\max} , K_s and K_{ic} values were multiplied by a factor of 100, 10 and 10, respectively.....	296
D9.2 Noncompetitive inhibition model fit to data identified as competitive inhibition of 1,1-DCA on 1,1,1-TCA transformation.....	297
D10.1 Comparison of parameters obtained from NLSR analysis fitting all inhibition models to data identified as competitive inhibition of 1,1,1-TCA on butane degradation. A y-axis is in logarithmic scale.....	298
D10.2 Mixed inhibition model fit to data identified as competitive inhibition of 1,1,1-TCA on butane degradation.....	299
D10.3 Noncompetitive inhibition model fit to data identified as competitive inhibition of 1,1,1-TCA on butane degradation.....	299

LIST OF APPENDIX FIGURES (Continued)

<u>Figure</u>	<u>Page</u>
D11.1 Comparison of parameters obtained from NLSR analysis fitting all inhibition models to data identified as competitive inhibition of 1,1,1-TCA on 1,1-DCE transformation. A y-axis is in logarithmic scale.....	300
D11.2 Mixed inhibition model fit to data identified as competitive inhibition of 1,1,1-TCA on 1,1-DCE transformation.....	301
D11.3 Noncompetitive inhibition model fit to data identified as competitive inhibition of 1,1,1-TCA on 1,1-DCE transformation.....	301
D12.1 Comparison of parameters obtained from NLSR analysis fitting all inhibition models to data identified as competitive inhibition of 1,1,1-TCA on 1,1-DCA transformation. A y-axis is in logarithmic scale....	302
D12.2 Noncompetitive inhibition model fit to data identified as competitive inhibition of 1,1,1-TCA on 1,1-DCA transformation.....	303
E2.1. Two linear plots using data showing competitive inhibition of 1,1-DCE on butane degradation.....	306
E2.2. Two linear plots using data showing competitive inhibition of 1,1-DCE on 1,1-DCA transformation.....	306
E2.3. Two linear plots using data showing competitive inhibition of 1,1-DCE on 1,1,1-TCA transformation.....	307
E2.4. Two linear plots using data showing competitive inhibition of 1,1-DCA on butane degradation.....	307
E2.5. Two linear plots using data showing competitive inhibition of 1,1-DCA on 1,1-DCE transformation.....	308
E2.6. Two linear plots using data showing competitive inhibition of 1,1-DCA on 1,1,1-TCA transformation.....	308
E2.7. Two linear plots using data showing competitive inhibition of 1,1,1-TCA on butane degradation.....	309

LIST OF APPENDIX FIGURES (Continued)

<u>Figure</u>	<u>Page</u>
E2.8. Two linear plots using data showing competitive inhibition of 1,1,1-TCA on 1,1-DCE transformation.....	309
E2.9. Two linear plots using data showing competitive inhibition of 1,1,1-TCA on 1,1-DCA transformation.....	310
F.1 Time-dependent inactivation of enzymes by mechanism-based enzyme inactivators (Silverman 1988).....	313
F.2 Substrate protection during mechanism-based inactivation (Silverman 1988).....	314

LIST OF APPENDIX TABLES

<u>Table</u>	<u>Page</u>
B2.1 The effects of inhibitors on the parameters of the Michaelis-Menten equation.....	193
C1.1 K_s^{app} and k_{max}^{app} values of 1,1-DCE in the presence of butane (0 μ M).....	198
C1.2 K_s^{app} and k_{max}^{app} values of 1,1-DCE in the presence of butane (1.8 \pm 0.01 μ M).....	199
C1.3 K_s^{app} and k_{max}^{app} values of 1,1-DCE in the presence of butane (4.6 \pm 0.01 μ M).....	199
C1.4 K_s^{app} and k_{max}^{app} values of 1,1-DCE in the presence of butane (8.6 \pm 0.02 μ M).....	200
C1.5 K_s^{app} and k_{max}^{app} values of 1,1-DCE in the presence of butane (13 \pm 0.1 μ M).....	201
C1.6 Values used for linearized plot in the case of mixed inhibition on 1,1-DCE transformation by butane.....	202
C1.7 Initial guesses of parameters obtained linearized plot in the case of inhibition on 1,1-DCE transformation by butane.....	202
C2.1 K_s^{app} and k_{max}^{app} values of 1,1-DCA in the presence of butane (0 μ M).....	204
C2.2 K_s^{app} and k_{max}^{app} values of 1,1-DCA in the presence of butane (0.62 \pm 0.02 μ M).....	205
C2.3 K_s^{app} and k_{max}^{app} values of 1,1-DCA in the presence of butane (1.7 \pm 0.01 μ M).....	205
C2.4 K_s^{app} and k_{max}^{app} values of 1,1-DCA in the presence of butane (3.2 \pm 0.13 μ M).....	206
C2.5 K_s^{app} and k_{max}^{app} values of 1,1-DCA in the presence of butane (4.9 \pm 0.07 μ M).....	207
C2.6 Values used for linearized plot in the case of mixed inhibition on 1,1-DCA transformation by butane.....	208

LIST OF APPENDIX TABLES (Continued)

<u>Table</u>	<u>Page</u>
C2.7. Initial guesses of parameters obtained linearized plot in the case of inhibition on 1,1-DCA transformation by butane.....	208
C3.1 K_s^{app} and k_{max}^{app} values of 1,1,1-TCA in the presence of butane (0 μ M).....	210
C3.2 K_s^{app} and k_{max}^{app} values of 1,1,1-TCA in the presence of butane (0.14 \pm 0.04 μ M).....	212
C3.3 K_s^{app} and k_{max}^{app} values of 1,1,1-TCA in the presence of butane (0.25 \pm 0.004 μ M).....	213
C3.4 K_s^{app} and k_{max}^{app} values of 1,1,1-TCA in the presence of butane (1.6 \pm 0.08 μ M).....	214
C3.5 K_s^{app} and k_{max}^{app} values of 1,1,1-TCA in the presence of butane (2.7 \pm 0.01 μ M).....	215
C3.6 K_s^{app} and k_{max}^{app} values of 1,1,1-TCA in the presence of butane (5.7 \pm 0.22 μ M).....	216
C3.7 Values used for linearized plot in the case of mixed inhibition on 1,1,1-TCA transformation by butane.....	217
C3.8 Initial guesses of parameters obtained linearized plot in the case of inhibition on 1,1,1-TCA transformation by butane.....	217
C4.1 K_s^{app} and k_{max}^{app} values of butane in the presence of 1,1-DCE (0 μ M).....	219
C4.2 K_s^{app} and k_{max}^{app} values of butane in the presence of 1,1-DCE (3.3 \pm 0.11 μ M).....	220
C4.3 K_s^{app} and k_{max}^{app} values of butane in the presence of 1,1-DCE 6.5 \pm 0.11 μ M).....	220
C4.4 K_s^{app} and k_{max}^{app} values of butane in the presence of 1,1-DCE (12.6 \pm 0.02 μ M).....	221

LIST OF APPENDIX TABLES (Continued)

<u>Table</u>	<u>Page</u>
C4.5 K_s^{app} and $k_{\text{max}}^{\text{app}}$ values of butane in the presence of 1,1-DCE ($22.2 \pm 0.10 \mu\text{M}$).....	222
C4.6 Values used for linearized plot in the case of competitive inhibition on butane degradation by 1,1-DCE.....	223
C4.7 Initial guesses of parameters obtained linearized plot in the case of inhibition on butane degradation by 1,1-DCE.....	223
C5.1 K_s^{app} and $k_{\text{max}}^{\text{app}}$ values of 1,1-DCA in the presence of 1,1-DCE ($0 \mu\text{M}$)....	225
C5.2 K_s^{app} and $k_{\text{max}}^{\text{app}}$ values of 1,1-DCA in the presence of 1,1-DCE ($5.4 \pm 0.37 \mu\text{M}$).....	226
C5.3 K_s^{app} and $k_{\text{max}}^{\text{app}}$ values of 1,1-DCA in the presence of 1,1-DCE ($16 \pm 0.36 \mu\text{M}$).....	226
C5.4 K_s^{app} and $k_{\text{max}}^{\text{app}}$ values of 1,1-DCA in the presence of 1,1-DCE ($25 \pm 1.03 \mu\text{M}$).....	227
C5.5 K_s^{app} and $k_{\text{max}}^{\text{app}}$ values of 1,1-DCA in the presence of 1,1-DCE ($46 \pm 1.00 \mu\text{M}$).....	228
C5.6 Values used for linearized plot in the case of competitive inhibition on 1,1-DCA transformation by 1,1-DCE.....	229
C5.7 Initial guesses of parameters obtained linearized plot in the case of inhibition on 1,1-DCA transformation by 1,1-DCE.....	229
C6.1 K_s^{app} and $k_{\text{max}}^{\text{app}}$ values of 1,1,1-TCA in the presence of 1,1-DCE ($0 \mu\text{M}$)....	231
C6.2 K_s^{app} and $k_{\text{max}}^{\text{app}}$ values of 1,1,1-TCA in the presence of 1,1-DCE ($1.4 \pm 0.14 \mu\text{M}$).....	232
C6.3 K_s^{app} and $k_{\text{max}}^{\text{app}}$ values of 1,1,1-TCA in the presence of 1,1-DCE ($4.3 \pm 0.16 \mu\text{M}$).....	232
C6.4 K_s^{app} and $k_{\text{max}}^{\text{app}}$ values of 1,1,1-TCA in the presence of 1,1-DCE ($7.3 \pm 0.15 \mu\text{M}$).....	233

LIST OF APPENDIX TABLES (Continued)

<u>Table</u>	<u>Page</u>
C6.5 K_s^{app} and k_{max}^{app} values of 1,1,1-TCA in the presence of 1,1-DCE ($12.6 \pm 0.15 \mu M$).....	234
C6.6 Values used for linearized plot in the case of competitive inhibition on 1,1,1-TCA transformation by 1,1-DCE.....	235
C6.7 Initial guesses of parameters obtained linearized plot in the case of inhibition on 1,1,1-TCA transformation by 1,1-DCE.....	235
C7.1 K_s^{app} and k_{max}^{app} values of butane in the presence of 1,1-DCA ($0 \mu M$).....	237
C7.2 K_s^{app} and k_{max}^{app} values of butane in the presence of 1,1-DCA ($238 \pm 4.8 \mu M$).....	238
C7.3 K_s^{app} and k_{max}^{app} values of butane in the presence of 1,1-DCA ($464 \pm 8.0 \mu M$).....	238
C7.4 K_s^{app} and k_{max}^{app} values of butane in the presence of 1,1-DCA ($693 \pm 5.4 \mu M$).....	239
C7.5 K_s^{app} and k_{max}^{app} values of butane in the presence of 1,1-DCA ($908 \pm 13.0 \mu M$).....	240
C7.6 Values used for linearized plot in the case of competitive inhibition on butane degradation by 1,1-DCA.....	241
C7.7 Initial guesses of parameters obtained linearized plot in the case of inhibition on butane degradation by 1,1-DCA.....	241
C8.1 K_s^{app} and k_{max}^{app} values of 1,1-DCE in the presence of 1,1-DCA ($0 \mu M$).....	243
C8.2 K_s^{app} and k_{max}^{app} values of 1,1-DCE in the presence of 1,1-DCA ($154 \pm 3.9 \mu M$).....	244
C8.3 K_s^{app} and k_{max}^{app} values of 1,1-DCE in the presence of 1,1-DCA ($387 \pm 24.3 \mu M$).....	244

LIST OF APPENDIX TABLES (Continued)

<u>Table</u>	<u>Page</u>
C8.4 K_s^{app} and k_{max}^{app} values of 1,1-DCE in the presence of 1,1-DCA ($608 \pm 14.8 \mu M$).....	245
C8.5 K_s^{app} and k_{max}^{app} values of 1,1-DCE in the presence of 1,1-DCA ($887 \pm 15.4 \mu M$).....	246
C8.6 Values used for linearized plot in the case of competitive inhibition on 1,1-DCE transformation by 1,1-DCA.....	247
C8.7 Initial guesses of parameters obtained linearized plot in the case of inhibition on 1,1-DCE transformation by 1,1-DCA.....	247
C9.1 K_s^{app} and k_{max}^{app} values of 1,1,1-TCA in the presence of 1,1-DCA ($0 \mu M$).....	249
C9.2 K_s^{app} and k_{max}^{app} values of 1,1,1-TCA in the presence of 1,1-DCA ($5.8 \pm 0.53 \mu M$).....	250
C9.3 K_s^{app} and k_{max}^{app} values of 1,1,1-TCA in the presence of 1,1-DCA ($9.8 \pm 1.12 \mu M$).....	250
C9.4 K_s^{app} and k_{max}^{app} values of 1,1,1-TCA in the presence of 1,1-DCA ($21 \pm 1.8 \mu M$).....	251
C9.5 K_s^{app} and k_{max}^{app} values of 1,1,1-TCA in the presence of 1,1-DCA ($29 \pm 2.15 \mu M$).....	252
C9.6 Values used for linearized plot in the case of competitive inhibition on 1,1,1-TCA transformation by 1,1-DCA.....	253
C9.7 Initial guesses of parameters obtained linearized plot in the case of inhibition on 1,1,1-TCA transformation by 1,1-DCA.....	253
C10.1 K_s^{app} and k_{max}^{app} values of butane in the presence of 1,1,1-TCA ($0 \mu M$).....	255
C10.2 K_s^{app} and k_{max}^{app} values of butane in the presence of 1,1,1-TCA ($184 \pm 4.84 \mu M$).....	256
C10.3 K_s^{app} and k_{max}^{app} values of butane in the presence of 1,1,1-TCA ($548 \pm 7.2 \mu M$).....	256

LIST OF APPENDIX TABLES (Continued)

<u>Table</u>	<u>Page</u>
C10.4 K_s^{app} and k_{max}^{app} values of butane in the presence of 1,1,1-TCA ($902 \pm 5.0 \mu M$).....	257
C10.5 K_s^{app} and k_{max}^{app} values of butane in the presence of 1,1,1-TCA ($1228 \pm 31 \mu M$).....	258
C10.6 Values used for linearized plot in the case of competitive inhibition on butane degradation 1,1,1-TCA.....	259
C10.7 Initial guesses of parameters obtained linearized plot in the case of inhibition on butane degradation by 1,1,1-TCA.....	259
C11.1 K_s^{app} and k_{max}^{app} values of 1,1-DCE in the presence of 1,1,1-TCA ($0 \mu M$)....	261
C11.2 K_s^{app} and k_{max}^{app} values of 1,1-DCE in the presence of 1,1,1-TCA ($66 \pm 2.6 \mu M$).....	262
C11.3 K_s^{app} and k_{max}^{app} values of 1,1-DCE in the presence of 1,1,1-TCA ($133 \pm 3.3 \mu M$).....	262
C11.4 K_s^{app} and k_{max}^{app} values of 1,1-DCE in the presence of 1,1,1-TCA ($278 \pm 6.6 \mu M$).....	263
C11.5 K_s^{app} and k_{max}^{app} values of 1,1-DCE in the presence of 1,1,1-TCA ($409 \pm 1.8 \mu M$).....	264
C11.6 Values used for linearized plot in the case of competitive inhibition on 1,1-DCE transformation 1,1,1-TCA.....	265
C11.7 Initial guesses of parameters obtained linearized plot in the case of inhibition on 1,1-DCE transformation by 1,1,1-TCA.....	265
C12.1 K_s^{app} and k_{max}^{app} values of 1,1-DCA in the presence of 1,1,1-TCA ($0 \mu M$)...	267
C12.2 K_s^{app} and k_{max}^{app} values of 1,1-DCA in the presence of 1,1,1-TCA ($16 \pm 0.32 \mu M$).....	268

LIST OF APPENDIX TABLES (Continued)

<u>Table</u>	<u>Page</u>
C12.3 K_s^{app} and $k_{\text{max}}^{\text{app}}$ values of 1,1-DCA in the presence of 1,1,1-TCA ($40.6 \pm 0.86 \mu\text{M}$).....	268
C12.4 K_s^{app} and $k_{\text{max}}^{\text{app}}$ values of 1,1-DCA in the presence of 1,1,1-TCA ($83 \pm 0.5 \mu\text{M}$).....	269
C12.5 K_s^{app} and $k_{\text{max}}^{\text{app}}$ values of 1,1-DCA in the presence of 1,1,1-TCA ($202 \pm 5.7 \mu\text{M}$).....	270
C12.6 Values used for linearized plot in the case of competitive inhibition on 1,1- DCA transformation 1,1,1-TCA.....	271
C12.7 Initial guesses of parameters obtained linearized plot in the case of inhibition on 1,1-DCA transformation by 1,1,1-TCA.....	271
C13.1 Comparison of k_{max} and K_s values of butane obtained from different methods.....	273
C13.2 Comparison of k_{max} and K_s values of 1,1-DCE obtained from different methods.....	273
C13.3 Comparison of k_{max} and K_s values of 1,1-DCA obtained from different methods.....	274
C13.4 Comparison of k_{max} and K_s values of 1,1,1-TCA obtained from different methods.....	274
C13.5 Comparison of K_{ic} and K_{iu} obtained with different methods.....	275
D1.1 Kinetic parameters (k_{max} and K_s) for 1,1-DCE and inhibition coefficients for butane obtained from NLSR analysis by fitting competitive and noncompetitive inhibition models to data identified as mixed inhibition of butane on 1,1-DCE transformation.....	280
D2.1 Kinetic parameters (k_{max} and K_s) for 1,1-DCA and inhibition coefficients for butane obtained from NLSR analysis by fitting competitive and noncompetitive inhibition models to data identified as mixed inhibition of butane on 1,1-DCA transformation.....	282

LIST OF APPENDIX TABLES (Continued)

<u>Table</u>	<u>Page</u>
D3.1 Kinetic parameters (k_{\max} and K_s) for 1,1-DCA and inhibition coefficients for butane obtained from NLSR analysis by fitting competitive and noncompetitive inhibition models to data identified as mixed inhibition of butane on 1,1,1-TCA transformation.....	284
D4.1 Kinetic parameters (k_{\max} and K_s) for butane and inhibition coefficients for 1,1-DCE obtained from NLSR analysis by fitting mixed and noncompetitive inhibition models to data identified as competitive inhibition of 1,1-DCE on butane degradation.....	286
D5.1 Kinetic parameters (k_{\max} and K_s) for 1,1-DCA and inhibition coefficients for 1,1-DCE obtained from NLSR analysis by fitting mixed and noncompetitive inhibition models to data identified as competitive inhibition of 1,1-DCE on 1,1-DCA transformation.....	288
D6.1 Kinetic parameters (k_{\max} and K_s) for 1,1,1-TCA and inhibition coefficients for 1,1-DCE obtained from NLSR analysis by fitting mixed and noncompetitive inhibition models to data identified as competitive inhibition of 1,1-DCE on 1,1,1-TCA transformation.....	290
D7.1 Kinetic parameters (k_{\max} and K_s) for butane and inhibition coefficients for 1,1-DCA obtained from NLSR analysis by fitting mixed and noncompetitive inhibition models to data identified as competitive inhibition of 1,1-DCA on butane degradation.....	292
D8.1 Kinetic parameters (k_{\max} and K_s) for 1,1-DCE and inhibition coefficients for 1,1-DCA obtained from NLSR analysis by fitting mixed and noncompetitive inhibition models to data identified as competitive inhibition of 1,1-DCA on 1,1-DCE transformation.....	294
D9.1 Kinetic parameters (k_{\max} and K_s) for 1,1,1-TCA and inhibition coefficients for 1,1-DCA obtained from NLSR analysis by fitting mixed and noncompetitive inhibition models to data identified as competitive inhibition of 1,1-DCA on 1,1,1-TCA transformation.....	296

LIST OF APPENDIX TABLES (Continued)

<u>Table</u>	<u>Page</u>
D10.1 Kinetic parameters (k_{\max} and K_s) for butane and inhibition Coefficients for 1,1,1-TCA obtained from NLSR analysis by fitting mixed and noncompetitive inhibition models to data identified as competitive inhibition of 1,1,1-TCA on butane degradation.....	298
D11.1 Kinetic parameters (k_{\max} and K_s) for 1,1-DCE and inhibition coefficients for 1,1,1-TCA obtained from NLSR analysis by fitting mixed and noncompetitive inhibition models to data identified as competitive inhibition of 1,1,1-TCA on 1,1-DCE transformation.....	300
D12.1 Kinetic parameters (k_{\max} and K_s) for 1,1-DCA and inhibition coefficients for 1,1,1-TCA obtained from NLSR analysis by fitting mixed and noncompetitive inhibition models to data identified as competitive inhibition of 1,1,1-TCA on 1,1-DCA transformation.....	302
E1.1 Kinetic parameters (K_s) for the CAHs and inhibition coefficients for butane obtained from the linear plots using the linearized equation for competitive inhibition model and the data identified as mixed inhibition of butane on CAHs transformation.....	305
E2.1 Kinetic parameters (k_{\max} and K_s) for the substrates and inhibition coefficients (K_{ic} and K_{iu}) for the inhibitors obtained from two linear plots for mixed inhibition model and the data identified as competitive inhibition.....	310

Aerobic Cometabolism of Chlorinated Aliphatic Hydrocarbons by a Butane-Grown Mixed Culture: Transformation Abilities, Kinetics and Inhibition

CHAPTER 1

Introduction

In my master's thesis, batch microcosm studies were carried out to screen for microorganisms from the subsurface of Hanford DOE site that could cometabolically transform chloroform (CF) under aerobic conditions (Kim et al., 1997a). Butane was found to be an effective substrate for stimulating aerobic microorganisms that cometabolically transformed 1,1,1-trichloroethane (1,1,1-TCA) as well as CF. It was also observed that butane-utilizers transformed mixtures of chlorinated ethanes and chlorinated ethenes (Kim et al., 1997b). These results indicated that the butane-utilizers likely had a good potential for transforming a broad range of chlorinated aliphatic hydrocarbons (CAHs), including chlorinated methanes, ethanes, and ethenes. Thus, this extended study with the butane-oxidizers was undertaken.

Several studies reported that phenol- and toluene-utilizers more effectively transformed chlorinated ethenes than methanotrophs (Semprini, 1997; Hopkins et al., 1993), and that methanotrophs (but not phenol- and toluene-oxidizers) have ability to transform both chlorinated methanes and ethanes (Chang and Alvarez-Cohen, 1995b). Although methanotrophs have a wide cometabolic substrate range, effective transformation with methanotrophs is usually induced under copper limited nutrient conditions, so that soluble methane monooxygenase (sMMO) is expressed (Oldenhuis

et al., 1989). This may be a limitation of methanotrophs in remediating CAHs in groundwater, because copper will likely be naturally present in groundwater.

For this study, a butane-grown mixed culture was isolated from the Hanford microcosms and enriched in media. A survey of the ability of this culture to aerobically cometabolize a broad range of CAHs was performed, and compared to other cometabolic systems. For this purpose the following were measured: 1) the amount of the CAHs transformed per unit time and cell mass, 2) the loss of butane uptake ability after exposure to CAH used as a measure of cell inactivation due to the CAH transformation, and 3) the amount chloride released resulting from CAHs transformation as an indicator of the extent of dehalogenation achieved.

The results of this survey indicated that the culture had a good potential for treating 1,1,1-TCA, 1,1-dichloroethene (1,1-DCE), and 1,1-dichloroethane (1,1-DCA). Mixtures of these contaminants are often found in groundwater due to abiotic and biotic transformations of 1,1,1-TCA (Vogel and McCarty, 1987). 1,1,1-TCA and 1,1-DCE have been problematic CAHs to treat via aerobic cometabolism. 1,1-DCE has high transformation product toxicity, and rates of 1,1,1-TCA transformation have been slow in in-situ methanotrophic treatment and with phenol and toluene driven system (Hopkins and McCarty, 1995; Hopkins et al., 1993; Semprini and McCarty, 1991).

Inhibition and kinetic studies were carried out with these CAHs to study the transformation of the CAH mixtures. Inhibition between CAHs and growth substrates has been found to be an important factor in designing an effective bioremediation system (Anderson and McCarty, 1996). Two assumptions have been made in kinetic and inhibition studies. As presented in Table 2.4, most studies assumed competitive

inhibition applies. Another assumption is that the inhibition coefficient (K_i) is equal to the independently measured half-saturation coefficient (K_s) of the inhibitor (Alvarez-Cohen and McCarty, 1991c; Chang and Alvarez-Cohen, 1997; Speitel Jr. et al., 1993; Strand and Stensel, 1990). These two assumptions may be valid for some cases, however, for many systems different inhibition types likely apply. For example, in the case of competitive inhibition, K_s may not be equal to K_i (Chang and Criddle, 1997, Landa et al., 1994). Mixed inhibition has also been observed with CAH transformation with nitrifying bacteria (Keener and Arp, 1993) and propane-oxidizing bacteria (Keenan et al., 1994). Systematic inhibition studies are therefore needed for determining inhibition types and for estimating the inhibition coefficients. One of the goals of this study was to develop a systematic method for performing kinetic and inhibition studies for the aerobic cometabolism of CAHs.

OBJECTIVES

The main objectives of this study were to evaluate the potential of the butane-oxidizers for transforming CAHs and to determine inhibition type and coefficients using systematic methods. The specific objectives of this study were:

- 1) To evaluate how effectively a butane-grown enrichment culture could transform a broad range of chlorinated methanes, ethanes, and ethenes in single contaminant tests.
- 2) To evaluate cell inactivation due to the CAH transformation.

- 3) To evaluate the extent of dechlorination achieved.
- 4) To develop systematic methods for determining inhibition type and inhibition coefficients.
- 5) To apply the methods for determining kinetic parameters, inhibition types between compounds, and inhibition coefficients, focusing on butane, 1,1,1-TCA, 1,1-DCE, and 1,1-DCA.

REFERENCES

- Alvarez-Cohen, L. M. and P. L. McCarty. 1991c. Product toxicity and cometabolic competitive inhibition modeling of chloroform and trichloroethylene transformation by methanotrophic resting cells. *Appl. Environ. Microbiol.* 57: 1031-1037.
- Anderson, J. E. and P. L. McCarty. 1996. Effect of three chlorinated ethenes on growth rates for a methanotrophic mixed culture. *Environ. Sci. Technol.* 30: 3517-3524.
- Chang, H. L. and L. Alvarez-Cohen. 1995b. Transformation capacities of chlorinated organics by mixed cultures enriched on methane, propane, toluene or phenol. *Biotech. Bioeng.* 45: 440-449.
- Chang, H. L. and L. Alvarez-Cohen. 1997. Two-stage methanotrophic bioreactor for the treatment of chlorinated organic wastewater. *Wat. Res.* 31:2026-2036.
- Chang, W-K. and C. S. Criddle. 1997. Experimental evaluation of a model for cometabolism: prediction of simultaneous degradation of trichloroethylene and methane by a methanotrophic mixed culture. *Biotech. Bioeng.* 54: 491-501.
- Hopkins, G. D. and P. L. McCarty. 1995. Field observations of in situ aerobic cometabolism of trichloroethylene and three dichloroethylene isomers using phenol and toluene as primary substrates. *Environ. Sci. Technol.* 29: 1628-1637.
- Hopkins, G. D., L. Semprini, and P. L. McCarty. 1993. Microcosm and in situ field studies of enhanced biotransformation of trichloroethylene by phenol-utilizing microorganisms. *Appl. Environ. Microbiol.* 59: 2277-2285.

- Keenan, J. E., S. E. Strand, and H. D. Stensel. 1994. Degradation kinetics of chlorinated solvents by a propane-oxidizing enrichment culture. In: R.E Hinchee, A. Leeson, L. Semprini, and S. K. Ong (Eds.) *Bioremediation of Chlorinated and Polycyclic Aromatic Hydrocarbon Compounds* Lewis Publishers, Boca Raton, FL, pp.1-13.
- Keener, W. K. and D. J. Arp. 1993. Kinetic studies of ammonia monooxygenase inhibition in *Nitrosomonas europaea* by hydrocarbons and halogenated hydrocarbons in an optimized whole-cell assay. *Appl. Environ. Microbiol.* 59: 2501-2510.
- Kim, Y., L. Semprini, and D. J. Arp. 1997a. Aerobic cometabolism of chloroform and 1,1,1-trichloroethane by butane-grown microorganisms. *Bioremediation J.* 2: 135-148.
- Kim, Y., L. Semprini, and D. J. Arp. 1997b. Aerobic cometabolism of chloroform, 1,1,1-trichloroethane, and the other chlorinated aliphatic hydrocarbons by butane-utilizing microorganisms. In: *In situ and On-site Bioremediation*; Alleman, B. C.; Leeson, A., Eds.; Battelle Press, Columbus, OH, Vol. 3, pp. 107-112.
- Landa, A. S., E. M. Sipkema, J. Weijma, A. A. C. M. Beenackers, J. Dolfig, and D. B. Janssen. 1994. Cometabolic degradation of trichloroethylene by *Pseudomonas cepacia* G4 in a chemostat with toluene as the primary substrate. *Appl. Environ. Microbiol.* 60: 3368-3374.
- Oldenhuis, R., R. L. J. M. Vink, D. B. Janssen, and B. Witholt. 1989. Degradation of chlorinated aliphatic hydrocarbons by *Methylosinus trichosporium* OB3b expressing soluble methane monooxygenase. *Appl. Environ. Microbiol.* 55: 2819-2826.
- Semprini, L. 1997. Strategies for the aerobic co-metabolism of chlorinated solvents. *Curr. Opin. Biotechnol.* 8: 296-308.
- Semprini, L. and P. L. McCarty. 1991. Comparison between model simulations and field results for in-situ bioremediation of chlorinated aliphatics: Part I. biostimulation of methanotrophic bacteria. *Ground Water.* 29: 365-374.
- Speitel Jr., G. E., R. L. Thompson, and D. Weissman. 1993. Biodegradation kinetics of *Methylosinus trichosporium* OB3b at low concentrations of chloroform in the presence and absence of enzyme competition by methane. *Wat. Res.* 27: 15-24.
- Strand, S. E., M. D. Bjelland, and H. D. Stensel. 1990. Kinetics of chlorinated hydrocarbon degradation by suspended cultures of methane-oxidizing bacteria. *Research Journal of the Water Pollution Control Federation.* 62: 124-129.
- Vogel, T. L. and P. L. McCarty. 1987. Abiotic and biotic transformations of 1,1,1-trichloroethane under methanogenic conditions. *Environ. Sci. Technol.* 21: 1208-1213.

CHAPTER 2

Literature Review

CAHs have become widely distributed environmental contaminants as a result of discharge of industrial wastewaters, seepage from landfills, and leakage from underground storage tanks. Analysis of volatile organic compounds (VOCs) in water supplies from ground water sources showed that the five most frequently observed CAHs were trichloroethylene (TCE), 1,1,1-trichloroethane (1,1,1-TCA), tetrachloroethylene (PCE), cis-1, 2-dichloroethylene (c-DCE), trans-1, 2-dichloroethylene (t-DCE) and 1, 1-dichloroethane (1,1-DCA) (Westrick, 1984). Nearly half of the water supplies were contaminated with multiple CAHs. The US EPA registers most of the chlorinated C1 and C2 aliphatic hydrocarbons as major pollutants due to their adverse effects on human health. The specific toxicity of CAHs varies between compounds. Most notably, vinyl chloride is a carcinogen, and its maximum contaminant level goal (MCLG) is 0 $\mu\text{g/L}$. Basic research on the remediation of CAH-contaminated ground water is required because of wide spread contamination, toxicity, and the high cost associated with treatment. A fair amount of research on bioremediation has been performed. The technology involved in bioremediation is a promising one, because of its cost-effectiveness and its potential to affect the direct transformation of CAHs as opposed to the partitioning of CAHs to other phases.

AEROBIC MICROORGANISMS THAT GROW ON CAHS

A few CAHs have been shown to support aerobic microbial growth. Most hydrocarbons substituted with single chlorine can be used as sole carbon source by specific microbial cultures (Dolfing et al., 1993). Compounds with two or more chlorines are more recalcitrant. Several pure cultures, however, have been grown on 1,2-dichloroethane (1,2-DCA) (Janssen et al., 1985). Dichloroethenes, TCE, and trichloroethanes do not support aerobic microbial growth (Janssen et al., 1985).

Specific aerobic dechlorination mechanisms have been identified in the microorganisms grown on the 1,2-DCA as shown in Figure 2.1 (Janssen et al., 1985; van den Wijngaard et al., 1992). The enzyme involved has been classified as hydrolytic dehalogenase. It is capable of hydrolytically cleaving the carbon-chlorine bond in 1,2-DCA, and converting 1,2-DCA to chloroethanol. No oxygen is required for the transformation of 1,2-DCA, and H_2O is the sole co-substrate.

In a recent paper (Hage and Hartmans, 1999), it was shown that instead of a hydrolytic dechlorination of 1,2-DCA, *Pseudomonas* sp. Strain DCA grew on 1,2-DCA as sole carbon and energy source through an oxidation reaction by monooxygenase. As shown in Figure 2.1, 1,2-DCA monooxygenase was responsible for the first step of 1,2-DCA degradation. The requirement of both O_2 and NAD(P) H, the conversion of propene to 1,2-epoxypropane, and the inhibition of propene on 1,2-DCA degradation suggested the involvement of monooxygenase. Only the initial attack of the 1,2-DCA molecules seemed to be different from the hydrolytic dechlorination pathway. The isolation of a CAH-grown bacterial strain offers

promising opportunities for the efficient biological removal of this compound from groundwater.

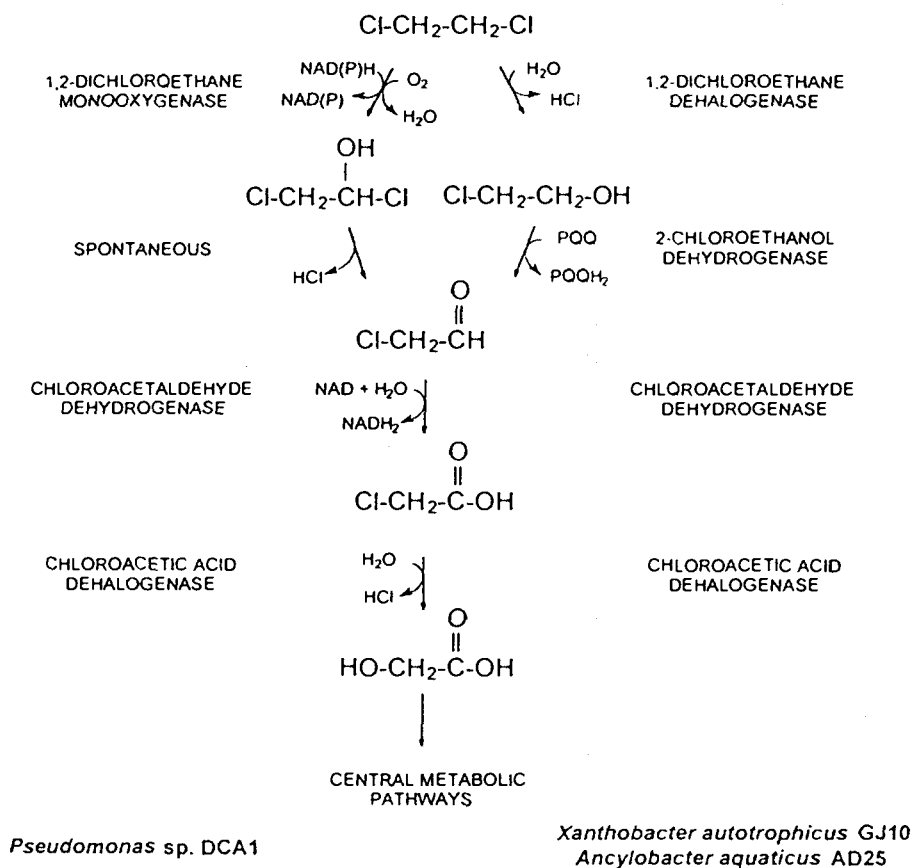


Figure 2.1. Different pathways of 1,2-DCA degradation by *Pseudomonas* sp. Strain DCA1 (proposed) (Hage and Hartmans, 1999), *Xanthobacter autotrophicus* GJ10 (Janssen et al. 1985) and *Ancylobacter aquaticus* AD25 (van den Wijngaard et al., 1992).

AEROBIC COMETABOLISM OF CAHs

When CAHs do not support microbial growth, aerobic cometabolism (the ability of microorganisms to transform non-growth-supporting substrates, typically in the presence of a growth supporting substrate) offers a biological method for CAH remediation from the contaminated environment. Since Wilson and Wilson (1985) reported TCE transformation by aerobic microorganisms exposed to natural gas, numerous laboratory and field investigation have been conducted regarding the aerobic cometabolism of CAHs by various oxygenase systems (Semprini, 1997).

The cometabolic CAHs transformation by oxygenase-expressing microorganisms is a complex process. The inhibition of enzyme by growth substrate or other CAHs, transformation product toxicity, and reducing energy regeneration such as NAD(P)H are important processes that affect cometabolic transformations.

Supply of Endogenous Reductant

The supply of endogenous reductant such as NAD(P)H, is one of the important factors that affect growth substrate degradation and CAH transformation. In this process methane-oxidizing and ammonia-oxidizing microorganisms insert one oxygen atom from an oxygen molecule into the growth substrate or CAH. The other oxygen atom is reduced concurrently to form H_2O , requiring the transfer of two electrons that must be provided from other reactions. In ammonia-oxidizing bacteria, these two electrons are provided from the subsequent oxidation of hydroxylamine to nitrite

(Keener and Arp, 1993). In methanotrophs, NAD(P)H provides the two electrons. The subsequent oxidation of methanol to formaldehyde, formaldehyde to formate, and/or formate to CO₂ provides NAD(P)H (Bedard and Knowles, 1989). If growth substrate degradation slows or stops, the reductant needed to support the degradation of the growth substrate or CAH or both may become depleted, although enzymes still remain active. To maintain the cell growth and drive CAH transformation, the reductant supply is critical.

Exogenous energy sources rather than endogenous sources have been studied to supply this energy. Formate was an effective external energy source for methanotrophs in the absence of the growth substrate, because its addition showed enhancement of CAH transformation rates and the transformation capacity (T_c : maximum mass of CAH that can be transformed per mass of cells prior to inactivation) (Alvarez-Cohen and McCarty, 1991b; Chang and Alvarez-Cohen, 1995a; Oldenhuis et al., 1989). Formate is catalyzed by formate dehydrogenase rather than monooxygenase. Thus, formate is not competing with CAH and growth substrate for active enzyme sites. This non-competing energy source in addition has a kinetic advantage.

Instead of an external energy source, the role of internal energy sources such as poly- β -hydroxybutyrate (PHB), in CAH transformation by methanotrophic mixed and pure cultures has been studied (Chu and Alvarez-Cohen, 1996; Henrysson and McCarty, 1993; Henry and Grbić-Galić, 1991; Shah et al., 1996). PHB accumulates in many microorganisms during unbalanced growth (Dawes and Senior, 1973; Shah et al., 1996). This accumulation can be advantageous to microorganisms (as proposed by

Dawes and Senior (1973)), since it can be used as an energy source. A positive correlation between PHB content and the TCE transformation rate and capacity was reported (Chu and Alvarez-Cohen, 1996; Henrysson and McCarty, 1993; Henry and Grbić-Galić, 1991; Shah et al., 1996).

Enzyme Inhibition

Since the same oxygenase enzyme initiates the oxidation of both the growth substrate and the CAHs, competition for the enzyme reduces the rates of growth substrate or CAH or both degradation. For example, several studies reported CAH inhibition on the cometabolism of another CAH or on the degradation of a primary substrate. Anderson and McCarty (1996) reported that TCE and t-DCE inhibition appeared to be an important factor in the reduction in growth rates of a methanotrophic mixed culture. In field studies, Hopkins and McCarty (1995) reported that 1,1-DCE strongly inhibited both transformation of TCE and degradation of phenol or toluene. 1,1-DCE also inhibited the transformation of VC in methane-utilizing soil columns (Dolan and McCarty, 1995).

Transformation Product Toxicity

Transformation product toxicity resulting from CAH transformation is an important process (Alvarez-Cohen and McCarty, 1991c; Oldenhuis et al., 1991;

Rasche et al., 1991). Studies of [^{14}C]TCE transformation by *Methylosinus trichosporium* OB3b expressing sMMO resulted in radiolabelling of various proteins including the component of sMMO. Oldenhuis et al. (1991) concluded that TCE-mediated inactivation of cells was caused by nonspecific covalent binding of transformation products to cellular proteins. The covalent radiolabelling of a number of cellular proteins was also observed when *Nitrosomonas europaea* cells were incubated with [^{14}C]TCE under conditions that allowed the turnover of ammonia monooxygenase (AMO) (Rasche et al., 1991). TCE-mediated inactivation was not observed in the presence of allylthiourea, a specific inhibitor of AMO, or under anaerobic conditions. Thus, the inactivation required AMO activity and resulted from TCE transformation products. It is generally thought that highly reactive transformation products inactivate the oxygenase enzyme or macromolecules by covalently binding to them and changing their structure.

Alvarez-Cohen and McCarty (1991a) introduced the T_c concept to quantify transformation product toxicity. The limiting of reductant supply or O_2 or both stops CAH transformation; thus T_c should be measured under the conditions where both are present in excess to separate limitation of reductant supply or O_2 (or both) from the toxicity. For example, in the case of methanotrophs, formate was used as exogenous energy source (Alvarez-Cohen and McCarty, 1991c; Dolan and McCarty, 1995). Some limitations for measuring T_c with different microorganisms, were reported, however, because a similar substrate like formate could not be identified for phenol-, propane-, and toluene-oxidizers (Chang and Alvarez-Cohen, 1995b).

The extent of cell inactivation resulting from transformation product toxicity was evaluated by different methods such as growth substrate uptake and growth substrate-dependent O_2 uptake (Alvarez-Cohen and McCarty; 1991c; Rasche et al., 1991). The growth substrate uptake assay has been widely used to evaluate toxicity effects on cells. This assay provides a good measure of the impacts on the cell of CAH transformation, because growth substrate degradation requires an active monooxygenase and an intact electron transport chain.

Figure 2.2 presents a log- log plot of methane uptake activity remaining versus T_c in the study with methanotrophs using data of Chang and Alvarez-Cohen (1996). I plotted the data in this form to show the capacity of methanotrophic resting cells to transform different CAHs. The compounds were divided into five classes, ranging from Class I (no transformation and minor inactivation) to Class V (major transformation and major inactivation). Cell incubations with many CAHs (except DCM, CA, 1,2-DCA and 1,1,1,2-TeCA) resulted in exhausted cell capacity due to transformation product toxicity. Thus, the amount transformed per unit cell mass of CA, 1,2-DCA and 1,1,1,2-TeCA may not represent T_c values, because fairly high cell activity was retained. In Chapter 3 of the thesis I generated a similar plot using my butane-utilizing culture.

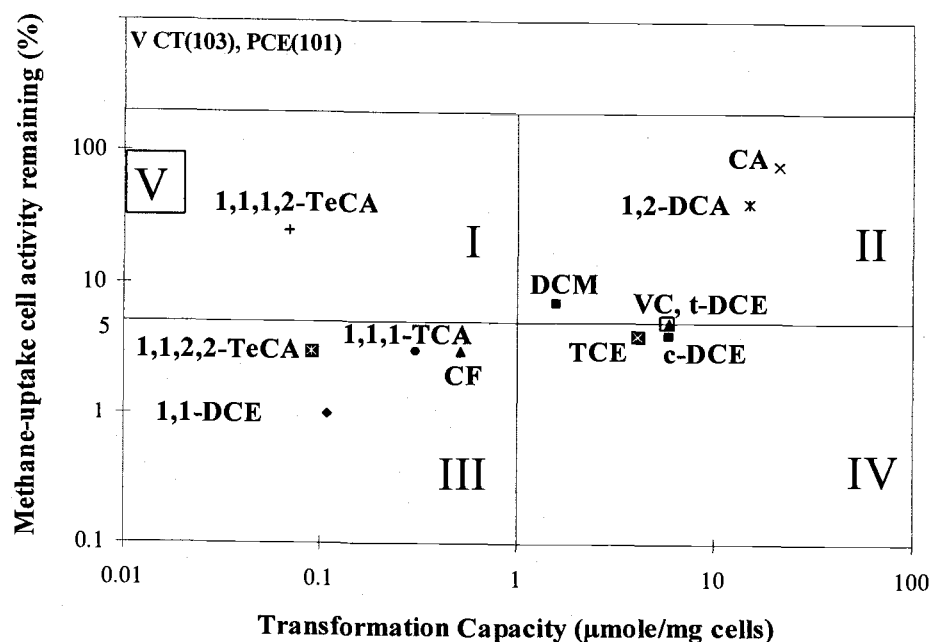


Figure 2.2. Transformation capacity versus methane uptake activity after 4 hours of exposure. Values in Class V box (no transformation) indicate percentage of methane uptake activity remaining after exposure to each compound.

ACETYLENE AS A MECHANISM-BASED INACTIVATOR OF OXYGENASE

Acetylene has been known to be an irreversible inactivator of particulate methane monooxygenase pMMO and sMMO from *Methylococcus capsulatus* (Bath) (Prior and Dalton, 1985), AMO from *N. europaea* (Keener et al., 1998), butane monooxygenase (BMO) from butane-grown *Pseudomonas butanovora*, *Mycobacterium vaccae* JOB5, and an environmental isolate, CF8 (Hamamura et al., 1999). This phenomenon has also been observed in studies with mixed cultures grown on methane (Alvarez-Cohen and McCarty, 1991c). Radiolabelled [^{14}C]acetylene was

used to define the active site protein of monooxygenase and to evaluate the monooxygenase inactivation mechanism. This assay was used to identify the diversity of BMO in three butane-grown strains (Hamamura et al., 1999). All three strains showed labeling of specific polypeptides in the presence of [^{14}C]acetylene. The [^{14}C]acetylene labeling patterns were different among the three bacteria, indicating the presence of three distinct types of butane monooxygenase in the three butane-grown bacteria. In Chapter 3 of the thesis acetylene was used to evaluate the involvement of a monooxygenase enzyme in my butane-grown mixed culture in CAHs transformation and butane-degradation.

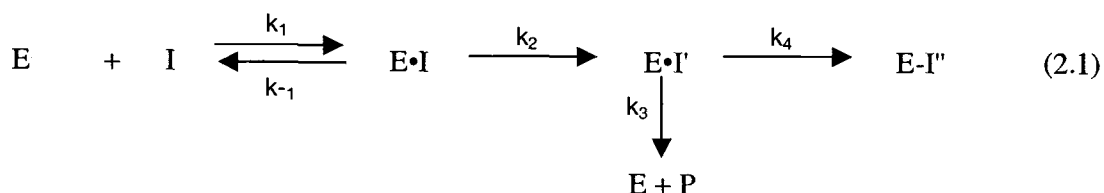
Mechanism-Based Inactivation

Acetylene is a mechanism-based inactivator (suicide substrate) of MMO (Prior and Doltan, 1985), AMO (Keener et al., 1998), and BMO (Hamamura et al., 1999). A mechanism-based enzyme inactivator is a relatively unreactive compound, having a structural similarity to the substrate for a particular enzyme. The enzyme converts the inactivator into a species through the normal degradation mechanism. Without prior release from the active site, an inactivator byproduct binds most often covalently to that enzyme (Silverman, 1988). The essential and unique feature of a mechanism-based enzyme inactivator is that the conversion to the activated form is at least initiated by the same catalytic steps involved in the reaction with normal substrates, and the products just happen to be more reactive than those produced from normal

substrates. An in-depth explanation of a mechanism-based inhibitor is presented in Appendix F.

Kinetics for Mechanism-Based Enzyme Inactivation

The characteristics of mechanism-based enzyme inactivation are believed to follow the equation 2.1 (Waley, 1980; 1985). The initial reversible binding of the inhibitor (I) to the enzyme (E) to form an enzyme inhibitor complex (E•I) is followed by a catalytic step (E•I \rightarrow E•I') which transforms the inhibitor to an activated species (I'). This reactive species can then either bind to the enzyme to produce a covalently modified inactive enzyme species (E-I'') or it can fully dissociate from the enzyme to produce a free product (P). According to equation 2.1, the ratio k_3/k_4 , the partition ratio, is important because it is a measure of the inactivator efficiency (Waley, 1980). The most efficient mechanism-based inactivators are those having partition ratios of 0, that is, every turnover produces inactivated enzyme. The partition ratio may depend on the reactivity of the activated intermediate, its diffusion rate from the active site, and the proximity of an appropriate nucleophile, radical, or electrophile on the enzyme for covalent bond formation (Silverman, 1988).



Waley (1980) applied the steady-state hypothesis to equation 2.1 and derived an equation 2.2 for the loss of enzyme activity as a function of time.

$$\frac{-d \ln a}{dt} = \frac{k_{inact} I_L}{K_I + I_L} \quad (2.2)$$

where, a = enzyme activity

I_L = aqueous inactivator concentration at a given time

k_{inact} = inactivator transformation rate into its activated form

K_I = the inactivator concentration at half the maximal inactivation rate

Assuming $K_I \gg I_L$ and $I_L \gg [E]$ (I_L = constant), analytical solution of equation 2.2 is equation 2.3.

$$\ln\left(\frac{a_t}{a_0}\right) = -\frac{k_{inact} I_L}{K_I} \cdot t \quad (2.3)$$

Assuming $K_I \ll I_L$, an analytical solution of equation 2.2 is given by equation 2.4.

$$\ln\left(\frac{a_t}{a_0}\right) = -k_{inact} \cdot t \quad (2.4)$$

Thus, under certain conditions, there is a linear relation between $\ln(a_t/a_0)$ and t , that is, pseudo first-order inactivation.

Biphasic kinetics (rather than pseudo first-order inactivation) as shown in Figure 2.3 can arise for several reasons (other reasons than experimental conditions).

When an inactivator generates a byproduct that binds much more tightly to the enzyme than does the inactivator, nonpseudo first-order kinetics, or biphasic kinetics, can be observed. This is because as inactivation progresses, a higher concentration of the product is formed, and this competes with the inactivator for the active site.

Biphasic kinetics can also arise for several different reasons, including that 1) two or more different inactivation processes are occurring simultaneously, 2) the inactivated enzyme is not stable and breakdown is rate determining, 3) there is negative cooperativity between two subunits in a multi-subunit enzyme (that is, attachment to one subunit renders an adjoining subunit less active), and 4) there is heterogeneity of subunit composition that results in nonequivalent binding to the subunits (Silverman, 1988). In Chapter 4 of the thesis an acetylene inactivation kinetic study was also performed to evaluate the kinetic diversity of butane-oxidizers in a butane-grown mixed culture studied here.

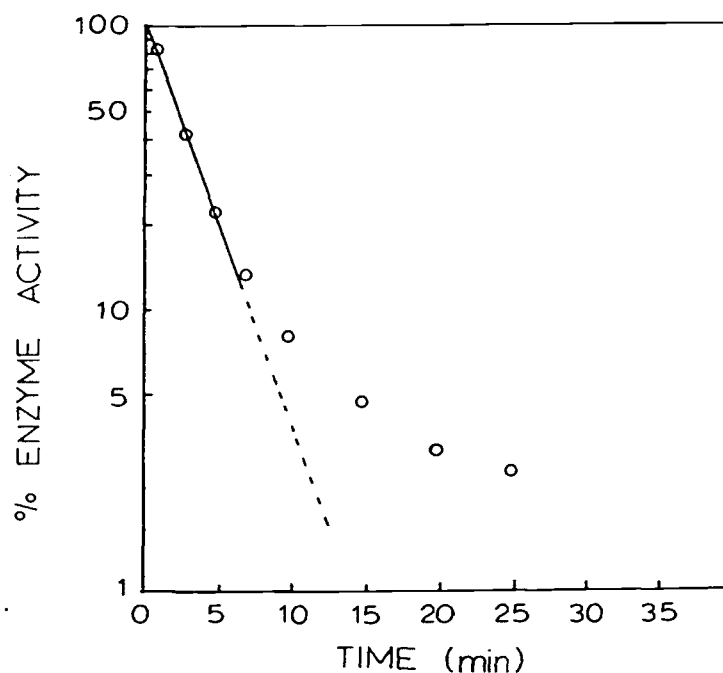


Figure 2.3. Nonpseudo first-order loss of enzyme activity (Silverman 1988).

SURVEY THE POTENTIAL OF AEROBIC MICROORGANISMS TO COMETABOLIZE CAHs

CAHs can be cometabolized by a wide range of oxygenase-expressing microorganisms, including those that grow on methane (Oldenhuis et al., 1989, 1991), propane (Kim, 1996; Tovanabootr and Semprini, 1998; Wackett et al., 1989), propene (Ensign et al., 1992), butane (Kim et al., 1997a; Hamamura et al., 1997), toluene (Nelson et al., 1986; Wackett et al., 1988), phenol (Folsom et al., 1990), and ammonia (Vannelli et al., 1990; Rasche et al., 1991). The range of CAHs that can be transformed by microbes grown on different substrates is of interest in determining the potential for bioremediation of these compounds. Surveys have been performed with

Methylosinus trichosporium OB3b (Oldenhuis et al. 1989), *Nitrosomonas europaea* (Rasche et al. 1991), and a methanotrophic mixed culture (Chang and Alvarez-Cohen 1996). Table 2.1 summarizes: 1) the amount of CAH transformed for certain period, 2) the T_c , 3) the cell inactivation caused by CAH transformations, 4) oxidative dechlorination measured by the amount of Cl^- released, and 5) byproducts detected. Table 2.1 is discussed in detail below.

Biotransformation

Chlorinated methanes, ethanes, and ethenes transformed by *Nitrosomonas europaea* (Rasche et al., 1991) and *Methylosinus trichosporium* OB3b (Oldenhuis et al., 1989) are presented to investigate the relative transformation potential among CAHs. *Nitrosomonas europaea* is an obligate chemolithotrophic nitrifying bacterium that derives its energy for growth exclusively from the oxidation of ammonia to nitrite. Nitrification is initiated by the action of AMO. *Nitrosomonas europaea* is capable of transforming all CAHs listed in Table 2.1 except fully chlorinated compounds such as CT and PCE.

When grown on methane, *Methylosinus trichosporium* OB3b is able to cometabolize CAHs. It is MMO that is the responsible catalyst. Two forms of MMO exist a soluble, sMMO, and a membrane bound form, pMMO. Their expression depends on growth conditions. sMMO is found only in Type II methanotrophs and is

Table 2.1 T_c values, cell activity remaining after exposure to each compound, the amount of chloride released and products detected by a methane-grown mixed culture (Chang and Alvarez-Cohen, 1996), *Methylosinus trichosporium* OB3b (Bartnicki and Castro, 1994; Oldenhuis et al., 1991; van Hylckama Vlieg et al., 1996), or *Nitrosomonas europaea* (Rasche et al., 1991)

^l Compound	^g Biodegradability (μ mol)			^h T_c (μ mol /mgTSS)	ⁱ Cell activity remaining (%)		^j Percentage of oxidative dechlorination (%)			Products detected	
	^a N	^b OB3b sMMO	^c OB3b pMMO		^a N	^d M	^a N	^b OB3b sMMO	^c OB3b pMMO	^a N	^{c,e,f} OB3b sMMO
CM	+	ND	ND	32	80	93	70	ND	ND	Formaldehyde CO	^e Halo-hydrin
DCM	+	11	9.5	1.6	60	7	125	105	75		
CF	+	12	11	0.52	1	3	73	100	77		
CT	-	< 2.5	< 2.5	~ 0	88	103	~ 0	~ 0	~ 0		
CA	+	^k ND	ND	21	97	79	110	ND	ND	Chloroethanol and acetaldehyde Acetic acid Chloro-acetaldehyde 2,2,2-trichloro-ethanol - Trichloro-acetaldehyde -	^e 2,2,2-trichloro-ethanol
1,1-DCA	+	13	< 1.3	ND	11	ND	105	100	10		
1,2-DCA	+	10	10	15	89	41	45	100	65		
1,1,1-TCA	+	11	< 1.8	0.31	53	3	~ 0	20	~ 0		
1,1,2-TCA	+	ND	ND	ND	8	-	67	ND	ND		
1,1,1,2-TeCA	ND	ND	ND	0.07	ND	25	ND	ND	ND		
1,1,2,2-TeCA	+	ND	ND	0.09	4	3	25	ND	ND		

Table 2.1 (Continued)

Compound	^g Biodegradability (μmol)			^h T _c (μmol /mgTSS)	ⁱ Cell activity remaining (%)		^j Percentage of oxidative dechlorination (%)			Products detected	
	^a N	^b OB3b sMMO	^c OB3b pMMO		^a N	^d M	^a N	^b OB3b sMMO	^c OB3b pMMO	^a N	^{c,e,f} OB3b sMMO
VC	+	ND	ND	5.8	30	5	40	ND	ND		^f VC epoxide
1,1-DCE	+	9.1	4.3	0.11	3	1	125	45	5		
c-DCE	+	12	6.7	5.9	4	4	50	105	50		^f c-DCE epoxide
t-DCE	+	15	15	5.9	50	5	~ 0	85	45		^f t-DCE epoxide
TCE	+	15	6.0	4.1	3	4	106	97	< 7		^f TCE epoxide
PCE	-	< 0.66	< 0.66	~ 0	88	101	~ 0	~ 0	~ 0		

a: N indicates *Nitrosomonas europaea* (Rasche et al., 1991). b: OB 3b sMMO indicates *M. Trichosporium* OB 3b grown without copper and with 20 mM formate (Oldenhuis et al., 1991). c: OB 3b pMMO indicates *M. Trichosporium* OB 3b grown with 4.8 μM copper and 20 mM formate (Oldenhuis et al., 1991). d: M indicates methanotrophs grown in the chemostat without copper. (Chang and Alvarez-Cohen, 1996). e: Results from the study by Bartnicki and Castro (1994). f: Results from the study by van Hylckama Vlieg et al. (1996). g: In study with *Nitrosomonas europaea*, biodegradability was presented + (indicating that compounds were transformed) and – (indicating that compounds were not transformed), while, in study with *M. Trichosporium* OB 3b, biodegradability was presented by the amount of CAH transformed for 24 hours with suspensions 0.3 to 0.4 mg of cells per ml and 0.2 mM of CAH. h: The T_c values of mixed chemostat-grown methanotrophs were measured in the presence of 20 mM of formate, exogenous energy source. i: For methanotrophs (M), cells were exposed to each compound 4 hours, and initial uptake rates of methane were measured. For *Nitrosomonas europaea*, cells were incubated for 1 hour with 5 mM (NH₄)₂SO₄ and the each compound. The rates of ammonia-dependent O₂ uptake were determined. j: The percentage of Cl⁻ released compared to that required for complete dechlorination of the amount of CAH transformed. k: ND indicates not determined. l: **Compound abbreviation.** CM (chloromethane), DCM (dichloromethane), CT (carbon tetrachloride), CA (chloroethane), 1,1,2-TCA (1,1,2-trichloroethane), 1,1,1,2-TeCA (1,1,1,2-tetrachloroethane), 1,1,1,2,2-TeCA (1,1,1,2,2-tetrachloroethane), and PCE (pentachloroethene)

expressed under conditions of Cu limitation. pMMO, in contrast, can be expressed in all methanotrophs, and is expressed under conditions of Cu sufficiency. As shown in Table 2.1, the amount of DCM and CF transformed by *Methylosinus trichosporium* OB3b expressing sMMO was comparable with that transformed by pMMO, while chlorinated ethanes and ethenes were more effectively transformed by those expressing sMMO than pMMO (Oldenhuis et al., 1991).

Transformation capacity (T_c) and cell inactivation

The T_c has been used to evaluate the capacity of resting cells to transform different CAHs. The T_c values for each CAH are inversely related to chlorine content within each aliphatic group (Figure 2.2 and Table 2.1). T_c for CF, 1,1-DCE, and 1,1,2,2-TeCA were the lowest among chlorinated methanes, ethanes, and ethenes, respectively, that is, transformation of those CAHs results in the greatest toxicity.

As shown in Table 2.1, Rasche et al. (1991) evaluated the degree of cell inactivation after exposure to a CAH for 1 hour by measuring the rates of ammonia-dependent O_2 uptake rather than measuring T_c . CT and PCE that were not transformed did not cause cell inactivation, suggesting that CT and PCE do not bind to AMO, or bind to AMO, but are not oxidized. Transformation of CM, CA, and 1,2-DCA caused minimal cell inactivation. The authors proposed that removing a single chlorine from a monochlorinated carbon produced the corresponding aldehydes (formaldehyde, acetaldehyde, and chloroaldehyde). These products were not toxic to

the cells during 1-hour exposures. Transformation of most CAHs containing a di- or trichlorinated carbon (DCM, CF, 1,1-DCA, and 1,1,1-TCA) resulted in substantial cell inactivation. The authors suggested that production of acyl chlorides from the compounds's transformation would account for the inactivation of AMO. Hydrolysis of chlorinated ethylene epoxides, the products of chlorinated ethylene oxidation by sMMO from *Methylosinus trichosporium* OB3b (van Hylckama Vlieg et al., 1996), may produce acyl chloride alkylating agents that would inactivate AMO. The authors also suggested that the production of alkylating agents from 1,1-DCA, 1,1,2-TCA, and 1,1,2,2-TeCA transformation may also provide the basis for AMO inactivation. The authors proposed that acyl chlorides could result from the hydroxylation of the dichlorinated carbon followed by the elimination of one of the chlorines.

Oxidative Dechlorination

Chloride released from CAH is an indicator of the extent of dehalogenation achieved. As show in Table 2.1, 1,1,1-TCA and 1,1-DCE were partially dechlorinated by *Methylosinus trichosporium* OB3b expressing sMMO, however, the other CAHs were completely dechlorinated. *Methylosinus trichosporium* OB3b expressing sMMO showed much greater dechlorination of CAH than that expressing pMMO.

In study with *Nitrosomonas europaea*, dechlorination of most CAHs was comparable with those by *Methylosinus trichosporium* OB3b expressing sMMO. Complete dechlorination of 1,1-DCE and no dechlorination of t-DCE and 1,1,1-TCA

by *Nitrosomonas europaea* were observed, while higher dechlorination of t-DCE and 1,1,1-TCA and lower 1,1-DCE dechlorination (45%) were observed by sMMO.

CAH Transformation Products Detected

During the degradation of TCE, c-DCE, t-DCE, and VC by *Methylosinus trichosporium* OB3b, the formation of the corresponding epoxides was observed (van Hylckama Vlieg et al., 1996), as indicated in Table 2.1. Cells expressing sMMO actively transformed the epoxides of c-DCE, but the epoxides of the other chlorinated ethenes were chemically degraded via first-order kinetics. The sMMO was involved in the c-DCE epoxide transformation.

Phenol- or toluene- oxidizers were not presented in Table 2.1, since butane-utilizers studied here are thought to have transformation characteristics more similar to ammonia-utilizers and methanotrophs. Phenol- and toluene-grown cultures have shown high potential for transforming chlorinated ethenes such as TCE. In a review paper by Semprini (1997), phenol- and toluene-utilizers appeared to be less effective in transforming chlorinated methanes and ethanes, but very effective in transforming chlorinated ethenes.

Aerobic cometabolism of chlorinated ethenes such as TCE, c-DCE, and VC by toluene- and phenol-oxidizers has been successfully demonstrated in the pilot and field studies (Hopkins et al., 1993; Hopkins and McCarty, 1995; McCarty et al., 1998). The results from these pilot and field studies showed that phenol-utilizers effectively

transformed TCE, c-DCE, and VC, and were less effective at transforming 1,1-DCE and t-DCE. Toluene-utilizers had very similar abilities as phenol-utilizers for all CAHs tested. However, both systems had showed no ability to transform of 1,1,1-TCA, a common contaminant in groundwater.

AEROBIC COMETABOLISM OF CAHs BY PROPANE- AND BUTANE-OXIDIZING MICROORGANISMS

Some butane- and propane-oxidizing microorganisms have the ability to transform CAHs (Hamamura et al., 1997; Kim et al, 1997a; Tovanabootr and Semprini, 1998; Wackett et al., 1989). There has been little study on propane- and butane-utilizing microorganisms compared with ammonia-, methane-, phenol- and toluene-utilizers.

Propane-Oxidizers

Aerobes using propane as carbon and energy source for growth also have an oxygenase of broad specificity. More attention has been given to CAH cometabolism by propane-oxidizers, since Wackett et al. (1989) found that *Mycobacterium vaccae* JOB5, grown on propane, had the ability to transform TCE, VC, 1,1-DCE, and c-DCE. It is of interest that the propane-oxidizing strains did not show identical properties. Four strains of the propane-oxidizing bacteria transformed 29 to 52 % of the TCE

present in incubation mixtures over 24 hours, while *M. vaccae* JOB5 transformed virtually all of the TCE in the reaction vials.

M. vaccae JOB5 has been studied in more detail to investigate its ability and potential to transform TCE and other CAHs. Vanderverg and Perry (1994) and Vanderverg et al. (1995) reported that *Mycobacterium vaccae* JOB5 has an inducible propane monooxygenase implicated in the transformation of TCE and 1-chlorobutane. Vanderverg and Perry (1994) reported that TCE was transformed with 53% dechlorination by *Mycobacterium vaccae* JOB5 when grown on propane. Intermediates in the transformation of TCE were 2,2,2-trichloroethanol and 2,2,2-trichloroacetaldehyde, and the amounts of the byproducts were 25% of TCE mass transformed. Transformation of TCE by *Methylosinus trichosporium* OB3b produced the same compounds as minor products (<10%) (Oldenhuis et al., 1989). Thus, the pattern of TCE transformation by propane oxygenase appears to be different compared with MMO.

Propane-grown microorganisms also showed the ability to transform chlorinated methanes and ethanes as well as chlorinated ethenes. In my soil microcosm studies (Kim and Semprini, Unpublished data), the ability of propane-utilizing microorganisms to transform chlorinated ethylenes (Figure 2.4.A) and chlorinated ethanes (Figure 2.4.B) was evaluated. Propane-utilizers transformed all chlorinated ethylenes except PCE, with c-DCE being most rapidly transformed followed by VC, TCE and t-DCE. Propane-utilizers also transformed all chlorinated ethanes tested, with 1,2-DCA being most rapidly transformed followed by 1,1-DCA,

1,1,2-TCA and 1,1,1-TCA. These results demonstrate the broad range of CAH transformation abilities of propane-utilizers.

The results are consistent with those of Tovanabootr and Semprini (1998) who found that propane-utilizing microorganisms enriched from the subsurface of McClellan AFB were able to transform mixtures of CF, 1,1,1-TCA, and TCE. Thus, microorganisms grown on propane appear to have a good potential to transform CAH mixtures. Although more studies of propane cometabolism are needed, propane-oxidizers appear to have a good potential for bioremediation of CAHs.

Butane-Oxidizers

A number of bacteria have been isolated that are capable of growth on butane. In one study, fifteen bacteria strains and four molds capable of growth on n-butane were isolated and partially classified (McLee et al. 1972). The bacteria were mostly *Arthrobacter* sp. and *Brevibacterium* sp.. All isolates were able to utilize ethane, propane, isobutane, n-hexadecane, sugar, and peptides. All of bacteria strains grew on all substrates tested except methane.

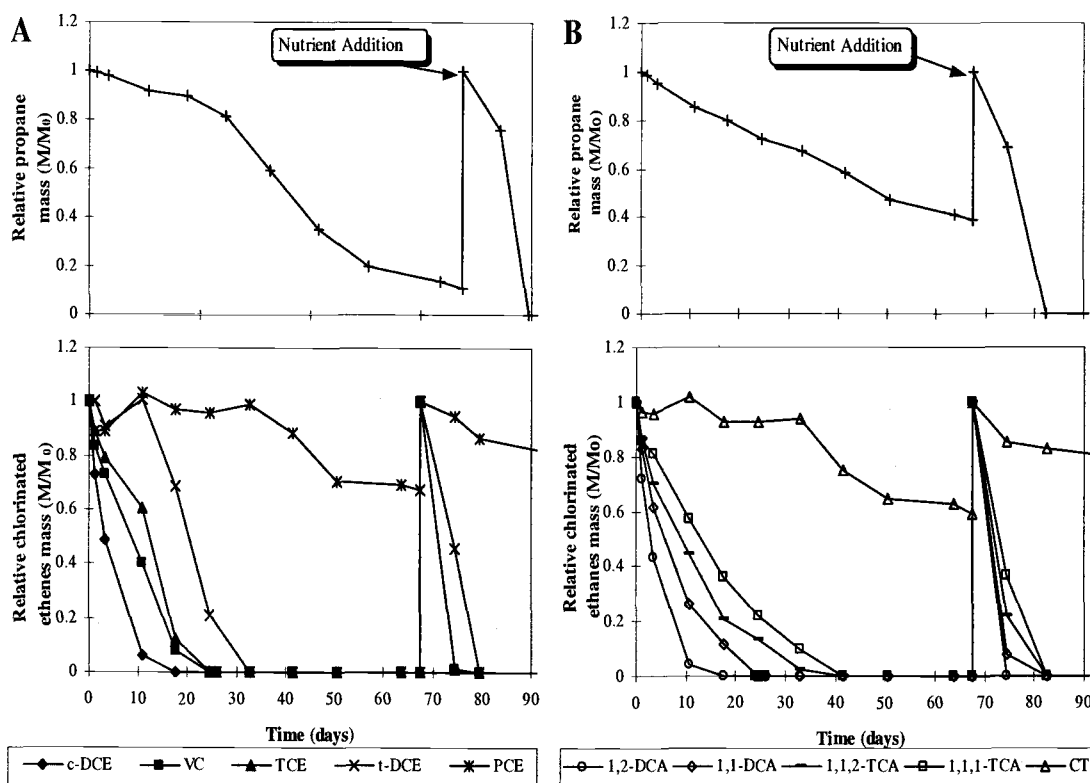


Figure 2.4. Propane degradation and transformation of mixtures of chlorinated ethylenes (A) and chlorinated ethanes (B) in propane microcosms. The total mass of propane was $0.09 \mu\text{mole}$ for each incubation, representing aqueous concentration of $51 \mu\text{M}$. Initial average aqueous concentrations of chlorinated ethanes and chlorinated ethylenes were 0.6 (Standard deviation [SD] ± 0.12) μM and 0.8 (SD ± 0.14) μM , respectively, representing total masses addition ranging from 0.03 to $0.09 \mu\text{mole}$ (Kim and Semprini, Unpublished data).

Nocardia TB1 was isolated with trans-2-butene as the carbon and energy source, and grew on several saturated straight-chain hydrocarbons, but not on 1-alkenes (Van Ginkel et al. 1987). Both trans-2-butene- and butane-grown cells of *Nocardia* TB1 oxidized a wide range of hydrocarbons including ethane, propane, cis-2-butene, 1,3-butadiene, ethene, propene, and 1-butene. The nature of the enzyme

involved in the attack on butane was investigated by measuring the disappearance of butane using cell-free extracts. Activity was observed only in the presence of NAD(P)H and molecular oxygen, indicating that a monooxygenase was probably responsible for the oxidation of butane. Based on these literature review on butane-utilizers, butane-utilizers have a non-specific monooxygenase that degrades saturated and unsaturated aliphatic hydrocarbons. Hamamura et al. (1999) reported the presence of butane monooxygenase (BMO) in butane-grown *Pseudomonas butanovora*, *Mycobacterium vaccae* JOB5, and CF8, isolated from a butane microcosms showing CF transformation of Kim et al. (1997a). The presence of BMO was indicated by: 1) the requirement of O₂ for butane degradation, 2) the production of 1-butanol during butane degradation, and 3) the inhibition of acetylene on both butane degradation and 1-butanol production. Thus, BMO in butane-grown bacteria was responsible for the initiation of butane degradation in the presence of NAD(P)H and O₂.

Phillips and Perry (1974) investigated the site on the butane molecule of initial oxidative attack by *Mycobacterium vaccae* JOB5. The fatty acid composition of hydrocarbon-utilizing microorganisms was used to determine the substrate oxidation pathway. *M. vaccae* JOB5 cells were grown on various substrates and analyzed for their fatty acid composition. *M. vaccae* JOB5, grown on propionate and 2-butanone (which would be the products of subterminal oxidation of n-butane) contained significant levels of fatty acids having an odd-carbon number chain length. Less than 1.0 % of the fatty acids in cells grown on n-butane, butyrate, β -hydroxybutyrate and acetate (which would be the products of terminal oxidation of n-butane) had odd-

carbon number chain lengths. These results suggested that 2-butanone could be metabolized to propionate yielding the precursor necessary for odd-carbon number fatty acid synthesis. The absence of significant amounts of odd-carbon number fatty acids in n-butane-grown cells suggested that n-butane was not oxidized through propionate. The similarity of the fatty acid composition in n-butane, butyrate, β -hydroxybutyrate, and acetate-grown cells implies that terminally oxygenated intermediates are involved in n-butane oxidation by *M. vaccae*. These results were consistent with those observed in the study with *Nocardia* TB1 (Van Ginkel et al. 1987). Van Ginkel and coworkers proposed a butane degradation pathway as shown in Figure 2.5. Arp (1999) also reported the terminal oxidation pathway of butane metabolism by butane-grown *Pseudomonas butanovora*.

Few studies have been performed on the butane-oxidizing microorganisms that are capable of cometabolizing CAHs. The potential for butane as an effective growth substrate for the aerobic cometabolism of CF and 1,1,1-TCA was first reported by Kim and co-researchers (1996; 1997a) using microcosms with groundwater and aquifer material from Hanford DOE in Washington. Butane was found to be an effective substrate for aerobic cometabolism of CF and 1,1,1-TCA (Kim et al., 1997a).

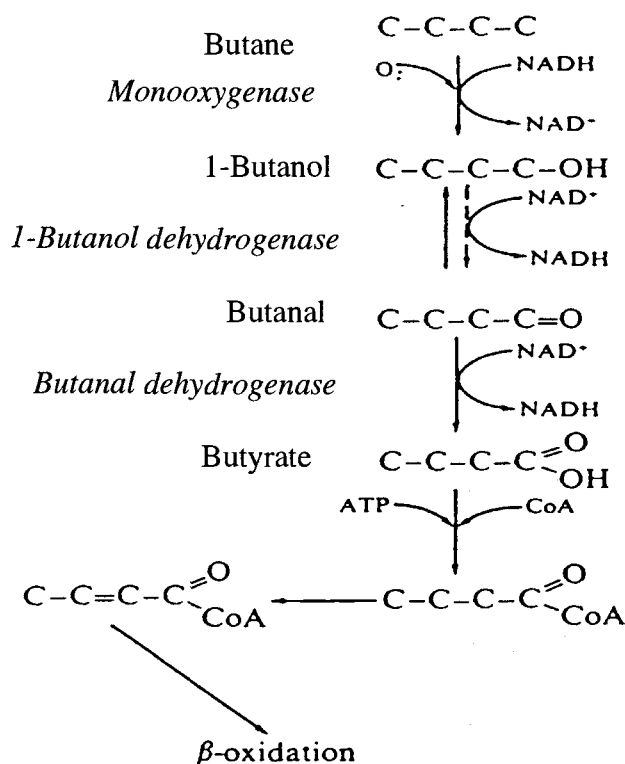


Figure 2.5. Proposed degradation pathway of butane in *Nocardia* TB1 (Van Ginkel et al. 1987)

The ability of butane-utilizers to transform mixtures of chlorinated ethylenes and chlorinated ethanes were also evaluated in microcosm studies (Kim et al., 1997b). The removal rate of VC, c-DCE, TCE, and t-DCE was different when these CAHs were spiked into one microcosm as a mixture with approximately 50 $\mu\text{g/L}$ of each compound. Complete and fast removal of VC and c-DCE was observed. Limited and slow transformation of TCE and trans-DCE was, however, also observed. The removal rate of 1,2-DCA, 1,1-DCA, 1,1,2-TCA, and 1,1,1-TCA was different. 1,2-

DCA was first transformed and followed by 1,1-DCA, 1,1,2-TCA, and 1,1,1-TCA, respectively. Complete removal of all CAHs was observed during a 7-day period.

The transformation of mixtures of 1,1-DCE and 1,1,1-TCA was also observed in butane-fed microcosms, as shown in Figure 2.6 (Kim and Semprini, Unpublished data). A 1,1-DCE / 1,1,1-TCA mixture was investigated, since the compounds are often observed as groundwater co-contaminants resulting from the abiotic transformation of 1,1,1-TCA to 1,1-DCE (Vogel and McCarty, 1987). After nutrient addition, complete removal of 1,1-DCE and 1,1,1-TCA was observed. 1,1-DCE appeared to be inhibitory to both butane degradation and 1,1,1-TCA transformation. Butane also appeared to inhibit 1,1,1-TCA transformation. These microcosm results indicate that butane-utilizers have potential for transforming 1,1-DCE and 1,1,1-TCA mixtures, and inhibition among compounds may play an important role in transforming these compounds. Thus detailed inhibition studies were performed and presented in Chapter 4 of this thesis.

Hamamura et al. (1997), with an enrichment culture, CF8, isolated from the Hanford microcosms of Kim et al. (1997a), found transformation of TCE, c-DCE, and VC when the culture was grown on butane. Butane monooxygenase was responsible for CF transformation. The authors also reported that *Pseudomonas butanovora* and *M. vaccae* JOB5 grown on butane transformed CF.

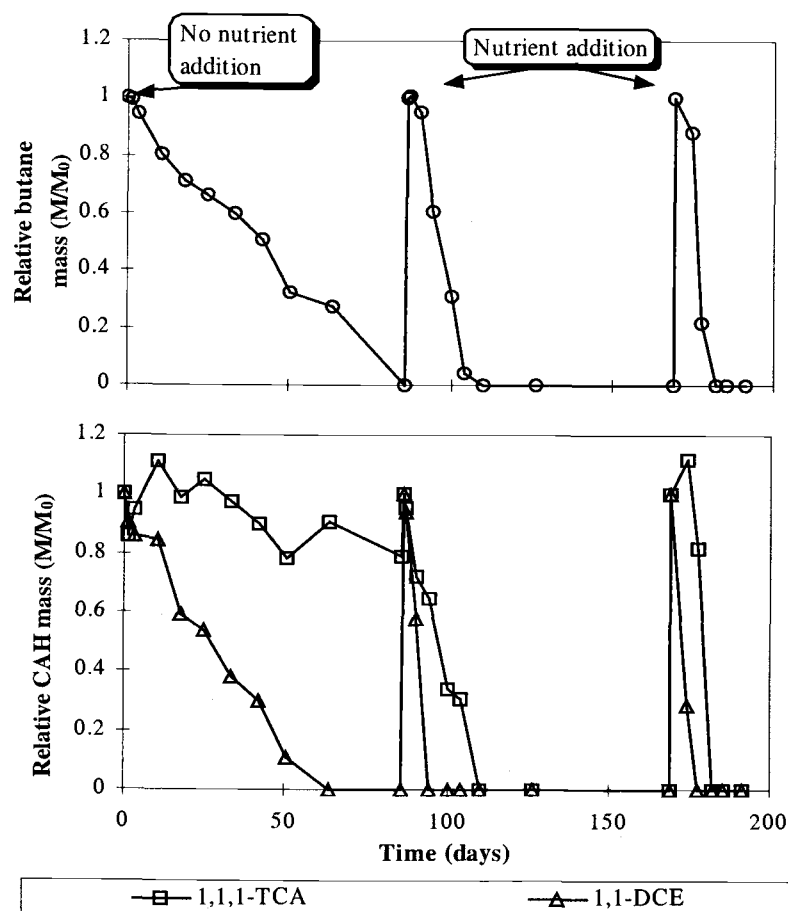


Figure 2.6. Butane degradation and transformation of mixtures of 1,1,1-TCA and 1,1-DCE before and after the addition of yeast extract (25 mg/L) in a butane microcosm (Kim and Semprini, Unpublished data)

KINETICS OF AEROBIC COMETABOLISM

The kinetics of growth substrate degradation and cometabolic CAH transformation have been described by several different models, ranging from simple first-order reaction models to complex multi-substrate mixed order models (Criddle, 1993; Schmidt et al., 1985). The most commonly applied approaches involve simplification and modification of the Michaelis-Menten/Monod expression:

$$v = \frac{-k_{\max}^{app} S_L}{K_s^{app} + S_L} \quad (2.5)$$

where v is the substrate degradation rate ($\mu\text{mol}/\text{mg TSS}/\text{hr}$), k_{\max}^{app} and K_s^{app} are the apparent values of the maximum degradation rate (k_{\max} in $\mu\text{mol}/\text{mg TSS}/\text{hr}$) and half-saturation coefficient (K_s in μM) in the presence of an inhibitor, respectively, and S_L is the aqueous substrate concentration (μM).

Estimation of Kinetic Parameters (k_{\max} and K_s)

Kinetic parameters such as k_{\max} and K_s have been estimated to characterize the interactions between substrate and enzyme. The kinetic values are determined by different methods as follows: 1) linearized forms of the Michaelis-Menten equation such as Lineweaver-Burk plot; 2) a direct linear plot (Eisenthal and Cornish-Bowden, 1974); 3) nonlinear least squares regression (NLSR) analysis fitting the differential form of Michaelis-Menten/Monod equation to the initial degradation rates measured; and 4) NLSR analysis fitting integrated forms of the Michaelis-Menten/Monod equation to substrate depletion data. These methods are discussed in detail below.

Linearized forms of Michaelis-Menten equation (Lineweaver Burk plot)

Linearized forms of the Michaelis-Menten equation such as Lineweaver-Burk, Hanes, and Eadie-Hofstee plots are commonly used for determining kinetic parameters. Deficiencies in these methods have been recognized for many years (Dowd and Riggs, 1965; Eisenthal and Cornish-Bowden, 1974; Robinson, 1985; Robinson and Charaklis, 1984). Most linearizations of nonlinear equations such as Michaelis-Menten equation involve data inversion, except direct linear plot (Eisenthal and Cornish-Bowden, 1974). Lineweaver-Burk plot has been most widely used, and the equation is derived by linearization:

$$\frac{1}{v} = \frac{1}{k_{\max}} + \frac{K_s}{k_{\max}} \frac{1}{S_L} \quad (2.6)$$

If $1/v$ is plotted against $1/S_L$, as shown Figure 2.7, a straight line is obtained with a slope of K_s/k_{\max} and a y intercept of $1/k_{\max}$. The inversion of v and S_L give the wrong impression about the experimental errors although it can be overcome by using a suitable weighting factor. For small values of v , small errors in v lead to enormous errors in $1/v$, but for large values of v , the same small errors in v lead to barely noticeable errors in $1/v$. This is visualized by the error bars shown in Figure 2.7, each of which is drawn for the same error range in v .

The inversion of v also results in the violation of a fundamental assumption of the unweighted least squares method. It is assumed that errors in dependent variables

are normally distributed. When v is inverted to fit to a linearized form, the inverted values ($1/v$) will not be normally distributed and their distributions will be unknown even though v are normally distributed (Robinson, 1985). Thus, unweighted linear regression on the plot of $1/v$ vs. $1/S_L$ is not theoretically recommendable.

Furthermore, linear regression yields estimates of combinations of the desired parameters such as $1/k_{\max}$ and K_s/k_{\max} , rather than the parameters themselves and their errors, as shown in Figure 2.7 (Robinson, 1985). This method does not provide a sound basis for calculating errors such as confidence intervals.

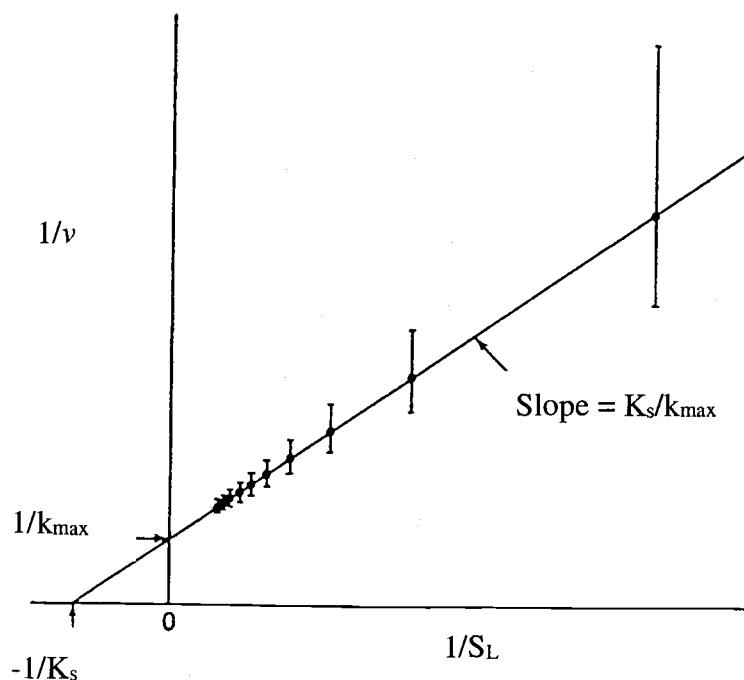


Figure 2.7. Lineweaver-Burk plot of $1/k_{\max}$ vs. $1/S_L$, with $\pm 0.05 v$ (Cornish-Bowden, 1994).

Direct linear Plot

Eisenthal and Cornish-Bowden (1974) described a different way of plotting the Michaelis-Menten equation, (known as direct linear plot) using equation 2.7.

$$k_{\max} = v + \frac{v}{S_L} K_s \quad (2.7)$$

If k_{\max} is plotted against K_s , a straight line is obtained with an x intercept of $-S_L$ and a y intercept of v (Figure 2.8). Values of v are plotted on the k_{\max} (vertical) axis and the corresponding negative S_L values are plotted on the K_s (horizontal) axis. The corresponding points are then joined and extrapolated. The intersection coordinates define the unique pair of k_{\max} and K_s values that satisfy both observations. The medians of each set of k_{\max} and K_s (rather than averages) are best estimates (closed circle). The median, unlike other types of averages, is less sensitive to extreme values that inevitably occur in the direct linear plot, because some of the lines are nearly parallel.

Cornish-Bowden and Eisenthal (1978) reported that some combinations of S_L and v can lead to the intersections in the second and third quadrants; that is, negative k_{\max} or K_s or both can be obtained. For example, when 1) both substrate concentrations ($K_s \ll S_{L1} < S_{L2}$) are large compared to K_s , 2) the corresponding rates of v_1 and v_2 are similar in magnitude to k_{\max} , and 3) v_1 is greater than v_2 , intersections in the second quadrant typically occur. The authors reported theoretical methods for treating negative values and finding medians (Cornish-Bowden and Eisenthal, 1978).

The negative values of k_{\max} are treated as if they are large and positive, and corresponding values of K_s are treated in the same way.

Although the other graphical methods using linear regression are better under ideal conditions, the direct linear plot has some advantages over those methods. The main advantage is that data inversion is not required. With linear regression methods, outliers can dramatically affect kinetic parameter estimates. However, the direct linear plot method is less sensitive to outliers, because the best estimate is the median rather than the mean.

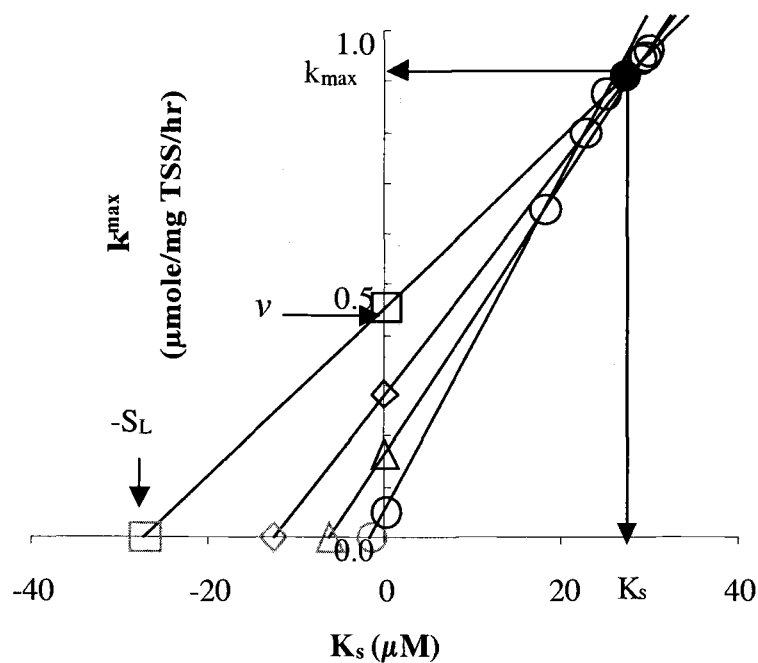


Figure 2.8. Direct linear plot of k_{\max} against K_s .

NLSR Analysis Using the Differential Form of Michaelis-Menten/Monod Equation

NLSR provides a tool for estimating the parameters of nonlinear models. Kinetic parameters can be determined by NLSR analysis fitting v measured at different substrate concentrations to the differential form of Michaelis-Menten equation (equation 2.5). NLSR analysis requires an initial guess for each unknown parameter as input. If the model has complicated multiparameters, the guesses may be very useful for converging the regression.

The advantages of this method are that: 1) it does not require linearization of the nonlinear equation; 2) it can be used for complicated multiparameter models; 3) the estimated parameter values are reliable; and 4) it provides a sound basis for calculating the errors such as the confidence interval of the parameters estimated.

NLSR Analysis using the Integrated Form of Michaelis-Menten/Monod Equation.

The NLSR analysis by fitting integrated form of the Michaelis-Menten/Monod equation to substrate depletion data was used to determine k_{\max} , K_s , initial substrate concentrations, and endogenous respiration rate (Robinson and Chracklis, 1984). This method was adapted to determine kinetic parameters for resting cell CAH transformation resulting in transformation product toxicity (Alvarez-Cohen and McCarty, 1991a; Smith et al., 1997). Alvarez-Cohen and McCarty (1991a) proposed a resting-cell cometabolic transformation model for CAHs exhibiting product toxicity.

The T_c of resting cells was used to incorporate the effects of product toxicity into a modified expression of Michaelis-Menten/Monod equation:

$$\frac{dS_L}{dt} = \frac{-k_{\max} X S_L}{(K_s + S_L)} \quad (2.8)$$

$$X = X_0 - \frac{1}{T_c} (S_{L,0} - S_L) \quad (2.9)$$

Substituting equation 2.9 into equation 2.8 and then integrating the equation derives equation 2.10.

$$t = \frac{1}{k_{\max}} \left[\left(\frac{K_s}{\frac{S_{L,0}}{T_c} - X_0} \right) \ln \left\{ \frac{S_L X_0}{\left[X_0 - \frac{(S_{L,0} - S_L)}{T_c} \right] S_{L,0}} \right\} + T_c \ln \left\{ \frac{X_0}{\left[X_0 - \frac{(S_{L,0} - S_L)}{T_c} \right]} \right\} \right] \quad (2.10)$$

Equation 2.10 relates the cometabolized contaminant concentration remaining at any time t to the initial contaminant and organism concentrations for a given T_c . Figure 2.9 presents an example showing how the parameters were determined by this method. TCE transformation in formate-amended batch bottles at seven initial TCE concentrations is plotted against time. From data fit with curve a in Figure 2.9, T_c was calculated, and k_{\max} and K_s were obtained by NLSR analysis fitting equation 2.10 to data (\square ; curve c). The other prediction lines were generated using the determined

kinetic parameters and measured T_c . As the authors reported, however, unique values of k_{\max} and K_s could not be obtained from the data due to high correlation between two parameters. Thus, it may not be possible to obtain unique parameter estimates, suggesting that for those experimental data the k_{\max}/K_s ratio may be a more useful kinetic parameter. Smith et al. (1998) also reported this limitation for evaluating the unique parameter estimates by this method.

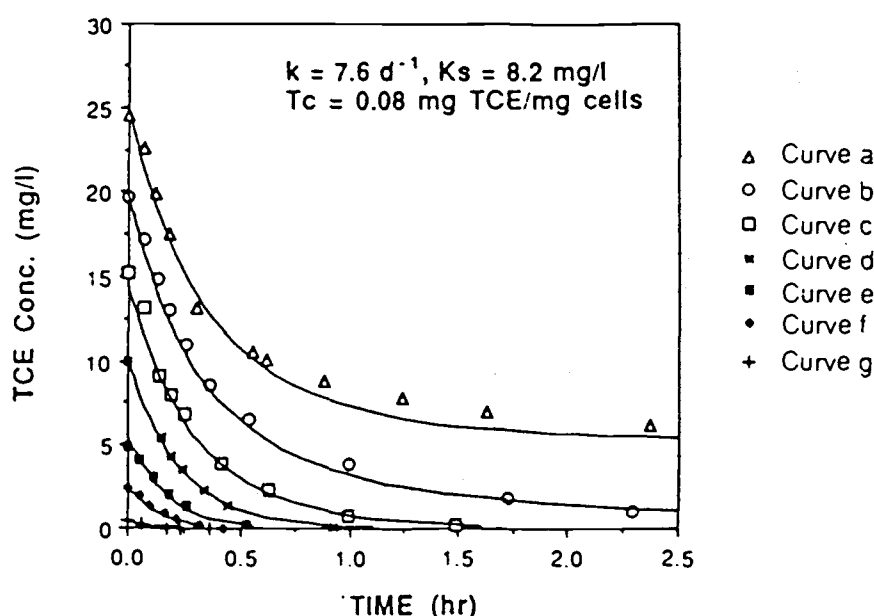


Figure 2.9. TCE disappearance in formate-amended batch bottles at seven initial TCE concentrations. Experiment data (symbols) are plotted along with predictions (lines) by use of the cometabolic transformation model and k (k_{\max}) and K_s determined from NLSR analysis of curve D (Alvarez-Cohen and McCarty, 1991a).

The advantage of this method is the economy of obtaining kinetic coefficients from a few batch experiments rather than using large numbers of initial rate

measurements. However, unique kinetic parameters can not be obtained in some cases. In more complicated cases involving effects such as endogenous cell decay and substrate losses by mechanisms other than bacterial reactions, the differential equation may not be integrated. If so, this method can not be directly applied to the model, but numerical methods can be employed.

Inhibition

A substance that reduces an enzyme's activity toward a substrate is called an inhibitor. The effects of the inhibitor on the enzyme activity depend on the mechanism of inhibitor binding to the enzyme. Four inhibition types are defined: competitive, uncompetitive, mixed and noncompetitive (Cornish-Bowden, 1994). Both mixed and noncompetitive inhibitions are sometimes called noncompetitive inhibition by other researchers (Keener and Arp, 1993; Keenan et al., 1994). A general model scheme for competitive, uncompetitive and mixed inhibition is presented in Figure 2.10.

The inhibition model is determined by the binding properties of the inhibitors (Cornish-Bowden, 1994). A competitive inhibitor (I_c) binds to E, and competes directly with a substrate for the same binding site of an enzyme. Thus, the degree of inhibition depends on the relative amounts of inhibitor and substrate present. At a fixed inhibitor concentration it is possible to drive all the inhibitor from the E converting it to ES by sufficient substrate addition. Thus, k_{max} will be unchanged by

the inhibitor. Because of the equilibrium between enzyme and inhibitor, K_s has to be displaced. More substrate will be necessary to reach k_{\max} , and therefore more substrate will be needed to reach half of the maximum rate in other words, K_s^{app} will be increased with increasing competitive inhibitor. With competitive inhibition, K_s^{app} increases with increasing I_L , while k_{\max}^{app} remains constant.

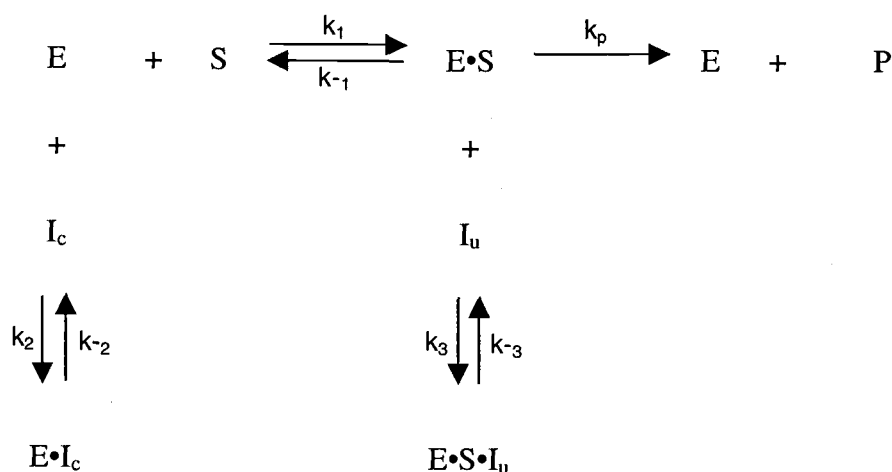


Figure 2.10. General model scheme for competitive, uncompetitive and mixed inhibition (Adapted from Cornish-Bowden, 1994).

An uncompetitive inhibitor (I_u) binds directly to the ES, but not to the E, indicating that the inhibitor and substrate binds at different sites on the enzyme. Thus, an uncompetitive inhibitor does not affect the binding of substrate to E. The I_u that binds to form ESI_u obviously decreases the amount of ES, and therefore k_{\max}^{app} decreases with increasing I_u . At a fixed I_u concentration it is impossible to drive all I_u from E converting it to ES by adding sufficient S. The reason is that more substrate

addition also generates more ESI_u . A lower amount of ES results in a decrease in the reaction rate of the ES to E and S, and therefore the K_s^{app} will also be decreased. Consequently, with uncompetitive inhibition, both k_{max}^{app} and K_s^{app} decrease with increasing I_L .

A mixed inhibitor or noncompetitive inhibitor binds to both the E and ES. Both types of inhibitions occur when there is a separate binding site for an inhibitor as well as the binding site for both substrate and inhibitor. Mixed inhibition is middle between competitive and uncompetitive inhibition. Thus, an inhibitor affects on both k_{max}^{app} and K_s^{app} .

Each inhibition model equation is derived based on the mechanisms presented in Figure 2.10, and the derivation is presented in Appendix B. Each inhibition equation can be presented by substituting both k_{max}^{app} and K_s^{app} (in Table 2.2) into equation 2.5. Table 2.2 also presents how k_{max}^{app} and K_s^{app} vary with increasing the level of I_L . Each inhibition shows different k_{max}^{app} or K_s^{app} or both with increasing the level of I_L : The level of competitive inhibitor concentrations does not affect k_{max} , while k_{max} approaches zero with

Table 2.2. The effects of inhibitors on the parameters of the Michaelis-Menten equation (Adapted from Cornish-Bowden, 1994).

Type of Inhibition	k_{\max}^{app}		K_s^{app}	
	$0 < I_L < \infty$	$I_L \rightarrow \infty$	$0 < I_L < \infty$	$I_L \rightarrow \infty$
Mixed	$\frac{k_{\max}}{(1 + \frac{I_L}{K_{iu}})}$	0	$\frac{K_s (1 + \frac{I_L}{K_{ic}})}{(1 + \frac{I_L}{K_{iu}})}$	$\frac{K_{iu} K_s}{K_{ic}}$
Noncompetitive	$\frac{k_{\max}}{(1 + \frac{I_L}{K_{iu}})}$	0	K_s	K_s
Competitive	k_{\max}	k_{\max}	$K_s (1 + \frac{I_L}{K_{ic}})$	∞
Uncompetitive	$\frac{k_{\max}}{(1 + \frac{I_L}{K_{iu}})}$	0	$\frac{K_s}{(1 + \frac{I_L}{K_{iu}})}$	0

Note: I_L is an inhibitor concentration in liquid phase, and K_{ic} and K_{iu} are inhibition coefficients representing the dissociation constants for binding of the inhibitor to the enzyme (E) and enzyme-substrate complex (ES), respectively.

increasing concentrations of other types inhibitors. The variation of K_s^{app} is different with different inhibition types. The variation patterns of both parameters with increasing I_L are evidence of the inhibition type as discussed above. Thus, the plot of k_{\max}^{app} vs. K_s^{app} (such as a direct linear plot) would be very useful in identifying the inhibition type, because it visualizes the parameter variation patterns (Cornish-Bowden, 1994).

Determination of Inhibition Types

The inhibition type and coefficients have been determined by various plots (Dixon and Webb, 1979). The Lineweaver-Burk plot has been widely used for distinguishing inhibition type and coefficients. The method provides visual confirmation of the inhibition type on a basis of the intersect position of linear regression lines (Figure 2.11).

With competitive inhibition, the lines intersect on the vertical axis, while with noncompetitive inhibition the lines intersect on the horizontal axis. With mixed inhibition the point of intersection is above or below the horizontal axis, and with uncompetitive inhibition the lines are parallel. The distinction between inhibition types is often difficult using this graphical analysis method. For example, the intersection point may be so close to the vertical axis that it is not easy to conclude whether the inhibition is mixed rather than competitive.

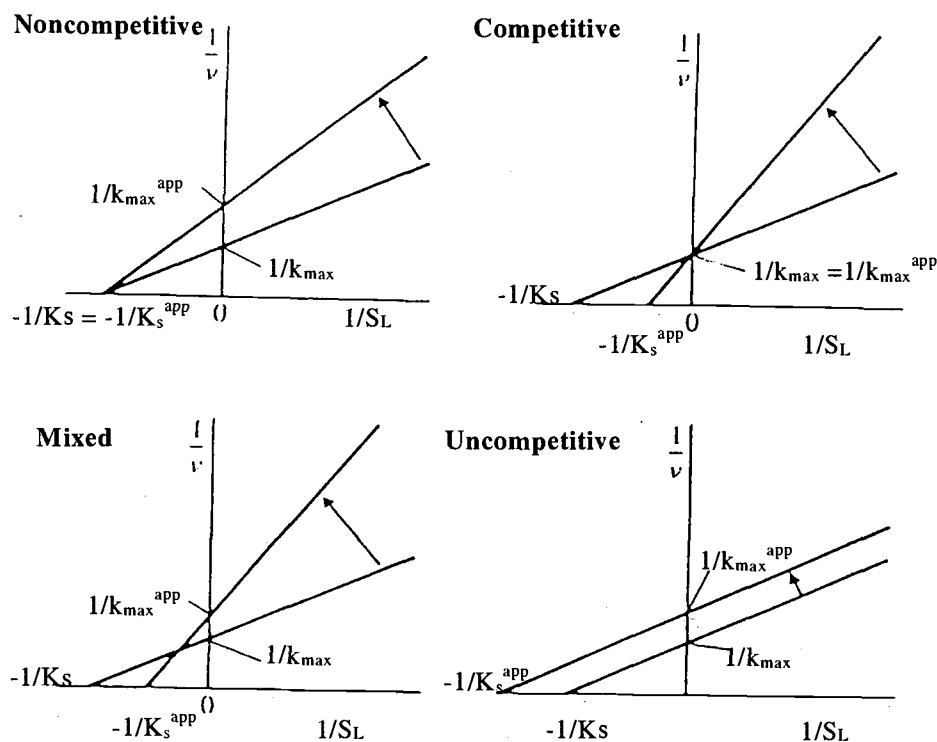


Figure 2.11. Lineweaver-Burk plots for different inhibitions (Adapted from Dixon and Webb, 1979).

Determination Inhibition Coefficients

A K_I can be obtained graphically from a Lineweaver-Burk plot made at a series of different inhibitor concentrations and secondary plot using slopes and intercepts obtained from Lineweaver-Burk plot. Expressions of the intercepts on both axes for various inhibition types are summarized in Table 2.3 (Dixon and Webb, 1979). The equations for y intercepts and/or slopes are linearized. If y intercepts and/or slopes are plotted against I_L , straight lines are obtained having x intercepts of negative K_I by

linear squares regression. The results of such plots for the each inhibition type are shown in Table 2.3.

Table 2.3. Intercepts and slopes of Lineweaver-Burk plot in the presence of inhibitor and graphical determination of inhibition coefficients (Adapted from Dixon and Webb, 1979).

Type of inhibition	Lineweaver-Burk plot			^a Slope and/or intercept vs. I_L	
	Y intercept	X intercept	Slope	Type of plot	X Intercept
Mixed	$\frac{K_s (1 + \frac{I_L}{K_{ic}})}{k_{max}}$	$\frac{-(1 + \frac{I_L}{K_{iu}})}{K_s (1 + \frac{I_L}{K_{ic}})}$	$\frac{(1 + \frac{I_L}{K_{iu}})}{k_{max}}$	Slope vs. I_L Y intercept vs. I_L	$-K_{iu}$ $-K_{ic}$
^b NonC	$\frac{K_s (1 + \frac{I_L}{K_{iu}})}{k_{max}}$	$\frac{-1}{K_s}$	$\frac{(1 + \frac{I_L}{K_{iu}})}{k_{max}}$	Y intercept vs. I_L	$-K_{iu}$
^c Comp	$\frac{K_s (1 + \frac{I_L}{K_{ic}})}{k_{max}}$	$\frac{-1}{K_s (1 + \frac{I_L}{K_{ic}})}$	$\frac{1}{k_{max}}$	Y intercept vs. I_L	$-K_{ic}$
^d UnC	$\frac{K_s}{k_{max}}$	$\frac{-(1 + \frac{I_L}{K_{iu}})}{K_s}$	$\frac{(1 + \frac{I_L}{K_{iu}})}{k_{max}}$	Slope vs. I_L	$-K_{iu}$

a: Slopes and intercepts of lines obtained from Lineweaver-Burk plot are plotted to obtain K_{ic} and K_{iu} .

b: NonC indicates noncompetitive inhibition. **c:** Comp indicates competitive inhibition. **d:** UnC indicates uncompetitive inhibition.

Figure 2.12 presents an example that shows the method for determining inhibition type and coefficients. The plot shows noncompetitive inhibition of C_2H_5Cl on NH_4^+ -dependent NO_2^- production in *N. europaea*, because the lines intersect on the

horizontal axis (Figure 2.11). From plot of y intercepts against I_L , K_{iu} (K_{iES}) was determined. K_{ic} (K_{iE}) was estimated from the plot of slope against I_L , and the value was equal to K_{iu} , indicating noncompetitive inhibition.

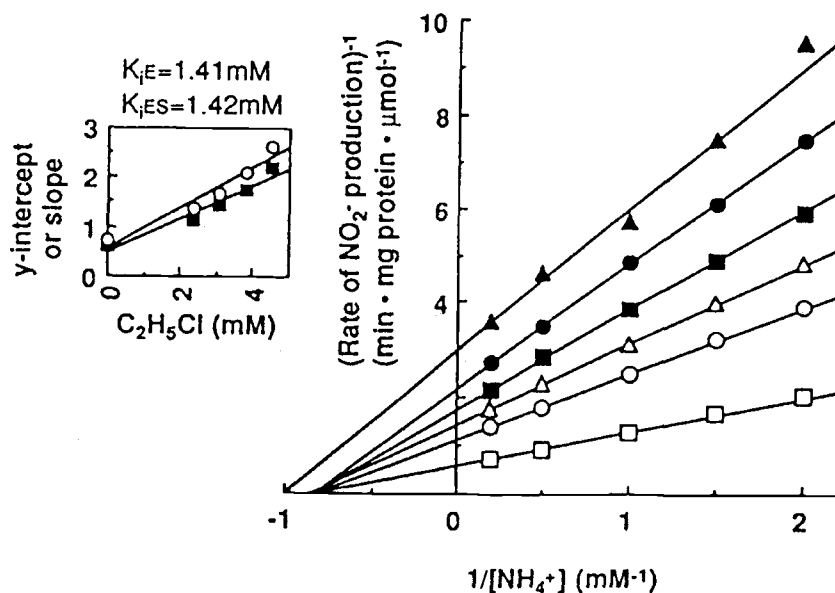


Figure 2.12. Lineweaver-Burk plot for various concentrations of C_2H_5Cl as an inhibitor of NH_4^+ -dependent NO_2^- production in *N. europaea*. Inset shows that y intercepts (■) and slopes (○) were replotted against the inhibitor concentrations to obtain K_{iE} (K_{ic}) and K_{iES} (K_{iu}), respectively (Keener and Arp, 1993).

Review Inhibition Studies in Aerobic CAH Cometabolism

Numerous inhibition studies have been performed due to the significance of inhibition in the aerobic CAH cometabolism process. To evaluate how the inhibition

type, K_s , and K_I have been determined in different studies, 18 kinetic studies are reviewed and summarized in Table 2.4. The table indicates the substrate, inhibitor, methods for determining inhibition type, K_s and K_I , and the values for K_s , K_I , and K_s/K_I .

Inhibition type

Two methods have frequently been used to diagnose the inhibition type: 1) linearized forms of Michaelis-Menten equation such as Lineweaver-Burk (Ref. 15 in Table 2.4) and Dixon (Ref. 14 in Table 2.4) plot; and 2) NLSR analysis that determines the best fitting inhibition model (Table 2.2) to initial rate data (Ref. 16 in Table 2.4). The second method for identifying inhibition types consists of fitting all inhibition types to the data using NLSR. The best model based on error analysis is then chosen. This method has been not been widely used, because it does not provide visual evidence for the inhibition pattern. However, this method is valuable for estimating parameter values if the inhibition type is known.

Competitive inhibition has been most widely used for the aerobic CAH cometabolism by pure and mixed cultures. In a few studies (Ref. 14 and 15 in Table 2.4) inhibition type was determined by a graphical method, but the predominant inhibition type was not competitive inhibition. However, many studies assumed

Table 2.4. Summary of methods for K_s , determination of inhibition types, and inhibition coefficients.

Culture (Ref.)	Substrate	Inhibitor	Inhibition type		Half-saturation and inhibition coefficients			
			Method	Type	Plot/Fitting method ^a	K_s of inhibitor (μM)	K_i of inhibitor (μM)	K_s/K_i of inhibitor (-)
Methanotrophic mixed culture (1)	1,1,1-TCA	methane	A ^a	C ⁱ	NLSR ^b	42	Assumed $K_i = K_s$	1
Methanotrophic mixed culture (2)	CF TCE	TCE	A	C	NLSR	11	Assumed $K_i = K_s$	1
		CF				11		
Methanotrophic mixed culture (4)	c-DCE	TCE	A	C	LB ^c	61 (TCE)	Assumed $K_i = K_s$	1
	TCE	c-DCE				81 (c-DCE)		
Methanotrophic mixed culture (5)	VC, c-DCE, or TCE	VC, c-DCE, or TCE	A	C	LB	56(VC), 31 (c-DCE), 47 (TCE)	Assumed $K_i = K_s$	1
Methanotrophic mixed culture (6)	Methane, 1,1-DCE, t-DCE, or TCE	Methane, 1,1-DCE, t-DCE, or TCE	A	C	NLSR	1.0 (methane), 4.5 (1,1-DCE), 1.8 (t-DCE), or 1.0 (TCE)	Assumed $K_i = K_s$	1
Methanotrophic mixed culture (7)	Methane	TCE or 1,1,1-TCA	A	C	NS ^d	NR ^h	TCE (91) 1,1,1-TCA (14)	NR
Methanotrophic mixed culture (8)	Methane or TCE	Methane or TCE	A	C	NS	NR	Assumed $K_i = K_s$	1
Methanotrophic mixed culture (9)	Methane or TCE	Methane or TCE	A	C	NLSR	428 (methane) 15 (TCE)	7.4 (methane) 82 (TCE)	58 (methane) 0.01 (TCE)
Methanotrophic mixed culture (10)	Methane or TCE	Methane or TCE	A	C	LB	67 (methane) 29 (TCE)	Assumed $K_i = K_s$	1

Table 2.4. (Continued)

Culture (Ref.)	Substrate	Inhibitor	Inhibition type		Half-saturation and inhibition coefficients			
			Method	Type	Plot/Fitting method ⁿ	K _s of inhibitor (μM)	K _I of inhibitor (μM)	K _s /K _I (-)
<i>M. trichosporium</i> OB3b (3)	CF	methane	A	C	NLSR and LSR ^e	19	Assumed	1
<i>M. trichosporium</i> OB3b PP358 (18)	TCE	Methanol	A	C	SOLVER ^f	NR	K _I = K _s 37500	NR
<i>Pseudomonas Cepacia</i> G4 (11)	Phenol	TCE	A	C	LB and DIXON ^g	3	3	1
<i>Pseudomonas Cepacia</i> G4 (13)	Toluene or TCE	Toluene or TCE	A	C	NR	25 (toluene) 6 (TCE)	5 (toluene) 30 (TCE)	5 (toluene) 0.2 (TCE)
Toluene-oxidizing Mixed culture (17)	Toluene	Toluene	A	C	NS	0.3 (Toluene) 1.3 (TCE)	0.3 (Toluene) 1.3 (TCE)	1
<i>Nitrosomonas europaea</i> (12)	Ammonia	TCE	A	C	SOLVER	10.7	10.7	1
<i>Nitrosomonas europaea</i> (14)	Ammonia	TCE	DIXON	C	DIXON	NR	30	NR
<i>Nitrosomonas europaea</i> (15)	Ammonia	Ethane Ethylene CM CA	LB	NC ^j C NC NC	LB	NR	220 (890) ^l 660 300 (1470) 1420 (1420)	NR
Propane-oxidizing Mixed culture (16)	1,1,1-TCA TCE	propane	NLSR	None ^k NC	NLSR	NR	10.6% ^m	NR

a: A indicates that inhibition type is assumed. b: NLSR indicates nonlinear least squares regression. c: LB indicates Lineweaver-Burk plot. d: NS indicates that numerical simulation that was used to minimize the errors between the observed and fitted values. e: LSR indicates linear least squares regression. f: Solver indicates that kinetic parameters were estimated by the solver optimization routine in Excel. g: DIXON indicates Dixon plot (Dixon and Webb, 1964). h: NR indicates not reported. i: C indicates competitive inhibition. j: NC indicates noncompetitive inhibition. k: None indicates that data did not fit to any of the inhibition models. l: Numbers in parenthesis are the dissociation constants for binding of the inhibitor to the enzyme-substrate complex (ES). m: inhibition coefficient (K_m) was presented as percentage of propane in headspace (vol/vol). n: In the studies that assumed K_I = K_s, the methods are for the determination of K_s.

Reference: 1. Strand et al. (1990); 2. Alvarez-Cohen and McCarty (1991c). 3. Speitel et al. (1993). 4. Chang and Alvarez-Cohen (1997). 5. Chang and Alvarez-Cohen (1996). 6. Anderson and McCarty (1996). 7. Broholm et al. (1990). 8. Broholm et al. (1992). 9. Chang and Criddle (1997). 10. Chang and Alvarez-Cohen (1995a). 11. Folsom et al. (1990). 12. Ely et al. (1995). 13. Landa et al. (1994). 14. Hyman et al. (1995). 15. Keener and Arp (1993). 16. Keenan et al. (1994). 17. Arcangeli and Arvin (1997). 18. Fitch et al. (1996).

competitive inhibition among CAHs or growth substrates or both, based on the hypothesis that growth substrate and CAH must bind to the same enzyme and compete for the same one active site of the enzyme. Although this assumption seems reasonable, several detailed studies show that other inhibition types may apply. In studies with *Nitrosomonas europaea*, the inhibition patterns were tested with respect to ammonia degradation using Lineweaver-Burk plots (Ref. 15 in Table 2.4). Although competitive inhibition was observed for ethylene, the predominant inhibition type was noncompetitive inhibition (ethane, CM, and CA) as shown in Table 2.4. These results suggest that there could be different inhibition types with different inhibitors, although the same enzyme is responsible for both the growth substrate and inhibitor oxidation. In the study with propane-oxidizers, Keenan and co-workers (Ref. 16 in Table 2.4) also reported that a noncompetitive inhibition model fit propane inhibition of TCE transformation.

Determination of inhibition coefficients

Three different methods have been adapted to estimate inhibition coefficients:

1) NLSR analysis using measured initial degradation rates and equation 2.5 (Ref. 9 and 16 in Table 2.4); 2) numerical simulation with trial and error fitting the data to inhibition models (Ref. 7 in Table 2.4); and 3) Lineweaver-Burk (Ref. 15 in Table 2.4) and Dixon plots (Ref. 11 and 14 in Table 2.4).

Most studies, especially with methanotrophs, assumed that the inhibition coefficient (K_I) was equal to the independently measured K_s of the inhibitor (Ref. 1, 2, 3, 4, 5, 6, 8, and 10 in Table 2.4). This assumption has been successfully used to model CAH transformation in the presence of growth substrate or other CAH. Several studies estimated K_I rather than assuming it, and deviation resulted (Ref. 9 and 13 in Table 2.4). Chang and Criddle (Ref. 9 in Table 2.4), using a mixed methanotrophic culture, found that the K_s of methane was about 60 times higher than K_{ic} for methane on TCE transformation. The K_s of TCE was a factor of 5 lower than K_{ic} for TCE on methane degradation. Similar inhibition results were reported for TCE transformation using *Pseudomonas cepacia* G4 grown on toluene (Ref. 13 in Table 2.4). The K_s of toluene was 5 times higher than K_{ic} of toluene inhibition on TCE transformation, while K_s of TCE was a factor of 5 lower than K_{ic} of TCE. Both studies showed that the assumption ($K_s = K_{ic}$) was not valid in their systems. The growth substrate was a stronger inhibitor than TCE, even though the K_s of the growth substrate was greater than that of CAH.

Two major assumptions exist in fitting inhibition models to the aerobic cometabolism of CAHs: 1) competitive inhibition is predominant; and 2) $K_s = K_I$. These two assumptions may be valid for some cases, however, for many systems, different inhibition types and inhibition constants likely apply. Systematic inhibition studies are needed for determining inhibition type and for estimating the inhibition coefficients.

METHOD USED IN THIS RESEARCH

In this research (Chapter 4) systematic kinetic and inhibition studies for aerobic CAH transformation are presented. The schematic diagram (Figure 2.13) describes the process used to determine the inhibition type and how kinetic parameters and inhibition coefficients were determined.

As discussed in the inhibition type section, the variation patterns of both k_{\max}^{app} and K_s^{app} (with increasing I_L) can provide evidence of the inhibition type. Direct linear plot prepared at various levels of I_L visualize the shifting directions of the best estimate point (k_{\max}^{app} , K_s^{app}) (Figure 2.14). Therefore, the inhibition pattern can be visually identified. (Cornish-Bowden, 1994). By definition, for competitive inhibition, the shift is to the right; for uncompetitive inhibition, it is directly towards to the origin; for mixed inhibition, it is intermediate between these extremes; and for special case of mixed inhibition, or noncompetitive inhibition, it shifts vertically down.

Initial guesses for kinetic parameters are needed to perform NLSR analysis. To obtain these values, equations for k_{\max}^{app} and K_s^{app} in Table 2.2 were linearized. The derivations are presented in Appendix B2, and the linearized equations are presented in Table 4.1. The k_{\max}^{app} and K_s^{app} values obtained from direct linear plot were used as inputs to plot the linearized equations. In the case of mixed inhibition, if $1/k_{\max}^{app}$ is

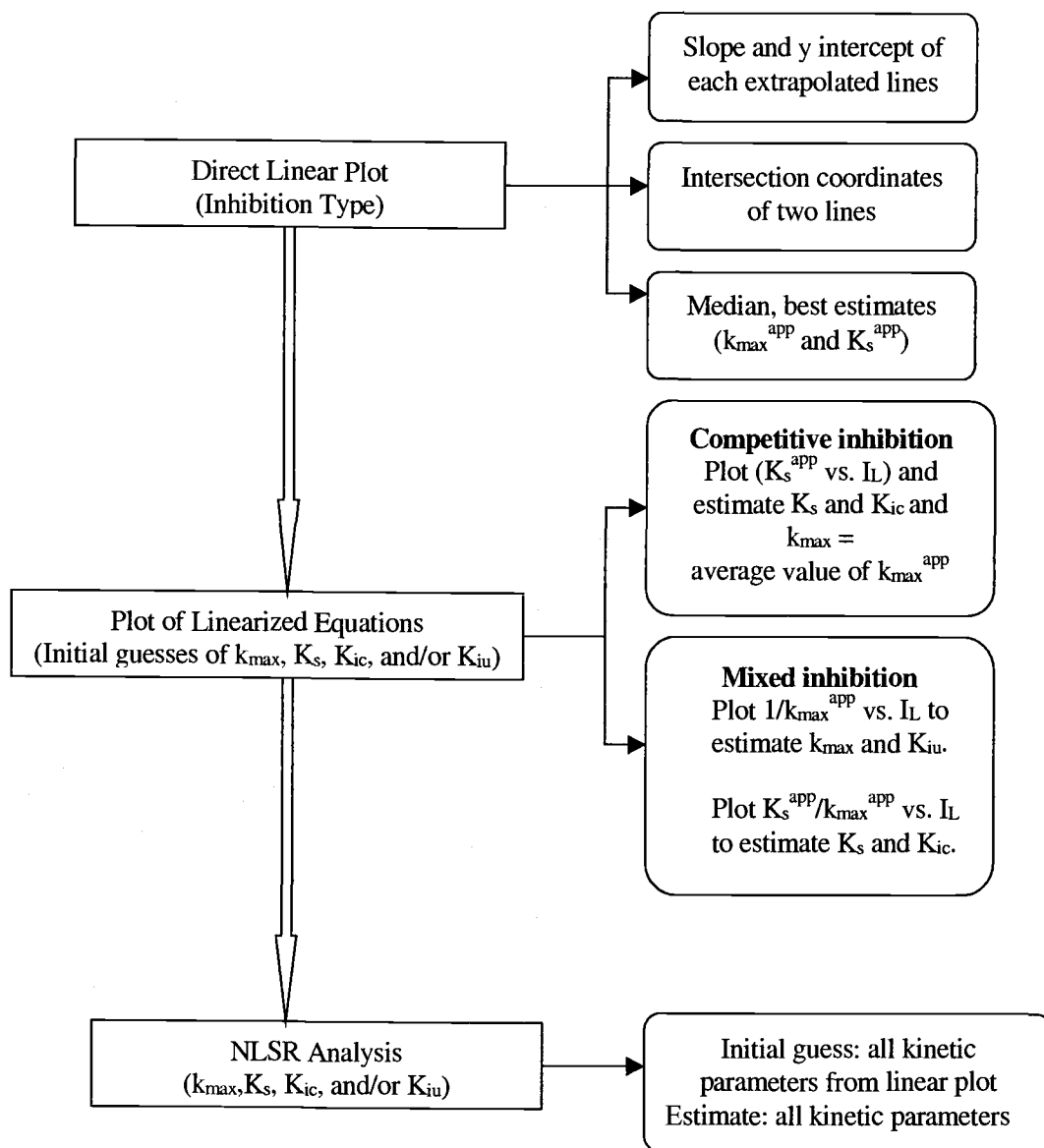


Figure 2.13. Schematic diagram for kinetic and inhibition studies.

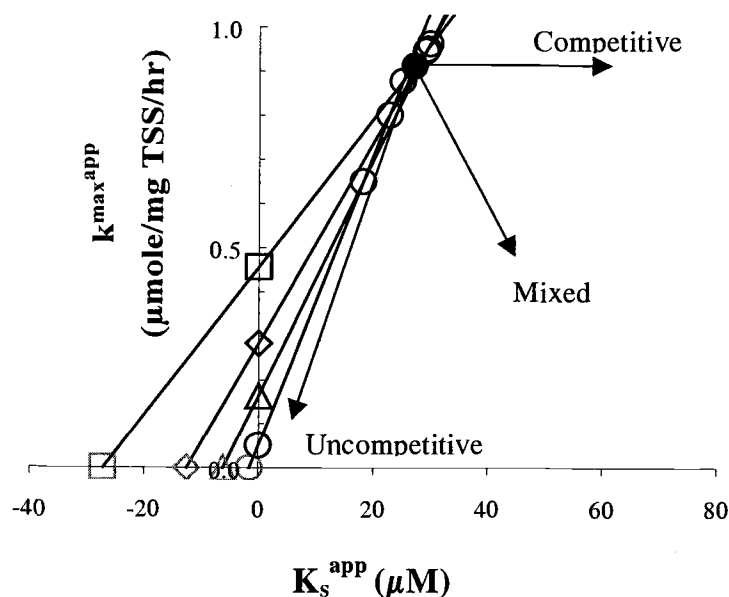


Figure 2.14. Direct linear plots showing the shifting directions of best estimate point $(k_{\max}^{\text{app}}, K_s^{\text{app}})$ at various levels of I_L providing visual evidence of inhibition type (Adapted from Cornish-Bowden, 1994).

plotted against I_L , a straight line is obtained. The slope and y intercept represents $1/(k_{\max}K_{iu})$ and $1/k_{\max}$, respectively. The values are obtained from linear squares regression. From these values, k_{\max} and K_{iu} were calculated. The values for K_s and K_{ic} were obtained from the second plot of $K_s^{\text{app}}/k_{\max}^{\text{app}}$ vs. I_L . Thus, all parameters were obtained from the two linearized plots. The same procedures can be applied to other inhibition cases to obtain kinetic parameters.

NLSR analysis using initial guesses from the linearized equations, the inhibition model determined from direct linear plot results in more accurate kinetic

parameters. The results and discussions for these systematic inhibition studies are presented in Chapter 4.

REFERENCES

- Alvarez-Cohen, L. M. , and P. L. McCarty. 1991a. A cometabolic biotransformation model for halogenated aliphatic compounds exhibiting product toxicity. *Environ. Sci. Technol.* 25: 1381-1387.
- Alvarez-Cohen, L. M. , and P. L. McCarty. 1991b. Effects of toxicity, aeration and reductant supply on trichloroethylene transformation by a mixed methanotrophic culture. *Appl. Environ. Microbiol.* 57:228-235.
- Alvarez-Cohen, L. M. and P. L. McCarty. 1991c. Product toxicity and cometabolic competitive inhibition modeling of chloroform and trichloroethylene transformation by methanotrophic resting cells. *Appl. Environ. Microbiol.* 57: 1031-1037.
- Anderson, J. E. and P. L. McCarty. 1996. Effect of three chlorinated ethenes on growth rates for a methanotrophic mixed culture. *Environ. Sci. Technol.* 30: 3517-3524.
- Arcangeli, J.-P. and E. Arvin. 1997. Modeling of the cometabolic biodegradation of trichloroethylene by toluene-oxidizing bacteria in a biofilm system. *Environ. Sci. Technol.* 31: 3044-3052.
- Arp, D. J. 1999. Butane metabolism by butane-grown '*pseudomonas butanovora*'. *Microbiology.* 145:1173-1180.
- Bartnicki, E. W. and C. E. Castro. 1994. Biodehalogenation: Rapid oxidative metabolism of mono- and polyhalomethanes by *Methylosinus trichosporium* OB-3b. *Environ. Toxicology and Chemistry.* 13: 241-245.
- Bedard, C. and R. Knowles. 1989. Physiology, biochemistry, and specific inhibitors of CH_4 , NH_4^+ and CO oxidation by methanotrophs and nitrifiers. *Microbio. Rev.* 53: 68-84.
- Broholm, K., T. H. Christensen, and B. K. Jensen. 1992. Modeling TCE degradation by a mixed culture of methane-oxidizing bacteria. *Water Res.* 9: 1177-1185.

- Broholm, K., K. Jensen, T. H. Christensen, and L. Olsen. 1990. Toxicity of 1,1,1-trichloroethane and trichloroethene on a mixed culture of methane-oxidizing bacteria. *Appl. Environ. Microbiol.* 56: 2488-2493.
- Chang, H. L. and L. Alvarez-Cohen. 1995a. Model for the cometabolic biodegradation of chlorinated organics. *Environ. Sci. Technol.* 29: 2357-2367.
- Chang, H. L. and L. Alvarez-Cohen. 1995b. Transformation capacities of chlorinated organics by mixed cultures enriched on methane, propane, toluene or phenol. *Biotech. Bioeng.* 45: 440-449.
- Chang, H. L. and L. Alvarez-Cohen. 1996. Biodegradation of individual and multiple chlorinated aliphatic hydrocarbons by methane-oxidizing cultures. *Appl. Environ. Microbiol.* 62: 3371-3377.
- Chang, H. L. and L. Alvarez-Cohen. 1997. Two-stage methanotrophic bioreactor for the treatment of chlorinated organic wastewater. *Wat. Res.* 31:2026-2036.
- Chang, W-K. and C. S. Criddle. 1997. Experimental evaluation of a model for cometabolism: prediction of simultaneous degradation of trichloroethylene and methane by a methanotrophic mixed culture. *Biotech. Bioeng.* 54: 491-501.
- Chu, K-H and L. Alvarez-Cohen. 1996. Trichloroethylene degradation by methane-oxidizing cultures grown with various nitrogen sources. *Water Environ. Res.* 68: 76-82.
- Cornish-Bowden, A. 1994. *Fundamentals of enzyme kinetics*. Protland press Ltd. London, UK.
- Cornish-Bowden, A and R. Eisenthal. 1978. Estimation of Michaelis constant and maximum velocity from the direct linear plot. *Biochim. Biophys. Acta.* 523: 268-272.
- Criddle, C. S. 1993. The kinetics of cometabolism. *Biotechnol. Bioeng.* 41:1048-1056.
- Dawes, E. A. and P. J. Senior. 1973. The role and regulation of energy reserve polymers in micro-organisms. *Adv. Microb. Physiol.* 10: 135-266.
- Dixon, M. and E. C. Webb. 1979. *Enzymes*. Academic Press. New York.
- Dolan, M. E. and P. L. McCarty. 1995. Methanotrophic chloroethene transformation capacities and 1,1-dichloroethene transformation product toxicity. *Environ. Sci. Technol.* 29: 2741-2747.
- Dolfing, J., A. J. van den Wijngaard, and D. B. Janssen. 1993. Microbiological aspects of the removal of chlorinated hydrocarbons from air. *Biodegradation.* 4: 261-281.

- Dowd, J. E. and D. S. Riggs. 1965. A comparison of estimates of Michaelis-Menten kinetic constants from various linear transformations. *J. Biol. Chem.* 240:863-869.
- Eisenthal, R. and A. Cornish-Bowden. 1974. The direct linear plot: a new graphical procedure for estimating enzyme kinetic parameters. *Biochem. J.* 139:715-720.
- Ely, R. L., M. R. Hyman, D. J. Arp, R. G. Guenther, and K. J. Williamson. 1995. A cometabolic biodegradation model incorporating enzyme inhibition, inactivation, and recovery. II: trichloroethylene degradation experiments. *Biotechnol. Bioeng.* 46: 232-245.
- Ensign, S. A., M. R. Hyman, and D. J. Arp. 1992. Cometabolic degradation of chlorinated alkenes by alkene monooxygenase in a propylene-grown *Xanobacter* strain. *Appl. Environ. Microbiol.* 58: 3038-3046.
- Fitch, M. W., G. E. Speitel Jr., and G. Georgiou. 1996. Degradation of trichloroethylene by methanol-grown cultures of *Methylosinus trichosporium* OB3b PP358. *Appl. Environ. Microbiol.* 62: 1124-1128.
- Folsom, B. R., P. J. Chapman, P. H. Pritchard. 1990. Phenol and trichloroethylene degradation by *Pseudomonas cepacia* G4: Kinetics and Interactions between Substrates. *Appl. Environ. Microbiol.* 56: 1279-1285.
- Hage, J. C. and S. Hartmans. 1999. Monooxygenase-mediated 1,2-dichloroethane degradation by *pseudomonas* sp. Strain DCA1. *Appl. Environ. Microbiol.* 65:2466-2470.
- Hamamura, N., C. Page., T. Long, L. Semprini, and D. J. Arp. 1997. Chloroform cometabolism by butane-grown CF8, *Pseudomonas butanovora*, and *Mycobacterium vaccae* JOB5 and methane-grown *Methylosinus trichosporium* OB3b. *Appl. Environ. Microbiol.* 63: 3607-3613.
- Hamamura, N., R. T. Storfa, L. Semprini, D. J. Arp. 1999. Diversity in butane monooxygenase among butane-grown bacteria. *Appl. Environ. Microbiol.* 65: 4586-4593.
- Henry, S. M. and D. Grbić-Galić. 1991. Influence of endogenous and exogenous electron donors and trichloroethylene oxidation toxicity on trichloroethylene oxidation by methanotrophic cultures from a groundwater aquifer. *Appl. Environ. Microbiol.* 57: 236-244.
- Henrysson, T. and P. L. McCarty. 1993. Influence of the endogenous storage lipid poly- β -hydroxybutyrate on the reducing power availability during cometabolism of trichloroethylene and naphthalene by resting methanotrophic mixed cultures. *Appl. Environ. Microbiol.* 59: 1602-1606.

- Hopkins, G. D. and P. L. McCarty. 1995. Field observations of in situ aerobic cometabolism of trichloroethylene and three dichloroethylene isomers using phenol and toluene as primary substrates. *Environ. Sci. Technol.* 29: 1628-1637.
- Hopkins, G. D., L. Semprini, and P. L. McCarty. 1993. Microcosm and in situ field studies of enhanced biotransformation of trichloroethylene by phenol-utilizing microorganisms. *Appl. Environ. Microbiol.* 59: 2277-2285.
- Hyman, M. R., S. A. Russell, R. L. Ely, K. J. Williamson, and D. J. Arp. 1995. Inhibition, inactivation and recovery of ammonia-oxidizing activity in cometabolism of trichloroethylene by *Nitrosomonas europaea*. *Appl. Environ. Microbiol.* 61: 1480-1487.
- Janssen, D. B., A. Scheper, and B. Witholt. 1985. Degradation of halogenated aliphatic compounds by *Xanthobacter autotrophicus* GJ10. *Appl. Environ. Microbiol.* 49: 673-677.
- Keenan, J. E., S. E. Strand, and H. D. Stensel. 1994. Degradation kinetics of chlorinated solvents by a propane-oxidizing enrichment culture. In: R.E Hinchey, A. Leeson, L. Semprini, and S. K. Ong (Eds.) *Bioremediation of Chlorinated and Polycyclic Aromatic Hydrocarbon Compounds* Lewis Publishers, Boca Raton, FL, pp.1-13.
- Keener, W. K. and D. J. Arp. 1993. Kinetic studies of ammonia monooxygenase inhibition in *Nitrosomonas europaea* by hydrocarbons and halogenated hydrocarbons in an optimized whole-cell assay. *Appl. Environ. Microbiol.* 59: 2501-2510.
- Kim, Y. 1996. Aerobic cometabolism of chloroform by butane and propane grown microorganisms from the Hanford subsurface. M.S. Thesis. Oregon State University, Corvallis, OR.
- Kim, Y. and L. Semprini. Unpublished data.
- Kim, Y., L. Semprini, and D. J. Arp. 1997a. Aerobic cometabolism of chloroform and 1,1,1-trichloroethane by butane-grown microorganisms. *Bioremediation J.* 2: 135-148.
- Kim, Y., L. Semprini, and D. J. Arp. 1997b. Aerobic cometabolism of chloroform, 1,1,1-trichloroethane, and the other chlorinated aliphatic hydrocarbons by butane-utilizing microorganisms. In: *In situ and On-site Bioremediation*; Alleman, B. C.; Leeson, A., Eds.; Battelle Press, Columbus, OH, Vol. 3, pp. 107-112.
- Landa, A. S., E. M. Sipkema, J. Weijma, A. A. C. M. Beenackers, J. Doling, and D. B. Janssen. 1994. Cometabolic degradation of trichloroethylene by *Pseudomonas*

cepacia G4 in a chemostat with toluene as the primary substrate. *Appl. Environ. Microbiol.* 60: 3368-3374.

McCarty, P. L., M. N. Goltz, G. D. Hopkins, M. E. Dolan, J. P. Allan, B. T. Kawakami, and T. J. Carrothers. 1998. Full-scale evaluation of in situ cometabolic degradation of trichloroethylene in groundwater through toluene Injection, *Environ. Sci. Technol.* 32:88-100.

McLee, A. G., A. C. Kormendy, and M. Wayman. 1972. Isolation and characterization of *n*-butane utilizing microorganisms. *Can. J. Microbiol.* 18: 1191-1195.

Nelson, M. J., S. O. Montgomery, and P. H. Pritchard. 1988. Trichloroethylene metabolism by microorganisms that degrade aromatic compounds. *Appl. Environ. Microbiol.* 54: 604-606.

Oldenhuis, R., J. Y. Oedzes, J. J. van der Waarde, and D. B. Janssen. 1991. Kinetic of chlorinated hydrocarbon degradation by *Methylosinus trichosporium* OB3b and toxicity of trichloroethylene. *Appl. Environ. Microbiol.* 57: 7-14.

Oldenhuis, R., R. L. J. M. Vink, D. B. Janssen, and B. Witholt. 1989. Degradation of chlorinated aliphatic hydrocarbons by *Methylosinus trichosporium* OB3b expressing soluble methane monooxygenase. *Appl. Environ. Microbiol.* 55: 2819-2826.

Phillips, W. E., and J. J. Perry. 1974. Metabolism of *n*-butane and 2-butanone by *Mycobacterium vaccae*. *J. Bacteriol.* 120: 987-989.

Prior, S. D. and H. Dalton. 1985. Acetylene as a suicide substrate and active site probe for methane monooxygenase from *Methylococcus capsulatus* (Bath). *FEMS Microbiol. Lett.* 29: 105-109.

Rasche, M. E., M. R. Hyman, and D. J. Arp. 1991. Factors limiting aliphatic chlorocarbon degradation by *Nitrosomonas europaea*: cometabolic inactivation of ammonia monooxygenase and substrate specificity. *Appl. Environ. Microbiol.* 57: 2986-2994.

Robinson, J. A. 1985. Determining microbial kinetic parameters using nonlinear regression analysis. *Adv. Microb. Ecol.* 8:61-114.

Robinson, J. A. and W. G. Charaklis. 1984. Simultaneous estimation of V_{\max} , K_m , and the rate of endogenous substrate production (R) from substrate depletion data. *Microb. Ecol.* 10:165-178.

Schmidt, S. K., S. Simkins, and M. Alexander. 1985. Models for the kinetics of biodegradation of organic compounds not supporting growth. *Appl. Environ. Microbiol.* 50: 323-331.

- Semprini, L. 1997. Strategies for the aerobic co-metabolism of chlorinated solvents. *Curr. Opin. Biotechnol.* 8: 296-308.
- Shah, N. N., M. L. Hanna, and R. T. Taylor. 1996. Batch cultivation of *Methylosinus trichosporium* OB3b:V. Characterization of poly- β -hydroxybutyrate production under methane-dependent growth conditions. *Biotechnol. Bioeng.* 49: 161-171.
- Silverman, R. B. 1988. *Mechanism-based enzyme inactivation: chemistry and enzymology*. Vol. 1. p3-30. CRC Press, Boca, Raton.
- Smith, L. H., P. L. McCarty, and P. K. Kitanidis. 1998. Spreadsheet method for evaluation of biochemical reaction rate coefficients and their uncertainties by weighted nonlinear least-squares analysis of the integrated Monod equation. *Appl. Environ. Microbiol.* 64: 2044-2050.
- Speitel Jr., G. E., R. L. Thompson, and D. Weissman. 1993. Biodegradation kinetics of *Methylosinus trichosporium* OB3b at low concentrations of chloroform in the presence and absence of enzyme competition by methane. *Wat. Res.* 27: 15-24.
- Strand, S. E., M. D. Bjelland, and H. D. Stensel. 1990. Kinetics of chlorinated hydrocarbon degradation by suspended cultures of methane-oxidizing bacteria. *Research Journal of the Water Pollution Control Federation.* 62: 124-129.
- Tovanabootr, A. and L. Semprini. 1998. Comparison of TCE transformation abilities of methane- and propane-utilizing microorganisms. *Bioremediation J.* 2:105-124.
- van den Wijngaard, A. J., K. W. H. J. van der Kamp, J. van der Ploeg, F. Pries, B. Kazemier, and D. B. Jassen. 1992. Degradation of 1,2-dichloroethane by *Ancylobacter aquaticus* and other facultative methylotrophs. *Appl. Environ. Microbiol.* 58: 976-983.
- Vanderberg, L. A., B. L. Burbach, and J. J. Perry. 1995. Biodegradation of trichloroethylene by *Mycobacterium vaccae*. *Can. J. Microbiol.* 41: 298-301.
- Vanderberg, L. A. and J. J. Perry. 1994. Dehalogenation by *Mycobacterium vaccae* JOB-5: Role of the propane monooxygenase. *Can. J. Microbiol.* 40: 169-172.
- Van Ginkel, C. G., H. G. J. Welten, S. Hartmans, and J. A. M. de Bont. 1987. Metabolism of trans-2-butene in *Nocardia* TB1. *Journal of General Microbiology.* 133: 1713-1720.
- van Hylckama Vlieg, J. E. T., W. de Koning, and D. B. Janssen. 1996. Transformation kinetic of chlorinated ethenes by *Methylosinus trichosporium* OB3b and detection of unstable epoxides by on-line gas chromatography. *Appl. Environ. Microbiol.* 62: 3304-3312.

- Vannelli, T., M. Logan, D. M. Arciero, and A. B. Hooper. 1990. Degradation of halogenated aliphatic compounds by the ammonia-oxidizing bacterium *Nitrosomonas europaea*. *Appl. Environ. Microbiol.* 56:1169-1171.
- Vogel, T. L. and P. L. McCarty. 1987. Abiotic and biotic transformations of 1,1,1-trichloroethane under methanogenic conditions. *Environ. Sci. Technol.* 21: 1208-1213.
- Wackett, L. P., G. A. Brusseau, S. R. Householder, and R. S. Hanson. 1989. Survey of microbial oxygenases: Trichloroethylene degradation by propane oxidizing bacteria. *Appl. Environ. Microbiol.* 55: 2960-2964.
- Wackett, L. P. and D. T. Gibson, 1988. Degradation of trichloroethylene by toluene dioxygenase in whole-cell studies with *Pseudomonas putida* F1. *Appl. Environ. Microbiol.* 54: 1703-1708.
- Waley, S. G. 1980. Kinetics of suicide substrate. *Biochem. J.* 185: 771-773.
- Waley, S. G. 1985. Kinetics of suicide substrate: Practical procedures for determining parameters. *Biochem. J.* 227: 843-849.
- Westrick, J. J., J. W. Mello, and R. F. Thomas. 1984. The ground water supply survey. *J. Am. Water Work Assoc.* 76: 52-59.
- Wilson, J. T. and B. H. Wilson. 1985. Biotransformation of trichloroethylene in soil. *Appl. Environ. Microbiol.* 49: 242-243.

CHAPTER 3

Aerobic Cometabolism of Chlorinated Methanes, Ethanes, and Ethenes by a Butane-Grown Mixed Culture: Transformation Abilities

SUMMARY

A survey of aerobic cometabolism of chlorinated aliphatic hydrocarbons (CAHs) by a butane-grown mixed culture was performed. The transformation of 1,1-dichloroethylene (1,1-DCE) and *cis*-1, 2-dichloroethylene (*c*-DCE) required O₂, and was inhibited by butane and inactivated by acetylene, indicating that a monooxygenase enzyme was likely involved in the transformations. The initial transformation rates and the quantities of CAHs transformed were inversely proportional to the chlorine contents within each group of chlorinated methanes, ethanes, and ethenes. Lower quantities of chloroform (CF) were transformed than chloromethane (CM) and dichloromethane (DCM), but CF transformation resulted in much higher cell inactivation. For the ethane group, chloroethane (CA) was most effectively transformed, but caused significant cell inactivation. Di- or trichloroethanes that have all chlorines on one carbon were more effectively transformed, and caused less cell inactivation than the isomers that have chlorine on both carbons. For chlorinated ethenes, 1,1-DCE was most rapidly transformed, while *trans*-1,2-dichloroethylene (*t*-DCE) was not transformed. Vinyl chloride (VC) was transformed to the greatest extent, while very limited transformation of trichloroethylene (TCE) was observed.

1,1-DCE transformation caused greater cell inactivation than the transformation of the other chlorinated ethenes. Chloride release studies showed nearly complete oxidative dechlorination of chlorinated methanes and CA, VC, and c-DCE (86% ~ 100%), while incomplete dechlorination of 1,1-dichloroethane (1,1-DCA), 1,2-dichloroethane (1,2-DCA), 1,1,1-trichloroethane (1,1,1-TCA), 1,1,2-trichloroethane (1,1,2-TCA), and 1,1-DCE (37% ~ 75%) was observed.

INTRODUCTION

Aerobic cometabolism is a potential method for remediating aquifers contaminated with chlorinated aliphatic hydrocarbons (CAHs) (McCarty and Semprini 1993). Microorganisms grown on a variety of substrates express oxygenase enzymes that are capable of transforming CAHs. The range of CAHs that can be transformed by microbes grown on different substrates is of interest to determine the potential for bioremediation. Surveys have been performed with *Methylosinus trichosporium* OB3b (Oldenhuis et al. 1989), *Nitrosomonas europaea* (Rasche et al. 1991), a propylene-grown *Xanthobacter* strain (Ensign et al. 1992), and methanotrophic mixed cultures (Dolan and McCarty 1995; Chang and Alvarez-Cohen 1996). The quantity of CAHs transformed and the inactivation of cells caused by CAH transformations were evaluated in these surveys.

McCarty and Semprini (1993) ranked the relative ability of specific oxygenase systems to cometabolically transform different CAHs. The rank was based on

maximum transformation rates, resting cell transformation capacities (T_c , the mass of CAHs ultimately transformed/mass of cells), and transformation yields (T_y , the maximum mass of CAHs transformed/ mass of growth substrates degraded). Chloroform (CF), 1,1,1-trichloroethane (1,1,1-TCA) and 1,1-dichloroethylene (1,1-DCE) were all shown to have limited potential for aerobic cometabolism by the systems known at that time. Thus, identification of cometabolic systems that perform well on these compounds are of interest.

In long-term microcosm studies with aquifer core material from Hanford in Washington, butane was found to be an effective substrate for aerobic cometabolism of CF and 1,1,1-TCA (Kim et al. 1997a). An enrichment culture, CF8, isolated from the Hanford DOE site microcosms transformed CF at rates comparable to those of *Methylosinus trichosporium* OB3b (Hamamura et al. 1997). Soil microcosm studies by Kim et al. (1997b) showed that butane-utilizers effectively transformed the mixtures of 1,1,1-TCA and 1,1-DCE when added at aqueous concentrations of 50 $\mu\text{g/L}$.

In this work, we evaluated how effectively a butane-grown enrichment culture could transform a broad range of chlorinated methanes, ethanes, and ethenes in single contaminant tests. CAHs were transformed in resting cell tests in the absence of exogenous energy sources. The effects of butyrate and formate, as exogenous energy sources, on the transformation of 1,1-DCE and cis-1, 2-dichloroethylene (c-DCE) were also evaluated. Loss of butane uptake ability after exposure to the compounds was used as a measure of cell inactivation due to the CAH transformation. Chloride

release was measured as an indicator of the extent of dehalogenation achieved. This study provides the first detailed evaluation of the range of CAHs that can be transformed by a butane-grown enrichment culture.

MATERIALS AND METHODS

A Butane-Utilizing Mixed Culture

The butane-utilizing enrichment was obtained from Hanford soil microcosms described by Kim et al. (1997a). The enrichment was batch grown in 750-mL capped-bottles containing 10% butane (vol/vol) in air and 250 ml of *Xanthobacter* Py2 medium (Wiegant and de Bont 1980) with the pH adjusted to 7.3, except NH_4NO_3 replaced by NaNO_3 . The bottles were rotary shaken at 200 rpm at 30 °C, and harvested at an optical density (OD_{600}) of 1.3, with a cell yield of 0.8 mg total suspended solid (TSS) per mg butane. Cells were harvested by centrifugation ($6,000 \times g$ for 15 minutes), washed and resuspended in a chloride-free phosphate buffer (adjusted pH 7.3; 2 mM KH_2PO_4 and 2 mM $\text{Na}_2\text{HPO}_4 \cdot 7\text{H}_2\text{O}$) to give a final cell density of 2000 mg/L (on a TSS basis). Resting cell transformation tests were performed within 2 hours of harvesting. Resting cell activity was stable for 30 hours after harvesting, based on butane uptake activity. Cell activities for different batches of cells were measured by determining butane uptake and 1,1-DCE transformation rates and the T_c of 1,1-DCE. 1,1-DCE was used to examine cell activities since it was

rapidly transformed, and its transformation led to complete cell inactivation (measured as a loss in butane uptake activity).

Chemicals

Methane (99%), butane ($\geq 99\%$), and acetylene (99.6%) were purchased from AIRCO (Vancouver, WA). Chloromethane (CM; 99.5%) was obtained from Liquid Carbonic Inc. (Chicago, IL). Butane (10% in nitrogen), carbon tetrachloride (CT; 99.9%), chloroethane (CA; 99.7%), 1,2-dichloroethane (1,2-DCA, $\geq 99\%$), 1,1,2-trichloroethane (1,1,2-TCA; 98%), 1,1,1,2-tetrachloroethane (1,1,1,2-TeCA; 99%), vinyl chloride (VC; $\geq 99.5\%$), 1,1-DCE (99%), trans-1,2-dichloroethene (t-DCE; 98%), c-DCE (97 %), trichloroethylene (TCE; $\geq 99.5\%$), and perchloroethylene (PCE; 99%) were purchased from Aldrich Chemical Co. (Milwaukee, WI). 1,1-dichloroethane (1,1-DCA, $\geq 99\%$), 1,1,2,2-tetrachloroethane (1,1,2,2-TeCA; 98.5%), pentachloroethane (PCA; 99%), and hexachloroethane (HCA; 99%) were obtained from Acros Organics (Pittsburgh, PA). Dichloromethane (DCM; 99.9%) and CF (99.9%) were obtained from Mallinckrodt Specialty Chemical Co. (Paris, KY). 1,1,1-TCA (95.5 %) was purchased from J. T. Baker Inc. (Phillipsburg, NJ).

Saturated aqueous stock solutions of CAHs were prepared at room temperature by adding specific amounts of the liquid or a solid compound to 125-mL serum bottles containing autoclaved deionized water. This procedure eliminated the use of carrier solvents, such as methanol. The bottles were shaken for 6 hours prior to use to ensure

saturation, and then allowed to settle for 6 hours before use. Gaseous compounds were directly transferred to the batch bottles.

Analysis

Gaseous concentrations were determined by a headspace analysis (Kampbell et al. 1989). The total compound mass in each test bottle was calculated, using the headspace and solution volumes and published Henry's constants (Mackay and Shiu 1981; Gossett 1987). All the experiments were conducted with vigorously shaken batch reactors to avoid mass transfer limitations. Calibration curves for all compounds were developed using external standards. Headspace concentrations of methane and butane were determined on a HP5890A series gas chromatograph (GC) using 3.2-mm x 1.2-m HayeSep D80/100-mesh, packed column (Alltech Associates, Deerfield, IL), operated at 130 °C, and a flame ionization detector (FID). CAH analysis was conducted by injecting headspace samples onto a HP 5890 series II GC with 0.25-mm x 30-m HP-624 capillary column operated at 140 °C and Model 5220 electrolytic conductivity detector (OI Analytical, College Station, TX).

Qualitative analysis of the c-DCE epoxide produced during c-DCE transformation was conducted using solid-phase micro-extraction of 1-mL aqueous samples with an 85- μ m acrylate fiber (Supelco Inc., Bellefonte, PA). The gas chromatograph equipped with mass spectrometer (GC/MS) analysis was conducted as previously reported by Vancheeswaran et al. (1999).

Culture density was determined as TSS (American Public Health Association 1985), using 0.1- μ m-membrane filter (Micro Separation Inc., Westboro, MA). The optical density (OD₆₀₀) of cultures was measured at 600 nm using an HP8453 UV-Visible spectrophotometer.

Transformation of CAHs

The transformation of each CAH was monitored for 30 hours. Autoclaved phosphate buffer solution (58 mL) was added to autoclaved 125-mL amber serum bottles that were crimp sealed with Teflon™-lined rubber septa (Kimble, Vineland, NJ). The CAH was added, and the initial CAH concentration was determined after 15 minutes of shaking. Washed and resuspended cells (4 to 6 mg on a TSS basis) were then added, and bottles were shaken at 180 rpm during the 30-hour incubation. Each CAH test included duplicate bottles with active cells, a bottle with acetylene-treated cells, and a bottle without cells. For the CAHs that were effectively transformed (CM, DCM, CA, and 1,1-DCA) multiple additions were made over the 30-hr incubation period. Acetylene blocking studies were performed on butane and CAH amended bottles. Acetylene inactivates activity of methane monooxygenase (MMO) and ammonia monooxygenases (AMO) (Bedard and Knowles 1989; Prior and Dalton 1985), and was shown to inactivate butane-utilization and CAH transformation in butane utilizing pure cultures (Hamamura et al. 1997). The harvested cells were exposed to acetylene [23 ml, 35 % (vol/vol) gas phase] with rapid shaking for 30

minutes, the bottles were purged with N₂, air was reintroduced, and the CAHs were added.

Cell Inactivation after Exposure to Compounds

Cell inactivation was determined from butane uptake measurements after CAH exposure. After the 30-hr incubation, the bottles were purged with N₂ to remove the CAH, and air was then reintroduced. The bottles were recapped, and 2 mL of 10% butane in N₂ was added. Butane was also added to control bottles of cells incubated for 30 hours without any CAH exposure. The headspace butane concentration was monitored to determine rates of butane uptake. Butane uptake rates of cells exposed to the CAH were compared to the control bottle of unexposed cells.

To evaluate the loss of butane uptake activity due to the 30-hour period of shaking, the initial rates of butane uptake were measured before and after shaking. Butane uptake rates after 30 hours of shaking were 82% to 93% of those with 0 hours of shaking. This small loss was accounted for by reporting the percentage of butane uptake rates for cells exposed to individual CAH for 30 hours, normalized by the butane uptake rates of cells shaken for 30 hours in the absence of CAH.

Chloride Release Study

To evaluate the degree of dechlorination of the CAHs, the amount of chloride released was measured. Aqueous chloride concentrations at the beginning and end of the 30-hour incubation were determined using a colorimetric method (Bergnam and Sanik 1957). This method was used to determine CAH dechlorination by *M. trichosporium* OB3b (Oldenhuis et al. 1989; van Hylckama Vlieg et al. 1996).

c-DCE or 1,1-DCE Transformation and Cell Inactivation

Duplicate batch bottles were prepared with combinations of c-DCE or 1,1-DCE, butane [0, 0.5, or 30% (vol/vol) gas phase], butyrate (2 mM), formate (20 mM), and with ambient air or no O₂ to evaluate the effects of exogenous energy source, butane concentration and O₂ on c-DCE or 1,1-DCE transformations. Preincubation effects of exogenous energy sources were evaluated by incubating resting cells with butyrate (2 mM) or formate (20 mM) for 1 hour before addition of c-DCE. In a cometabolic process, the presence of physiological substrate at sufficiently high concentrations is expected to inhibit the transformation of another substrate (Colby and Dalton 1976). To provide a qualitative evaluation of inhibition (competing for active site of enzyme), butane was added into batch bottles with active cells at two concentrations of either 0.5 or 30% (vol/vol, gas phase) along with c-DCE or 1,1-

DCE. O₂ depleted bottles were constructed with three vacuum cycles and N₂ gas purging. Four different kinds of cell activity control bottles were constructed: 1) no substrate with cells; 2) butyrate with cells; 3) formate with cells; and 4) c-DCE or 1,1-DCE with acetylene-treated cells.

RESULTS AND DISCUSSION

Cell Activities for Different Cell Preparation Batches

Rates of butane uptake and 1,1-DCE transformation and the T_c of 1,1-DCE were measured to evaluate the cell activities for different cell batches. The average initial transformation rates with standard deviations (SD) for 10 cell batches were 0.35 ± 0.14 μmol 1,1-DCE transformed / mg TSS-hr and 0.61 ± 0.31 μmol butane degraded/mg TSS-hr. The average T_c with SD was 0.92 ± 0.23 μmol 1,1-DCE/ mg TSS. These rates and transformation capacities were of sufficient reproducibility for the surveys of CAH transformation abilities assessed in the study.

Transformations of 1,1-DCE and c-DCE and the Effects of Their Transformation on Cell Inactivation

The effects of O₂, butane, butyrate, formate or cell treatment with acetylene [35% (vol/vol) gas phase] on the transformation of 1,1-DCE and c-DCE were examined. The results with duplicate bottles were essentially identical, thus the results from only one bottle are presented in Figure 3.1. No transformation of 1,1-DCE or c-DCE was observed in the absence of O₂. Acetylene-treated cells transformed less than 15% of the amount of 1,1-DCE or c-DCE achieved by untreated cells. Untreated cells rapidly transformed 1,1-DCE, with most of the transformation occurring within the first 4 hours of exposure. c-DCE was transformed more slowly than 1,1-DCE, with an initial transformation rate being 0.20 $\mu\text{mol/mg TSS-hr}$ compared with 0.34 $\mu\text{mol/mg TSS-hr}$ for 1,1-DCE. The transformation of c-DCE decreased significantly after 12 hours of incubation.

1,1-DCE and c-DCE transformation rates in the presence of butane [30% (vol/vol) gas phase] were about 22% and 13% of the rate in the absence of butane, respectively. The amount of 1,1-DCE and c-DCE transformed decreased by 50 and 60%, respectively. However, 0.5% butane did not inhibit the transformation. Butane degradation was also inhibited by both c-DCE and 1,1-DCE, with 1,1-DCE being a stronger inhibitor (data not presented).

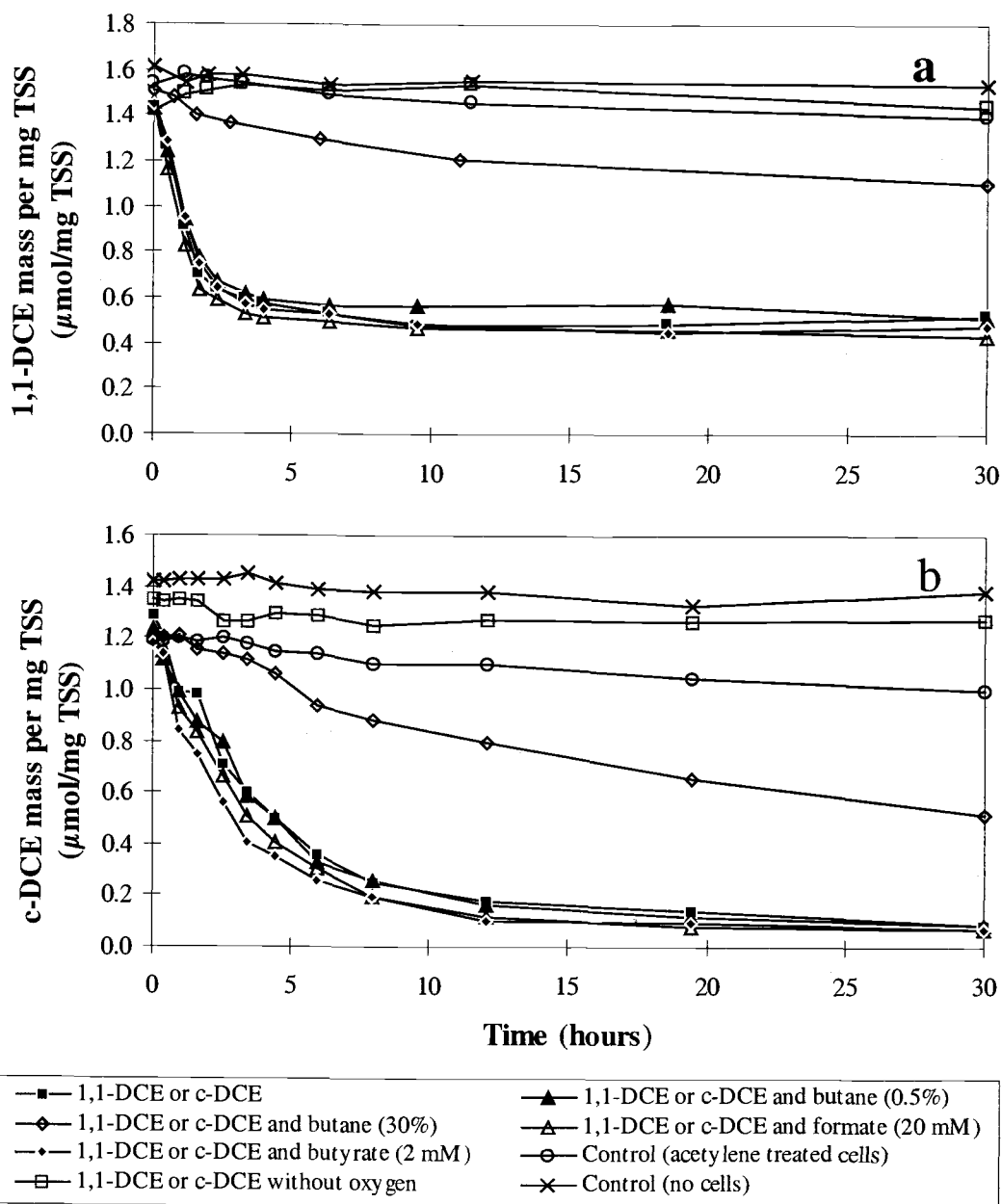


Figure. 3.1. Resting cell transformation of (a) 1,1-DCE and (b) c-DCE in the presence or absence of O_2 , butane, butyrate, or formate. 3.4 mg TSS and 4.5 mg TSS were used for 1,1-DCE and c-DCE transformation experiments, respectively.

The transformation of *c*-DCE resulted in the production of *c*-DCE epoxide. Mass spectrometry confirmed the presence of a compound with mass to charge fragment ratios (*m/z*) 112, 83, 48, and 35. The values are in agreement with the spectra of a chemically synthesized DCE epoxide (Janssen et al. 1988).

A monooxygenase enzyme was likely involved in the transformation of the CAHs, based on the lack of transformation in the absence of O₂ and the inactivation of CAH transformation by acetylene and the inhibition of CAH transformation by butane. The possible involvement of butane monooxygenase in the transformation of CAHs is consistent with the results obtained with pure butane-utilizing cultures and an enrichment of the culture tested here (Hamamura et al. 1997). More detailed enzyme analyses are needed to verify the involvement of a monooxygenase enzyme.

Butyrate and formate addition had no effect on transformation of 1,1-DCE and *c*-DCE. Transformation rates and extents and cell activation with or without preincubation or incubation with butyrate and formate were similar. Cells incubated with 1,1-DCE or *c*-DCE in the absence of O₂ retained 80% or 91% of butane-uptake activity, respectively, after 30 hours of exposure, while cells incubated with 1,1-DCE or *c*-DCE in the presence of O₂ retained less than 1% activity. Cells were also highly inactivated after the transformation of each compound in the presence of O₂ and butyrate or formate, with less than 1% activity remaining. The rapid inactivation of 1,1-DCE and *c*-DCE transformation likely resulted from transformation product toxicity. The results indicate that either butyrate and formate are not effective

exogenous energy sources, or the butane-grown mixed culture is using internal energy reserves such as poly- β -hydroxybutyrate (PHB).

Based on our resting-cell transformation results, internal energy reserves such as PHB are likely driving the CAH transformation. A positive correlation between PHB content of methanotrophs and the TCE transformation rate and capacity was reported (Chu and Alvarez-Cohen 1996; Henry and Grbić-Galić 1991; Henrysson and McCarty 1993; Shah et al. 1996). The synthesis of PHB by *Nocardia* 107-332 grown on butane was reported, and the PHB and other polymers constituted about 12 to 14% of the cell mass (Davis 1964).

For both c-DCE and 1,1-DCE, similar extents of cell inactivation occurred in the absence or presence of 0.5% butane, with less than 2% activity remaining. However, with 30% butane, very different cell inactivation was observed. For 1,1-DCE, only 10% activity remained, while, for c-DCE, 96% remained. These results indicate that toxicity resulting from c-DCE transformation could be greatly reduced in the presence of butane, while the toxicity resulting from 1,1-DCE transformation was only slightly reduced.

Transformation of Chlorinated Methanes, Ethanes, and Ethylenes

Transformation tests were performed for chlorinated methanes, ethanes, and ethylenes in the absence of butane using the same procedures as the 1,1-DCE and c-DCE tests. Butyrate and formate were not added as external energy sources. The

tests, therefore, relied on the internal energy reserves to drive the CAH transformations. The transformations of all the compounds tested were inhibited by the treating cells with acetylene.

The results for the chlorinated methanes (a), ethanes (b), and ethenes (c) are presented in Figure 3.2 where the amounts of CAH transformed per TSS mass versus time are plotted. For CAHs that were effectively transformed (CM, DCM, CA, and 1,1-DCA) the compounds were successively added to the batch reactors. The cumulative transformation amounts are presented (Figure 3.2). Single-chlorine substituted CAHs, CM, CA and VC, were transformed to the greatest extent in each of the three groups. Generally, the molecules with more chlorine atoms showed decreased transformation rates.

As expected, no transformation of fully chlorinated CAHs (CT, HCA, and PCE) was observed. The transformations of CM, DCM, and 1,1-DCA continued during the 30-hour time course, while transformations of all other compounds ceased. For chlorinated methanes the transformation rate of CF quickly decreased and CF transformation ceased.

No transformation of 1,1,1,2-TeCA, 1,1,2,2-TeCA, and PCA was observed (data not shown). The relative amounts of chlorinated ethane transformed per unit mass of TSS in the order of the highest to lowest were: CA; 1,1-DCA; 1,2-DCA;

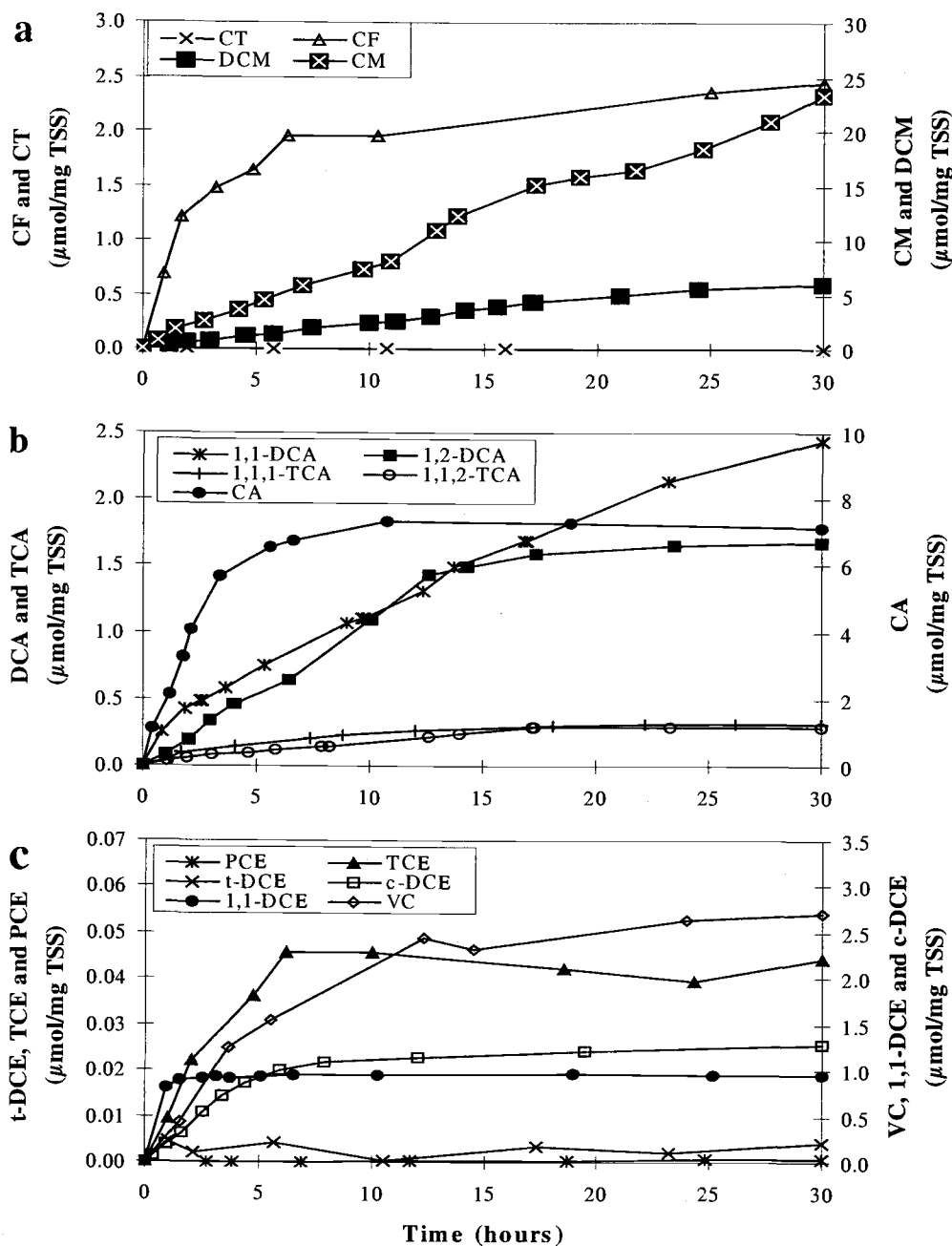


Figure 3.2. Resting cell transformation of (a) chlorinated methanes, (b) chlorinated ethanes, and (c) chlorinated ethylenes. CM, DCM, CA, and 1,1-DCA values (scale on the right Y-axis) are cumulative amounts following multiple additions of CAH. The addition times in hours are as follows: CM (9.8, 22), DCM (4.6, 11, and 17), CA (1.2 and 3.4), and 1,1-DCA (2.7, 9.8, and 17).

1,1,1-TCA; and 1,1,2-TCA. The amount transformed decreased in proportion to chlorine content, and also depended on the location of the chlorine substitution. The transformation rate of CA decreased more quickly than that of 1,2-DCA, 1,1,1-TCA and 1,1,2-TCA.

The amounts transformed per unit mass of TSS for the chlorinated ethenes in the order of the highest to lowest was: VC > c-DCE > 1,1-DCE > TCE. The transformation of the DCE isomers differed, with no observable transformation of t-DCE, while similar amounts of c-DCE and 1,1-DCE were transformed, but at different rates. Transformation rates decreased most rapidly for 1,1-DCE, followed by TCE, c-DCE, and VC.

The initial transformation rates of each CAH are presented in Table 3.1. For all three classes of compounds, the trend is towards decreasing rates of transformation with increasing number of chlorines. Whether this trend reflects difference in maximum transformation rates (k_{\max}), or half-saturation coefficients (K_s) or both is not yet known. A more detailed kinetic study is needed to evaluate whether a direct relationship exists between chlorine content and the k_{\max} of the butane-grown mixed culture.

Table 3.1. Average initial transformation rates of chlorinated methanes, ethanes, and ethylenes

Chlorinated	Initial rates ^a	Chlorinated	Initial rates ^a	Chlorinated	Initial rates ^a
Methanes	($\mu\text{mol}/\text{mg TSS}/\text{hr}$)	ethanes	($\mu\text{mol}/\text{mg TSS}/\text{hr}$)	Ethenes	($\mu\text{mol}/\text{mg TSS}/\text{hr}$)
CM	0.95	CA	1.68	VC	0.29
DCM	0.28	1,1-DCA	0.19	1,1-DCE	0.34
CF	0.11	1,2-DCA	0.11	c-DCE	0.20
CT	≈ 0.00	1,1,1-TCA	0.03	TCE	0.01
		1,1,2-TCA	0.03	t-DCE	≈ 0.00
		TeCA	≈ 0.00	PCE	≈ 0.00
		PCA	≈ 0.00		
		HCA	≈ 0.00		

Note: Average initial aqueous concentrations (μM) were CM (428), DCM (90), CF (84), CT (4.0), CA (302), 1,1-DCA (47), 1,2-DCA (52), 1,1,1-TCA (25), 1,1,2-TCA (16), 1,1,1,2-TeCA (8.6), 1,1,2,2-TeCA (28), PCA (39), HCA (9.3), VC (129), 1,1-DCE (37), c-DCE (87), TCE (19), and PCE (6.5).

a: Results from duplicate bottles were used in calculating the average initial transformation rates.

CAHs Transformation Effects on Cell Inactivation

To compare the degree of CAH transformation and the transformation effect on cell inactivation, CAHs were divided into classes based on the amount of CAH transformed and the degree of cell inactivation that occurred. Cell inactivation was based on the rate of butane-uptake after 30-hour exposure to the CAH. Cell inactivation is presented as the ratio of rates for CAH exposed cells to those of controls with no exposure, which were also incubated for 30 hours.

The compounds were divided into five classes, ranging from Class I (no transformation and minor inactivation) to Class V (major transformation and major inactivation). Values below 1 μmol CAHs transformed/mg TSS after 30 hours of incubation and above 5% of cell activity remaining were considered “minor” for classification purposes, while values above these benchmarks were considered “major”. These criteria are based on the range for practical use in remediation purposes, and the ability of cells likely to recover with 5% butane activity remaining. The results of this comparison are shown in Figure 3.3.

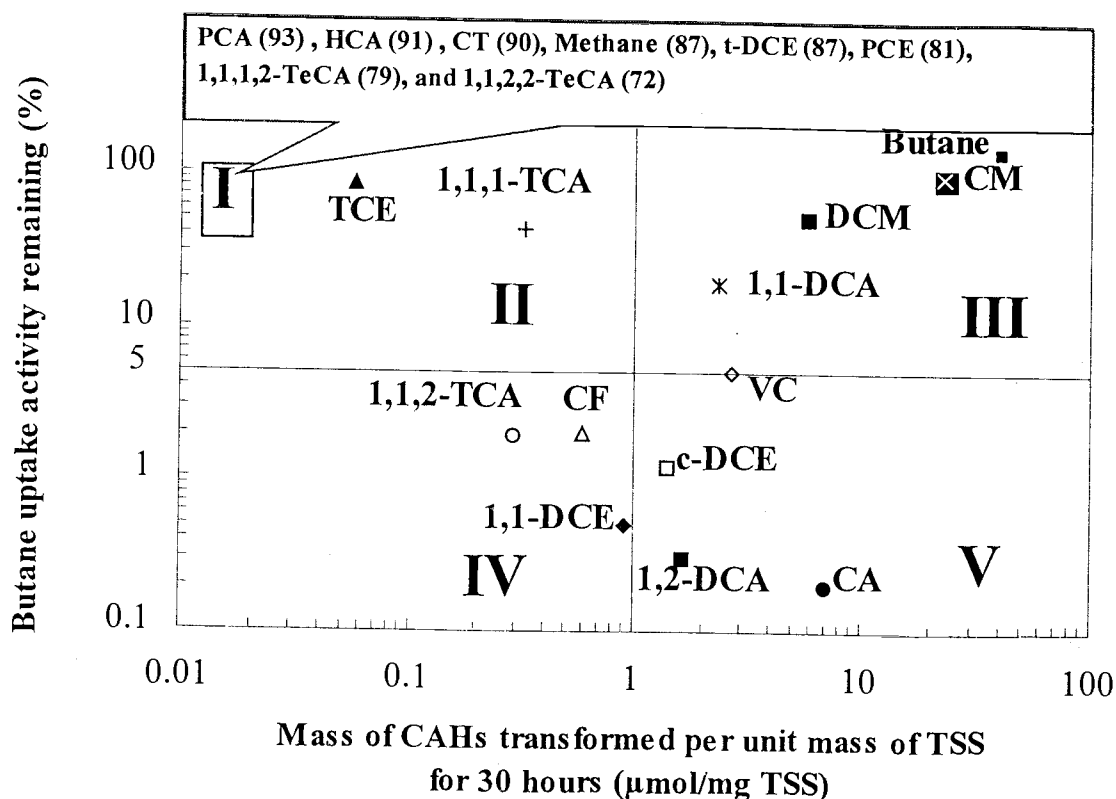


Figure. 3.3. The mass of CAHs transformed per mg TSS after 30 hours of incubation versus butane uptake activity after the exposure. Values in Class I box (no transformation) indicate percentage of butane uptake activity remaining after exposure to each compound.

Class I ($\approx 0 \mu\text{mol transformed/mg TSS}$ and more than 70% of activity remaining)

Exposure to fully chlorinated aliphatic hydrocarbons (CT, HCA, and PCE), chlorinated ethanes with four or more chlorines, methane, and t-DCE did not greatly reduce cell activity. These compounds were not effectively transformed and general

transformation product toxicity was not observed. Exposure to 1,1,2,2-TeCA resulted in loss of some activity, however transformation was not detected.

The lack of transformation of methane by butane-grown microorganisms is consistent with previous observations of 15 isolated butane-grown bacteria (McLee et al., 1972) and *Nocardia* TB1 grown on butane (Van Ginkel et al., 1987). In contrast, ammonia oxygenase, which can oxidize butane, can also oxidize methane (Hyman et al., 1988).

Class II (less than 1 μ mol transformed/mg TSS and more than 5% of cell activity remaining)

TCE and 1,1,1-TCA were classified as Class II compounds, with limited transformation and limited cell inactivation. In studies with *M. trichosporium* OB3b, high cell inactivation followed TCE transformation, however the amount transformed was 20 times that of the butane enrichment. Inactivation was attributed to nonspecific covalent binding of transformation products to cellular proteins (Oldenhuis et al., 1991).

Class III (more than 1 μ mol transformed/mg TSS and more than 5% of activity remaining)

Class III compounds have the highest potential for cometabolic treatment due to relatively high transformation amounts and low cell inactivation. CM, DCM, and 1,1-DCA are in this class. CM was most effectively transformed among CAHs tested.

CM transformation caused little loss in cell activity in studies with *N. europaea* (Rasche et al., 1991) and methanotrophs (Chang and Alvarez-Cohen, 1996). It is plausible that monooxygenase-mediated transformation of CM may produce formaldehyde through oxidative dechlorination pathway (Rasche et al., 1991). Its transformation with little loss in rate and with essentially no loss in activity indicates it may, upon being transformed, serve as an energy source for butane-utilizers. In contrast less DCM was transformed and more inactivation occurred.

1,1-DCA was effectively transformed and caused moderate cell inactivation. Rasche et al. (1991) suggested that AMO-turnover-dependent inactivation (loss in ammonia-dependent O₂ uptake activity) of ammonia oxidation by *N. europaea* resulted from the transformation of compounds having dichlorinated carbons. They suggested that the production of alkylating agents may provide the basis for inactivation by 1,1-DCA transformation. Such alkylating agents could account for the relatively higher cell inactivation resulting from transformation of 1,1-DCA than transformation of the other compounds in Class III.

Class IV (less than 1 μ mol transformed/mg TSS and less than 5% of activity remaining)

Compounds in Class IV (CF, 1,1,2-TCA, and 1,1-DCE) are problematic for this enrichment due to relatively low amounts transformed and high degree of cell inactivation. Among the chlorinated methanes, only CF was in this class. Previous observations with a methane-utilizing mixed culture suggested toxicity of transformation products of CF cometabolism (Alvarez-Cohen and McCarty, 1991c). Alvarez-Cohen and McCarty (1991c) proposed phosgene as a potential intermediate product of the CF transformation, and Bartnicki and Castro (1994) confirmed this pathway with *M. trichosporium* OB3b. A similar pathway could account for high inactivation by CF transformation for the butane enrichment.

For *M. trichosporium* OB3b expressing soluble methane monooxygenase (sMMO), 1,1-DCE transformation activity rapidly decreased during transformation, and cell viability was greatly reduced (van Hylckama Vlieg et al., 1997). 1,1-DCE transformation resulted in loss of O₂ uptake ability in *N. europaea* (Rasche et al., 1991). Similar transformation products and toxicity mechanisms likely affected the butane enrichment. The transformation of 1,1,2-TCA caused much greater cell inactivation than 1,1,1-TCA. In the case of TCA isomers, distribution of chlorine on the two carbons results in greater toxicity.

Class V (more than 1 μmol transformed/mg TSS and less than 5% of activity remaining)

Class V compounds (CA, 1,2-DCA, c-DCE, and VC) are problematic contaminants due to the high cell inactivation, however relatively large amounts are transformed. Transformation of VC and c-DCE resulted in a high degree of cell inactivation. Cells exposed to CA were essentially completely inactivated. Despite less transformation, exposure to 1,2-DCA caused much higher cell inactivation than 1,1-DCA. As observed with 1,1,1-TCA and 1,1,2-TCA, the isomer with chlorine on each carbon caused more inactivation.

During the transformation of CA, less inactivation occurred with *N. europaea* (Rasche et al., 1991) and methanotrophs (Chang and Alvarez-Cohen, 1996), with exposure times of 1 and 4 hours, respectively. The major CA transformation product with *N. europaea* was acetaldehyde, and greater inactivation occurred with longer exposures (Rasche et al., 1990; 1991). The 30-hour exposures of the butane culture may have resulted in greater inactivation, especially if acetaldehyde was present.

Cell inactivation resulting from CAH transformation was based on the loss of butane uptake ability. This assay provides a good measure of the impacts on the cell of CAH transformation, because butane consumption requires an active butane monooxygenase and an intact electron transport chain. The immediate and stable response to butane indicated that induction and de novo enzyme synthesis were not required. Because reductant is required for the monooxygenase reaction, measurement of butane consumption can not distinguish between damage to the monooxygenase and

to the flow of reductant. Activity studies with a readily degraded CAH can also be used to assay oxygenase enzyme activity and could be used in conjunction with the butane assay.

Chloride Release

The degree of dechlorination of the CAHs was determined by measuring the amount of chloride released after 30 hours of incubation. The chloride release observed was compared with stoichiometric release of chloride required for the amount of CAH transformed. The dechlorination extent is presented on a percentage basis (Figure 3.4).

Chlorinated methanes and ethylenes were more highly dechlorinated than the chlorinated ethanes, except CA. Nearly complete dechlorination of chlorinated methanes (90% to 95%) indicates that transformations proceeded past an initial oxidation. Oldenhuis et al. (1989) reported 100% and 76% dechlorination of CF by *M. trichosporium* OB3b expressing sMMO and particulate methane monooxygenase (pMMO) after 24 hours of incubation, respectively, while after 1 hour of incubation 73% dechlorination of CF by *N. europaea* was reported (Rasche et al., 1991). The degree of dechlorination was likely affected by the experimental protocol used here where excess CAH was added during a 30-hour exposure period. If the CAHs were permitted to be completely transformed, by adding lesser amounts, biotic

transformation of products may have occurred resulting in more complete dechlorination.

Partial dechlorination of 1,1-DCA, 1,2-DCA, 1,1,2-TCA and 1,1,1-TCA indicates that chlorinated transformation products exist. 1,1-DCA and 1,2-DCA were completely dechlorinated by *M. trichosporium* OB3b expressing sMMO (Oldenhuis et al., 1989). 1,1-DCA was completely dechlorinated by *N. europaea*, but 1,2-DCA was only partially dechlorinated (Rasche et al., 1991). The ability to transform products of chlorinated ethanes therefore differs between butane-utilizers and the MMO and AMO systems.

Nearly complete oxidative dechlorination of VC and c-DCE was observed, while 75% dechlorination of 1,1-DCE was achieved. c-DCE was completely dechlorinated by *M. trichosporium* OB3b expressing sMMO, but incomplete 1,1, - DCE dechlorination was observed (Oldenhuis et al., 1989). Dolan and McCarty (1995) speculated that methanotrophic transformation of 1,1-DCE may produce 1,1-DCE epoxide that rearranges to form chlorinated products of acyl chlorides (strong alkylating agents). It is plausible that chlorinated products of 1,1-DCE may result in high cell inactivation consistent with observations with other systems.

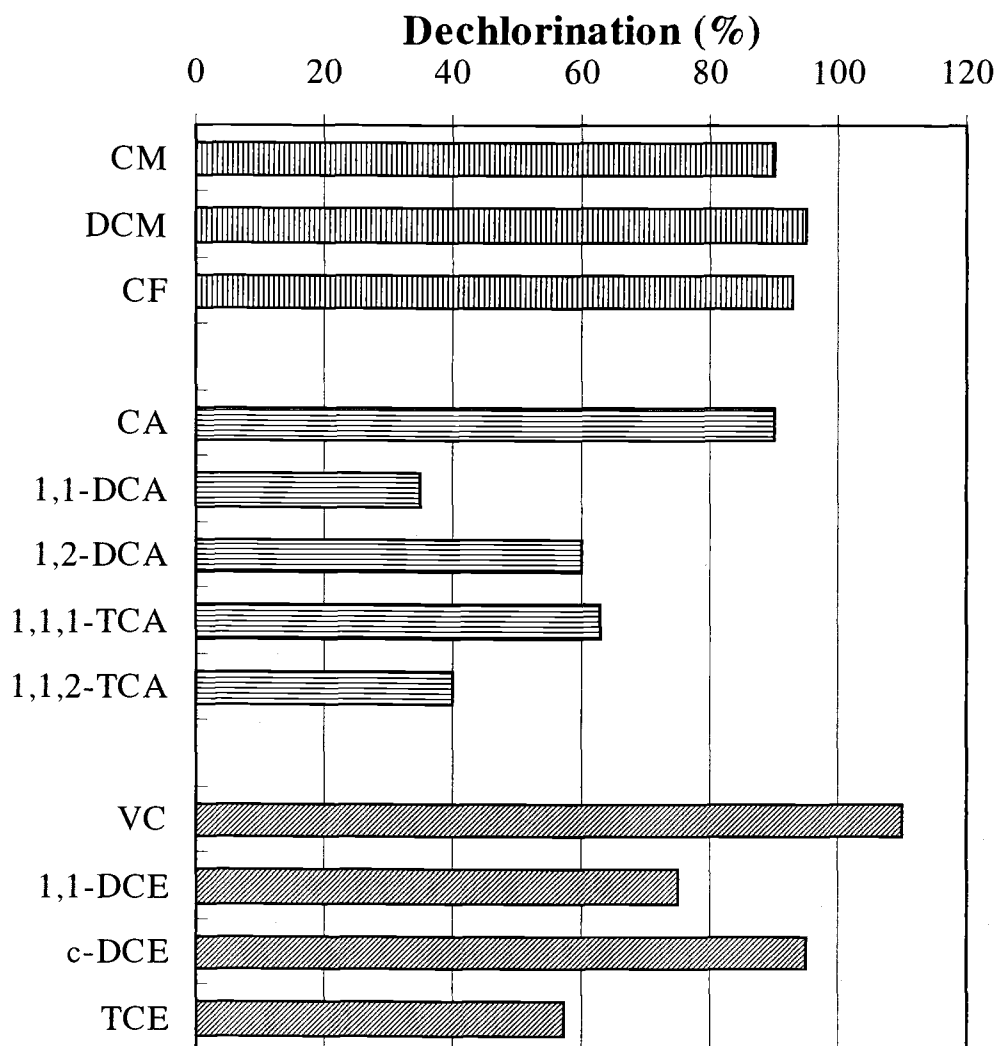


Figure. 3.4. Average percent dechlorination of the CAHs after 30 hours of incubation.

van Hylckama Vlieg et al. (1996) found that c-DCE epoxide produced from c-DCE transformation could be biologically transformed by *M. trichosporium* OB3b expressing sMMO. c-DCE epoxide was formed by the butane enrichment as previously discussed. As shown in Figure 3.4, 95% Cl⁻ release occurred after 30 hours of incubation of c-DCE. The half-life of c-DCE epoxide is approximately 72 hours

(Janssen et al., 1988). The nearly complete oxidative dechlorination of c-DCE within 30 hours of incubation, suggests c-DCE epoxide transformation by the butane-utilizers. The high degree in inactivation of the butane-utilizers potentially resulted from the biotic transformation of the epoxide.

CONCLUSIONS

An enrichment culture grown on butane transformed chlorinated methanes (CM, DCM, and CF), chlorinated ethanes (CA, 1,1-DCA, 1,2-DCA, 1,1,1-TCA, and 1,1,2-TCA), and chlorinated ethylenes (VC, 1,1-DCE, and c-DCE). A butane monooxygenase enzyme is likely involved in the transformation of CAHs, based on the lack of transformation in the absence of O₂ and the inactivation of CAH transformation by acetylene and inhibition of CAH transformation by butane. More detailed enzyme analyses are needed to verify the involvement of a monooxygenase enzyme.

Many sites are contaminated with mixtures of 1,1,1-TCA, 1,1-DCE, and 1,1-DCA as biotic and abiotic transformation products of 1,1,1-TCA (Vogel and McCarty, 1987). 1,1,1-TCA and 1,1-DCE have been problematic CAHs for aerobic cometabolism. Limited 1,1,1-TCA transformation has been observed with methane-grown cultures (Henson et al., 1989; Strand et al., 1990). During in-situ studies with methane-utilizing microorganisms (Semprini et al., 1990) or with phenol utilizing

microorganisms (Hopkins et al., 1993; Hopkins and McCarty, 1995), 1,1,1-TCA was not transformed, despite effective transformation of chlorinated ethenes. 1,1-DCE can also be cometabolized by microorganisms grown on methane (van Hylckama Vlieg et al., 1996) and ammonia (Rasche et al., 1991). The transformation of 1,1-DCE has been shown to be toxic to nitrifying bacteria and methane-utilizing microorganisms (Rasche et al., 1991; Dolan and McCarty, 1995; van Hylckama Vlieg et al., 1997).

The butane culture has good potential for transforming 1,1,1-TCA, 1,1-DCE, and 1,1-DCA. Butane-utilizers may have advantages over methanotrophs for these contaminants. Our butane-grown culture had a greater ability to transform 1,1,1-TCA on a basis of amount transformed per unit mass cells than a methane-grown mixed culture (Chang and Alvarez-Cohen, 1996). The initial transformation rates of 1,1-DCE were comparable with that achieved by *M. trichosporium* OB3b expressing sMMO (Oldenhuis et al., 1991), while the T_c was a factor of 4 to 9 higher than achieved with methanotrophs (Chang and Alvarez-Cohen, 1996). Thus butane-utilizers may have better potential for remediating 1,1-DCE contamination than other oxygenase systems, despite being more toxic to the culture than other CAHs.

CAH transformations by the butane-utilizing culture were achieved without the addition of an exogenous energy source, while the results with methanotrophs were typically achieved with the addition of 20-mM formate (Chang and Alvarez-Cohen, 1996; Oldenhuis et al., 1991). A higher percentage of butane uptake activity was retained after 30 hours exposure to 1,1,1-TCA than the percentage of methane uptake activity retained by methanotrophs exposed to 1,1,1-TCA for 4 hours (Chang and

Alvarez-Cohen, 1996). T_y values of the butane enrichment for 1,1-DCE and 1,1,1-TCA were also higher than those obtained by Chang and Alvarez-Cohen (1996) with chemostat-grown methanotrophs, likely because the cell yield of the butane enrichment was a factor of 2.5 higher than the methanotrophs. 1,1-DCA was also very effectively transformed by the butane enrichment, and showed a low degree of inactivation. The enrichment results are consistent with the groundwater/soil microcosm results (Kim et al., 1997b) which indicated that butane is an effective substrate for treating mixtures of 1,1,1-TCA, 1,1-DCE and 1,1-DCA, as well as chlorinated methanes, VC, and c-DCE. The enrichment, however, did not effectively transform TCE, which is a common groundwater contaminant.

Effective transformation with methanotrophs is usually induced under copper limited nutrient conditions, so that soluble MMO (sMMO) is expressed. Copper was not limiting ($0.1 \mu\text{M}$ as $\text{CuCl}_2 \cdot 2\text{H}_2\text{O}$) in the media formulation used here. Thus butane-utilizers might also have an advantage for in-situ remediation, where it is difficult to limit copper available.

The results presented are for one butane enrichment that shows a broad range of CAH transformation abilities. More studies are needed with pure cultures and enrichments from other sites to determine how CAH transformation abilities differ among cultures and growth conditions.

ACKNOWLEDGMENTS

The research was supported by Research Grant from the R2D2 program of the U.S. Environmental Protection Agency-sponsored Western Region Hazardous Substance Research Center under agreement R-815738. This article has not been reviewed by the agency, and no official endorsement should be inferred.

REFERENCES

- Alvarez-Cohen, L. M. and P. L. McCarty. 1991c. Product toxicity and cometabolic competitive inhibition modeling of chloroform and trichloroethylene transformation by methanotrophic resting cells. *Appl. Environ. Microbiol.* 57: 1031-1037.
- American Public Health Association. (1985). *Standard methods for the examination of water and wastewater*. 16th ed. APHA, New York, N.Y.
- Bartnicki, E. W. and C. E. Castro. 1994. Biodehalogenation: Rapid oxidative metabolism of mono- and polyhalomethanes by *Methylosinus trichosporium* OB-3b. *Environ. Toxicology and Chemistry*. 13: 241-245.
- Bedard, C. and R. Knowles. 1989. Physiology, biochemistry, and specific inhibitors of CH₄, NH₄⁺ and CO oxidation by methanotrophs and nitrifiers. *Microbio. Rev.* 53: 68-84.
- Bergnam, J. G. and J. Sanik. 1957. Determination of trace amounts of chloride in naphtha. *Anal. Chem.* 29: 241-243.
- Chang, H. L. and L. Alvarez-Cohen. 1996. Biodegradation of individual and multiple chlorinated aliphatic hydrocarbons by methane-oxidizing cultures. *Appl. Environ. Microbiol.* 62: 3371-3377.

- Chu, K-H and L. Alvarez-Cohen. 1996. Trichloroethylene degradation by methane-oxidizing cultures grown with various nitrogen sources. *Water Environ. Res.* 68: 76-82.
- Colby, J. and H. Dalton. 1976. Some properties of a soluble methane mono-oxygenase from *Methylococcus capsulatus* Strain Bath. *Biochem. J.* 157, 495-497.
- Davis, J. B. 1964. Cellular lipids of a *Nocardia* grown on propane and n-butane. *Appl. Microbiol.* 12: 301-304.
- Dolan, M. E. and P. L. McCarty. 1995. Methanotrophic chloroethene transformation capacities and 1,1-dichloroethene transformation product toxicity. *Environ. Sci. Technol.* 29: 2741-2747.
- Ensign, S. A., M. R. Hyman, and D. J. Arp. 1992. Cometabolic degradation of chlorinated alkenes by alkene monooxygenase in a propylene-grown *Xanobacter* strain. *Appl. Environ. Microbiol.* 58: 3038-3046.
- Gossett, J. M. 1987. Measurements of Henry's law constants for C1 and C2 chlorinated hydrocarbons. *Environ. Sci. Technol.* 21: 202-208.
- Hamamura, N., C. Page., T. Long, L. Semprini, and D. J. Arp. 1997. Chloroform cometabolism by butane-grown CF8, *Pseudomonas butanovora*, and *Mycobacterium vaccae* JOB5 and methane-grown *Methylosinus trichosporium* OB3b. *Appl. Environ. Microbiol.* 63: 3607-3613.
- Henry, S. M. and D. Grbić-Galić. 1991. Influence of endogenous and exogenous electron donors and trichloroethylene oxidation toxicity on trichloroethylene oxidation by methanotrophic cultures from a groundwater aquifer. *Appl. Environ. Microbiol.* 57: 236-244.
- Henrysson, T. and P. L. McCarty. 1993. Influence of the endogenous storage lipid poly- β -hydroxybutyrate on the reducing power availability during cometabolism of trichloroethylene and naphthalene by resting methanotrophic mixed cultures. *Appl. Environ. Microbiol.* 59: 1602-1606.
- Henson, J. M., M. V. Yates, and J. W. Cochran. 1989. Metabolism of chlorinated methanes, ethanes and ethylenes by a mixed bacterial culture growing on methane. *J. Industr. Microbiol.* 4: 29-35.
- Hopkins, G. D., L. Semprini, and P. L. McCarty. 1993. Microcosm and in situ field studies of enhanced biotransformation of trichloroethylene by phenol-utilizing microorganisms. *Appl. Environ. Microbiol.* 59: 2277-2285.

- Hopkins, G. D. and P. L. McCarty. 1995. Field evaluation of *in situ* aerobic cometabolism of trichloroethylene and three dichloroethylene isomers using phenol and toluene as primary substrates. *Environ. Sci. Technol.* 29: 1628-1637.
- Hyman, M. R., I. B. Murton, and D. J. Arp. 1988. Interaction of ammonia monooxygenase from *Nitrosomonas europaea* with alkanes, alkenes, and alkynes. *Appl. Environ. Microbiol.* 54: 3187-3190.
- Janssen, D. B., G. Grobбен, R. Hoekstra, R. Oldehuis, and B. Witholt. 1988. Degradation of trans-1,2-dichloroethylene by mixed and pure cultures of methanotrophic bacteria. *Appl. Microbiol. Biotechnol.* 29: 392-399.
- Kampbell, D. H., J. T. Wilson, and S. A. Vandergrift. 1989. Dissolved oxygen and methane in water by a GC headspace equilibration technique. *J. Environ. Anal. Chem.* 36: 249-259.
- Kim, Y., L. Semprini, and D. J. Arp. 1997a. Aerobic cometabolism of chloroform and 1,1,1-trichloroethane by butane-grown microorganisms. *Bioremediation J.* 2: 135-148.
- Kim, Y., L. Semprini, and D. J. Arp. 1997b. Aerobic cometabolism of chloroform, 1,1,1-trichloroethane, and the other chlorinated aliphatic hydrocarbons by butane-utilizing microorganisms. In: *In situ and On-site Bioremediation*; Alleman, B. C.; Leeson, A., Eds.; Battelle Press, Columbus, OH, Vol. 3, pp. 107-112.
- Mackay, D. and W. Y. Shiu. 1981. A critical review of Henry's law constants for chemicals of environmental interest. *J. Phys. Chem. Ref. Data.* 10: 1175-1199.
- McCarty, P. L. and L. Semprini. 1993. Ground-water treatment of chlorinated solvents. In *Handbook of Bioremediation*, Lewis Publisher Inc., Chelsea, MI, pp87-116.
- McLee, A. G., A. C. Kormendy, and M. Wayman. 1972. Isolation and characterization of *n*-butane utilizing microorganisms. *Can. J. Microbiol.* 18: 1191-1195.
- Oldenhuis, R., J. Y. Oedzes, J. J. van der Waarde, and D. B. Janssen. 1991. Kinetic of chlorinated hydrocarbon degradation by *Methylosinus trichosporium* OB3b and toxicity of trichloroethylene. *Appl. Environ. Microbiol.* 57: 7-14.
- Oldenhuis, R., R. L. J. M. Vink, D. B. Janssen, and B. Witholt. 1989. Degradation of chlorinated aliphatic hydrocarbons by *Methylosinus trichosporium* OB3b expressing soluble methane monooxygenase. *Appl. Environ. Microbiol.* 55: 2819-2826.

- Prior, S. D. and H. Dalton. 1985. Acetylene as a suicide substrate and active site probe for methane monooxygenase from *Methylococcus capsulatus* (Bath). *FEMS Microbiol. Lett.* 29: 105-109.
- Rasche, M. E., R. E. Hicks, M. R. Hyman, and D. J. Arp. 1990. Oxidation of monohalogenated ethenes and n-chlorinated alkanes by whole cells of *Nitrosomonas europaea*. *J. Bacteriol.* 172: 5368-5373.
- Rasche, M. E., M. R. Hyman., and D. J. Arp. 1991. Factors limiting aliphatic chlorocarbon degradation by *Nitrosomonas europaea*: cometabolic inactivation of ammonia monooxygenase and substrate specificity. *Appl. Environ. Microbiol.* 57: 2986-2994.
- Shah, N. N., M. L. Hanna, and R. T. Taylor. 1996. Batch cultivation of *Methylosinus trichosporium* OB3b:V. Characterization of poly- β -hydroxybutyrate production under methane-dependent growth conditions. *Biotechnol. Bioeng.* 49: 161-171.
- Semprini, L., P. V. Roberts, G. D. Hopkins, and P. L. McCarty. 1990. A field evaluation of in-situ biodegradation of chlorinated ethenes: Part 2. The results of biostimulation and biotransformation experiments. *Ground Water.* 28: 715-727.
- Strand, S. E., M. D. Bjelland, and H. D. Stensel. 1990. Kinetics of chlorinated hydrocarbon degradation by suspended cultures of methane-oxidizing bacteria. *Research Journal of the Water Pollution Control Federation.* 62: 124-129.
- Vancheeswaran, S., R. U. Halden, K. J. Williamson, J. D. Ingle, and L. Semprini. 1999. Abiotic and biological transformation of tetraalkoxysilanes and trichloroethene/cis-1,2-dichloroethene cometabolism driven by tetrabutoxysilane-degrading microorganisms. *Environ. Sci. Technol.* 33: 1077-1085.
- Vanginkel, C. G., H. G. J. Welten, S. Hartmans, and J. A. M. de Bont. 1987. Metabolism of trans-2-butene in *Nocardia* TB1. *Journal of General Microbiology.* 133: 1713-1720.
- van Hylckama Vlieg, J. E. T., W. de Koning, and D. B. Janssen. 1996. Transformation kinetic of chlorinated ethenes by *Methylosinus trichosporium* OB3b and detection of unstable epoxides by on-line gas chromatography. *Appl. Environ. Microbiol.*, 62: 3304-3312
- van Hylckama Vlieg, J. E. T., W. de Koning, and D. B. Janssen. 1997. Effect of chlorinated ethene conversion on viability and activity of *Methylosinus trichosporium* OB3b. *Appl. Environ. Microbiol.* 63: 4961-4964.

Vogel, T. L. and P. L. McCarty. 1987 Abiotic and biotic transformations of 1,1,1-trichloroethane under methanogenic conditions. *Environ. Sci. Technol.* 21: 1208-1213.

Wiegant, L. P. and J. A. M. de Bont. 1980. "A new route for ethylene glycol metabolism in *Mycobacterium* E44. *J. Gen. Microbiol.*, 120: 325-331.

CHAPTER 4

Kinetic and Inhibition Studies for Aerobic Cometabolism of 1,1,1-Trichloroethane, 1,1-Dichloroethylene, 1,1-Dichloroethane by a Butane-Grown Mixed Culture

SUMMARY

Batch kinetics of the aerobic cometabolism of chlorinated aliphatic hydrocarbons (CAHs) by a butane-grown mixed culture was investigated. This study focused on 1,1,1-trichloroethane (1,1,1-TCA), 1,1-dichloroethylene (1,1-DCE) and 1,1-dichloroethane (1,1-DCA), which are often found together as co-contaminants in ground water. The inhibition type was determined using direct linear plots at various substrate and inhibitor concentrations. The maximum degradation rates (k_{\max}) and half-saturation coefficients (K_s) were determined by performing single compound tests. Inhibition coefficients (K_{ic} and K_{iu}) were determined by nonlinear least squares regression (NLSR) fits to the inhibition model determined from the direct linear plots. Initial guesses of the kinetic parameters were determined from linearized equations that were derived from the correlations between apparent maximum degradation rates (k_{\max}^{app}) and/or the apparent half-saturation coefficient (K_s^{app}) and the k_{\max} , K_s and inhibitor concentration (I_L) in each inhibition equation. Good agreement was achieved between independently measured k_{\max} and K_s values and those obtained from the fitting of all parameters using inhibition study data. Two different inhibition types were observed among the compounds. Competitive inhibition among CAHs was

indicated from direct linear plots, and the CAHs were also competitively inhibited by butane. Mixed inhibition of 1,1,1-TCA, 1,1-DCA, and 1,1-DCE transformation by butane was observed. The initial guesses of all the kinetic parameters determined from linear plots were in the range of the values estimated from NLSR analysis. In the case of competitive inhibition between CAHs, the ratio of K_s values was a good indicator of competitive inhibition observed. However, the ratio of K_s values of CAH and butane were not a good indicator by the competitive inhibition of CAH on butane degradation. Butane was a strong inhibitor of CAH transformation, having a much lower inhibitor coefficients than the K_s value of butane, however, the CAHs were weak inhibitors of butane degradation. Overall the results show that use of the direct linear plot method to identify the inhibition type, coupled with initial guesses of parameters to provide initial guesses for NLSR analysis results in an accurate method for determining inhibition types and coefficients.

INTRODUCTION

Aerobic cometabolism of chlorinated aliphatic hydrocarbons (CAHs) has been widely studied with methane-, ammonia-, phenol- and toluene-oxidizing microorganisms (Alvarez-Cohen and McCarty, 1991c; Chang and Criddle, 1997; Ely et al., 1997; Folsom et al., 1990; Landa et al., 1994). Phenol- and toluene-utilizers effectively transform chlorinated ethenes, however, chlorinated methanes and ethanes such as 1,1,1-trichloroethane (1,1,1-TCA) are not effectively transformed (Chang and

Alvarez-Cohen, 1995b; Hopkins and McCarty, 1995). Methanotrophs expressing soluble methane monooxygenase (sMMO) effectively transformed 1,1,1-TCA, while those expressing particulate methane monooxygenase (pMMO) are not effective (Chang and Alvarez-Cohen, 1996; Oldenhuis et al., 1991). 1,1-DCE has been a problematic CAH to transform via aerobic cometabolism due to high transformation product toxicity (Anderson and McCarty, 1996; Dolan and McCarty, 1995; Hopkins and McCarty, 1995; Rasche et al., 1991). 1,1,1-TCA, 1,1-DCE and 1,1-DCA are often found together in groundwater, since 1,1-DCE and 1,1-DCA are produced abiotically and biologically from 1,1,1-TCA (Vogel and McCarty, 1987), and their wide use as a solvent also results in subsurface contamination. Thus, aerobic systems for effective transformation of 1,1,1-TCA and 1,1-DCE are of interest.

In my previous resting cell studies (Chapter 3), a butane-grown mixed culture had the ability to effectively transform 1,1-DCE, 1,1,1-TCA, and 1,1-DCA (Kim et al., 1999). Our butane-grown culture had a greater ability to transform 1,1,1-TCA on the basis of amount transformed per unit mass cells than a methane-grown mixed culture (Chang and Alvarez-Cohen, 1996). The initial transformation rates of 1,1-DCE were comparable with that achieved by *M. trichosporium* OB3b expressing sMMO (Oldenhuis et al., 1991), while the transformation capacity (T_c : maximum mass of CAH that can be transformed per mass of cells prior to inactivation) was a factor of 4 to 9 higher than achieved with methanotrophs (Chang and Alvarez-Cohen, 1996). Thus butane-utilizers have potential for remediating 1,1-DCE. 1,1-DCA was also very effectively transformed by the butane enrichment. Thus, this kinetic study focused on

the transformation of these contaminants and inhibition among the CAHs and butane, when mixtures are present.

For aerobic cometabolism, competitive inhibition is an important process to consider, since there is competition between CAHs and growth substrates for enzyme active sites due to lack of enzyme specificity. Cell growth rates and CAH transformation rates can be affected (Alvarez-Cohen and McCarty, 1991c; Anderson and McCarty, 1996; Dolan and McCarty, 1995). As presented in Table 2.4, competitive inhibition during aerobic cometabolism has been most widely proposed and successfully modeled with methane oxidizers, *N. europaea*, and *Pseudomonas cepacia* G4 (Anderson and McCarty, 1994, 1996; Chang and Alvarez-Cohen, 1995b; Chang and Criddle, 1997; Ely et al., 1997; Landa et al., 1994). However, different inhibition types have also been observed. Keener and Arp (1993) reported noncompetitive inhibition of chloromethane and chloroethane and competitive inhibition of methane and ethylene on NH_4^+ - dependent NO_2^- production in *N. europaea*. Keenan and co-workers (1994) reported that propane inhibited trichloroethylene (TCE) transformation which fitted a noncompetitive inhibition model. There, however, have been limited detailed studies of inhibition among CAHs and CAHs and growth substrates.

As presented in Table 2.4, many competitive inhibition models assume that the half-saturation coefficient (K_s) is equal to the competitive inhibition coefficient (K_{ic}) for given substrate/inhibitor (Alvarez-Cohen and McCarty, 1991c; Anderson and McCarty, 1996; Broholm et al., 1992; Chang and Alvarez-Cohen, 1995b; Strand et al., 1990). However, there has been some debate about the use of K_s as K_{ic} values (Chang

and Criddle, 1997; Landa et al., 1994). In studies of Chang and Criddle (1997) and Landa et al. (1994), the K_{ic} for growth substrate on TCE transformation was much smaller than the K_s for the substrate, and K_{ic} for TCE on growth substrate degradation was much greater than K_s for TCE.

Convenient linearized plots, especially Lineweaver-Burk plot, have been widely used to determine the inhibition type and estimate kinetic parameters (Alvarez-Cohen and McCarty, 1991c; Chang and Alvarez-Cohen, 1995b, 1996, 1997; Keener and Arp, 1993). Visual determination of inhibition type and the estimation of kinetic parameters from classical linear plotting is not straightforward as discussed in the literature review, Chapter 2 (Dowd and Riggs, 1965; Eisenthal and Cornish-Bowden, 1974; Robinson, 1985; Robinson and Charaklis, 1984).

In this study, the direct linear plot method of Eisenthal and Cornish-Bowden (1974) was used to determine the inhibition type. This method has several advantages over other convenient linearized plots such as Lineweaver-Burk and Hanse plot as discussed in Chapter 2. Nonlinear least squares regression (NLSR) analysis has been shown to be a better method for estimating the kinetic parameters than the convenient linearized plots (Robinson, 1985; Robinson and Charaklis, 1984).

Present here is a systematic kinetic and inhibition study for aerobic cometabolism of CAHs by a butane-grown mixed culture. The schematic diagram of the study is presented and discussed in Figure 2.13. Batch kinetic studies were performed to measure degradation rates at various substrates and inhibitor concentrations. To determine the inhibition types among the compounds, the direct linear plots were prepared using the measured rates. Initial estimates of all kinetic

parameters such as maximum degradation rates (k_{\max}), K_s , and competitive inhibition coefficient (K_{ic}), and uncompetitive inhibition coefficient (K_{iu}) were obtained from linearized equations presented in Table 4.1. Values determined from linear regression were used as initial guesses of NLSR analysis. The equation derivations are presented in Appendix B2 and plotting method is described in Chapter 2. The inhibition model determined by direct linear plots was fitted to the experimental rate data using NLSR analysis to obtain all the kinetic parameters.

MATERIALS AND METHODS

A Butane-Utilizing Mixed Culture

The butane-utilizing enrichment was obtained from Hanford soil microcosms as described in the Butane-Oxidizers section (Chapter 2). The enrichment was stained with 4' 6'-diamidino-2-phenylindole for living cells and propidium iodide for nonliving cells. Observation under a fluorescence microscope showed 1 to 2 μm long rods that form chains of up to two or three microorganisms (Figure 4.1). Gram stain test indicates that the larger cells (2 μm) are gram-positive and smaller cells (1 μm) are gram-negative.

The enrichment was batch grown in 750-mL capped-bottles containing 10%

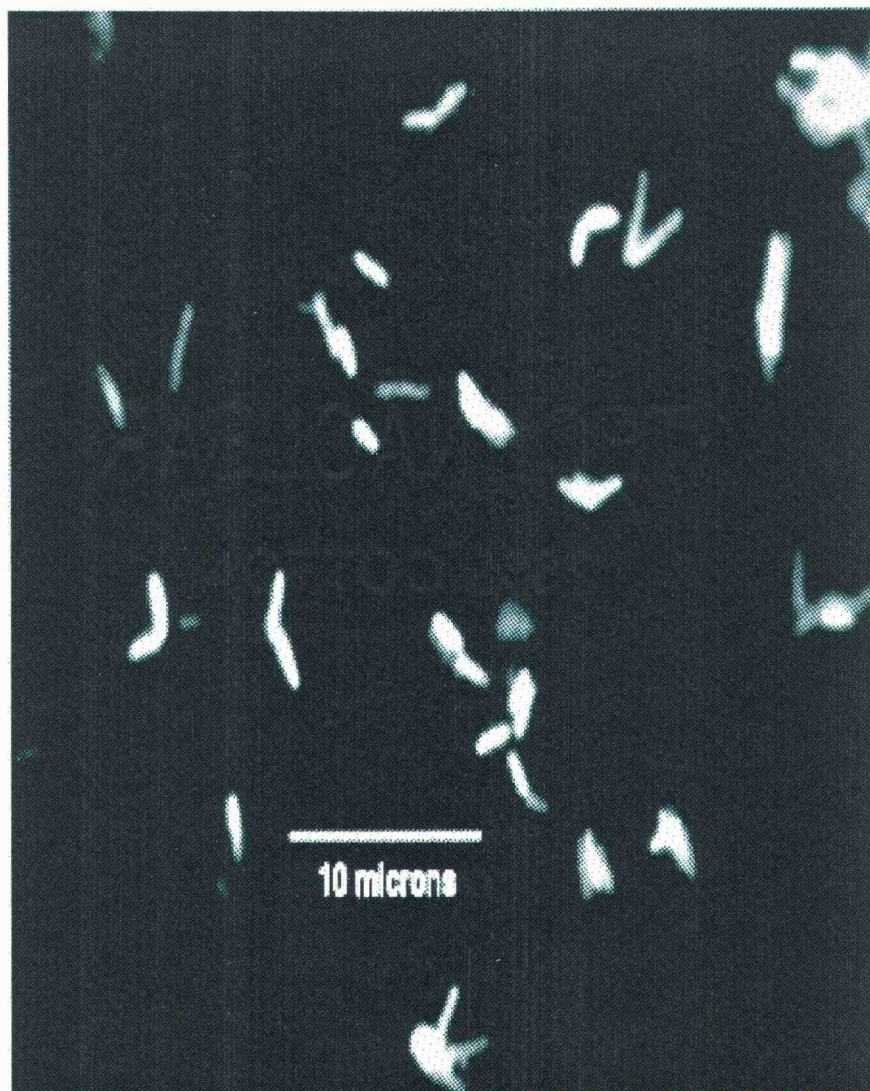


Figure 4.1. A butane-grown mixed culture viewed under a fluorescence microscope.

butane (vol/vol) in air and 250 mL of mineral medium, using *Xanthobacter* Py2 medium (Wiegant and de Bont, 1980), except NH_4NO_3 replaced NaNO_3 and the pH was adjusted to 7.3. Cells were harvested at an optical density of 0.6 @ 600 nm (OD_{600}) (approximately 0.1 mg TSS/mL) which is in the late exponential growth phase. In order to obtain a reproducible mixed culture the cells were washed and cell suspensions (1 mL) were added in autoclaved 2-mL cryogenic vials (Nalgene Company, Rochester, NY). Each vial received a total of 70 μL of dimethyl sulfoxide (DMSO), and was then stored in a cryogenic dewar containing liquid nitrogen (-80°C) to ensure a consistent inoculum for the sets of experiments. This method of storing cells showed stable activity in methanotrophic studies (Anderson and McCarty, 1996, 1997).

For the batch kinetic tests, the frozen cells were thawed, washed and rinsed three times to remove DMSO and grown on 10% butane (vol/vol) in air as previously described (Chapter 3). The batch growth reactors were incubated in the dark at 30°C while shaken at 210 rpm on a rotary table. Cells were harvested at OD_{600} of 0.6. The cells were concentrated by three cycles of centrifuging ($6,000 \times g$ for 15 minutes), washing and resuspending in the same media described above. Based on butane uptake activity, resting cell activity was stable for 10 hours after harvesting, thus all kinetic tests were performed within 10 hours of harvesting the cells.

Chemicals

Butane ($\geq 99\%$) and acetylene (99.6%) were purchased from AIRCO (Vancouver, WA). 1,1,1-TCA (99.5 % anhydrous) and 1,1-DCE (99%) were purchased from Aldrich Chemical Co. (Milwaukee, WI). 1,1-DCA, ($\geq 99\%$) was obtained from Acros Organics (Pittsburgh, PA).

Saturated aqueous stock solutions of CAHs were prepared at 20 °C by adding specific amounts of the pure liquid compound to 125-mL serum bottles containing autoclaved deionized water. This procedure eliminated the use of carrier solvents, such as methanol. The bottles were shaken for 6 hours prior to use to ensure saturation, and then allowed to settle for 6 hours before use. Butane was volumetrically transferred to the batch bottles using gas-tight syringes (Precision Sampling Corp., Baton Rouge, LA).

Analysis

The gaseous concentrations of butane and the CAHs of interest were determined by headspace analysis. The total compound mass in each test bottle was calculated, using the headspace and solution volumes and published Henry's constants (Gossett 1987; Mackay and Shiu, 1981). Calibration curves for all compounds were developed using external standards. Headspace concentrations of the CAHs and butane were determined by injecting 100 μL of the headspace sample into a HP5890 series gas chromatograph (GC) connected to a photoionization detector (PID)

followed by a flame ionization detector (FID) at 250 °C. The GC was operated at the following conditions: oven temperature, 190 °C; carrier gas (He) flow, 15 mL/min; H₂ flow to detectors, 35 mL/min; air flow to detectors, 165 mL/min; and FID detector makeup gas (He) flow, 15 mL/min. Chromatographic separation was performed with a 30-m megabore GSQ-PLOT column from J&W Scientific (Folsom, CA).

In mass transfer studies the measurement of aqueous phase 1,1-DCE concentrations was also required. EPA 8010 method was adapted and modified to measure aqueous 1,1-DCE concentrations using HP purge autosampler and HP trap concentrator. Aqueous samples (100 µL) were periodically taken from the batch bottles. Each sample was added to 5 mL of gas tight syringe with fixed luer lock (Alltech, Deerfield, IL) that was filled with 5 mL of deionized water, and injected to purge-tubes. Chromatographic separation was performed by HP 5890 series II GC with 0.25-mm x 30-m HP-624 capillary column. GC was operated the following conditions: oven temperature, 160 °C; carrier gas (helium) flow, 1.8 mL/min; and total hydrogen and helium flow; 130 mL/min. Detection was made on a Model 5220 electrolytic conductivity detector (ELCD) operating at 900 °C (OI analytical, College station, TX).

Culture density was determined as total suspended solids (TSS) (American Public Health Association 1985), using 0.1-µm-membrane filter (Micro Separation Inc., Westboro, MA). The OD₆₀₀ of cultures was measured using an HP8453 UV-Visible spectrophotometer.

Batch Experiments

Batch kinetic studies were performed using 26-mL glass vials at 20 °C. Autoclaved mineral medium (4.5 mL) described above was added to vials, and the vials were crimp sealed with Teflon™-lined rubber septa (Kimble, Vineland, NJ).

A volumetric amount of saturated aqueous stock solution of CAHs of interest or butane or both was added into the vials to achieve desired initial aqueous concentrations. The vials were shaken on a rotary shaker at 260 rpm to adjust temperature of medium to 20 °C. A headspace sample was taken to measure initial concentrations just before adding prepared cells, to initiate transformation reactions. After cell addition, the bottles were vigorously hand-shaken for 10 seconds, and then shaken at 260 rpm on a rotary shaker. Headspace concentrations were measured at five equally spaced time intervals over a period 10- to 20-min. Initial transformation/degradation rates were determined by linear regression of six temporal observations. Based on the results presented in Chapter 3, the amount of CAH transformed per cell mass for 30 hours were 2.4, 0.33, and 0.92 $\mu\text{mol/mg}$ TSS for 1,1-DCA, 1,1,1-TCA, and 1,1-DCE, respectively. In kinetic studies, the amount of CAHs transformed per mg TSS over the time period ranged from 5 to 21% of these values. Thus, the ratio of the amount of CAH transformed to mass of cells added was high enough that loss in cell activity resulting from CAH transformation was minimal and did not affect the transformation rate.

Procedures for performing inhibition studies followed batch kinetic test method described by Cornish-Bowden (1994). For single substrate kinetic test to

determine k_{\max} and K_s values, duplicate or triplicate vials were prepared at 10 different concentrations. For inhibition test the inhibitor was added at five different concentrations and four different substrate concentrations. The studies were prepared in single vials, thus 20 reactors were required for a test. Preliminary inhibition experiments were performed to determine the range of concentrations for use in the studies. Concentrations were chosen to achieve less than half of maximum rate with inhibitor present at its highest concentration.

Mass Transfer Experiments

In the kinetic studies, headspace analysis for CAHs and butane was performed to measure initial rates. To insure the Henry equilibrium partitioning could be applied to estimate liquid concentration mass transfer tests were performed under the conditions of kinetic experiment. The overall liquid-phase mass transfer rate coefficient (K_{LaL}) and the overall gas-phase mass transfer rate coefficient (K_{GaG}) were measured. 1,1-DCE was used, because it has the highest Henry's coefficient of the CAHs tested. Studies were performed to measure mass transfer of 1,1-DCE from the vapor to aqueous phase and also from the aqueous phase to the vapor phase. 1,1-DCE was added either to the aqueous phase or air phase of the batch reactor. After addition, the appearance of 1,1-DCE concentrations, rather than disappearance in the headspace or aqueous solution, was measured as a function of time until equilibrium was reached. The 1,1-DCE concentrations in the phases and their dependence on the

$K_L a_L$ and $K_G a_G$ in time are described by equations 4.1 and 4.2. The detailed derivations of equations of 4.1 and 4.2 are presented in Appendix A1.

$$\frac{dS_G}{dt} = -K_L a_L \left(\frac{S_G}{H_{cs}} - \frac{M_s}{V_L} + \frac{S_G V_G}{V_L} \right) \frac{V_L}{V_G} \quad (4.1)$$

$$\frac{dS_L}{dt} = -K_G a_G \left(H_{cs} S_L - \frac{M_s}{V_G} + \frac{S_L V_L}{V_G} \right) \frac{V_G}{V_L} \quad (4.2)$$

S_G is substrate concentration in gas phase (μM), S_L is substrate concentration in liquid phase (μM), M_s is total substrate mass in bottle (μmol), H_{cs} is dimensionless Henry's constant of substrate, V_L is volume of liquid phase (L), and V_G is volume of gas phase (L). Equation 4.1 and 4.2 can be solved to give equations 4.3 and 4.4, respectively, as presented in Appendix A1.

$$S_G = \frac{H_{cs} M_s}{H_{cs} V_G + V_L} + \left(S_{G,0} - \frac{H_{cs} M_s}{H_{cs} V_G + V_L} \right) \exp \left(-K_L a_L \left(1 + \frac{V_L}{V_G H_{cs}} \right) \cdot t \right) \quad (4.3)$$

$$S_L = \frac{M_s}{H_{cs} V_G + V_L} + \left(S_{L,0} - \frac{M_s}{H_{cs} V_G + V_L} \right) \exp \left(-K_G a_G \left(1 + \frac{V_G H_{cs}}{V_L} \right) \cdot t \right) \quad (4.4)$$

where t is time (min) and $S_{G,0}$ and $S_{L,0}$ are the concentrations at time zero. The experimental data was fit to analytical solutions of equations 4.3 and 4.4 by NLSR in

S-PLUS (MathSoft Inc., Cambridge, MA) to determine the K_{LaL} and the K_{GaG} for 1,1-DCE.

Acetylene Inactivation Experiment

As discussed in Chapter 2, acetylene is a mechanism-based inactivator of MMO, AMO, and BMO (Bedard and Knowles 1989; Prior and Dalton 1985; Hamamura et al., 1999). Different inactivation characteristics among different cultures have been reported by Hamamura et al. (1999), Keener et al. (1998), and Yeager et al. (1999). As presented in Chapter 3, CAH transformation was inhibited in acetylene-treated butane-grown mixed culture. These results suggest that acetylene inactivates the monooxygenase activity of the butane-grown mixed culture. An experiment to evaluate the loss of butane uptake activity upon exposure to acetylene as a function of time was performed. The experiment evaluates the kinetic diversity of butane-oxidizers in the mixed culture. If a plot of the log percent of enzyme activity remaining vs. time follows a single phase kinetic and/or fits to first order kinetic (as shown in Figures F1 and F2, Appendix F), it indicates the mixed culture consists of kinetically similar butane-oxidizers. However, if not (as shown Figure 2.3), the mixed culture may include kinetically very different butane-oxidizers.

In order to measure a time-dependent loss of butane uptake activity upon exposure to acetylene, 100 μ L acetylene (0.33% vol./vol. in headspace) was added into the 50-mL gastight syringe (Unimetrics No 7450, Folsom, CA) containing cell

suspension in media (20 mL) and air (30 mL). The syringe was sealed and hand-shaken throughout the experiment. Samples of the acetylene-treated cell suspension (1.5 mL) were taken as a function of time from the 50-mL gas tight syringe using 5-mL syringes. During the cell sampling, gas phase volume of 50-mL syringe was kept constant in order to keep the aqueous acetylene concentration constant throughout the experiment. The acetylene was removed from the samples by equilibrating with air and expelling air. The 1 mL cell suspensions were added into 26-mL batch bottles containing growth media (4 mL), butane (0.5 mL pure butane), and headspace air (22 mL). Initial butane degradation rates were measured as described above.

Determination of Inhibition Types

For batch kinetic and inhibition studies the Michaelis-Menten equation can be modified to include a mass balance between the air and aqueous phase, assuming equilibrium partitioning. Based on the results of our mass transfer experiments the assumption of equilibrium is valid over the time scale of the kinetic experiments. The validity of this assumption is discussed in detail in Appendix A.2.

$$v = \frac{-k_{\max}^{app} S_L}{K_s^{app} + S_L} \quad (4.5)$$

$$S_L = \left(\frac{M_s}{V_L + V_G H_{cs}} \right) \quad (4.6)$$

where v is substrate degradation rate ($\mu\text{mol}/\text{mg TSS}/\text{hr}$), k_{\max}^{app} and K_s^{app} are the apparent values of k_{\max} and K_s in the presence of inhibitor, respectively.

For each of the four inhibition types, competitive, uncompetitive, mixed and noncompetitive inhibition (Cornish-Bowden, 1994) inhibition model equation can be written by substituting k_{\max}^{app} and K_s^{app} presented in Table 4.1 into equation 4.5. Details of derivation of these equations are discussed in Appendix B1. In Table 4.1, I_L is inhibitor concentration in liquid phase (μM), M_i is total mass of inhibitor in bottle (μmol), H_{ci} is the inhibitor Henry's constant, and K_{ic} and K_{iu} are inhibition coefficients (μM). For purified enzymes with one substrate and an unreactive inhibitor, K_{ic} and K_{iu} are the equilibrium constants for inhibitor binding to the free enzyme (E) and the enzyme-substrate complex (ES), respectively (Cornish-Bowden, 1994). We assume that the kinetics for purified enzymes can be applied to whole cells.

The direct linear plot reported by Eisenthal and Cornish-Bowden (1974) and Cornish-Bowden and Eisenthal (1978) was used to determine the inhibition types. The advantages of this method over the least-square method are discussed in Chapter 2. Equation 4.5 may be rearranged to show the dependence of k_{\max}^{app} on K_s^{app} :

$$k_{\max}^{app} = v + \frac{v}{S_L} K_s^{app} \quad (4.7)$$

The plotting procedure is described in Chapter 2. Values of v on a vertical k_{\max}^{app} axis and the corresponding negative S_L are plotted on the horizontal K_s^{app} axis.

Table 4.1. The effects of inhibitors on the parameters of the Michaelis-Menten equation and linearized equations of the parameters.

Type of inhibition	k_{\max}^{app}	K_s^{app}	^a Linearized equation
Mixed	$\frac{k_{\max}}{(1 + \frac{I_L}{K_{iu}})}$	$\frac{K_s(1 + \frac{I_L}{K_{ic}})}{(1 + \frac{I_L}{K_{iu}})}$	$\frac{K_s^{app}}{k_{\max}^{app}} = \frac{K_s}{k_{\max}} + \frac{K_s}{k_{\max}K_{ic}}I_L$ $\frac{1}{k_{\max}^{app}} = \frac{1}{k_{\max}} + \frac{1}{k_{\max}K_{iu}}I_L$
Noncompetitive	$\frac{k_{\max}}{(1 + \frac{I_L}{K_{iu}})}$	K_s	$\frac{1}{k_{\max}^{app}} = \frac{1}{k_{\max}} + \frac{1}{k_{\max}K_{iu}}I_L$ $K_s = K_s^{app}$
Competitive	k_{\max}	$K_s(1 + \frac{I_L}{K_{ic}})$	$K_s^{app} = K_s + \frac{K_s}{K_{ic}}I_L$ $k_{\max} = k_{\max}^{app}$
Uncompetitive	$\frac{k_{\max}}{(1 + \frac{I_L}{K_{iu}})}$	$\frac{K_s}{(1 + \frac{I_L}{K_{iu}})}$	$\frac{1}{K_s^{app}} = \frac{1}{K_s} + \frac{1}{K_sK_{iu}}I_L$ $\frac{1}{k_{\max}^{app}} = \frac{1}{k_{\max}} + \frac{1}{k_{\max}K_{iu}}I_L$

a: The linearized equations are derived from the equations for k_{\max}^{app} and K_s^{app} to graphically evaluate the kinetic parameters that are used for initial guess of NLSR analysis. These parameters are derived in

Appendix B1. Note: $I_L = \left(\frac{M_i}{V_L + V_G H_{ci}} \right)$ where I_L is an inhibitor concentration in liquid phase (μM),

M_i is total mass of inhibitor in bottle (μmol), H_{ci} is a Henry's constant of inhibitor, K_{ic} and K_{iu} are inhibition coefficients (μM).

A line is drawn and extrapolated between the v and negative S_L . The coordinates of the intersection on lines define an unique pair of k_{\max}^{app} and K_s^{app} values that satisfy the

sets of observations. The medians of intersections provide estimates of k_{\max}^{app} and K_s^{app} .

As discussed in Chapter 2, the shift in the direction of best estimate point of k_{\max}^{app} and K_s^{app} at each value of I_L is an indicator of the inhibition type. For competitive inhibition, the shift is to the right; for uncompetitive inhibition, the shift is towards the origin; for mixed inhibition, the shift is between these extremes; and for the special case of mixed inhibition (noncompetitive inhibition), the shift is vertically down.

Determination of k_{\max} , K_s , and K_I

For single compound batch kinetic studies, k_{\max} and K_s were determined by fitting the data to equation 4.5 and 4.6 using NLSR. Initial estimates (guesses) of k_{\max} and K_s for NLSR routine were obtained by plots of rate versus substrate concentration.

In the inhibition study, k_{\max} , K_s , K_{ic} , and K_{iu} were determined by NLSR analysis for the inhibition model determined by direct linear plot. The linearized forms presented in Table 4.1 were used to obtain the initial guesses of all kinetic parameters for the NLSR fitting. The derivations of the linearized forms and the method of obtaining initial guesses from plots of linearized equations are provided in Chapter 2 and Appendix B2. For mixed inhibition model, good initial parameter

guesses are needed for NLSR method to converge. This is due to more complex kinetic expression with more parameters compared to the other kinetic equations.

RESULTS

Liquid and Gas Mass Transfer Coefficients

The rates of mass transfer achieved in the batch reactors under experimental conditions of the kinetic studies were determined by measuring the overall liquid-phase (Figure 4.2A) and gas-phase (Figure 4.2B) mass transfer rate coefficients of 1,1-DCE. An excellent match was obtained between the experimental results and model simulations using equations 4.3 and 4.4. Both the transfer from the liquid phase to the gas phase (Figure 4.2A) and from the gas phase to the liquid phase (Figure 4.2B) were modeled equally well. The K_{LaL} and K_{GaG} with 95% confidence intervals for 1,1-DCE were $1.3 \pm 0.1/\text{min}$ and $2.0 \pm 0.2/\text{min}$.

The K_{LaL} values for the other compounds studied were determined based on theoretical considerations. The K_{LaL} for a compound is dependent on its diffusivity and can be calculated by multiplying the K_{LaL} obtained for 1,1-DCE with the third root of the molecular weight of 1,1-DCE relative to the molecular weight of the compound of interest (Perry's chemical engineering handbook, 1984). The K_{GaG} also can be calculated by multiplying K_{LaL} by the dimensionless Henry's constant of interest

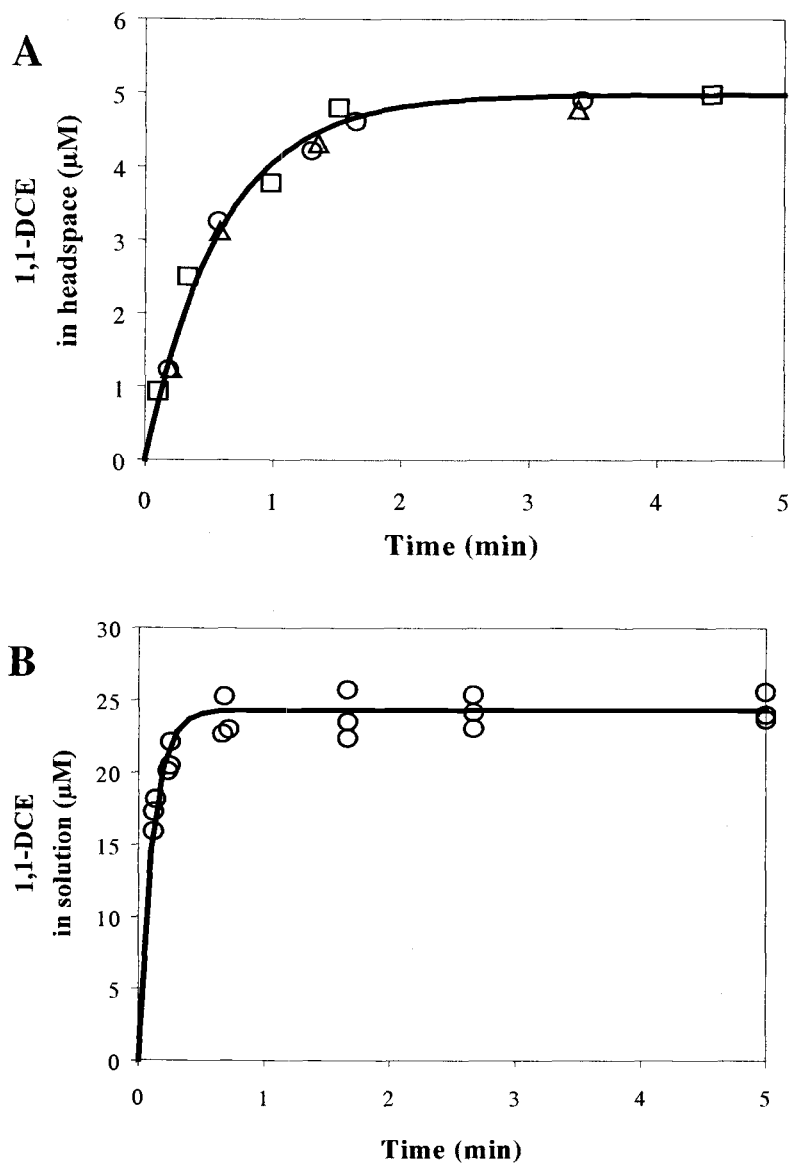


Figure 4.2. Determination of K_{LaL} (A) and K_{GaG} (B) for 1,1-DCE. The aqueous stock solution of 1,1-DCE was injected in the liquid phase (A), and gaseous 1,1-DCE was added in the headspace (B). The data were fit to equations 4.3 and 4.4. Input parameters: $H_{cc} = 0.86$; $V_L = 0.005$ L; $V_G = 0.021$ L; $C_{G,0} = C_{L,0} = 0$ μM ; and $M_{\text{tot}} = 0.13$ μmol (A) and 0.56 μmol (B).

Table 4.2. Overall mass transfer coefficients (K_{La} and K_{Ga}) for 1,1-DCE, 1,1-DCA, 1,1,1-TCA, and butane.

Compound	K_{La} (1/min)	K_{Ga} (1/min)
Butane	1.6	0.04
1,1-DCE	1.3 ± 0.1^a	2.0 ± 0.2 (1.5 ^b)
1,1-DCA	1.3	7.3
1,1,1-TCA	1.2	2.2

a: 95% confidence interval. ^b Value theoretically calculated.

compound. As shown in Table 4.2, the measured K_{GaG} for 1,1-DCE is in good agreement with the calculated value. The agreement indicates the theoretical calculations of K_{LaL} and K_{GaG} for the other compounds are reasonable.

In headspace reactors, mass transfer is required from the gas phase to the liquid, with the reaction occurring in the liquid phase. The analysis of the rate data is simplified if equilibrium partitioning can be inferred. Based on the estimates provided in Table 4.2, K_{GaG} for other CAHs was a factor of 40 to 200 greater than that for butane. The result indicates that butane was the most susceptible to mass transfer limitations.

In order to determine cell mass additions that achieve butane-utilization rates were not mass transfer limited, model simulations were performed and presented in Appendix A2. The initial rates were not mass transfer limited at cell concentrations lower than 13000 mg TSS/L, while the rates decreased due to mass transfer limitations at higher than the concentrations (Figure A2.2 in Appendix A2). The TSS was kept below 13000 mg TSS/L through all the studies so that the mass transfer limitations did not influence the initial rate measurements.

Acetylene Blocking Experiment

The acetylene inactivation experiment was performed to evaluate the kinetic diversity of butane-oxidizers in the mixed culture. The results of the acetylene inactivation experiment are presented in Figure 4.3. A progressive loss of butane uptake rate was observed as a function of time upon addition of acetylene to the 50 mL syringe. Residual butane uptake activity [rate at time t (r) to rate at time zero (r_0)] plotted as a function of time followed a single phase kinetic, and it fit a first-order

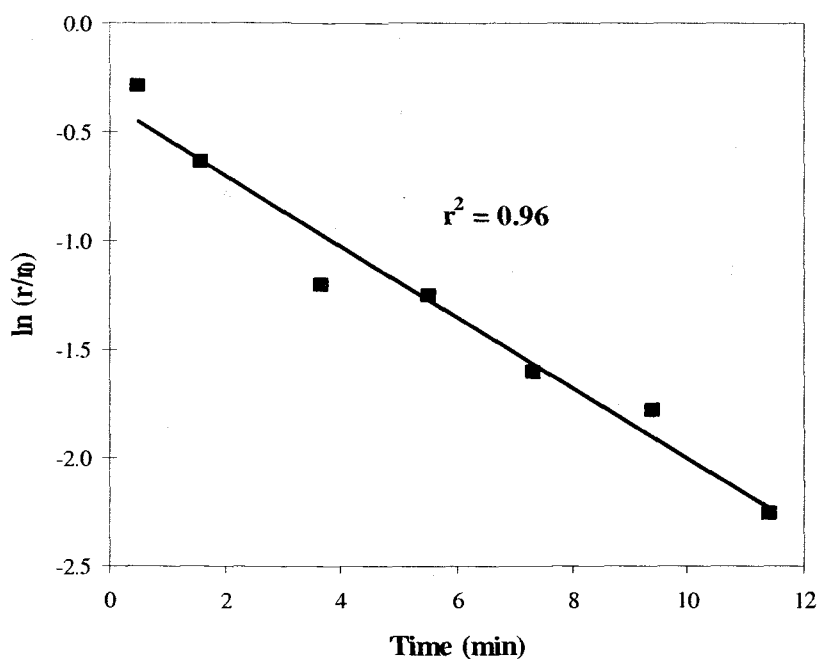


Figure 4.3. Decay of butane degradation rate as a function of time after acetylene exposure. Data were fit to first order decay model. r/r_0 indicates the ratio of the rate at time t to that at time zero.

kinetics model ($r^2 = 0.96$). Thus, the loss of butane uptake activity was time-dependent and followed first-order decay reaction model, consistent with observation of Keener et al. (1998) with nitrifying bacteria. This single-phase good fit indicates that kinetically similar monooxygenases are present in a butane-grown mixed culture.

k_{\max} and K_s for Butane, 1,1-DCE, 1,1-DCA, and 1,1,1-TCA

The results of the single compound tests to determine k_{\max} and K_s are provided in Figure 4.4. The measured degradation rates versus concentrations and best-fit curves to equation 4.5 achieved by NLSR as shown. The estimated k_{\max} and K_s along with their 95% confidence intervals and the pseudo first order rate ($k_1 = k_{\max} / K_s$) are summarized in Table 4.3. Excellent agreement to equation 4.5 was achieved, based on the 95% confidence intervals that were obtained. The order of k_{\max} from the highest to lowest was butane, 1,1-DCE, 1,1-DCA, and 1,1,1-TCA. The order of K_s from the highest to lowest was 1,1-DCA, butane, 1,1,1-TCA and 1,1-DCE. The K_s for 1,1-DCE was one order of magnitude lower than those for the other compounds, indicating that 1,1-DCE has a higher binding affinity to enzyme than the other compounds. The pseudo-first order rate coefficient k_1 for 1,1-DCE was greater than that for the other compounds.

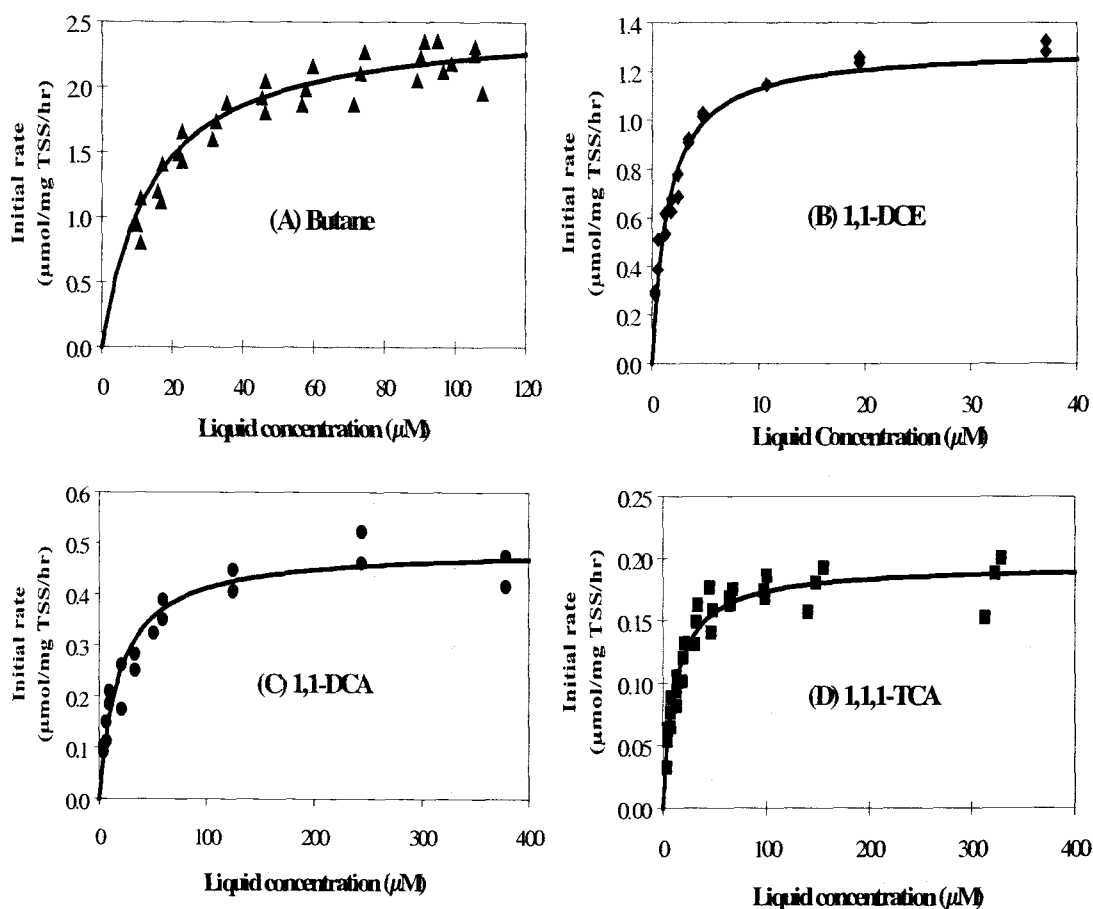


Figure 4.4. Initial degradation rates at various initial concentrations of butane (A), 1,1-DCE (B), 1,1-DCA (C), and 1,1,1-TCA (D). The curve represents the best fit of data to equation 4.5 using NLSR.

Table 4.3. k_{\max} and K_s with their 95% confidence intervals for butane, 1,1-DCE, 1,1-DCA, and 1,1,1-TCA.

	Butane	1,1-DCE	1,1-DCA	1,1,1-TCA
k_{\max} ($\mu\text{mol/mg TSS/hr}$)	2.6 ± 0.14	1.3 ± 0.09	0.49 ± 0.03	0.19 ± 0.01
K_s (μM)	19 ± 3.3	1.5 ± 0.39	19 ± 5.0	12 ± 2.8
k_{\max}/K_s (L/mg TSS/hr)	0.14	0.87	0.03	0.02

Inhibition Types and Inhibition Coefficients

Inhibition among CAHs

Inhibition types among CAHs were first investigated. The direct linear plot showing inhibition of 1,1-DCA on 1,1-DCE transformation is presented in Figure 4.5.

The points of intersection, shown as smaller symbols give the estimate of k_{\max}^{app} and

K_s^{app} . The best estimate of k_{\max}^{app} and K_s^{app} shown as the larger symbols are the

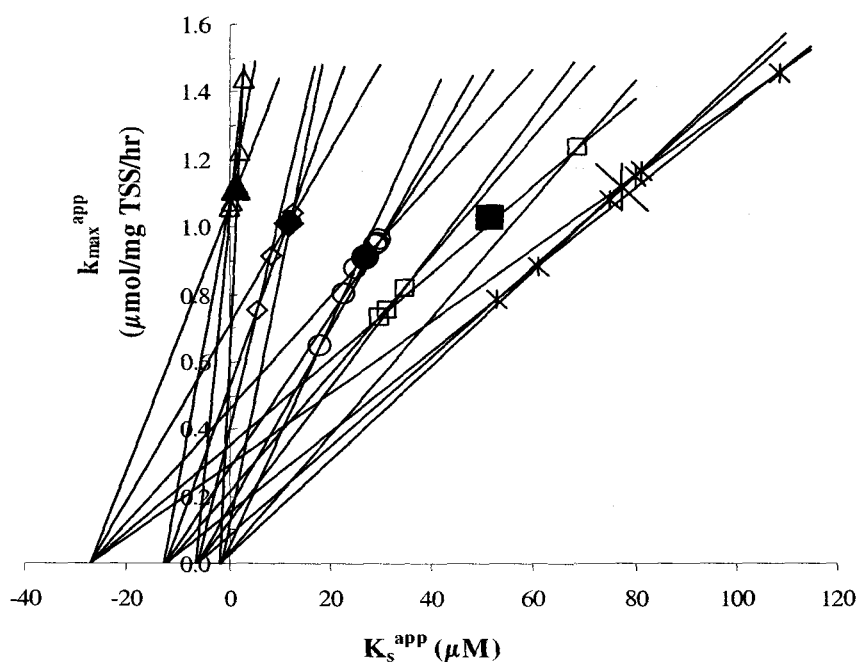


Figure 4.5. Direct linear plot showing competitive inhibition of 1,1-DCA on 1,1-DCE transformation. Aqueous 1,1-DCA concentrations were 0 (Δ), 153 (\blacklozenge), 387 (\bullet), 608 (\blacksquare), and 887 (\times) μM .

medians of the individual values at the various I_L concentrations (1,1-DCA). As inhibitor concentrations increased, the K_s^{app} for 1,1-DCE increased, while k_{max}^{app} for 1,1-DCE remained essentially constant, indicating competitive inhibition of 1,1-DCA on 1,1-DCE transformation.

The direct linear plot showing the inhibition of 1,1,1-TCA on 1,1-DCA transformation is presented in Figure 4.6A. Competitive inhibition of 1,1,1-TCA on 1,1-DCA transformation was also indicated. Kinetic parameters (K_{ic} and K_s) were graphically estimated by the plot of K_s^{app} versus I_L (Figure 4.6B). For the competitive inhibition model the plot of these variables should yield a linear correlation with K_s/K_{ic} equal to the slope and K_s equal to y intercept (Table 4.1). As shown in Figure 4.6B, a linear plot was achieved with r^2 value of 0.97. The regression yielded a K_s value of 15 μM for 1,1-DCA and a K_{ic} value of 12 μM for 1,1,1-TCA. The K_s value for 1,1-DCA was close to the value (19 μM) estimated from single compound kinetic test (Table 4.3). The k_{max} value of 1,1-DCA (0.46 $\mu\text{mol/mg TSS/hr}$) calculated by averaging the k_{max}^{app} values obtained from direct linear plot was also within the range of the value (0.49 $\mu\text{mol/mg TSS/hr}$) measured in single compound kinetic test (Table 4.3). The linear regression values of k_{max} , K_s , and K_{ic} were used as initial guesses in the NLSR fit of the experimental data.

All kinetic parameters (k_{max} , K_s , and K_{ic}) were determined by NLSR analysis of the measured rates with the competitive inhibition model determined by the direct linear plot. The data converged with very small residual standard error (RSE) of 0.012

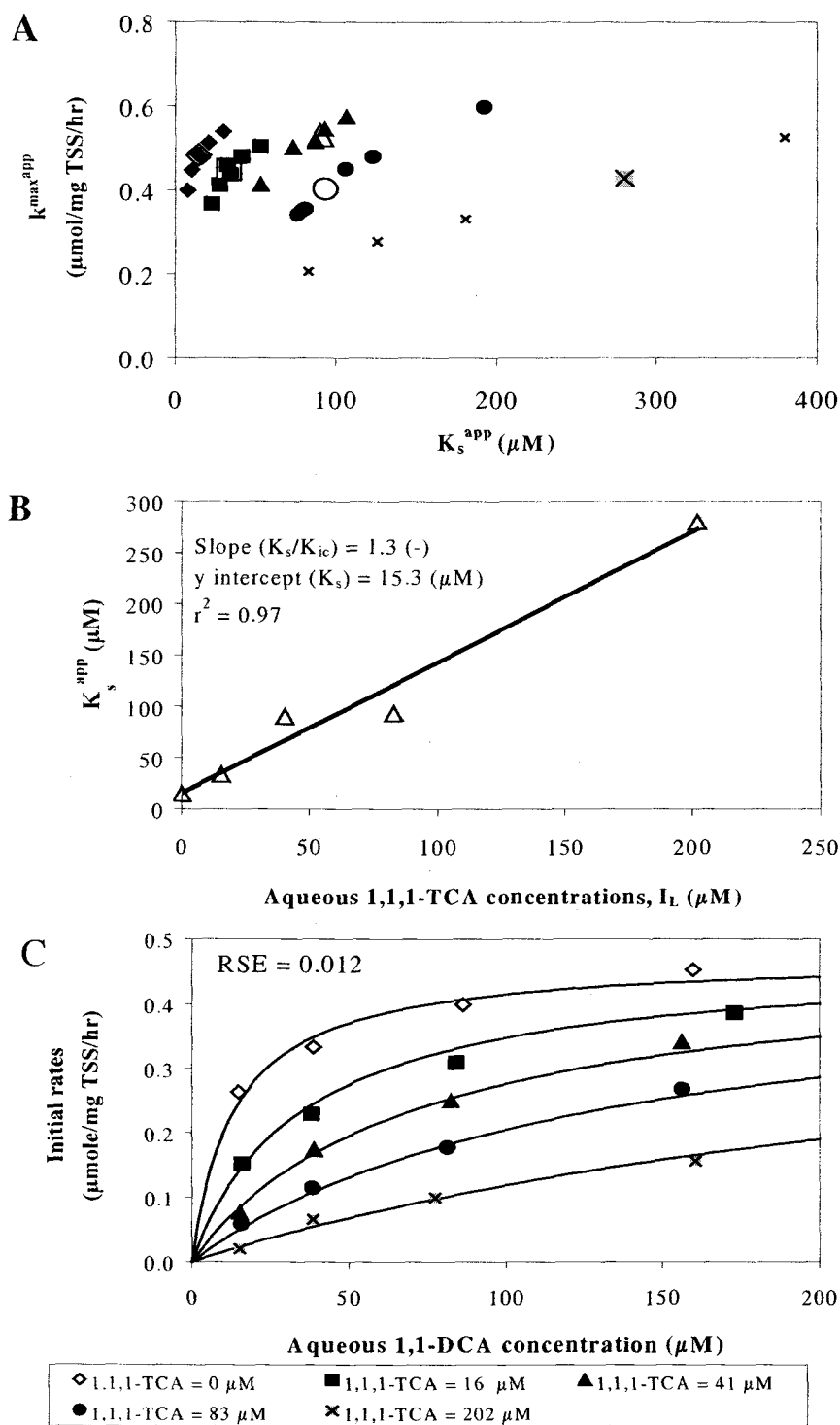


Figure 4.6. Direct linear plot showing competitive inhibition of 1,1,1-TCA on 1,1-DCA transformation (A), linearized plot of K_s^{app} vs. I_L to graphically evaluate K_s and K_{ic} (B), and the NLSR best fit of the data to the competitive inhibition equation (C).

(Figure 4.6C). NLSR yielded a K_{ic} value of $9.8 \pm 2.2 \mu\text{M}$ for 1,1,1-TCA, which was in the range of the linearized K_{ic} value of $12 \mu\text{M}$ used as initial guess (Table 4.5). In the experiments with the other CAHs, competitive inhibition was observed among CAHs, as shown in Table 4.4. The estimated inhibition coefficients with their initial guesses obtained from linear plot are presented in Table 4.5. The results of competitive inhibition studies among CAHs are presented in Appendices C5, C6, C8, C9, C11, and C12.

Table 4.4. Summary of determined inhibition types.

Substrate	Inhibitor			
	Butane	1,1-DCE	1,1-DCA	1,1,1-TCA
Butane	-	C ^a	C	C
1,1-DCE	M ^a	-	C	C
1,1-DCA	M	C	-	C
1,1,1-TCA	M	C	C	-

a: C indicates competitive inhibition. ^b:M indicates mixed inhibition.

CAH inhibition on butane

Figure 4.7A shows the direct linear plot of 1,1,1-TCA inhibition on butane degradation. The best estimates shift to the right with increasing inhibitor (1,1,1-TCA) concentrations, indicating competitive inhibition of 1,1,1-TCA on butane degradation. The linearized plot of K_s^{app} versus I_L (1,1,1-TCA) is shown in Figure

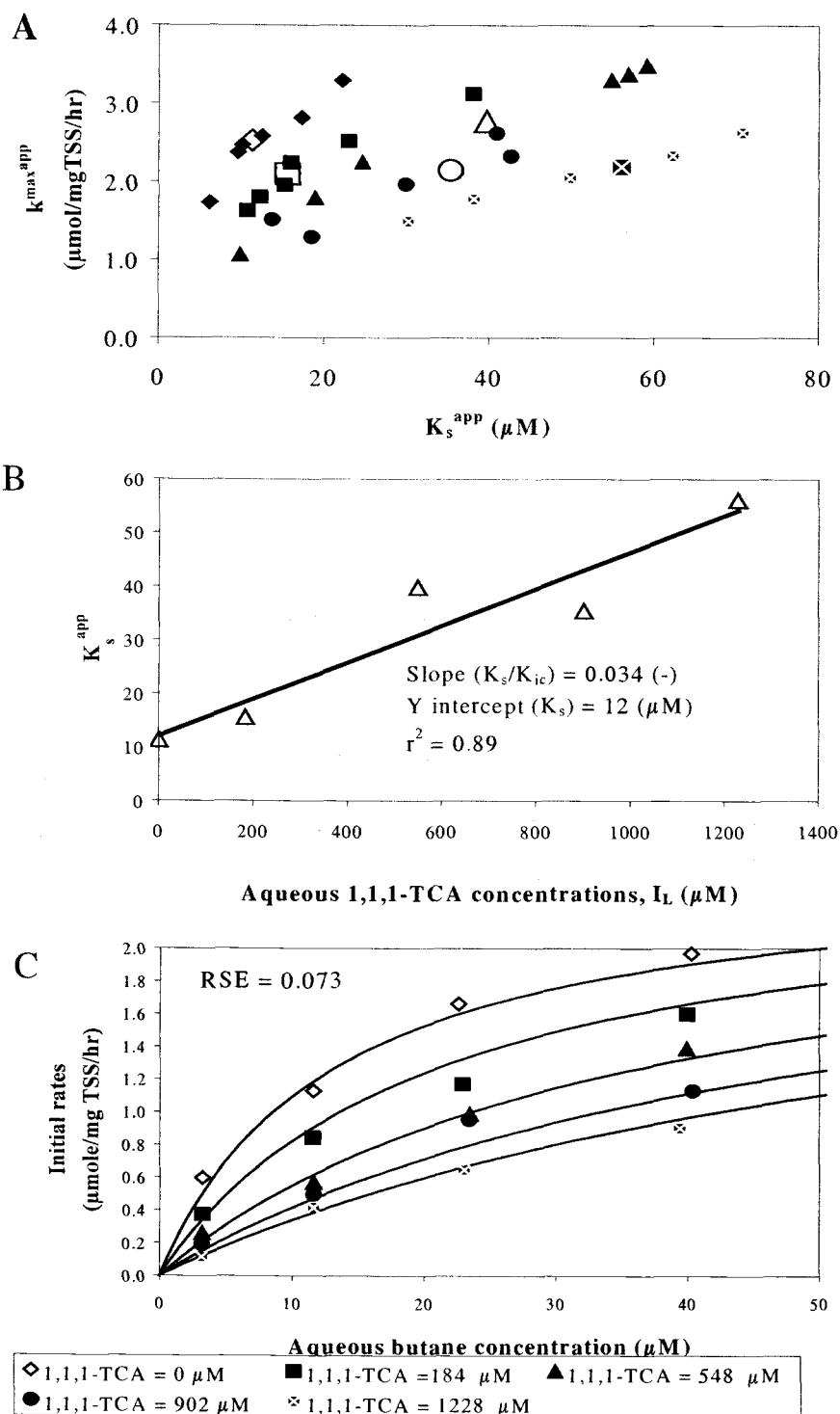


Figure 4.7. Direct linear plot showing competitive inhibition of 1,1,1-TCA on butane degradation (A), plot of K_s^{app} versus I_L to graphically evaluate K_s and K_{ic} (B), and the NLSR best fit of the data to the competitive inhibition equation (C).

4.7B. A linear plot was achieved with an r^2 value of 0.89. The regression yielded a K_s value of 12 μM for butane and a K_{ic} value of 364 μM for 1,1,1-TCA. The K_s value for butane is in good agreement with the value of 19 μM measured in single compound kinetic test (Table 4.3). The k_{\max} of 2.4 $\mu\text{mol/mg TSS/hr}$ based on average k_{\max}^{app} values is close to the measured value of 2.6 $\mu\text{mol/mg TSS/hr}$ obtained in single compound test (Table 4.3). NLSR analysis using competitive inhibition model with linearized kinetic parameters as initial guesses fit the observations very well (Figure 4.7C). The linearized value of K_{ic} (364 μM) for 1,1,1-TCA was close to the value of 313 μM obtained by NLSR analysis. As shown in Table 4.4, all CAHs competitively inhibited butane degradation. The results of all tests and the NLSR analyses are provided in Appendices C4, C7 and C10.

Butane inhibition on CAH

Inhibition of butane on each CAH was also evaluated. As shown in Figure 4.8A, k_{\max}^{app} and K_s^{app} of 1,1-DCA shifted with increasing inhibitor (butane) concentrations in the direction of decreasing k_{\max}^{app} and increasing K_s^{app} . This trend indicates mixed inhibition of butane on 1,1-DCA transformation. The kinetic parameters (k_{\max} , K_s , K_{iu} , and K_{ic}) were estimated by a linearized plot using the equations in Table 4.1 for the mixed inhibition case (Figure 4.8B). Excellent fits to

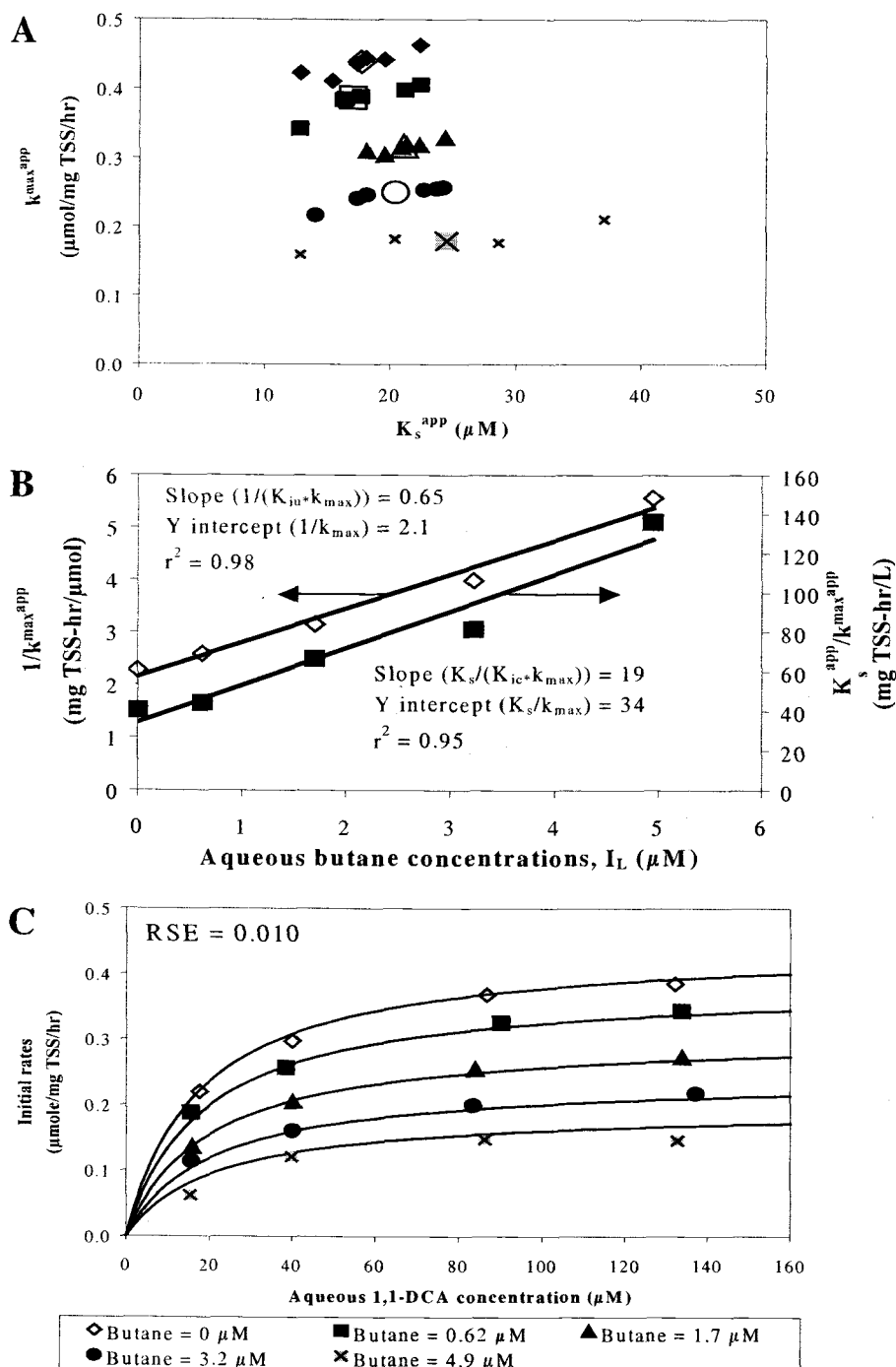


Figure 4.8. Direct linear plot showing mixed inhibition of butane on 1,1-DCA transformation (A), plot of $1/k_{max}^{app}$ or K_s^{app}/k_{max}^{app} versus I_L to graphically evaluate k_{max} , K_s , K_{ic} , and K_{iu} (B), and the NLSR best fit of the data to the mixed inhibition equation (C).

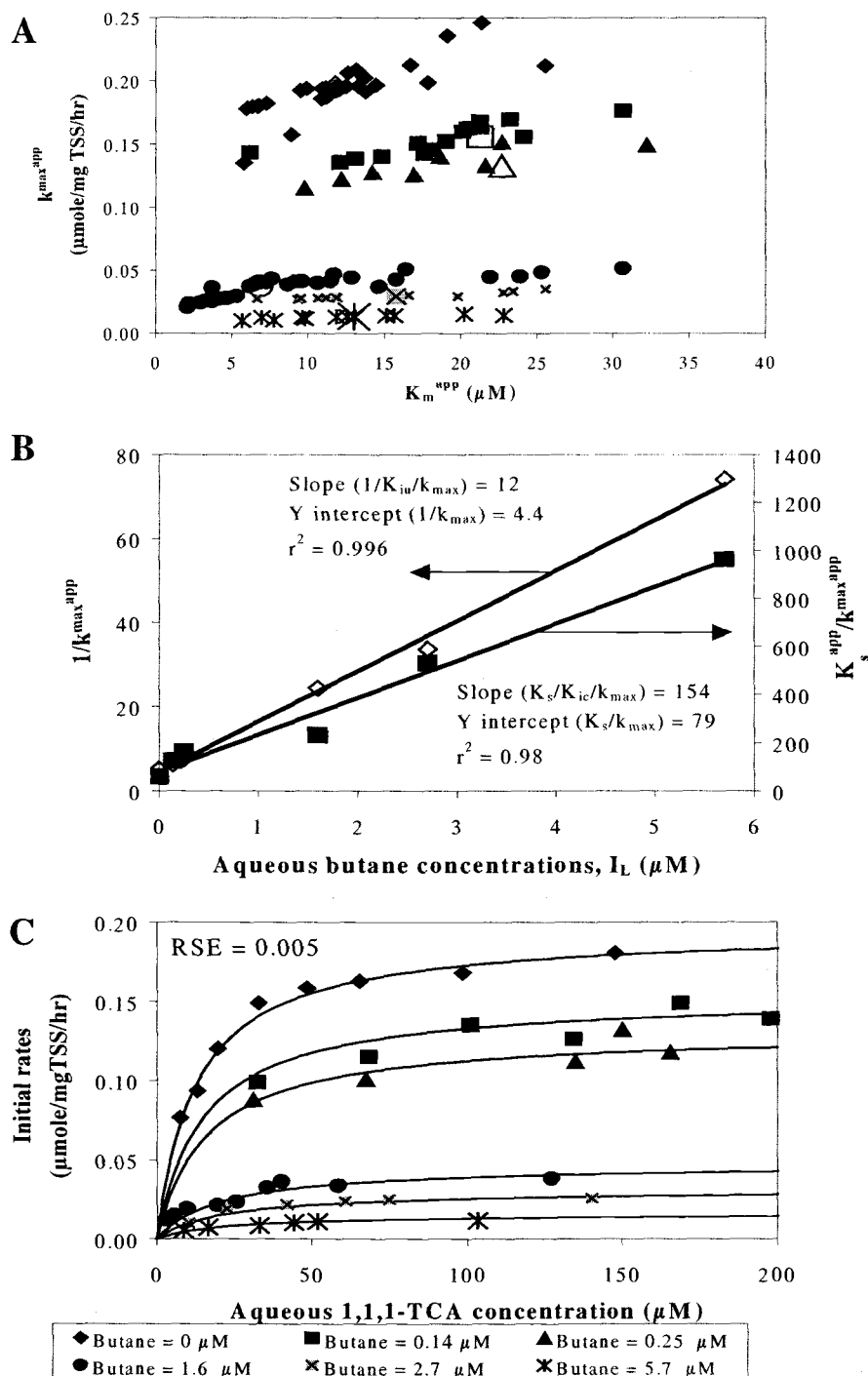


Figure 4.9. Direct linear plot showing mixed inhibition of butane on 1,1,1-TCA transformation (A), plot of $1/k_{\max}^{\text{app}}$ or $K_s^{\text{app}}/k_{\max}^{\text{app}}$ versus I_L to graphically evaluate k_{\max} , K_s , K_{ic} , and K_{iu} (B) and the NLSR best fit of the data to the mixed inhibition equation (C).

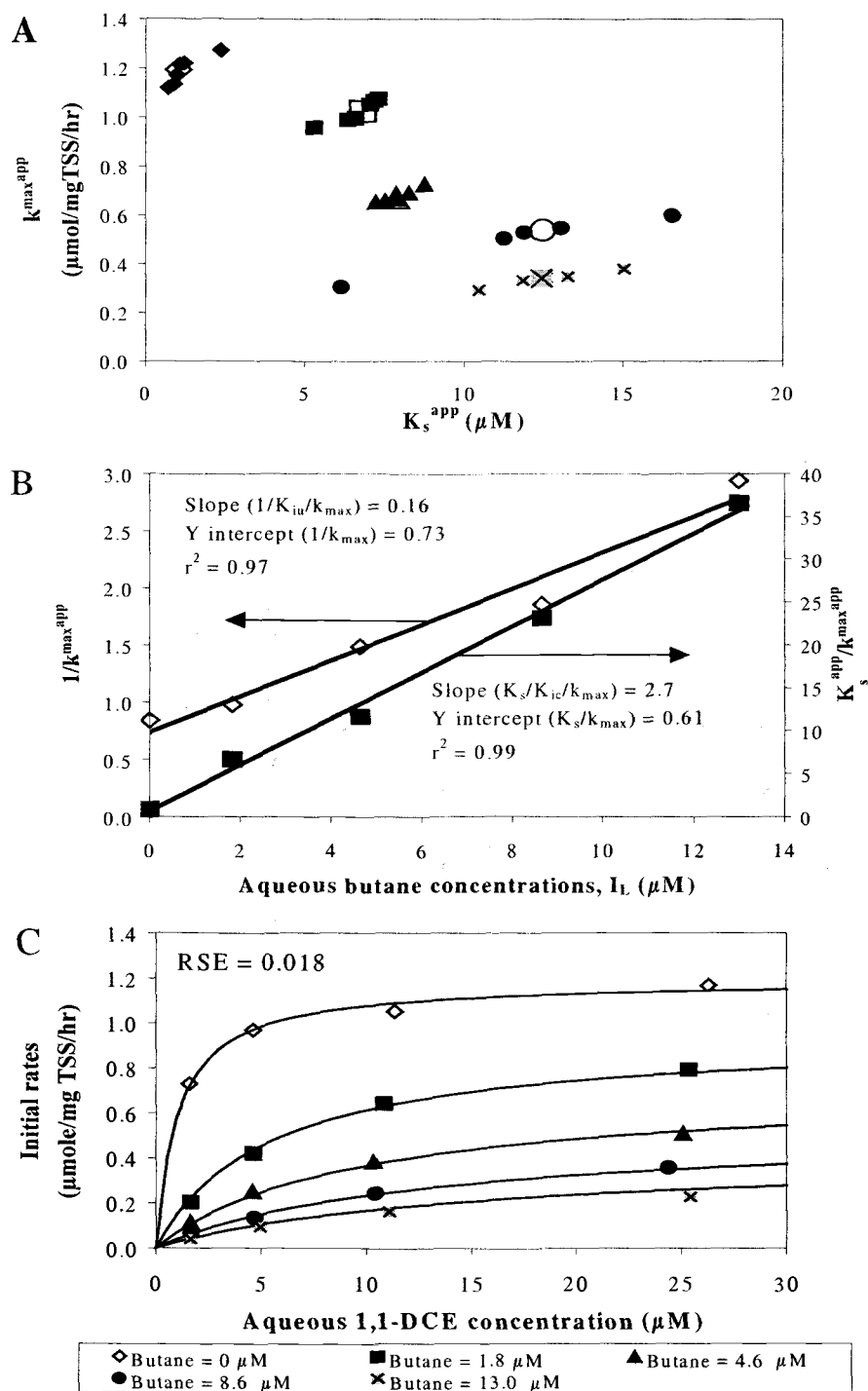


Figure 4.10. Direct linear plot showing mixed inhibition of butane on 1,1-DCE transformation (A), plot of $1/k_{max}^{app}$ or K_s^{app}/k_{max}^{app} versus I_L to graphically evaluate k_{max} , K_s , K_{ic} , and K_{iu} (B) and the NLSR best fit of the data to the mixed inhibition equation (C).

the linearized forms were obtained. The k_{\max} and K_s values for 1,1-DCA were 0.47 $\mu\text{mol/mg TSS-hr}$, and 16 μM , respectively, which agreed well with the values obtained in the single compound tests. K_{iu} , and K_{ic} for butane were, 3.3 μM , and 1.8 μM , respectively (Table 4.5). An excellent agreement by NLSR analysis to the mixed inhibition model is indicated (Figure 4.8C). Both inhibition coefficients were comparable with the values from the linear plot. Also, butane showed mixed inhibition on 1,1-DCE and 1,1,1-TCA transformation, as shown in Figure 4.9A and 4.10A. In both cases excellent fits to the linearized forms were obtained and the kinetic parameters obtained from linearized plots agreed well with the values obtained from single compound tests and NLSR analyses (Table 4.5 and Figure 4.11).

The data also fit the mixed inhibition model well. The detailed results of butane inhibition on 1,1,1-TCA and 1,1-DCE are provided in Appendices C1, C2 and C3. Although a negative value of K_{ic} for 1,1-DCA was obtained from the linearized plot for the case of 1,1-DCA inhibition on 1,1-DCE, inhibition coefficients values obtained from linearized plots generally well in good agreement with those estimated by NLSR analysis. As shown in Table 4.5, both inhibition coefficients (K_{ic} and K_{iu}) for butane are smaller than K_{ic} for CAHs, showing butane more strongly inhibits CAHs transformation. Among CAHs, K_{ic} for 1,1-DCE is smaller than for 1,1-DCA and 1,1,1-TCA, thus 1,1-DCE is a stronger inhibitor than the other CAHs. K_{ic} and K_{iu} for butane on 1,1,1-TCA and 1,1-DCA transformation were very similar. However, K_{iu} for butane on 1,1-DCE transformation was a factor of 20 higher than K_{ic} for butane on 1,1-DCE transformation, indicating that butane more competitively inhibited 1,1-DCE transformation.

Table 4.5. Inhibition coefficients estimated from linearized equation and NLSR analysis.

Inhibitor (Parameter)	Method	Substrate			
		Butane	1,1-DCE	1,1-DCA	1,1,1-TCA
Butane (K_{ic})	Linearized	-	0.23	1.82	0.52
	NLSR	-	0.33 ± 0.07^a	2.8 ± 1.60	0.28 ± 0.13
Butane (K_{iu})	Linearized	-	4.64	3.3	0.36
	NLSR	-	6.9 ± 1.6	3.8 ± 0.88	0.51 ± 0.09
1,1-DCE (K_{ic})	Linearized	12.8	-	8.6	0.95
	NLSR	8.7 ± 2.3	-	3.6 ± 1.5	1.1 ± 0.30
1,1-DCA (K_{ic})	Linearized	253	-16.3	-	9.6
	NLSR	403 ± 51	18 ± 4.9	-	16 ± 4.8
1,1,1-TCA (K_{ic})	Linearized	350	81	12	-
	NLSR	313 ± 88	17 ± 4.0	9.8 ± 2.2	-

a: The values of inhibition coefficients with their 95% confidence intervals are presented in μM .

Comparison of Kinetic Parameters Determined with Different Methods

Kinetic parameters were determined by different methods. k_{\max} and K_s were determined using single compound tests, and also through inhibition tests. In the inhibition tests, both linear plots and NLSR analyses that permitted all parameters to vary estimated k_{\max} , K_s , K_{ic} , and K_{iu} . Thus, the values determined by different methods can be compared. Figure 4.11 presents a comparison of k_{\max} (A) and K_s (B) determined by single compound tests, linearized equation plots, and NLSR analysis, using inhibition test data. In the case of the two latter methods, k_{\max} and K_s were the average of three values obtained from three inhibition studies (Appendix C13). While the K_s of butane determined by both the linear plots and NLSR analysis are slightly

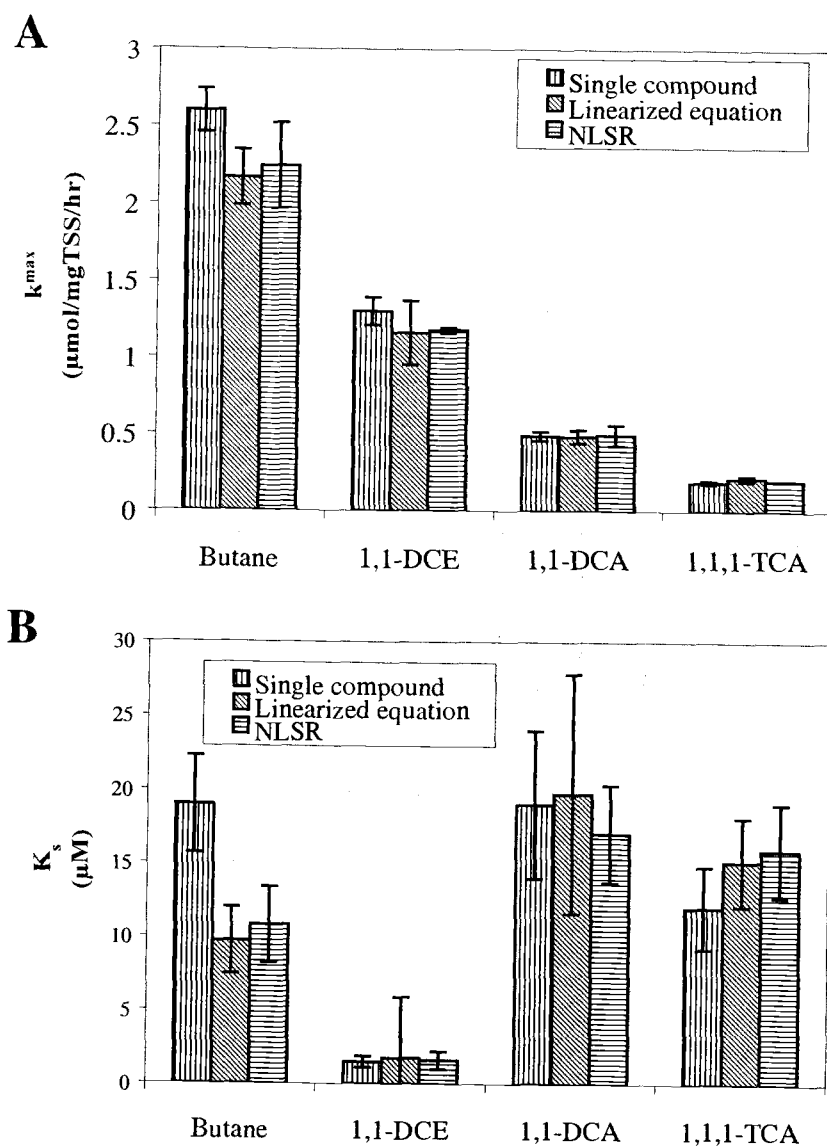


Figure 4.11 Comparison of k_{\max} and K_s that are separately estimated from single-compound batch kinetic studies, linear plots, and NLSR analysis using rate data in the presence of inhibitors. The error bars represent the 95% confidence intervals.

lower than the values obtained from the single compound tests, and K_s value of 1,1-DCE obtained from linearized plot has larger errors, all methods yielded very comparable K_s values for 1,1-DCE, 1,1-DCA, and 1,1,1-TCA. The k_{max} values determined by all three methods were in excellent agreement. The results suggest that k_{max} and K_s values can be very effectively determined by either the linear plot method, or NLSR analysis using initial guesses obtained from the linear plot.

Comparison of K_s with K_{ic}

To evaluate if the K_s value is a good indicator of competitive inhibition, the ratios of K_s of substrate over K_s of inhibitor and K_s of substrate over K_{ic} of inhibitor are compared (Figure 4.12). If K_s value is a good indicator of competitive inhibition, the slope of the linear regression line should be 1. The slope for data obtained from CAHs inhibition on butane was 0.17, however, the slope for data from inhibition among CAHs was 0.69. For the case of inhibition among CAHs, the slope was 1.3 when one outlier value at a high ratio was omitted. The results indicate that the ratios of K_s values of CAHs are good indicators for competitive inhibition among CAHs. However, for the case of CAH inhibition on the growth substrate degradation, the ratios of K_s values are not a good indicator of the observed competitive inhibition.

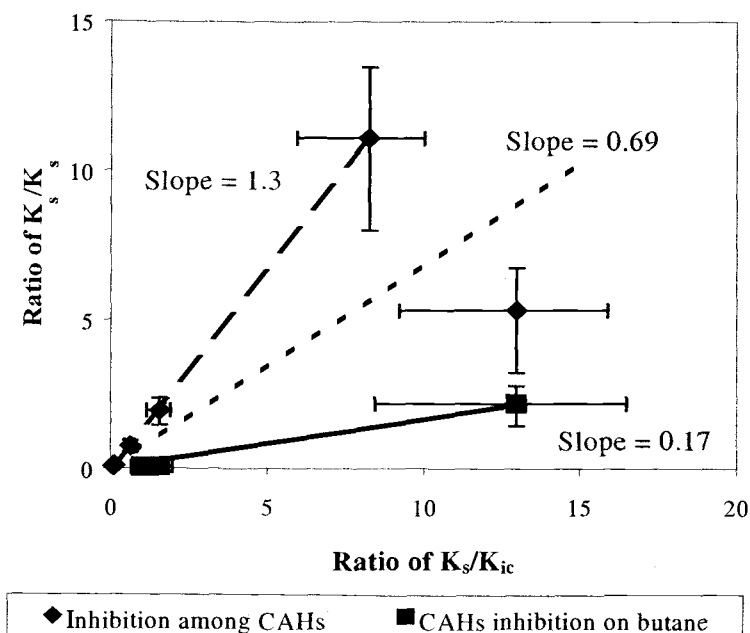


Figure 4.12 Comparison of the ratio of K_s of the substrate over K_s of the inhibitor and the K_s of substrate over estimated K_i of the inhibitor. The data obtained from competitive inhibition among the CAHs (◆) and the data obtained from competitive inhibition of CAHs on butane degradation (□) are separately fit by linear least squares regression.

Effects of k_{max} and/or K_s on Inhibition Coefficients in NLSR Analysis

In previous NLSR analysis all kinetic parameters in the inhibition equation were permitted to vary in obtaining the model fit to the experimental data. In order to evaluate how k_{max} and/or K_s affect on the determination of inhibition coefficients (K_{ic} and K_{iu}) during NLSR analysis, k_{max} and/or K_s obtained from the single compound tests were given as constants for the NLSR analysis. Four different ways of NLSR analyses were performed with the inhibition data: 1) varying all 4 kinetic parameters

(k_{\max} , K_s , K_{ic} , and/or K_{iu}); 2) constant k_{\max} and K_s and varying inhibition coefficients; 3) constant k_{\max} and varying K_s and inhibition coefficients; and 4) constant K_s and varying k_{\max} and inhibition coefficients.

Figure 4.13 presents comparison of butane inhibition coefficients, K_{ic} (A) and K_{iu} (B), determined with the four different NLSR analyses using initial guesses of the inhibition parameters from the linearized plot. In all cases of butane inhibition on CAHs, each NLSR analysis yielded estimated inhibition coefficients that were within the range of values determined by the other methods. These results suggest that prior determination of k_{\max} and/or K_s is not required for determining the inhibition coefficients (K_{ic} and K_{iu}). NLSR analysis with varying or constant k_{\max} and K_s yielded very comparable inhibition coefficients for butane, suggesting k_{\max} and K_s may be successfully estimated by NLSR analysis using inhibition data. The good agreement of k_{\max} and K_s values obtained using different methods, shown in Figure 4.11, indicate that this would be the likely result. The results of this analysis for the other compounds are presented in Table C13.5 and Figures C13.3, C13.4 and C13.5 (Appendix C13). All these results were very similar with those of butane inhibition on CAHs.

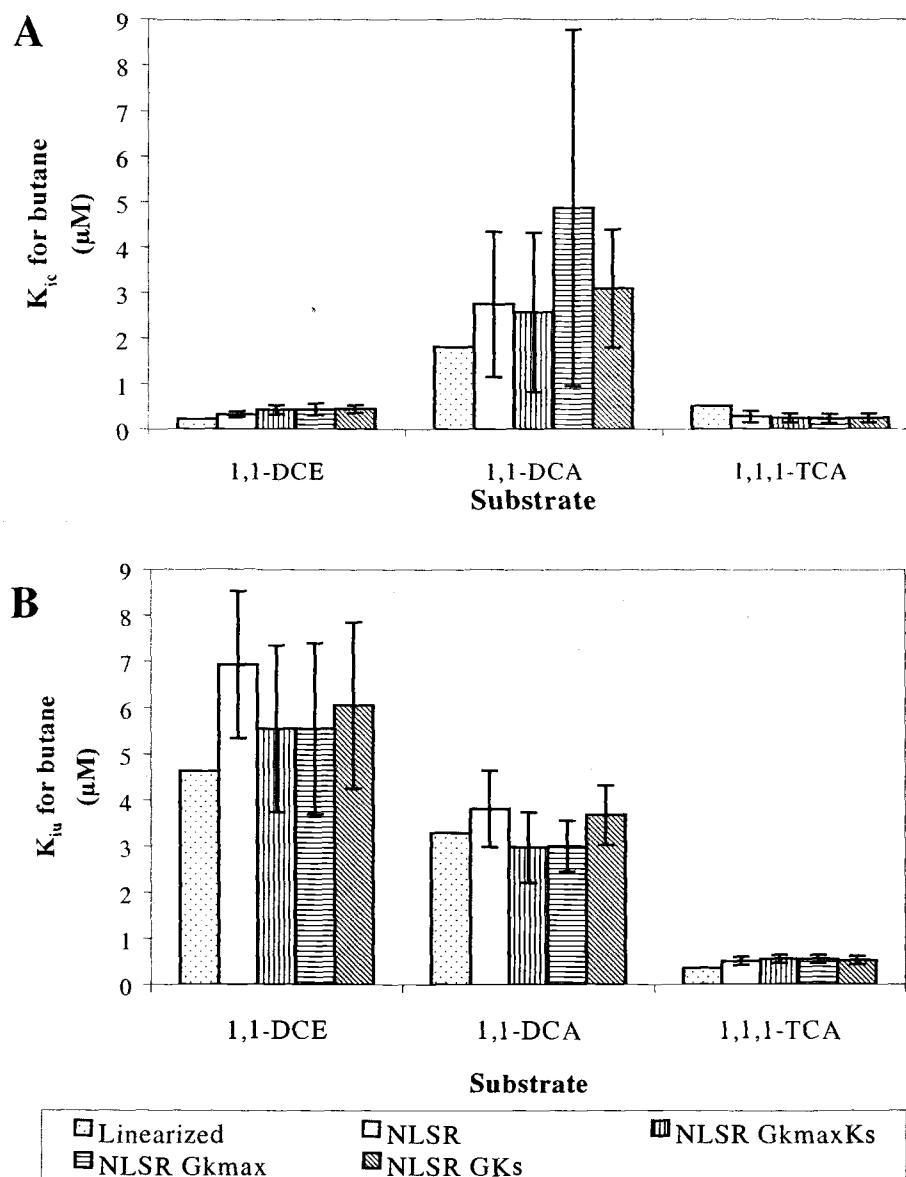


Figure 4.13. Comparison of butane inhibition coefficients, K_{ic} (A) and K_{iu} (B), determined by four different NLSR analyses along with values from the linearized plot. Linearized indicates linear plot; NLSR indicates NLSR with all 4 kinetic parameters varying (k_{max} , K_s , K_{ic} , and/or K_{iu}); NLSR GkmaxKs indicates NLSR with constant k_{max} and K_s and with 2 inhibition coefficients varying; NLSR Gkmax indicates NLSR with constant k_{max} and with K_s and inhibition coefficients varying; and NLSR GKs indicates NLSR with constant K_s , and with k_{max} and inhibition coefficients varying.

NLSR Analysis with Different Inhibition Models

In order to evaluate how the data fit to different inhibition models and how the models affect the estimated kinetic parameters, NLSR analysis using three different inhibition model equations was performed for all inhibition data. For this comparison all kinetic parameters were varied and minimized. This analysis evaluated how the data best fit by a mixed inhibition model would be fit using a competitive inhibition model and vice versa. Evaluations were also made on how the data fit by a mixed inhibition model would be fit a noncompetitive inhibition model.

Figure 4.14A presents kinetic coefficients determined by NLSR analysis using mixed, noncompetitive and competitive inhibition models for the case of butane inhibition on 1,1-DCA transformation. The best data fit to the noncompetitive inhibition model and competitive inhibition model are presented Figure 4.14B and Figure 4.14C, respectively. As described previously, butane showed mixed inhibition on 1,1-DCA transformation. The data could also be well fit to noncompetitive inhibition model, having the same RSE of 0.010 as mixed inhibition fit. The k_{\max} , K_s , and K_{iu} were in the range of the values determined from fit the to mixed inhibition model. The reason for good fit of the noncompetitive inhibition model is that K_{ic} and K_{iu} for butane were very close, thus K_s^{app} is equal to K_s resulting in noncompetitive inhibition model as shown in Table 4.1. This result is consistent with the near vertical shift in k_{\max} shown Figure 4.8. Data for mixed inhibition of butane on 1,1,1-TCA transformation were also well fit to the noncompetitive inhibition model with RSE of 0.005 (Figure D3.2 in

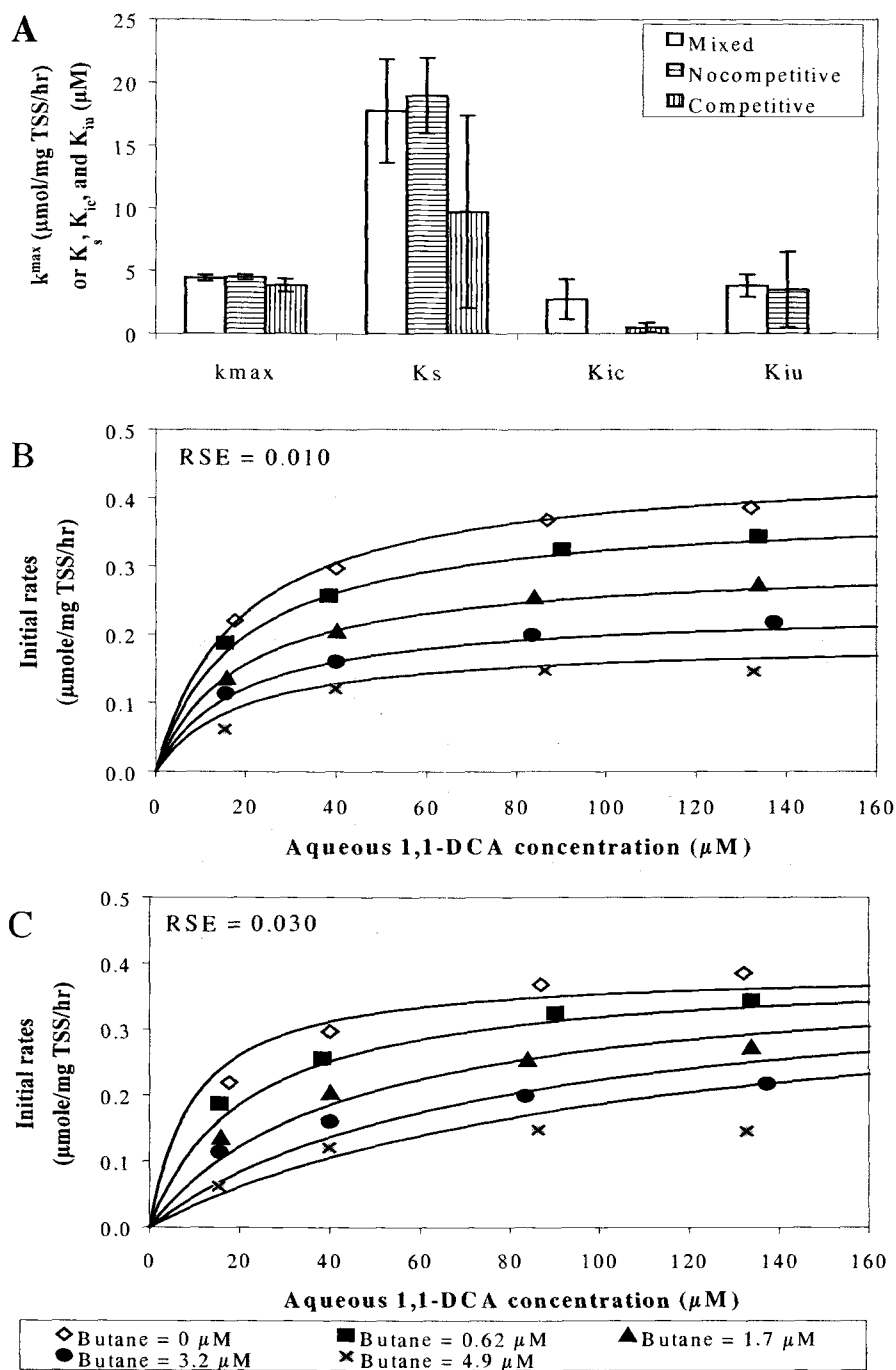


Figure 4.14. Kinetic coefficients determined by NLSR analysis using mixed, noncompetitive, and competitive inhibition models for the case of butane inhibition on 1,1-DCA transformation (A), the best fit of the data to the noncompetitive inhibition model (B), and the competitive inhibition model (C). The k_{\max} values in panel (A) are presented by multiplying the estimated values by a factor of 10.

Appendix D3). Comparable values of k_{\max} and K_s for 1,1,1-TCA with the values determined from fitting the mixed inhibition (Table D3.1 in Appendix D3). The data fit noncompetitive inhibition model well for the same reasons as the 1,1-DCA data. This is also consistent with the near vertical shift in k_{\max} in Figure 4.9.

Data when fit to competitive inhibition model resulted in a higher RSE than those achieved with the mixed and noncompetitive inhibition models. The poorer fit is evident in Figure 4.14C. The k_{\max} , and K_s for 1,1-DCA and K_{ic} for butane were within the range of the values obtained using the mixed inhibition model, however, K_s for 1,1-DCA and K_{ic} for butane converged with higher standard errors than those obtained with mixed and noncompetitive inhibition models. Similar results were observed when butane inhibition on 1,1,1-TCA transformation was modeled (Table D3.1 and Figure D3.3 in Appendix D3).

Figure 4.15A presents kinetic coefficients determined by NLSR analysis using mixed, noncompetitive, and competitive inhibition model for the case of butane inhibition on 1,1-DCE transformation. Fits to the noncompetitive inhibition model and competitive inhibition model are presented in Figure 4.15B and Figure 4.15C, respectively. As described previously, butane showed mixed inhibition on 1,1-DCE transformation. The K_{iu} of butane was a factor of 20 greater than K_{ic} in the case of

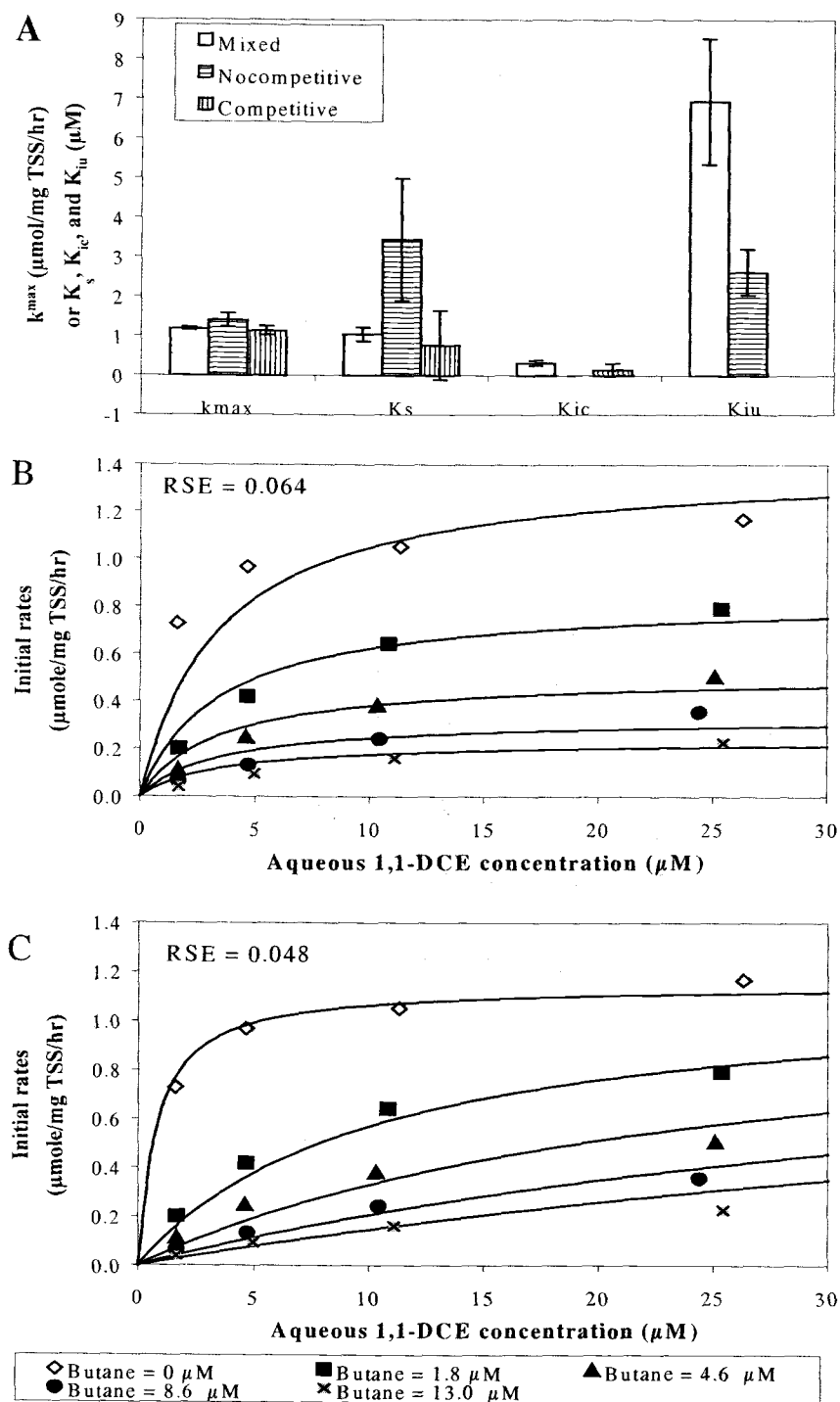


Figure 4.15. Kinetic coefficients determined by NLSR analysis using mixed, noncompetitive and competitive inhibition models for the case of butane inhibition on 1,1-DCE transformation (A), the best fit of the data to the noncompetitive inhibition model (B), and the competitive inhibition model (C).

butane inhibition on 1,1-DCE, which is indicated by shifts shown in Figure 4.10A. Data were better fit to competitive inhibition model than noncompetitive inhibition model, based on RSE. The competitive inhibition model yielded k_{\max} and K_s that were in the range of the values determined using the mixed inhibition model. The noncompetitive inhibition model resulted in very similar k_{\max} to those determined using the mixed inhibition model, however the K_s was a factor of 2.5 greater than the value estimated using mixed inhibition model. The reason for better fit to competitive inhibition model than noncompetitive inhibition is that the K_{iu} of butane was a factor of 20 greater than K_{ic} , thus butane more competitively inhibited 1,1-DCE transformation.

Figure 4.16A presents kinetic coefficients determined by NLSR analysis using mixed, noncompetitive, and competitive inhibition models for the case of 1,1-DCA inhibition on 1,1-DCE transformation. The mixed inhibition and the noncompetitive inhibition model fits are shown in Figure 4.16B and Figure 4.16C, respectively. The competitive inhibition fit of 1,1-DCA on 1,1-DCE transformation is shown in Figure C8.3. The k_{\max} and K_s values were in the range determined using the competitive inhibition model. For the case of mixed inhibition model, K_{ic} was in the range determined using the competitive inhibition model. However, the estimated K_{iu} value was a factor of 37 greater than K_{ic} , and K_{iu} had much greater error than the K_{ic} estimate. Data showing competitive inhibition may be represented by a mixed inhibition model having a very high K_{iu} to compensate for the inhibitor effect on K_{\max} .

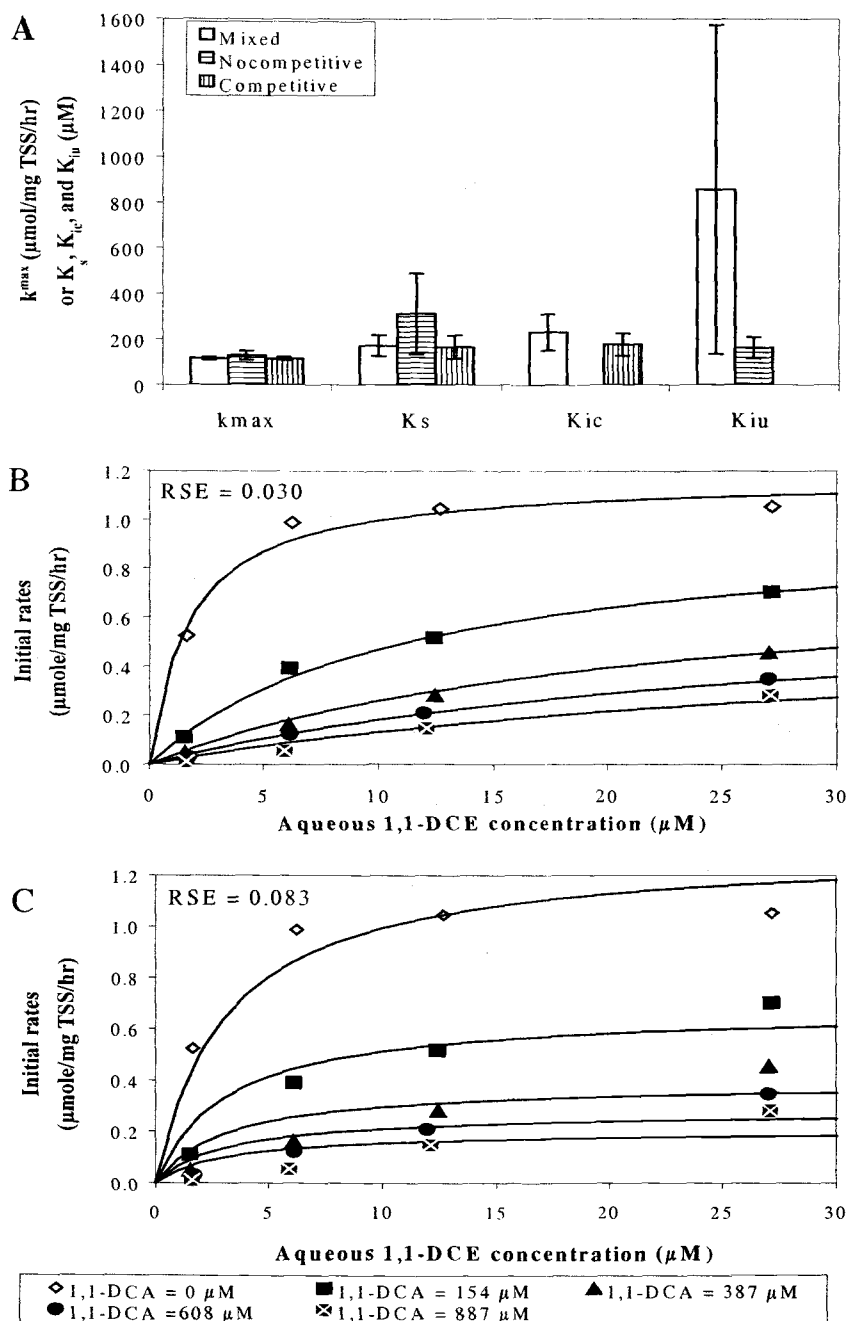


Figure 4.16. Kinetic coefficients determined by NLSR analysis using mixed, noncompetitive, and competitive inhibition models for the case of 1,1-DCA inhibition on 1,1-DCE inhibition (A), the best fit of the data to the mixed inhibition model (B), and the noncompetitive inhibition model (C). The values for k_{max} , K_s and K_{ic} in panel (A) are presented by multiplying the estimated values by a factor of 100, 100 and 10, respectively.

When the K_{iu} value is much greater than K_{ic} value, the mixed inhibition model equation can be expressed using the competitive inhibition model equation, as shown in Table 4.1. Most of the competitive inhibition data showed similar results, and the data when fit to mixed inhibition model resulted in a K_{iu} that compensated for the inhibitor affect on K_{max} . Some of the competitive inhibition data when fit to the mixed inhibition model resulted in negative values for the kinetic parameters or inhibition coefficients or both (Appendices D4 through D12).

The results of NLSR analysis using three different inhibition models suggest that, in some cases, inhibition type can not be conclusively determined by the fit error analysis.

DISCUSSION

Practical applications of CAHs groundwater clean-up via aerobic cometabolism will likely involve the use of mixed cultures rather than pure cultures or purified enzymes. Thus, kinetic studies, rate models, and parameters obtained with mixed cultures are needed. The results of this study showed inhibition models and kinetic parameters could be reproducibly studied using a butane-grown mixed culture. The method of a reproducibly grown mixed culture from a stock of culture frozen at -80°C , worked well for this purpose.

This study investigated inhibition kinetics for the aerobic cometabolism of 1,1-DCE, 1,1-DCA and 1,1,1-TCA, by a butane-grown mixed culture. The method that combined both direct linear plots to identify the inhibition type and NLSR analysis to

estimate the kinetic parameters (using graphically estimated kinetic parameters as initial guesses) proved to be very effective.

The kinetic results can be compared to other systems. The kinetic parameters for 1,1-DCE and 1,1,1-TCA were determined with *M. trichosporium* OB3b producing sMMO (Oldenhuis et al., 1991). The K_s for 1,1-DCE measured here is a factor of 4 lower than that reported by Oldenhuis et al. (1991), while k_{max} for 1,1-DCE is a factor of 5 greater. The greater k_{max} and lower K_s indicates that the butane-grown culture has a higher affinity for 1,1-DCE than *M. trichosporium* OB3b. The K_s for 1,1,1-TCA measured here was a factor of 20 lower than the value they reported, while k_{max} is an order of magnitude lower. Thus, this comparison suggests that the butane-grown culture also has higher affinity for 1,1,1-TCA, but slower maximum transformation rates.

With respect to in situ cometabolism of CAH, the contaminant concentrations are often much lower than the K_s . Thus, the pseudo first-order rate, k_1 is a more important parameter. The k_1 for 1,1-DCE measured here is a factor of 4 greater than the value for *M. trichosporium* OB3b expressing sMMO, and two orders of magnitude greater than achieved with pMMO (Oldenhuis et al., 1991; van Hylckama Vlieg et al., 1996). The k_1 for 1,1,1-TCA obtained with our enrichment is comparable to that with *M. trichosporium* OB3b (Oldenhuis et al., 1991). The k_1 with methane- or propane-grown mixed culture studied by Strand et al. (1990) and Keenan et al. (1994) is 2 to 4 orders of magnitude lower than observed here. Thus, the butane-grown culture studied here has potential advantages for bioremediation of 1,1-DCE and 1,1,1-TCA.

The identification of inhibition types and the estimated kinetic parameters are often not easy to determine using graphical analysis, such as Lineweaver-Burk, Woolf, and Eadie-Hofstee plots (Dowd and Riggs, 1965; Eisenthal and Cornish-Bowden, 1974; Robinson, 1985; Robinson and Charaklis, 1984). The problem of discriminating between competitive inhibition and the limiting case of mixed inhibition was discussed in detail by Eisenthal and Cornish-Bowden (1974). They argued against the use of graphical plots using linearized equations for diagnostic purposes.

However, the method performed here involved combining direct linear plot, linearized plot, and NLSR analysis for better indication of the type of inhibition was very effective. An example is shown in Figure 4.6. The data suggests competitive inhibition is the dominant form, but mixed inhibition can not be completely ruled out. When nonlinear curve fitting using competitive and mixed inhibition model was performed with these data, the mixed inhibition model fit the observations with a K_{iu} a factor of 170 greater than K_{ic} , suggesting that it is likely competitive inhibition. As shown in Figure E2.9 (Appendix E), when the data were used in linearized plots using mixed inhibition model equations (K_s^{app}/k_{max}^{app} or $1/k_{max}^{app}$ v s. I_L), an r^2 value of 0.99 was achieved for the plot of K_s^{app}/k_{max}^{app} vs. I_L . However, a linear plot was achieved with an r^2 value of 0.26 from the plot of $1/k_{max}^{app}$ vs. I_L and a K_{iu} achieved was a factor of 175 greater than K_{ic} (Appendix E, Table E2.1). Thus, the linearized plots can be the supporting evidence for inhibition type identified. Although inhibition type can not be conclusive by an better r^2 value and smaller error of fit in the linearized plot and

NLSR fit, the linearized plot or NLSR analysis or both can confirm inhibition type determined by the direct linear plot by reducing some uncertainty.

NLSR analysis requires initial guesses of the parameters, which, if good, will result in a convergence to best-fit estimates. For the mixed inhibition model, the initial guesses need to be close to the best estimates since more parameters are being estimated. The linearized equations presented in Table 4.1 are useful in providing these estimates. Shown in Table 4.5, Figures 4.11 and 4.13 is the comparison of values obtained from the linearized equations, and for the initial guesses for NLSR, and the final values obtained by NLSR. Most of estimates obtained from the linearized method for k_{max} , K_s , K_{ic} , and K_{iu} are in the range of the final estimated values (Table 4.5 and Figure 4.11). The results indicate that the method of linearization proposed here provides estimates close to the final values achieved by NLSR. The direct linear plots also provide visual insight into the inhibition type and initial guesses to get the best estimates. Most cases this approach resulted in a distribution of data that was amendable to linear regression.

The values for k_{max} and K_s were compared with those estimated by single-compound batch kinetic studies. An excellent agreement was obtained between the values estimated from the inhibition studies and those obtained from single compound tests. These results indicated that these parameters can be accurately obtained by NLSR analysis of the combined data without the need for single compound tests.

Inhibition of CAHs on growth substrate utilization or vice versa is an important consideration in the design the effective systems for cometabolizing CAHs, because it is strongly related with microorganism growth and/or viability and enzyme

activity (Alvarez-Cohen and McCarty, 1991c; Anderson and McCarty, 1996; van Hylckama Vlieg et al., 1997). Most modeling of inhibition of CAH cometabolism has assumed or found competitive inhibition kinetics (Semprini, 1995; Chang and Alvarez-Cohen, 1995a, 1996; Chang and Criddle, 1997; Anderson and McCarty, 1996). However, there are reports that other inhibition models may apply. For example, the inhibitory effect of 1,1,1-TCA on methane consumption (Broholm et al., 1992) and propane on 1,1,1-TCA transformation (Keenan et al., 1994) did not fit a competitive inhibition model. Also, in a study with *N. europaea*, the ability of several alternative substrates to inhibit ammonia monooxygenase (AMO) oxidation of NH_3 , was tested. Some nonhalogenated C1 and C2 compounds, such as ethylene and methane, were competitive inhibitors of NH_3 oxidation. Larger nonhalogenated compounds such as propane, butane and monohalogenated compounds such as chloromethane, and chloroethane noncompetitively (in this study, defined as mixed inhibition) inhibited NH_3 oxidation. In results present here, competitive inhibition among CAHs was observed, and CAHs also competitively inhibited butane degradation. However, butane showed mixed inhibition on the CAHs. Thus, competitive inhibition and mixed inhibition, both are important in cometabolism of CAHs. The types of inhibition mechanisms observed may differ with different microorganisms, growth substrates, and CAHs.

Competitive inhibition results from substrate and inhibitor binding to the same enzyme site, while mixed inhibition occurs when there is a separate binding site for the inhibitor. The butane-degradation dependent inactivation of cells by acetylene was well fit by a first-order-decay model. These results suggest that a kinetically similar

population of butane-oxidizers were responsible for the degradation of butane and the CAHs. Thus, mixed inhibition of butane on CAHs transformation does not likely result from the kinetic diversity of mixed culture, and likely indicates that separate binding sites for butane and the CAHs. Other mechanisms can not be ruled out since the measurements were done with whole cells and not with purified enzymes. Thus, substrate transport to the enzyme and other cell dynamic processes may have an influence on the inhibition observed.

Many competitive inhibition models that have been developed have assumed that the K_s are equal to K_{ic} for the respective substrates (Alvarez-Cohen and McCarty, 1991c; Chang and Alvarez-Cohen, 1995a, 1996; Anderson and McCarty, 1997). In this study, K_s and K_{ic} were measured rather than assuming K_{ic} .

Among CAHs, the K_{ic} of CAH was comparable to the K_s of the respective substrate, suggesting that K_s of CAH is a good indicator for the competitive inhibition observed. However, for inhibition of butane utilization the K_{ic} of CAH was a factor of 6 to 25 greater than K_s of the respective substrate. Thus the K_s of CAH was not a good estimate of the K_{ic} in the expressing competitive inhibition of CAH on butane utilization. In a study with a mixed methanotrophic culture, the K_s of methane was about 60 times higher than the K_{ic} of methane on TCE transformation, while the K_s of TCE was a factor of 5 lower than K_{ic} of TCE on methane degradation (Chang and Criddle, 1997). Similar observations were reported for toluene and TCE in the study using *Pseudomonas cepacia* G4 (Landa et al., 1994). The K_s of toluene was 5 times higher than K_{ic} of toluene, and K_s of TCE was a factor of 5 lower than K_{ic} of TCE. These results are consistent with results presented in this study, that is, K_s of CAH was

smaller than K_{ic} of the respective substrate, and K_s for growth substrate was greater than that K_{ic} of the respective substrate.

Butane is a strong inhibitor of CAH transformation, and this inhibition needs to be considered in remediation applications. Strong inhibition of butane on CAH transformation may allow the butane-grown enrichment culture to be effectively stimulated in the presence of CAHs (such as 1,1-DCE) that exert transformation product toxicity. This may be accomplished by adding butane at high concentrations during the initial phase of biostimulation.

ACKNOWLEDGMENTS

The research was supported by Research Grant from the R2D2 program of the U.S. Environmental Protection Agency-sponsored Western Region Hazardous Substance Research Center under agreement R-815738. This article has not been reviewed by the agency, and no official endorsement should be inferred. I thank Dr. Mark Dolan, George Pon, Adisorn Tovanabootr and Incheol Pang for helping to measure overall mass transfer coefficients.

NOMENCLATURE

H_{cs}	dimensionless Henry's constant of substrate (-)
H_{ci}	dimensionless Henry's constant of inhibitor (-)
I_L	inhibitor concentrations in liquid phase (μM)
I_{tot}	total inhibitor mass (μmol)

k_1	pseudo first order rate constant (L/mg TSS/hr)
k_{max}^{app}	apparent maximum degradation/transformation rates (μmol substrate/mg TSS/hr)
K_s^{app}	apparent half-saturation coefficient (μM)
K_{GaG}	overall gas-side mass transfer rate coefficient (min^{-1})
K_{ic}	competitive inhibition coefficient (μM)
K_{iu}	uncompetitive inhibition coefficient (μM)
K_{LaL}	overall liquid-side mass transfer rate coefficient (min^{-1})
k_{max}	maximum degradation/transformation rates (μmol substrate/mg TSS/hr)
K_s	half-saturation coefficient (μM)
S_{tot}	total substrate mass (μmol)
S_G	substrate concentrations in gas phase (μM)
S_L	substrate concentrations in liquid phase (μM)
t	time (minutes or hour)
TSS	total suspended solids (mg)
v	degradation rates ($\mu\text{mol}/\text{mg TSS/hr}$)
V_L	volume of liquid phase (L)
V_G	volume of gas phase (L)
X	biomass concentrations (mg TSS/L)

REFERENCES

- Alvarez-Cohen, L. M. and P. L. McCarty. 1991c. Product toxicity and cometabolic competitive inhibition modeling of chloroform and trichloroethylene transformation by methanotrophic resting cells. *Appl. Environ. Microbiol.* 57: 1031-1037.
- American Public Health Association. 1985. *Standard methods for the examination of water and wastewater*. 16th ed. APHA, New York, N.Y.
- Anderson, J. E. and P. L. McCarty. 1994. Model for treatment of trichloroethylene by methanotrophic biofilms. *J. Environ. Eng.* 120: 379-400.
- Anderson, J. E. and P. L. McCarty. 1996. Effect of three chlorinated ethenes on growth rates for a methanotrophic mixed culture. *Environ. Sci. Technol.* 30: 3517-3524.
- Anderson, J. E. and P. L. McCarty. 1997. Transformation yield of chlorinated ethenes by a methanotrophic mixed culture expressing particulate methane monooxygenase. *Appl. Environ. Microbiol.* 63: 687-693.

- Bedard, C. and R. Knowles. 1989. Physiology, biochemistry, and specific inhibitors of CH_4 , NH_4^+ and CO oxidation by methanotrophs and nitrifiers. *Microbio. Rev.* 53: 68-84.
- Broholm, K., T. H. Christensen, and B. K. Jensen. 1992. Modeling TCE degradation by a mixed culture of methane-oxidizing bacteria. *Water Res.* 9: 1177-1185.
- Chang, H. L. and L. Alvarez-Cohen. 1995a. Model for the cometabolic biodegradation of chlorinated organics. *Environ. Sci. Technol.* 29: 2357-2367.
- Chang, H. L. and L. Alvarez-Cohen. 1995b. Transformation capacities of chlorinated organics by mixed cultures enriched on methane, propane, toluene or phenol. *Biotech. Bioeng.* 45: 440-449.
- Chang, H. L. and L. Alvarez-Cohen. 1996. Biodegradation of individual and multiple chlorinated aliphatic hydrocarbons by methane-oxidizing cultures. *Appl. Environ. Microbiol.* 62: 3371-3377.
- Chang, H. L. and L. Alvarez-Cohen. 1997. Two-stage methanotrophic bioreactor for the treatment of chlorinated organic wastewater. *Wat. Res.* 31:2026-2036.
- Chang, W-K. and C. S. Criddle. 1997. Experimental evaluation of a model for cometabolism: prediction of simultaneous degradation of trichloroethylene and methane by a methanotrophic mixed culture. *Biotech. Bioeng.* 54: 491-501.
- Cornish-Bowden, A. 1994. *Fundamentals of enzyme kinetics*. Protland press Ltd. London, UK.
- Cornish-Bowden, A and R. Eisenthal. 1974. Estimation of Michaelis constant and maximum velocity from the direct linear plot. *Biochim. Biophys. Acta.* 523: 268-272.
- Dolan, M. E. and P. L. McCarty. 1995. Methanotrophic chloroethene transformation capacities and 1,1-dichloroethene transformation product toxicity. *Environ. Sci. Technol.* 29: 2741-2747.
- Dowd, J. E. and D. S. Riggs. 1965. A comparison of estimates of Michaelis-Menten kinetic constants from various linear transformations. *J. Biol. Chem.* 240:863-869.
- Eisenthal, R. and A. Cornish-Bowden. 1974. The direct linear plot: a new graphical procedure for estimating enzyme kinetic parameters. *Biochem. J.* 139:715-720.
- Ely, R. L., K. J. Williamson, M. R. Hyman, and D. J. Arp. 1997. Cometabolism of chlorinated solvents by nitrifying bacteria: kinetics, substrate interaction, toxicity effects, and bacterial response. *Biotechnol. Bioeng.* 54: 520-534.

- Folsom, B. R., P. J. Chapman, P. H. Pritchard. 1990. Phenol and trichloroethylene degradation by *Pseudomonas cepacia* G4: Kinetics and Interactions between Substrates. *Appl. Environ. Microbiol.* 56: 1279-1285.
- Gossett, J. M. 1987. Measurements of Henry's law constants for C1 and C2 chlorinated hydrocarbons. *Environ. Sci. Technol.* 21: 202-208.
- Hamamura, N., R. T. Storfa, L. Semprini, D. J. Arp. 1999. Diversity in butane monooxygenase among butane-grown bacteria. *Appl. Environ. Microbiol.* 65: 4586-4593.
- Hopkins, G. D. and P. L. McCarty. 1995. Field observations of in situ aerobic cometabolism of trichloroethylene and three dichloroethylene isomers using phenol and toluene as primary substrates. *Environ. Sci. Technol.* 29: 1628-1637.
- Keenan, J. E., S. E. Strand, and H. D. Stensel. 1994. Degradation kinetics of chlorinated solvents by a propane-oxidizing enrichment culture. In: R.E Hinchee, A. Leeson, L. Semprini, and S. K. Ong (Eds.) *Bioremediation of Chlorinated and Polycyclic Aromatic Hydrocarbon Compounds* Lewis Publishers, Boca Raton, FL, pp.1-13.
- Keener, W. K. and D. J. Arp. 1993. Kinetic studies of ammonia monooxygenase inhibition in *Nitrosomonas europaea* by hydrocarbons and halogenated hydrocarbons in an optimized whole-cell assay. *Appl. Environ. Microbiol.* 59: 2501-2510.
- Kim, Y., D. J. Arp, L. Semprini. 1999. Aerobic cometabolism of chlorinated methanes, ethanes, and ethenes, by a butane-grown mixed culture. Submitted in *J. of Environ. Engr.*
- Kim, Y., L. Semprini, and D. J. Arp. 1997a. Aerobic cometabolism of chloroform and 1,1,1-trichloroethane by butane-grown microorganisms. *Bioremediation J.* 2: 135-148.
- Kim, Y., L. Semprini, and D. J. Arp. 1997b. Aerobic cometabolism of chloroform, 1,1,1-trichloroethane, and the other chlorinated aliphatic hydrocarbons by butane-utilizing microorganisms. In: *In situ and On-site Bioremediation*; Alleman, B. C.; Leeson, A., Eds.; Battelle Press, Columbus, OH, Vol. 3, pp. 107-112.
- Landa, A. S., E. M. Sipkema, J. Weijma, A. A. C. M. Beenackers, J. Dolfing, and D. B. Janssen. 1994. Cometabolic degradation of trichloroethylene by *Pseudomonas cepacia* G4 in a chemostat with toluene as the primary substrate. *Appl. Environ. Microbiol.* 60: 3368-3374.
- Lange C. C. and L. P. Wackett. 1997. Oxidation of aliphatic olefins by toluene dioxygenase: Enzyme rates and production identification. *J. Bacteriol.* 179: 3858-3865.

- Mackay, D. and W. Y. Shiu. 1981. A critical review of Henry's law constants for chemicals of environmental interest. *J. Phys. Chem. Ref. Data*. 10: 1175-1199.
- Oldenhuis, R., J. Y. Oedzes, J. J. van der Waarde, and D. B. Janssen. 1991. Kinetic of chlorinated hydrocarbon degradation by *Methylosinus trichosporium* OB3b and toxicity of trichloroethylene. *Appl. Environ. Microbiol.* 57: 7-14.
- Oldenhuis, R., R. L. J. M. Vink, D. B. Janssen, and B. Witholt. 1989. Degradation of chlorinated aliphatic hydrocarbons by *Methylosinus trichosporium* OB3b expressing soluble methane monooxygenase. *Appl. Environ. Microbiol.* 55: 2819-2826.
- Perry, R. H., D. W. Green, and J. O. Maloney. 1984. *Perry's chemical engineers handbook*, 6th ed., table 3-137. McGraw-Hill Book Co., New York.
- Prior, S. D. and H. Dalton. 1985. Acetylene as a suicide substrate and active site probe for methane monooxygenase from *Methylococcus capsulatus* (Bath). *FEMS Microbiol. Lett.* 29: 105-109.
- Rasche, M. E., M. R. Hyman, and D. J. Arp. 1991. Factors limiting aliphatic chlorocarbon degradation by *Nitrosomonas europaea*: cometabolic inactivation of ammonia monooxygenase and substrate specificity. *Appl. Environ. Microbiol.* 57: 2986-2994.
- Robinson, J. A. 1985. Determining microbial kinetic parameters using nonlinear regression analysis. *Adv. Microb. Ecol.* 8:61-114.
- Robinson, J. A. and W. G. Charaklis. 1984. Simultaneous estimation of V_{max} , K_m , and the rate of endogenous substrate production (R) from substrate depletion data. *Microb. Ecol.* 10:165-178.
- Semprini, L. 1995. In situ bioremediation of chlorinated solvents. *Environmental Health Perspectives*. 103:10-105.
- Strand, S. E., M. D. Bjelland, and H. D. Stensel. 1990. Kinetics of chlorinated hydrocarbon degradation by suspended cultures of methane-oxidizing bacteria. *Research Journal of the Water Pollution Control Federation*. 62: 124-129.
- van Hylckama Vlieg, J. E. T., W. de Koning, and D. B. Janssen. 1996. Transformation kinetic of chlorinated ethenes by *Methylosinus trichosporium* OB3b and detection of unstable epoxides by on-line gas chromatography. *Appl. Environ. Microbiol.* 62: 3304-3312.
- van Hylckama Vlieg, J. E. T., W. de Koning, and D. B. Janssen. 1997. Effect of chlorinated ethene conversion on viability and activity of *Methylosinus trichosporium* OB3b. *Appl. Environ. Microbiol.* 63: 4961-4964.

Vogel, T. L. and P. L. McCarty. 1987. Abiotic and biotic transformations of 1,1,1-trichloroethane under methanogenic conditions. *Environ. Sci. Technol.* 21: 1208-1213.

Wiegant, L. P. and J. A. M. de Bont. 1980. A new for ethylene glycol metabolism in *Mycobacterium* E44. *J. Gen. Microbiol.*, 120: 325-331.

Yeager, C. M., P. J. Bottomley, D. J. Arp, and M. R. Hyman. 1999. Inactivation of toluene 2-monooxygenase in *Burkholderia cepacia* G4 by Alkynes. *Appl. Environ. Microbiol.* 65: 632-639.

CHAPTER 5

Engineering Significance and Conclusions

ENGINEERING SIGNIFICANCE

The suitability of microorganisms for application in a cometabolic CAH remediation process is determined by several factors including substrate range, kinetics of the transformation, and transformation efficiency. A broad substrate range is desirable, since contaminated groundwater often contains more than one contaminant. The kinetics of the transformation are also important, since high transformation rates may allow high volumetric transformation capacity, and high affinity (e.g., low K_s) making it easier to transform contaminants to low concentrations. However, the kinetics of cometabolic transformations are often complex and are influenced by a number of factors including transformation toxicity. Transformation efficiencies are also important since they dictate the amount of cometabolic substrate and oxygen that must be fed to transform a given amount of contaminant. Therefore, high T_c or T_y values are also advantageous.

The butane-growth mixed culture studied here is highly suitable for treating CAH mixtures based on its broad substrate range. Of particular interest are mixtures of 1,1,1-TCA, 1,1-DCE, and 1,1-DCA, since they are commonly observed as groundwater contaminants. The butane culture has the ability to transform the chlorinated ethanes (1,1,1-TCA and 1,1-DCA) and ethenes (1,1-DCE) as effectively as

methanotrophs expressing sMMO. The pseudo first-order rate (k_1) values for 1,1-DCE and 1,1,1-TCA were a factor of 2 to 4 greater than those reported for a methanotrophic culture (Oldenhuis et al., 1991). The culture also had a higher T_c for these three CAHs than observed with methanotrophs by Chang and Alvarez-Cohen (1996). Possible reasons for higher T_y values are: 1) the cell yield of the butane enrichment was a factor of 2.5 higher than that of the methanotrophs, and 2) the butane culture produced and effectively used internal energy reserves, such as PHB.

Bioaugmentation using this culture may be a promising means for treating the CAH mixtures in groundwater. Transformation of the three CAH mixtures is a function of inhibition among compounds and transformation product toxicity. Assuming the concentrations of each compound are same, butane would be most rapidly degraded followed by 1,1-DCE, 1,1-DCA, and 1,1,1-TCA. The reasons for the sequence transformation may be: 1) the lower inhibition coefficients for butane (i.e. strong inhibition on the transformation of the other compounds), 2) the greatest k_{max} value for butane, 3) the greater k_{max} value for 1,1-DCE than the other CAHs, 4) the lower K_s (or K_{ic}) value for 1,1-DCE than the other CAHs, and 5) the greater k_{max} of 1,1-DCA than 1,1,1-TCA.

The transformation extent of each compound may depend on cell inactivation resulting from CAH transformation product toxicity. 1,1-DCE transformation would most highly affect the transformation of the other compounds, because it is highly inhibitory, and its transformation results in the greatest cell inactivation. Thus, an effective 1,1-DCE treatment would be an important factor to consider when designing a bioremediation system for these CAH mixtures. During bioaugmentation, to

overcome 1,1-DCE transformation product toxicity, high concentrations of the culture can be injected into the groundwater. However, this may result in clogged well screens or pores, so this approach may not be a good one for stimulating the bioaugmented culture. Another approach would be adding the culture with growth substrate or adding the culture after growth substrate addition. With this method, butane cultures may be effectively stimulated in the presence of 1,1-DCE as well as the other CAHs. Strong inhibition of butane on 1,1-DCE transformation may allow the butane-grown enrichment culture to be effectively stimulated. This may be accomplished by adding butane at high concentrations during the initial phase of biostimulation. After the culture is stimulated in groundwater, butane injection concentrations can be reduced.

Butane as a growth substrate has several advantages over the other growth substrates. In-situ bioremediation of aquifers can be accomplished by dissolving butane and oxygen in groundwater. Butane is approximately 3 times more soluble in water than methane, and thus it can be more easily added to groundwater. It can also be supplied to sites in a liquefied form, and it can therefore be easily implemented at remote sites. Another potential advantage of butane-utilizers is that they will not be as sensitive as methane-utilizers to tracer nutrient conditions in the subsurface that can affect the cometabolism potential, such as copper availability. The butane culture was enriched without copper limitations and an effective transformation was achieved. As a gaseous substrate butane might also be applied for remediation of the unsaturated zone. One potential advantage of butane over toluene and phenol is that butane is not

a regulated chemical. Thus, it will likely be easier to obtain regulatory approval to add butane to the subsurface.

CONCLUSIONS

In summary, the research in this dissertation supports the following conclusions:

- A butane-grown mixed culture effectively transformed chlorinated methanes, chlorinated ethanes, and selective chlorinated ethenes such as 1,1-DCE, VC, and c-DCE.
- The amounts of CAHs transformed per unit cell mass and unit time were inversely proportional to chlorine contents within each group of chlorinated methanes, ethanes, and ethylenes, with the exception of t-DCE.
- Butane utilization was completely inactivated by the transformation of 1,1-DCE, CA, and 1,2-DCA, and highly inactivated by the transformation of CF, 1,1,2-TCA, c-DCE, and VC.
- Cells were more highly inactivated by the transformation of 1,2-DCA and 1,1,2-TCA than by 1,1-DCA and 1,1,1-TCA, suggesting less cell inactivation by transformation of di- or tri-chloroethanes that have all chlorines on one carbon.
- Nearly complete oxidative dechlorination of CM, DCM, CF, CA, VC, and c-DCE was observed, but not of di- or tri-chloroethanes and 1,1-DCE.

- A good potential for treating 1,1-DCE, 1,1-DCA and 1,1,1-TCA was achieved. These compounds are often observed together as subsurface contaminants.
- The method of combining both direct linear plot, initial parameter guesses using graphical methods, and NLSR analysis can be used systematically to obtain kinetic coefficients, inhibition type and inhibition parameters.
- Competitive inhibition among CAHs was identified from the direct linear plot method. The CAHs also competitively inhibited butane degradation. Butane caused mixed inhibition on 1,1-DCE, 1,1-DCA, and 1,1,1-TCA transformation.
- The values of the competitive inhibition coefficients (K_{ic}) for each CAH were a factor of 8 to 20 higher than the corresponding K_s for each CAH in the presence of butane. Without butane, the K_s values were good indicators of competitive inhibition among CAHs.
- Butane was a strong inhibitor of CAH transformation, having a much lower inhibitor coefficient than the K_s value of butane, however, the CAHs were weak inhibitors of butane degradation.

FUTURE WORK

In order to develop a model for the cometabolism of CAH mixtures and butane utilization more inhibition studies are needed to evaluate if kinetic parameters, inhibition types, and inhibition coefficients determined in Chapter 4 can be successful with mixtures of two or more compounds. Inhibition studies with three or four

compounds can also be accomplished using the methods developed, including direct linear plot and NLSR analysis used in Chapter 4.

In addition to inhibition studies, further work on CAH transformation product toxicity needs to be performed. Cell inactivation resulting from single CAH transformation needs to be investigated and then extended to the CAH mixtures in the absence or presence of butane. For these studies the models developed including transformation capacity model (Alvarez-Cohen and McCarty, 1991c) and transformation yield model (Chang and Criddle, 1997) can be tested to determine if these models can be applied to this system. If not, a new model needs to be developed. The inactivation model (equation 2.1) is one possible approach to evaluate CAH transformation product toxicity, since the model can account for transformation product toxicity on cells that transformed CAHs and toxicity of byproducts released to solution on new cells grown.

Inhibition of CAH transformation by butane was modeled by mixed inhibition. Based on the definitions of mixed and competitive inhibition, butane may bind two active sites of the monooxygenase, while the CAHs may bind one active site. To understand this mechanism better more detailed studies should be carried out with a pure culture isolated from the mixed culture. One experimental approach is the method reported by Hamamura et al., 1999. They used [^{14}C] acetylene labeling technique to identify the diversity in BMO among butane-grown bacteria. The method can be adapted to define the active protein site of the monooxygenase enzyme using radiolabelled [^{14}C] acetylene, [^{14}C] butane, or [^{14}C] CAH. The labeling patterns between [^{14}C] butane and [^{14}C] CAH may be different. The pattern in the presence of

[^{14}C] acetylene may be the combination of both patterns, since no degradation of butane and CAH was observed by the acetylene-treated butane culture. The comparison of labeling pattern may be an indicator of binding and inhibition mechanisms.

The butane-culture has a good potential for bioremediating a wide range CAHs in the unsaturated and saturated zone. More studies with the culture may help to better understand the transformation mechanisms of CAH mixtures in the presence of butane and to successfully apply the butane culture to the bioremediation of CAHs.

REFERENCES

- Alvarez-Cohen, L. M., and P. L. McCarty. 1991a. A cometabolic biotransformation model for halogenated aliphatic compounds exhibiting product toxicity. *Environ. Sci. Technol.* 25: 1381-1387.
- Chang, H. L. and L. Alvarez-Cohen. 1996. Biodegradation of individual and multiple chlorinated aliphatic hydrocarbons by methane-oxidizing cultures. *Appl. Environ. Microbiol.* 62: 3371-3377.
- Chang, W-K. and C. S. Criddle. 1997. Experimental evaluation of a model for cometabolism: prediction of simultaneous degradation of trichloroethylene and methane by a methanotrophic mixed culture. *Biotech. Bioeng.* 54: 491-501.
- Hamamura, N., R. T. Storfa, L. Semprini, D. J. Arp. 1999. Diversity in butane monooxygenase among butane-grown bacteria. *Appl. Environ. Microbiol.* 65: 4586-4593.
- Oldenhuis, R., J. Y. Oedzes, J. J. van der Waarde, and D. B. Janssen. 1991. Kinetic of chlorinated hydrocarbon degradation by *Methylosinus trichosporium* OB3b and toxicity of trichloroethylene. *Appl. Environ. Microbiol.* 57: 7-14.

BIBLIOGRAPHY

- Alvarez-Cohen, L. M. , and P. L. McCarty. 1991a. A cometabolic biotransformation model for halogenated aliphatic compounds exhibiting product toxicity. *Environ. Sci. Technol.* 25: 1381-1387.
- Alvarez-Cohen, L. M. , and P. L. McCarty. 1991b. Effects of toxicity, aeration and reductant supply on trichloroethylene transformation by a mixed methanotrophic culture. *Appl. Environ. Microbiol.* 57:228-235.
- Alvarez-Cohen, L. M. and P. L. McCarty. 1991c. Product toxicity and cometabolic competitive inhibition modeling of chloroform and trichloroethylene transformation by methanotrophic resting cells. *Appl. Environ. Microbiol.* 57: 1031-1037.
- American Public Health Association. 1985. *Standard methods for the examination of water and wastewater*. 16th ed. APHA, New York, N.Y.
- Anderson, J. E. and P. L. McCarty. 1994. Model for treatment of trichloroethylene by methanotrophic biofilms. *J. Environ. Eng.* 120: 379-400.
- Anderson, J. E. and P. L. McCarty. 1996. Effect of three chlorinated ethenes on growth rates for a methanotrophic mixed culture. *Environ. Sci. Technol.* 30: 3517-3524.
- Anderson, J. E. and P. L. McCarty. 1997. Transformation yield of chlorinated ethenes by a methanotrophic mixed culture expressing particulate methane monooxygenase. *Appl. Environ. Microbiol.* 63: 687-693.
- Arcangeli, J.-P. and E. Arvin. 1997. Modeling of the cometabolic biodegradation of trichloroethylene by toluene-oxidizing bacteria in a biofilm system. *Environ. Sci. Technol.* 31: 3044-3052.
- Arp, D. J. 1999. Butane metabolism by butane-grown '*pseudomonas butanovora*'. *Microbiology*. 145:1173-1180.
- Bartnicki, E. W. and C. E. Castro. 1994. Biodehalogenation: Rapid oxidative metabolism of mono- and polyhalomethanes by *Methylosinus trichosporium* OB-3b. *Environ. Toxicology and Chemistry*. 13: 241-245.
- Bedard, C. and R. Knowles. 1989. Physiology, biochemistry, and specific inhibitors of CH_4 , NH_4^+ and CO oxidation by methanotrophs and nitrifiers. *Microbio. Rev.* 53: 68-84.

- Bergnam, J. G. and J. Sanik. 1957. Determination of trace amounts of chloride in naphtha. *Anal. Chem.* 29: 241-243.
- Broholm, K., T. H. Christensen, and B. K. Jensen. 1992. Modeling TCE degradation by a mixed culture of methane-oxidizing bacteria. *Water Res.* 9: 1177-1185.
- Broholm, K., K. Jensen, T. H. Christensen, and L. Olsen. 1990. Toxicity of 1,1,1-trichloroethane and trichloroethene on a mixed culture of methane-oxidizing bacteria. *Appl. Environ. Microbiol.* 56: 2488-2493.
- Chang, H. L. and L. Alvarez-Cohen. 1995a. Model for the cometabolic biodegradation of chlorinated organics. *Environ. Sci. Technol.* 29: 2357-2367.
- Chang, H. L. and L. Alvarez-Cohen. 1995b. Transformation capacities of chlorinated organics by mixed cultures enriched on methane, propane, toluene or phenol. *Biotech. Bioeng.* 45: 440-449.
- Chang, H. L. and L. Alvarez-Cohen. 1996. Biodegradation of individual and multiple chlorinated aliphatic hydrocarbons by methane-oxidizing cultures. *Appl. Environ. Microbiol.* 62: 3371-3377.
- Chang, H. L. and L. Alvarez-Cohen. 1997. Two-stage methanotrophic bioreactor for the treatment of chlorinated organic wastewater. *Wat. Res.* 31:2026-2036.
- Chang, W-K. and C. S. Criddle. 1997. Experimental evaluation of a model for cometabolism: prediction of simultaneous degradation of trichloroethylene and methane by a methanotrophic mixed culture. *Biotech. Bioeng.* 54: 491-501.
- Chu, K-H and L. Alvarez-Cohen. 1996. Trichloroethylene degradation by methane-oxidizing cultures grown with various nitrogen sources. *Water Environ. Res.* 68: 76-82.
- Colby, J. and H. Dalton. 1976. Some properties of a soluble methane mono-oxygenase from *Methylococcus capsulatus* Strain Bath. *Biochem. J.* 157, 495-497.
- Cornish-Bowden, A. 1994. *Fundamentals of enzyme kinetics*. Protland press Ltd. London, UK.
- Cornish-Bowden, A and R. Eisenthal. 1978. Estimation of Michaelis constant and maximum velocity from the direct linear plot. *Biochim. Biophys. Acta.* 523: 268-272.
- Criddle, C. S. 1993. The kinetics of cometabolism. *Biotechnol. Bioeng.* 41:1048-1056.
- Davis, J. B. 1964. Cellular lipids of a *Nocardia* grown on propane and n-butane. *Appl. Microbiol.* 12: 301-304.

Dawes, E. A. and P. J. Senior. 1973. The role and regulation of energy reserve polymers in micro-organisms. *Adv. Microb. Physiol.* 10: 135-266.

Dixon, M. and E. C. Webb. 1979. *Enzymes*. Academic Press. New York.

Dolan, M. E. and P. L. McCarty. 1995. Methanotrophic chloroethene transformation capacities and 1,1-dichloroethene transformation product toxicity. *Environ. Sci. Technol.* 29: 2741-2747.

Dolfing, J., A. J. van den Wijngaard, and D. B. Janssen. 1993. Microbiological aspects of the removal of chlorinated hydrocarbons from air. *Biodegradation.* 4: 261-281.

Dowd, J. E. and D. S. Riggs. 1965. A comparison of estimates of Michaelis-Menten kinetic constants from various linear transformations. *J. Biol. Chem.* 240:863-869.

Eisenthal, R. and A. Cornish-Bowden. 1974. The direct linear plot: a new graphical procedure for estimating enzyme kinetic parameters. *Biochem. J.* 139:715-720.

Ely, R. L., M. R. Hyman, D. J. Arp, R. G. Guenther, and K. J. Williamson. 1995. A cometabolic biodegradation model incorporating enzyme inhibition, inactivation, and recovery. II: trichloroethylene degradation experiments. *Biotechnol. Bioeng.* 46: 232-245.

Ely, R. L., K. J. Williamson, M. R. Hyman, and D. J. Arp. 1997. Cometabolism of chlorinated solvents by nitrifying bacteria: kinetics, substrate interaction, toxicity effects, and bacterial response. *Biotechnol. Bioeng.* 54: 520-534.

Ensign, S. A., M. R. Hyman, and D. J. Arp. 1992. Cometabolic degradation of chlorinated alkenes by alkene monooxygenase in a propylene-grown *Xanobacter* strain. *Appl. Environ. Microbiol.* 58: 3038-3046.

Fitch, M. W., G. E. Speitel Jr., and G. Georgiou. 1996. Degradation of trichloroethylene by methanol-grown cultures of *Methylosinus trichosporium* OB3b PP358. *Appl. Environ. Microbiol.* 62: 1124-1128.

Folsom, B. R., P. J. Chapman, P. H. Pritchard. 1990. Phenol and trichloroethylene degradation by *Pseudomonas cepacia* G4: Kinetics and Interactions between Substrates. *Appl. Environ. Microbiol.* 56: 1279-1285.

Gossett, J. M. 1987. Measurements of Henry's law constants for C1 and C2 chlorinated hydrocarbons. *Environ. Sci. Technol.* 21: 202-208.

Hage, J. C. and S. Hartmans. 1999. Monooxygenase-mediated 1,2-dichloroethane degradation by *pseudomonas* sp. Strain DCA1. *Appl. Environ. Microbiol.* 65:2466-2470.

- Hamamura, N., C. Page, T. Long, L. Semprini, and D. J. Arp. 1997. Chloroform cometabolism by butane-grown CF8, *Pseudomonas butanovora*, and *Mycobacterium vaccae* JOB5 and methane-grown *Methylosinus trichosporium* OB3b. *Appl. Environ. Microbiol.* 63: 3607-3613.
- Hamamura, N., R. T. Storfa, L. Semprini, D. J. Arp. 1999. Diversity in butane monooxygenase among butane-grown bacteria. *Appl. Environ. Microbiol.* 65: 4586-4593.
- Henry, S. M. and D. Grbić-Galić. 1991. Influence of endogenous and exogenous electron donors and trichloroethylene oxidation toxicity on trichloroethylene oxidation by methanotrophic cultures from a groundwater aquifer. *Appl. Environ. Microbiol.* 57: 236-244.
- Henrysson, T. and P. L. McCarty. 1993. Influence of the endogenous storage lipid poly- β -hydroxybutyrate on the reducing power availability during cometabolism of trichloroethylene and naphthalene by resting methanotrophic mixed cultures. *Appl. Environ. Microbiol.* 59: 1602-1606.
- Henson, J. M., M. V. Yates, and J. W. Cochran. 1989. Metabolism of chlorinated methanes, ethanes and ethylenes by a mixed bacterial culture growing on methane. *J. Industr. Microbiol.* 4: 29-35.
- Hopkins, G. D. and P. L. McCarty. 1995. Field observations of in situ aerobic cometabolism of trichloroethylene and three dichloroethylene isomers using phenol and toluene as primary substrates. *Environ. Sci. Technol.* 29: 1628-1637.
- Hopkins, G. D., L. Semprini, and P. L. McCarty. 1993. Microcosm and in situ field studies of enhanced biotransformation of trichloroethylene by phenol-utilizing microorganisms. *Appl. Environ. Microbiol.* 59: 2277-2285.
- Hyman, M. R., I. B. Murton, and D. J. Arp. 1988. Interaction of ammonia monooxygenase from *Nitrosomonas europaea* with alkanes, alkenes, and alkynes. *Appl. Environ. Microbiol.* 54: 3187-3190.
- Hyman, M. R., S. A. Russell, R. L. Ely, K. J. Williamson, and D. J. Arp. 1995. Inhibition, inactivation and recovery of ammonia-oxidizing activity in cometabolism of trichloroethylene by *Nitrosomonas europaea*. *Appl. Environ. Microbiol.* 61: 1480-1487.
- Janssen, D. B., G. Grobbsen, R. Hoekstra, R. Oldehuis, and B. Witholt. 1988. Degradation of trans-1,2-dichloroethylene by mixed and pure cultures of methanotrophic bacteria. *Appl. Microbiol. Biotechnol.* 29: 392-399.

- Janssen, D. B., A. Scheper, and B. Witholt. 1985. Degradation of halogenated aliphatic compounds by *Xanthobacter autotrophicus* GJ10. *Appl. Environ. Microbiol.* 49: 673-677.
- Kampbell, D. H., J. T. Wilson, and S. A. Vandergrift. 1989. Dissolved oxygen and methane in water by a GC headspace equilibration technique. *J. Environ. Anal. Chem.* 36: 249-259.
- Keenan, J. E., S. E. Strand, and H. D. Stensel. 1994. Degradation kinetics of chlorinated solvents by a propane-oxidizing enrichment culture. In: R.E Hincsee, A. Leeson, L. Semprini, and S. K. Ong (Eds.) *Bioremediation of Chlorinated and Polycyclic Aromatic Hydrocarbon Compounds* Lewis Publishers, Boca Raton, FL, pp.1-13.
- Keener, W. K. and D. J. Arp. 1993. Kinetic studies of ammonia monooxygenase inhibition in *Nitrosomonas europaea* by hydrocarbons and halogenated hydrocarbons in an optimized whole-cell assay. *Appl. Environ. Microbiol.* 59: 2501-2510.
- Kim, Y. 1996. Aerobic cometabolism of chloroform by butane and propane grown microorganisms from the Hanford subsurface. M.S. Thesis. Oregon State University, Corvallis, OR.
- Kim, Y. and L. Semprini. Unpublished data.
- Kim, Y., D. J. Arp, L. Semprini. 1999. Aerobic cometabolism of chlorinated methanes, ethanes, and ethenes, by a butane-grown mixed culture. Submitted in *J. of Environ. Engr.*
- Kim, Y., L. Semprini, and D. J. Arp. 1997a. Aerobic cometabolism of chloroform and 1,1,1-trichloroethane by butane-grown microorganisms. *Bioremediation J.* 2: 135-148.
- Kim, Y., L. Semprini, and D. J. Arp. 1997b. Aerobic cometabolism of chloroform, 1,1,1-trichloroethane, and the other chlorinated aliphatic hydrocarbons by butane-utilizing microorganisms. In: *In situ and On-site Bioremediation*; Alleman, B. C.; Leeson, A., Eds.; Battelle Press, Columbus, OH, Vol. 3, pp. 107-112.
- Landa, A. S., E. M. Sipkema, J. Weijma, A. A. C. M. Beenackers, J. Doling, and D. B. Janssen. 1994. Cometabolic degradation of trichloroethylene by *Pseudomonas cepacia* G4 in a chemostat with toluene as the primary substrate. *Appl. Environ. Microbiol.* 60: 3368-3374.
- Lange C. C. and L. P. Wackett. 1997. Oxidation of aliphatic olefins by toluene dioxygenase: Enzyme rates and production identification. *J. Bacteriol.* 179: 3858-3865.

- Mackay, D. and W. Y. Shiu. 1981. A critical review of Henry's law constants for chemicals of environmental interest. *J. Phys. Chem. Ref. Data*. 10: 1175-1199.
- McCarty, P. L., M. N. Goltz, G. D. Hopkins, M. E. Dolan, J. P. Allan, B. T. Kawakami, and T. J. Carrothers. 1998. Full-scale evaluation of in situ cometabolic degradation of trichloroethylene in groundwater through toluene Injection, *Environ. Sci. Technol.* 32:88-100.
- McCarty, P. L. and L. Semprini. 1993. Ground-water treatment of chlorinated solvents. In *Handbook of Bioremediation*, Lewis Publisher Inc., Chelsea, MI, pp87-116.
- McLee, A. G., A. C. Kormendy, and M. Wayman. 1972. Isolation and characterization of *n*-butane utilizing microorganisms. *Can. J. Microbiol.* 18: 1191-1195.
- Nelson, M. J., S. O. Montgomery, and P. H. Pritchard. 1988. Trichloroethylene metabolism by microorganisms that degrade aromatic compounds. *Appl. Environ. Microbiol.* 54: 604-606.
- Oldenhuis, R., J. Y. Oedzes, J. J. van der Waarde, and D. B. Janssen. 1991. Kinetic of chlorinated hydrocarbon degradation by *Methylosinus trichosporium* OB3b and toxicity of trichloroethylene. *Appl. Environ. Microbiol.* 57: 7-14.
- Oldenhuis, R., R. L. J. M. Vink, D. B. Janssen, and B. Witholt. 1989. Degradation of chlorinated aliphatic hydrocarbons by *Methylosinus trichosporium* OB3b expressing soluble methane monooxygenase. *Appl. Environ. Microbiol.* 55: 2819-2826.
- Phillips, W. E., and J. J. Perry. 1974. Metabolism of *n*-butane and 2-butanone by *Mycobacterium vaccae*. *J. Bacteriol.* 120: 987-989.
- Perry, R. H., D. W. Green, and J. O. Maloney. 1984. *Perry's chemical engineers handbook*, 6th ed., table 3-137. McGraw-Hill Book Co., New York.
- Prior, S. D. and H. Dalton. 1985. Acetylene as a suicide substrate and active site probe for methane monooxygenase from *Methylococcus capsulatus* (Bath). *FEMS Microbiol. Lett.* 29: 105-109.
- Rasche, M. E., R. E. Hicks, M. R. Hyman, and D. J. Arp. 1990. Oxidation of monohalogenated ethenes and *n*-chlorinated alkanes by whole cells of *Nitrosomonas europaea*. *J. Bacteriol.* 172: 5368-5373.
- Rasche, M. E., M. R. Hyman, and D. J. Arp. 1991. Factors limiting aliphatic chlorocarbon degradation by *Nitrosomonas europaea*: cometabolic inactivation of ammonia monooxygenase and substrate specificity. *Appl. Environ. Microbiol.* 57: 2986-2994.

- Robinson, J. A. 1985. Determining microbial kinetic parameters using nonlinear regression analysis. *Adv. Microb. Ecol.* 8:61-114.
- Robinson, J. A. and W. G. Charaklis. 1984. Simultaneous estimation of V_{\max} , K_m , and the rate of endogenous substrate production (R) from substrate depletion data. *Microb. Ecol.* 10:165-178.
- Schmidt, S. K., S. Simkins, and M. Alexander. 1985. Models for the kinetics of biodegradation of organic compounds not supporting growth. *Appl. Environ. Microbiol.* 50: 323-331.
- Semprini, L. 1995. In situ bioremediation of chlorinated solvents. *Environmental Health Perspectives.* 103:10-105.
- Semprini, L. 1997. Strategies for the aerobic co-metabolism of chlorinated solvents. *Curr. Opin. Biotechnol.* 8: 296-308.
- Semprini, L. and P. L. McCarty. 1991. Comparison between model simulations and field results for in-situ bioremediation of chlorinated aliphatics: Part 1. biostimulation of methanotrophic bacteria. *Ground Water.* 29: 365-374.
- Semprini, L., P. V. Roberts, G. D. Hopkins, and P. L. McCarty. 1990. A field evaluation of in-situ biodegradation of chlorinated ethenes: Part 2. The results of biostimulation and biotransformation experiments. *Ground Water.* 28: 715-727.
- Shah, N. N., M. L. Hanna, and R. T. Taylor. 1996. Batch cultivation of *Methylosinus trichosporium* OB3b:V. Characterization of poly- β -hydroxybutyrate production under methane-dependent growth conditions. *Biotechnol. Bioeng.* 49: 161-171.
- Silverman, R. B. 1988. *Mechanism-based enzyme inactivation: chemistry and enzymology*. Vol. 1. p3-30. CRC Press, Boca, Raton.
- Smith, L. H., P. L. McCarty, and P. K. Kitanidis. 1998. Spreadsheet method for evaluation of biochemical reaction rate coefficients and their uncertainties by weighted nonlinear least-squares analysis of the integrated Monod equation. *Appl. Environ. Microbiol.* 64: 2044-2050.
- Speitel Jr., G. E., R. L. Thompson, and D. Weissman. 1993. Biodegradation kinetics of *Methylosinus trichosporium* OB3b at low concentrations of chloroform in the presence and absence of enzyme competition by methane. *Wat. Res.* 27: 15-24.
- Strand, S. E., M. D. Bjelland, and H. D. Stensel. 1990. Kinetics of chlorinated hydrocarbon degradation by suspended cultures of methane-oxidizing bacteria. *Research Journal of the Water Pollution Control Federation.* 62: 124-129.

- Tovanabootr, A. and L. Semprini. 1998. Comparison of TCE transformation abilities of methane- and propane-utilizing microorganisms. *Bioremediation J.* 2:105-124.
- Vancheeswaran, S., R. U. Halden, K. J. Williamson, J. D. Ingle, and L. Semprini. 1999. Abiotic and biological transformation of tetraalkoxysilanes and trichloroethene/cis-1,2-dichloroethene cometabolism driven by tetrabutoxysilane-degrading microorganisms. *Environ. Sci. Technol.* 33: 1077-1085.
- van den Wijngaard, A. J., K. W. H. J. van der Kamp, J. van der Ploeg, F. Pries, B. Kazemier, and D. B. Jassen. 1992. Degradation of 1,2-dichloroethane by *Ancylobacter aquaticus* and other facultative methylotrophs. *Appl. Environ. Microbiol.* 58: 976-983.
- Vanderberg, L. A., B. L. Burbach, and J. J. Perry. 1995. Biodegradation of trichloroethylene by *Mycobacterium vaccae*. *Can. J. Microbiol.* 41: 298-301.
- Vanderberg, L. A. and J. J. Perry. 1994. Dehalogenation by *Mycobacterium vaccae* JOB-5: Role of the propane monooxygenase. *Can. J. Microbiol.* 40: 169-172.
- Van Ginkel, C. G., H. G. J. Welten, S. Hartmans, and J. A. M. de Bont. 1987. Metabolism of trans-2-butene in *Nocardia* TB1. *Journal of General Microbiology*. 133: 1713-1720.
- van Hylckama Vlieg, J. E. T., W. de Koning, and D. B. Janssen. 1996. Transformation kinetic of chlorinated ethenes by *Methylosinus trichosporium* OB3b and detection of unstable epoxides by on-line gas chromatography. *Appl. Environ. Microbiol.* 62: 3304-3312.
- van Hylckama Vlieg, J. E. T., W. de Koning, and D. B. Janssen. 1997. Effect of chlorinated ethene conversion on viability and activity of *Methylosinus trichosporium* OB3b. *Appl. Environ. Microbiol.* 63: 4961-4964.
- Vannelli, T., M. Logan, D. M. Arciero, and A. B. Hooper. 1990. Degradation of halogenated aliphatic compounds by the ammonia-oxidizing bacterium *Nitrosomonas europaea*. *Appl. Environ. Microbiol.* 56:1169-1171.
- Vogel, T. L. and P. L. McCarty. 1987. Abiotic and biotic transformations of 1,1,1-trichloroethane under methanogenic conditions. *Environ. Sci. Technol.* 21: 1208-1213.
- Wackett, L. P., G. A. Brusseau, S. R. Householder, and R. S. Hanson. 1989. Survey of microbial oxygenases: Trichloroethylene degradation by propane oxidizing bacteria. *Appl. Environ. Microbiol.* 55: 2960-2964.
- Wackett, L. P. and D. T. Gibson, 1988. Degradation of trichloroethylene by toluene dioxygenase in whole-cell studies with *Pseudomonas putida* F1. *Appl. Environ. Microbiol.* 54: 1703-1708.

- Waley, S. G. 1980. Kinetics of suicide substrate. *Biochem. J.* 185: 771-773.
- Waley, S. G. 1985. Kinetics of suicide substrate: Practical procedures for determining parameters. *Biochem. J.* 227: 843-849.
- Westrick, J. J., J. W. Mello, and R. F. Thomas. 1984. The ground water supply survey. *J. Am. Water Work Assoc.* 76: 52-59.
- Wiegant, L. P. and J. A. M. de Bont. 1980. A new for ethylene glycol metabolism in *Mycobacterium* E44. *J. Gen. Microbiol.*, 120: 325-331.
- Wilson, J. T. and B. H. Wilson. 1985. Biotransformation of trichloroethylene in soil. *Appl. Environ. Microbiol.* 49: 242-243.
- Yeager, C. M., P. J. Bottomley, D. J. Arp, and M. R. Hyman. 1999. Inactivation of toluene 2-monooxygenase in *Burkholderia cepacia* G4 by Alkynes. *Appl. Environ. Microbiol.* 65: 632-639.

APPENDICES

APPENDIX A

Derivation of the Analytical Solutions for the Mass Transfer of Volatile Compounds in a Batch Reactor and Tests of the Validity of Equilibrium Assumption in the Batch Kinetic Studies

A1. DERIVATION OF ANALYTICAL SOLUTIONS FOR MASS TRANSFER

To evaluate overall mass transfer coefficients of a volatile compound, an analytical solution of the mass transfer model was derived. In the mass transfer experiment, the appearance of a compound into the vapor or aqueous phase via mass transfer was measured rather than disappearance of the compound for the phase. Thus the analytical solutions were derived to match the experimental procedures. Mass balances of the volatile compound in a batch reactor were incorporated into mass transfer model.

The mass flux from liquid phase to the gas phase is:

$$V_L \frac{dS_L}{dt} = JA \quad (\text{A.1})$$

where, V_L = liquid volume (L)

S_L = substrate concentration in liquid phase (μM)

J = mass flux ($\mu\text{mol}/\text{min}/\text{m}^2$)

A = gas and liquid phase interfacial area (m^2)

Mass flux from gas phase to liquid phase is:

$$V_G \frac{dS_G}{dt} = JA \quad (\text{A.2})$$

where, V_G = headspace volume (L)

S_G = substrate concentration in gas phase (μM)

The flux can be expressed in terms of the liquid phase and gas phase concentrations by assuming hypothetical concentrations S_L^* and S_G^* corresponding to equilibrium with bulk liquid and gas phase concentrations.

$$JA = -K_L(S_L^* - S_L)A = -K_G(S_G^* - S_G)A \quad (\text{A.3})$$

$$S_L^* = \frac{S_G}{H_{cs}} \quad (\text{A.4})$$

$$S_G^* = H_{cs} \cdot S_L \quad (\text{A.5})$$

where, K_L = overall liquid phase mass transfer coefficient (m/min)

K_G = overall gas phase mass transfer coefficient (m/min)

S_L^* = hypothetical liquid concentration that would be in equilibrium with the
bulk gas

S_G^* = hypothetical gas concentration that would be in equilibrium with the bulk
liquid

H_{cs} = dimensionless Henry's constant of the substrate

Substituting equation A.3 into A.1, equation A.1 can be written as

$$\frac{dS_L}{dt} = -K_L (S_L^* - S_L) \frac{A}{V_L} = -K_L a_L (S_L^* - S_L) \quad (\text{A.6})$$

where, a_L = specific liquid-side interfacial area ($= A/V_L$)

The equation for dependence of gas phase concentration on K_L was derived.

At equilibrium, flux from gas phase to liquid phase and flux from liquid phase to gas phase are same.

$$V_L \frac{dS_L}{dt} = V_G \frac{dS_G}{dt} \quad (\text{A.7})$$

Thus,

$$\frac{dS_L}{dt} = \frac{V_G}{V_L} \frac{dS_G}{dt} \quad (\text{A.8})$$

Substituting equations A.8 and A.4 into A.6 results in equations A.9 and A.10, respectively,

$$\frac{dS_G}{dt} = -K_L a_L (S_L^* - S_L) \frac{V_L}{V_G} \quad (\text{A.9})$$

$$\frac{dS_G}{dt} = -K_L a_L \left(\frac{S_G}{H_{cs}} - S_L \right) \frac{V_L}{V_G} \quad (\text{A.10})$$

The mass balance on substrate in a batch reactor can be written as

$$M_s = S_L \cdot V_L + S_G \cdot V_G \quad (\text{A.11})$$

Here, M_s symbolizes total substrate mass in the bottle.

Rearranging equation A.11 results in the following equation,

$$S_L = \frac{M_s}{V_L} - \frac{S_G \cdot V_G}{V_L} \quad (\text{A.12})$$

Substituting equation A.12 into A.10 yields the following equation,

$$\frac{dS_G}{dt} = -K_L \cdot a_L \left(\frac{S_G}{H_{cs}} - \frac{M_s}{V_L} + \frac{S_G V_G}{V_L} \right) \cdot \frac{V_L}{V_G} \quad (\text{A.13})$$

The equation for dependence of liquid phase concentration on K_G was also derived

$$\frac{dS_G}{dt} = -K_G (S_G^* - S_G) \cdot \frac{A}{V_G} = -K_G \cdot a_G (S_G^* - S_G) \quad (\text{A.14})$$

where, a_G = specific gas-side interfacial area ($= A/V_G$)

Substituting equations A.7 and A.5 into equation A.14 yields the following equation

$$\frac{dS_L}{dt} = -K_G \cdot a_G (H_{cs} \cdot S_L - S_G) \frac{V_G}{V_L} \quad (\text{A.15})$$

Equation A.11 can be written in terms of S_G .

$$S_G = \frac{M_s}{V_G} - \frac{S_L V_L}{V_G} \quad (\text{A.16})$$

Substituting equation A.16 into equation A.15 results in the following equation

$$\frac{dS_L}{dt} = -K_G \cdot a_G \left(H_{cs} \cdot S_L - \frac{M_s}{V_G} + \frac{S_L V_L}{V_G} \right) \cdot \frac{V_G}{V_L} \quad (\text{A.17})$$

Equations A.13 and A.17 were solved to obtain analytical solutions.

In equation A.13 S_G and S_L are variables, and H_{cs} , S_{tot} , V_L , V_G , and $K_L a_L$ are constants.

Rearranging equation A.13 yields equation A.18.

$$\begin{aligned} \frac{dS_G}{dt} &= -K_L \cdot a_L \left(\frac{V_L}{V_G H_{cs}} \cdot S_G - \frac{M_s}{V_G} + S_G \right) \\ &= -K_L \cdot a_L \left\{ \frac{-M_s}{V_G} + \left(1 + \frac{V_L}{V_G H_{cs}} \right) S_G \right\} \end{aligned} \quad (\text{A.18})$$

If we assume

$$P = \left(\frac{M_s}{V_G} \right) \cdot (K_L \cdot a_L) \quad (\text{A.19})$$

$$Q = \left(1 + \frac{V_L}{V_G H_{cs}} \right) (-K_L \cdot a_L) \quad (\text{A.20})$$

Equation A.18 can be rewritten as

$$\frac{dS_G}{dt} = P + QS_G \quad (\text{A.21})$$

If we assume

$$P + QS_G = X \quad (\text{A.22})$$

$$QdS_G = dX \quad (\text{A.23})$$

Equation A.21 can be rewritten by substituting equation A.23 into equation A.21

$$\frac{\left(\frac{dX}{Q} \right)}{dt} = X \quad (\text{A.24})$$

Rearranging equation A.24 results in the following equation.

$$\frac{dX}{X} = Qdt \quad (\text{A.25})$$

Integrating the equation A.25 yields equation A.27.

$$\int_{X_0}^{X_t} \frac{dX}{X} = Q \int_0^t dt \quad (\text{A.26})$$

$$X_t = X_0 \cdot e^{Qt} \quad (\text{A.27})$$

Substituting equation A.22 into equation A.27, and rearranging for $S_{G,t}$ yields equation (A.28).

$$P + QS_{G,t} = (P + QS_{G,0}) \cdot e^{Qt}$$

$$S_{G,t} = \left(\frac{(P + QS_{G,0}) \cdot e^{Qt}}{Q} \right) - \frac{P}{Q} \quad (\text{A.28})$$

Substituting equations A.19 and A.20 into equation A.28 results in the equation A.29

$$\frac{P}{Q} + S_{G,0} = \frac{-H_{cs} \cdot M_s}{V_G H_{cs} + V_L} + S_{G,0}$$

$$-\frac{P}{Q} = \frac{H_{cs} \cdot M_s}{V_G H_{cs} + V_L}$$

$$S_{G,t} = \frac{H_{cs} \cdot M_s}{V_G H_{cs} + V_L} + \left(S_{G,0} - \frac{H_{cs} \cdot M_s}{V_G H_{cs} + V_L} \right) \cdot e^{-K_L \cdot a_L \left(1 + \frac{V_L}{V_G H_{cs}} \right) t} \quad (\text{A.29})$$

Equation A.17 can also be solved, and the analytical solution is

$$S_{L,0} = \frac{M_s}{H_{cs} V_G + V_L} + \left(S_{L,0} - \frac{M_s}{H_{cs} V_G + V_L} \right) e^{-K_G \cdot a_G \left(1 + \frac{V_G H_{cs}}{V_L} \right) t} \quad (\text{A.30})$$

NLSR analysis using experimental data and the analytical solution (equations A29 and A30) was used to evaluate the overall mass transfer coefficients.

A2. VALIDITY OF EQUILIBRIUM ASSUMPTION

Model simulations were performed in order to determine the experimental conditions where mass transfer does not affect on the transformation rates. The effect of mass transfer on the estimation of zero-order degradation rates of butane (k_{\max}) at high butane concentrations ($150 \mu\text{M}$) was estimated. Hamamura et al. (1999) reported the K_s value for butane-grown CF8, isolated from the same butane-supplemented microcosms as our mixed culture enriched, was below $5 \mu\text{M}$. Thus K_s was assumed to be much smaller than S_L , while k_{\max} was set at $3 \mu\text{mol/mg TSS/hr}$. Equations 4.5 and 4.6 in Chapter 4 for butane degradation were simulated with using STELA Research software (High Performance Systems, Inc., Hanover, NH). Initial rates were estimated at different levels of TSS.

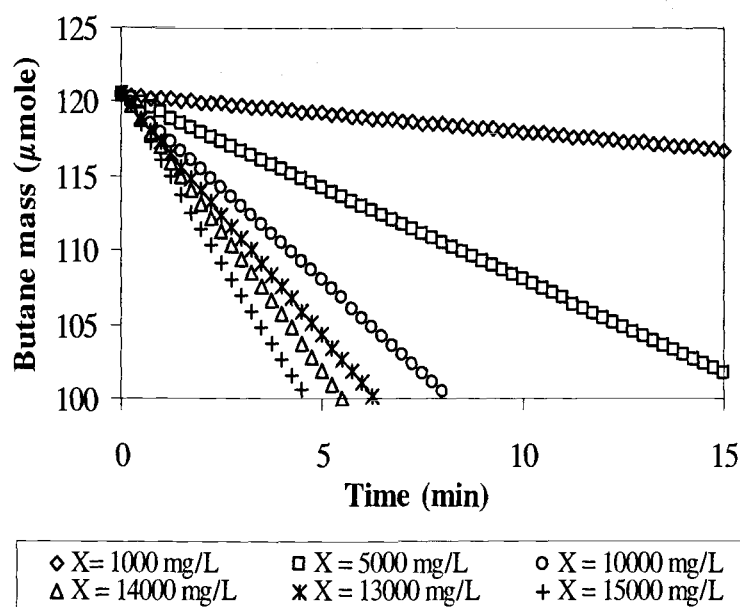


Figure A2.1. Simulation results of butane degradation at different levels of TSS

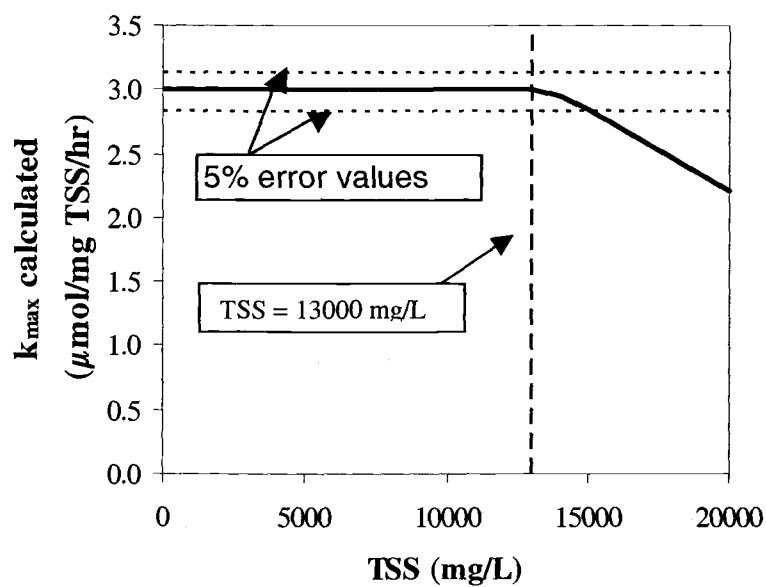


Figure A2.2. The k_{\max} calculated versus TSS

The k_{\max} remained constant at lower than 13000 mg TSS/L, however, the rates decreased due to mass transfer limitations at higher than the concentrations.

APPENDIX B

Derivation of Inhibition Equations and Linearized Inhibition Equations

B1. DERIVATION OF INHIBITION MODEL EQUATIONS

The general model for competitive inhibition and mixed inhibition is presented by the following reaction scheme (Cornish-Bowden, 1994):



Here, E, S, ES, EI, ESI, and P symbolize enzyme, substrate, enzyme-substrate complex, enzyme-inhibitor complex, enzyme-substrate-inhibitor complex, and product, respectively. I_{c1} , I_{c2} , I_{c3} , and I_{m1} , are competitive inhibitors, and I_{m4} is an inhibitor of mixed inhibition. The K is an equilibrium constant and k_p is an rate coefficient of the product production reaction.

The mass balance on enzyme yields

$$[E]_t = [E] + [ES] + [EI_{c1}] + [EI_{c2}] + [EI_{c3}] + [EI_{m1}] + [ESI_{m1}] \quad (\text{B.7})$$

Assuming equilibrium (the forward reaction rate is equal to the reverse reaction rate),

$$K_{ic,1} = \frac{[E][I_{c1}]}{[EI_{c1}]} \quad [EI_{c1}] = \frac{[E][I_{c1}]}{K_{ic,1}} \quad (\text{B.8})$$

$$K_{ic,2} = \frac{[E][I_{c2}]}{[EI_{c2}]} \quad [EI_{c2}] = \frac{[E][I_{c2}]}{K_{ic,2}} \quad (\text{B.9})$$

$$K_{ic,3} = \frac{[E][I_{c3}]}{[EI_{c3}]} \quad [EI_{c3}] = \frac{[E][I_{c3}]}{K_{ic,3}} \quad (\text{B.10})$$

$$K_{ic,m1} = \frac{[E][I_{m1}]}{[EI_{m1}]} \quad [EI_{m4}] = \frac{[E][I_{m1}]}{K_{ic,4}} \quad (\text{B.11})$$

$$K_{iu,m1} = \frac{[ES][I_{m1}]}{[ESI_{m1}]} \quad [ESI_{m1}] = \frac{[ES][I_{m1}]}{K_{iu,m1}} \quad (\text{B.12})$$

$$K_s = \frac{[E][S]}{[ES]} \quad [E] = \frac{K_s[ES]}{[S]} \quad (\text{B.13})$$

Substituting equation B.13 into equations B.8, B.9, B.10, and B.11 results in the following equations.

$$[EI_{c1}] = \frac{[I_{c1}]}{K_{ic,1}} \frac{K_s[ES]}{[S]} \quad (\text{B.14})$$

$$[EI_{c2}] = \frac{[I_{c2}]}{K_{ic,2}} \frac{K_s[ES]}{[S]} \quad (\text{B.15})$$

$$[EI_{c3}] = \frac{[I_{c3}] K_s [ES]}{K_{ic,3} [S]} \quad (\text{B.16})$$

$$[EI_{m1}] = \frac{[I_{m1}] K_s [ES]}{K_{ic,m1} [S]} \quad (\text{B.17})$$

$$v = k_p [ES] \quad (\text{B.18})$$

$$k_{\max} = k_p [E]_t \quad (\text{B.19})$$

Here, k is an initial degradation rate and k_{\max} is a maximum degradation rate.

Substituting equations B.12, B.13, B.14, B.15, B.16, and B.17 into equation B.7 yields the following equation.

$$[E]_t = \frac{K_s [ES]}{[S]} + [ES] + \frac{[I_{c1}] K_s [ES]}{K_{ic,1} [S]} + \frac{[I_{c2}] K_s [ES]}{K_{ic,2} [S]} + \frac{[I_{c3}] K_s [ES]}{K_{ic,3} [S]} + \frac{[I_{m1}] K_s [ES]}{K_{ic,m1} [S]} + \frac{[ES][I_{m1}]}{K_{iu,m1}} \quad (\text{B.20})$$

The equation B.20 can be written in terms of $[ES]$.

$$[ES] = \frac{[E]_t}{\frac{K_s}{[S]} + 1 + \frac{[I_{c1}] K_s}{K_{ic,1} [S]} + \frac{[I_{c2}] K_s}{K_{ic,2} [S]} + \frac{[I_{c3}] K_s}{K_{ic,3} [S]} + \frac{[I_{m1}] K_s}{K_{ic,m1} [S]} + \frac{[I_{m1}]}{K_{iu,m1}}} \quad (\text{B.21})$$

Substituting equation B.21 in equation B.18 results in the following equation.

$$v = \frac{k_p \cdot [E]_t}{\frac{K_s}{[S]} + 1 + \frac{[I_{c1}]}{K_{ic,1}} \frac{K_s}{[S]} + \frac{[I_{c2}]}{K_{ic,2}} \frac{K_s}{[S]} + \frac{[I_{c3}]}{K_{ic,3}} \frac{K_s}{[S]} + \frac{[I_{m1}]}{K_{ic,m1}} \frac{K_s}{[S]} + \frac{[I_{m1}]}{K_{iu,m1}}} \quad (\text{B.22})$$

Substituting equation B.19 into equation B.22 and rearranging it yields the following equations.

$$v = \frac{k_{\max}}{\frac{K_s}{[S]} \left(1 + \frac{[I_{c1}]}{K_{ic,1}} + \frac{[I_{c2}]}{K_{ic,2}} + \frac{[I_{c3}]}{K_{ic,3}} + \frac{[I_{m1}]}{K_{ic,mq}}\right) + \left(1 + \frac{[I_{m1}]}{K_{iu,m1}}\right)} \quad (\text{B.23})$$

$$= \frac{k_{\max} [S]}{K_s \left(1 + \frac{[I_{c1}]}{K_{ic,1}} + \frac{[I_{c2}]}{K_{ic,2}} + \frac{[I_{c3}]}{K_{ic,3}} + \frac{[I_{m1}]}{K_{ic,m1}}\right) + \left(1 + \frac{[I_{m1}]}{K_{iu,m1}}\right) [S]}$$

$$v = \frac{\frac{k_{\max}}{\left(1 + \frac{[I_{m1}]}{K_{iu,m1}}\right)} \cdot [S]}{K_s \left\{ \frac{1 + \frac{[I_{c1}]}{K_{ic,1}} + \frac{[I_{c2}]}{K_{ic,2}} + \frac{[I_{c3}]}{K_{ic,3}} + \frac{[I_{m1}]}{K_{ic,m1}}}{\left(1 + \frac{[I_{m1}]}{K_{iu,m1}}\right)} \right\} + [S]} \quad (\text{B.24})$$

Thus, generally equation B.24 can be written:

$$v = \frac{\frac{k_{\max}}{(1 + \sum_{l=1}^l \frac{[I_{ml}]}{K_{iu,l}})} \cdot [S]}{K_s \left\{ \frac{1 + \sum_{j=1}^j \frac{[I_{cj}]}{K_{ic,j}} + \sum_{l=1}^l \frac{[I_{ml}]}{K_{ic,ml}}}{(1 + \sum_{l=1}^l \frac{[I_{ml}]}{K_{iu,l}})} \right\} + [S]} \quad (\text{B.25})$$

If there is only one competitive inhibitor present, equation B.25 results in the following equation.

$$v = \frac{k_{\max} [S]}{K_s \left\{ 1 + \frac{[I_{c1}]}{K_{ic,1}} \right\} + [S]} \quad (\text{B.26})$$

If there is only one mixed inhibitor present, equation B.25 results in the following equation.

$$v = \frac{\frac{k_{\max}}{(1 + \frac{[I_{m1}]}{K_{iu,m1}})} \cdot [S]}{K_s \left\{ \frac{1 + \frac{[I_{m1}]}{K_{ic,m1}}}{1 + \frac{[I_{m1}]}{K_{iu,m1}}} \right\} + [S]} \quad (\text{B.27})$$

If $K_{iu,m1} = K_{ic,m1}$, the equation yields noncompetitive inhibition model.

$$v = \frac{\frac{k_{\max}}{(1 + \frac{[I_{m1}]}{K_{iu,m1}})} \cdot [S]}{K_s + [S]} \quad (\text{B.28})$$

B2. DERIVATION OF LINEARIZED EQUATIONS USED TO EVALUATE THE INITIAL GUESS OF KINETIC PARAMETERS FOR NLSR ANALYSIS

The linearized equations are derived from the correlation between k_{\max}^{app} or K_s^{app} and k_{\max} , K_s , or I_L as presented in Table B2.1.

Table B2.1. The effects of inhibitors on the parameters of the Michaelis-Menten equation.

Type of Inhibition	k_{\max}^{app}	K_s^{app}
Mixed	$\frac{k_{\max}}{(1 + \frac{I_L}{K_{iu}})}$	$\frac{K_s (1 + \frac{I_L}{K_{ic}})}{(1 + \frac{I_L}{K_{iu}})}$
Noncompetitive	$\frac{k_{\max}}{(1 + \frac{I_L}{K_{iu}})}$	K_s
Competitive	k_{\max}	$K_s (1 + \frac{I_L}{K_{ic}})$
Uncompetitive	$\frac{k_{\max}}{(1 + \frac{I_L}{K_{iu}})}$	$\frac{K_s}{(1 + \frac{I_L}{K_{iu}})}$

Mixed Inhibition

As shown in Table B2.1,

$$k_{\max}^{app} = \frac{k_{\max}}{(1 + \frac{I_L}{K_{iu}})} \quad (B.29)$$

$$K_s^{app} = \frac{K_s (1 + \frac{I_L}{K_{ic}})}{(1 + \frac{I_L}{K_{iu}})} \quad (B.30)$$

Inverting equation B.29 and then linearizing result equation B.31

$$\frac{1}{k_{\max}^{app}} = \frac{(1 + \frac{I_L}{K_{iu}})}{k_{\max}} = \frac{1}{k_{\max}} + \frac{1}{k_{\max} K_{iu}} I_L \quad (B.31)$$

This equation can be plotted using known k_{\max}^{app} determined from direct linear plot and

I_L . Slope ($1/k_{\max}/K_{iu}$) and y intercept ($1/k_{\max}$) can be obtained from linear plot of

$1/k_{\max}^{app}$ versus I_L . From the slope and y intercept, k_{\max} and K_{iu} can be calculated.

Rearranging equation 29 yields the following equation

$$(1 + \frac{I_L}{K_{iu}}) = \frac{k_{\max}}{k_{\max}^{app}} \quad (B.32)$$

Substituting equation B.32 into equation B.30 and then linearizing result the following equations

$$K_s^{app} = \frac{K_s (1 + \frac{I_L}{K_{ic}})}{(\frac{k_{\max}}{k_{\max}^{app}})} = \frac{k_{\max}^{app} K_s}{k_{\max}} (1 + \frac{I_L}{K_{ic}}) \quad (B.33)$$

$$K_s^{app} = \frac{k_{\max}^{app} K_s}{k_{\max}} + \frac{k_{\max}^{app} K_s}{k_{\max} K_{ic}} I_L \quad (B.34)$$

Dividing both side by $1/k_{\max}^{app}$ yields the following equation.

$$\frac{K_s^{app}}{k_{\max}^{app}} = \frac{K_s}{k_{\max}} + \frac{K_s}{k_{\max} K_{ic}} I_L \quad (B.35)$$

This equation can be plotted using known k_{\max}^{app} , K_s^{app} , and I_L . The slope ($K_s/k_{\max}/K_{ic}$)

and y intercept (K_s/k_{\max}) can be obtained from the plot of K_s^{app}/k_{\max}^{app} versus I_L . From

the slope and y intercept, K_s and K_{ic} can be calculated. Thus, all kinetic parameters, K_s , k_{max} , K_{ic} , and K_{iu} can be estimated from two linear plots using equations B.31 and B.35.

Noncompetitive Inhibition

Equation B.29 can be applied for the case of noncompetitive inhibition, thus the k_{max} and K_{iu} values can be calculated using equations B.31. In the case of noncompetitive inhibition K_s^{app} is equal to K_s , thus K_s can be estimated by averaging the values of K_s^{app} at various I_L that are determined using the direct linear plot.

Competitive Inhibition

As shown in Table B2.1,

$$K_s^{app} = K_s \left(1 + \frac{I_L}{K_{ic}}\right) \quad (B.36)$$

Linearizing equation B.36 yields

$$K_s^{app} = K_s + \frac{K_s}{K_{ic}} I_L \quad (B.37)$$

The equation B.37 can be plotted using K_s^{app} determined from direct linear plot and I_L .

The slope (K_s/K_{ic}) and the y intercept (K_s) can be obtained from the plot of

K_s^{app} versus I_L , and then K_s and K_{ic} can be calculated. For the case of competitive

inhibition k_{max}^{app} is equal to k_{max} , thus k_{max} can be estimated by averaging the values of

k_{max}^{app} at various I_L that are determined using the direct linear plot. Thus, a linear plot

of equation B.37 using values from the direct linear plot yields k_{max} , K_s , and K_{ic} .

Uncompetitive Inhibition

As shown in Table B2.1,

$$k_{\max}^{app} = \frac{k_{\max}}{(1 + \frac{I_L}{K_{iu}})} \quad (B.38)$$

$$K_s^{app} = \frac{K_s}{(1 + \frac{I_L}{K_{iu}})} \quad (B.39)$$

Inverting equations B.38 and B.39 and then linearizing results in equations B.40 and (B.41), respectively

$$\frac{1}{k_{\max}^{app}} = \frac{1}{k_{\max}} + \frac{1}{k_{\max} K_{iu}} I_L \quad (B.40)$$

$$\frac{1}{K_s^{app}} = \frac{1}{K_s} + \frac{1}{K_s K_{iu}} I_L \quad (B.41)$$

Both equation can be plotted using K_s^{app} and k_{\max}^{app} values determined using the direct linear plot and I_L . In equation B.40, the slope ($1/k_{\max}/K_{iu}$) and the y intercept ($1/k_{\max}$) can be obtained from plot of $1/k_{\max}^{app}$ versus I_L , and then K_{\max} and K_{iu} can be calculated. In equation B.41, the slope ($1/K_s/K_{iu}$) and the y intercept ($1/K_s$) can be obtained from plot of $1/K_s^{app}$ versus I_L , and then K_s can be calculated. Thus all kinetic parameters can be estimated from the linear plot using equations B.40 and B.41.

Consequently, linearized equations derived above can be used to estimate the all kinetic parameters such as k_{\max} , K_s , K_{ic} , K_{iu} . These parameters might be used in the absence of NLSR analysis, or for the first guesses of parameters for NLSR analysis.

APPENDIX C

Estimation Methods Combining the Direct Linear Plot to Determine Inhibition Type and Values of K_s^{app} and $k_{\text{max}}^{\text{app}}$, Linearized Equations to Obtain the Initial Guesses of Kinetic Parameters, and NLSR Analysis to Determine the Kinetic Parameters

C1. MIXED INHIBITION ON 1,1-DCE TRANSFORMATION BY BUTANE

K_s^{app} and k_{max}^{app} Values of 1,1-DCE in the Presence of Butane

Table C1.1. K_s^{app} and k_{max}^{app} values of 1,1-DCE in the presence of butane (0 μ M).

- Slope and y intercept of extrapolated linear lines

Batch vial #	Substrate, S_L 1,1-DCE (μ M)	Inhibitor, I_L Butane (μ M)	$-S_L$ (μ M)	Initial degradation rate, v (μ mol/mg TSS/hr)	Extrapolated line	
					Slope	Y intercept
BUDE#17-2	1.61	0	-1.61	0.728	0.45	0.73
BUDE #18	4.65	0	-4.65	0.968	0.21	0.97
BUDE #19	11.34	0	-11.34	1.052	0.09	1.05
BUDE #20	26.32	0	-26.32	1.167	0.04	1.17

- Intersection coordinates and best estimate (median) of K_s^{app} and k_{max}^{app}

Number of data	Batch vial #	Batch vial #	Coordinate of intersection		Order from the lowest to highest	
			K_s^{app} (μ M)	k_{max}^{app} (μ mol/mg TSS/hr)	K_s^{app} (μ M)	k_{max}^{app} (μ mol/mg TSS/hr)
1	BUDE#17-2	BUDE#18	0.98	1.17	0.72	1.12
2	BUDE#17-2	BUDE#19	0.90	1.14	0.90	1.14
3	BUDE#17-2	BUDE#20	1.07	1.21	0.98	1.17
Median	-	-	-	-	1.03	1.19
4	BUDE#18	BUDE#19	0.72	1.12	1.07	1.21
5	BUDE#18	BUDE#20	1.21	1.22	1.21	1.22
6	BUDE#19	BUDE#20	2.37	1.27	2.37	1.27

Table C1.2. K_s^{app} and k_{max}^{app} values of 1,1-DCE in the presence of butane ($1.8 \pm 0.01 \mu\text{M}$).

- Slope and y intercept of extrapolated linear lines

Batch vial #	Substrate, S_L 1,1-DCE (μM)	Inhibitor, I_L Butane (μM)	$-S_L$ (μM)	Initial degradation rate, v ($\mu\text{mol/mg TSS/hr}$)	Extrapolated line	
					Slope	Y intercept
BUDE#1	1.68	1.84	-1.68	0.202	0.121	0.202
BUDE#2	4.67	1.84	-4.67	0.419	0.090	0.419
BUDE#3	10.84	1.82	-10.84	0.643	0.059	0.643
BUDE#4	25.37	1.83	-25.37	0.792	0.031	0.792

- Intersection coordinates and best estimate (median) of K_s^{app} and k_{max}^{app}

Number of data	Batch vial #	Batch vial #	Coordinate of intersection		Order from the lowest to highest	
			K_s^{app} (μM)	k_{max}^{app} ($\mu\text{mol/mg TSS/hr}$)	K_s^{app} (μM)	k_{max}^{app} ($\mu\text{mol/mg TSS/hr}$)
1	BUDE#1	BUDE#2	7.05	1.05	5.29	0.96
2	BUDE#1	BUDE#3	7.18	1.07	6.35	1.00
3	BUDE#1	BUDE#4	6.59	1.00	6.59	1.00
Median	-	-	-	-	6.82	1.03
4	BUDE#2	BUDE#3	7.32	1.08	7.05	1.05
5	BUDE#2	BUDE#4	6.35	1.00	7.18	1.07
6	BUDE#3	BUDE#4	5.29	0.96	7.32	1.08

Table C1.3. K_s^{app} and k_{max}^{app} values of 1,1-DCE in the presence of butane ($4.6 \pm 0.01 \mu\text{M}$).

- Slope and y intercept of extrapolated linear lines

Batch vial #	Substrate, S_L 1,1-DCE (μM)	Inhibitor, I_L Butane (μM)	$-S_L$ (μM)	Initial degradation rate, v ($\mu\text{mol/mg TSS/hr}$)	Extrapolated line	
					Slope	Y intercept
BUDE#5	1.65	4.76	-1.65	0.115	0.070	0.115
BUDE#6	4.61	4.68	-4.61	0.251	0.054	0.251
BUDE#7	10.33	4.50	-10.33	0.385	0.037	0.385
BUDE#8	25.09	4.61	-25.09	0.508	0.020	0.508

- Intersection coordinates and best estimate (median) of K_s^{app} and k_{max}^{app}

Number of data	Batch vial #	Batch vial #	Coordinate of intersection		Order from the lowest to highest	
			K_s^{app} (μM)	k_{max}^{app} ($\mu mol/mg$ TSS/hr)	K_s^{app} (μM)	k_{max}^{app} ($\mu mol/mg$ TSS/hr)
1	BUDE#5	BUDE#6	8.75	0.73	7.22	0.65
2	BUDE#5	BUDE#7	8.26	0.69	7.52	0.66
3	BUDE#5	BUDE#8	7.90	0.67	7.82	0.67
Median	-	-	-	-	7.86	0.67
4	BUDE#6	BUDE#7	7.82	0.68	7.90	0.68
5	BUDE#6	BUDE#8	7.52	0.66	8.26	0.69
6	BUDE#7	BUDE#8	7.22	0.65	8.75	0.73

Table C1.4. K_s^{app} and k_{max}^{app} values of 1,1-DCE in the presence of butane ($8.6 \pm 0.02 \mu M$).

- Slope and y intercept of extrapolated linear lines

Batch vial #	Substrate, S_L 1,1-DCE (μM)	Inhibitor, I_L Butane (μM)	$-S_L$ (μM)	Initial degradation rate, v ($\mu mol/mg$ TSS/hr)	Extrapolated line	
					Slope	Y intercept
BUDE#9	1.67	8.74	-1.67	0.065	0.039	0.065
BUDE#10	4.71	8.66	-4.71	0.133	0.028	0.133
BUDE#11	10.43	8.47	-10.43	0.243	0.023	0.243
BUDE#12	24.40	8.71	-24.40	0.357	0.015	0.357

- Intersection coordinates and best estimate (median) of K_s^{app} and k_{max}^{app}

Number of data	Batch vial #	Batch vial #	Coordinate of intersection		Order from the lowest to highest	
			K_s^{app} (μM)	k_{max}^{app} ($\mu mol/mg$ TSS/hr)	K_s^{app} (μM)	k_{max}^{app} ($\mu mol/mg$ TSS/hr)
1	BUDE#9	BUDE#10	6.14	0.31	6.14	0.31
2	BUDE#9	BUDE#11	11.2	0.51	11.2	0.51
3	BUDE#9	BUDE#12	11.9	0.53	11.9	0.53
Median	-	-	-	-	12.5	0.54
4	BUDE#10	BUDE#11	22.8	0.77	13.1	0.55
5	BUDE#10	BUDE#12	16.5	0.60	16.5	0.60
6	BUDE#11	BUDE#12	13.1	0.55	22.8	0.77

Table C1.5. K_s^{app} and k_{max}^{app} values of 1,1-DCE in the presence of butane ($13 \pm 0.1 \mu\text{M}$).

- Slope and y intercept of extrapolated linear lines

Batch vial #	Substrate, S_L 1,1-DCE (μM)	Inhibitor, I_L Butane (μM)	$-S_L$ (μM)	Initial degradation rate, v ($\mu\text{mol/mg TSS/hr}$)	Extrapolated line	
					Slope	Y intercept
BUDE#13	1.67	12.87	-1.67	0.040	0.024	0.040
BUDE#14	4.97	12.92	-4.97	0.094	0.019	0.094
BUDE#15	11.10	13.08	-11.10	0.161	0.014	0.161
BUDE#16	25.46	13.13	-25.46	0.227	0.009	0.227

- Intersection coordinates and best estimate (median) of K_s^{app} and k_{max}^{app}

Number of data	Batch vial #	Batch vial #	Coordinate of intersection		Order from the lowest to highest	
			K_s^{app} (μM)	k_{max}^{app} ($\mu\text{mol/mg TSS/hr}$)	K_s^{app} (μM)	k_{max}^{app} ($\mu\text{mol/mg TSS/hr}$)
1	BUDE#13	BUDE#14	10.5	0.29	10.5	0.29
2	BUDE#13	BUDE#15	12.6	0.34	11.8	0.33
3	BUDE#13	BUDE#16	12.3	0.34	12.3	0.34
Median	-	-	-	-	12.4	0.34
4	BUDE#14	BUDE#15	15.0	0.38	12.6	0.34
5	BUDE#14	BUDE#16	13.3	0.35	13.3	0.35
6	BUDE#15	BUDE#16	11.8	0.33	15.0	0.38

Direct Linear Plot

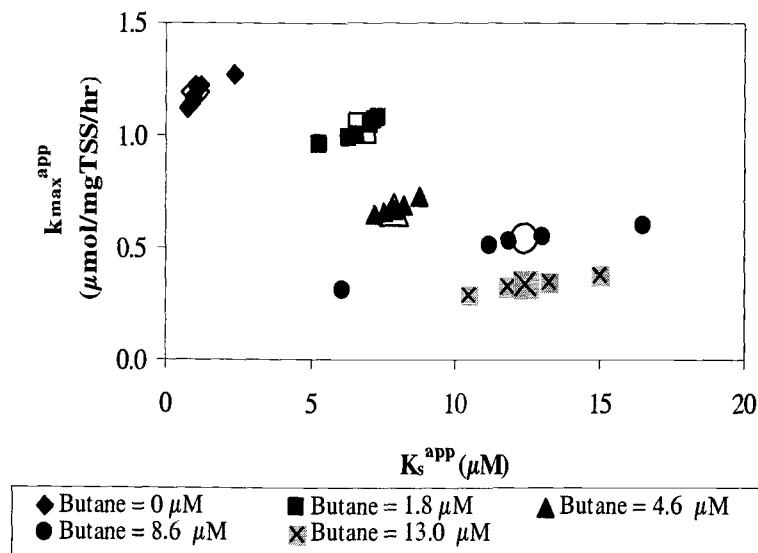


Figure C1.1. Direct linear plot showing mixed inhibition on 1,1-DCE transformation by butane.

Linearized Plot

Table C1.6. Values used for linearized plot in the case of mixed inhibition on 1,1-DCE transformation by butane

Inhibitor (Butane) (μM)	K_s^{app} (μM)	k_{max}^{app} ($\mu\text{mol/ mg TSS/hr}$)	$1/k_{max}^{app}$ ($\text{mg TSS-hr}/\mu\text{mol}$)	K_s^{app}/k_{max}^{app} (mg TSS-hr/L)
0.0	1.03	1.19	0.84	0.9
1.8	6.82	1.03	0.98	6.7
4.6	7.86	0.67	1.49	11.7
8.6	12.5	0.54	1.86	23.1
13	12.4	0.34	2.94	36.6

Table C1.7. Initial guesses of parameters obtained linearized plot in the case of inhibition on 1,1-DCE transformation by butane

Plot ($1/k_{max}^{app}$ vs. I_L)	Y intercept ($=1/k_{max}$) ($\text{mg TSS-hr}/\mu\text{mol}$)	Slope ($= 1/K_{iu}/k_{max}$) ($\text{mg TSS-hr-L}/\mu\text{mol}^2$)	k_{max} ($\mu\text{mol/ mg TSS/hr}$)	K_{iu} (μM)
	0.73	0.16	1.37	4.64
Plot (K_s^{app}/k_{max}^{app} vs. I_L)	Y intercept ($=K_s/k_{max}$) (mg TSS-hr/L)	Slope ($= K_s/K_{ic}/k_{max}$) ($\text{mg TSS-hr}/\mu\text{mol}$)	K_s ($\mu\text{mol/ mg TSS/hr}$)	K_{ic} (μM)
	0.61	2.7	0.83	0.23

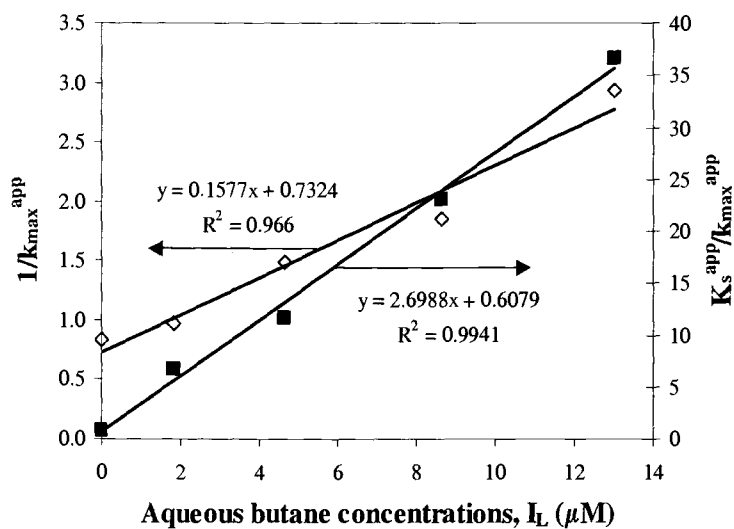


Figure C1.2. Linearized plot in the case of mixed inhibition of 1,1-DCE transformation by butane

NLSR Analysis

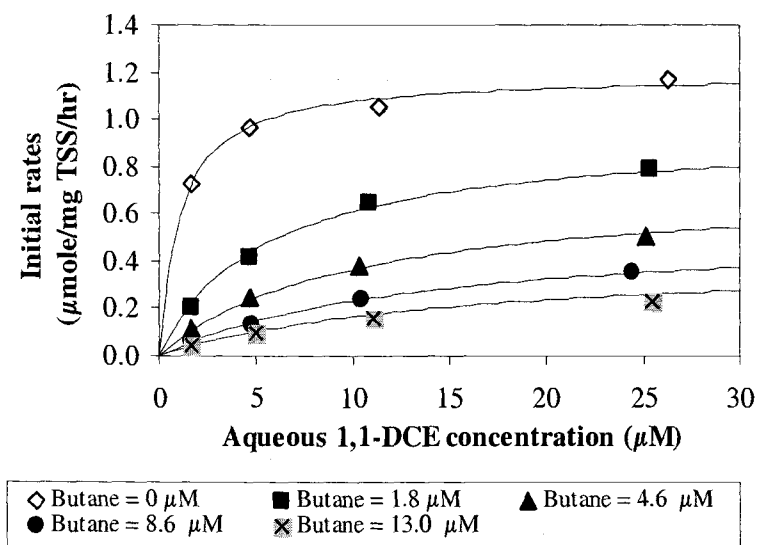


Figure C1.3. Best fit obtained from NLSR analysis using mixed inhibition model. (Residual Standard Error = 0.018, $k_{\text{max}} = 1.2 \pm 0.04 \mu\text{mol/mg TSS/hr}$, $K_s = 1.05 \pm 0.18 \mu\text{M}$, $K_{ic} = 0.33 \pm 0.07 \mu\text{M}$ and $K_{iu} = 6.9 \pm 1.6 \mu\text{M}$)

C2. MIXED INHIBITION ON 1,1-DCA TRANSFORMATION BY BUTANE

K_s^{app} and k_{max}^{app} Values of 1,1-DCA in the Presence of Butane

Table C2.1. K_s^{app} and k_{max}^{app} values of 1,1-DCA in the presence of butane (0 μ M).

- Slope and y intercept of extrapolated linear lines

Batch Vial #	Substrate, S_L 1,1-DCA (μ M)	Inhibitor, I_L Butane (μ M)	$-S_L$ (μ M)	Initial degradation rate, v (μ mol/mg TSS/hr)	Extrapolated line	
					Slope	Y intercept
BUDA#21	17.7	0.00	-17.7	0.212	0.013	0.220
BUDA#22	40.1	0.00	-40.1	0.297	0.007	0.297
BUDA#23	86.8	0.00	-86.8	0.368	0.004	0.368
BUDA#24	132	0.00	-132	0.386	0.003	0.385

- Intersection coordinates and best estimate (median) of K_s^{app} and k_{max}^{app}

Number of data	Batch vial #	Batch vial #	Coordinate of intersection		Order from the lowest to highest	
			K_s^{app} (μ M)	k_{max}^{app} (μ mol/mg TSS/hr)	K_s^{app} (μ M)	k_{max}^{app} (μ mol/mg TSS/hr)
1	BUDA#21	BUDA#22	15.4	0.41	15.4	0.411
2	BUDA#21	BUDA#23	18.1	0.45	12.9	0.423
3	BUDA#21	BUDA#24	17.4	0.44	17.4	0.436
Median	-	-	-	-	17.7	0.44
4	BUDA#22	BUDA#23	22.4	0.46	18.1	0.443
5	BUDA#22	BUDA#24	19.6	0.44	19.6	0.445
6	BUDA#23	BUDA#24	12.9	0.42	22.4	0.463

Table C2.2. K_s^{app} and k_{max}^{app} values of 1,1-DCA in the presence of butane ($0.62 \pm 0.02 \mu\text{M}$).

- Slope and y intercept of extrapolated linear lines

Batch Vial #	Substrate, S_L 1,1-DCA (μM)	Inhibitor, I_L Butane (μM)	$-S_L$ (μM)	Initial degradation rate, v ($\mu\text{mol/mg TSS/hr}$)	Extrapolated line	
					Slope	Y intercept
BUDA#5	15.6	0.63	-15.6	0.188	0.012	0.188
BUDA#9	38.5	0.61	-38.5	0.257	0.007	0.257
BUDA#13	90.2	0.60	-90.2	0.325	0.004	0.325
BUDA#17	134	0.64	-134	0.344	0.003	0.344

- Intersection coordinates and best estimate (median) of K_s^{app} and k_{max}^{app}

Number of data	Batch vial #	Batch vial #	Coordinate of intersection		Order from the lowest to highest	
			K_s^{app} (μM)	k_{max}^{app} ($\mu\text{mol/mg TSS/hr}$)	K_s^{app} (μM)	k_{max}^{app} ($\mu\text{mol/mg TSS/hr}$)
1	BUDA#5	BUDA#9	12.8	0.34	12.8	0.34
2	BUDA#5	BUDA#13	16.3	0.38	16.3	0.38
3	BUDA#5	BUDA#17	16.4	0.39	16.4	0.39
Median	-	-	-	-	17.1	0.39
4	BUDA#9	BUDA#13	22.4	0.41	17.7	0.39
5	BUDA#9	BUDA#17	21.2	0.40	21.2	0.40
6	BUDA#13	BUDA#17	17.7	0.39	22.3	0.41

Table C2.3. K_s^{app} and k_{max}^{app} values of 1,1-DCA in the presence of butane ($1.7 \pm 0.01 \mu\text{M}$).

- Slope and y intercept of extrapolated linear lines

Batch Vial #	Substrate, S_L 1,1-DCA (μM)	Inhibitor, I_L Butane (μM)	$-S_L$ (μM)	Initial degradation rate, v ($\mu\text{mol/mg TSS/hr}$)	Extrapolated line	
					Slope	Y intercept
BUDA#6	15.9	1.69	-15.9	0.136	0.009	0.136
BUDA#10	40.2	1.69	-40.2	0.205	0.005	0.205
BUDA#14	84.0	1.72	-84.0	0.255	0.003	0.255
BUDA#18	134	1.72	-134	0.273	0.002	0.273

- Intersection coordinates and best estimate (median) of K_s^{app} and k_{max}^{app}

Number of data	Batch vial #	Batch vial #	Coordinate of intersection		Order from the lowest to highest	
			K_s^{app} (μM)	k_{max}^{app} ($\mu mol/mg$ TSS/hr)	K_s^{app} (μM)	k_{max}^{app} ($\mu mol/mg$ TSS/hr)
1	BUDA#6	BUDA#10	19.5	0.31	18.1	0.305
2	BUDA#6	BUDA#14	21.3	0.32	19.5	0.310
3	BUDA#6	BUDA#18	20.9	0.32	20.9	0.316
Median	-	-	-	-	21.1	0.318
4	BUDA#10	BUDA#14	24.4	0.33	21.3	0.319
5	BUDA#10	BUDA#18	22.4	0.32	22.4	0.320
6	BUDA#14	BUDA#18	18.1	0.31	24.4	0.329

Table C2.4. K_s^{app} and k_{max}^{app} values of 1,1-DCA in the presence of butane ($3.2 \pm 0.13 \mu M$).

- Slope and y intercept of extrapolated linear lines

Batch vial #	Substrate, S_L 1,1-DCA (μM)	Inhibitor, I_L Butane (μM)	$-S_L$ (μM)	Initial degradation rate, v ($\mu mol/mg$ TSS/hr)	Extrapolated line	
					Slope	Y intercept
BUDA#7	15.6	3.29	-15.6	0.114	0.007	0.114
BUDA#11	40.1	3.26	-40.1	0.161	0.004	0.161
BUDA#15	83.5	3.32	-83.5	0.200	0.002	0.200
BUDA#19	137	3.03	-137	0.218	0.002	0.218

- Intersection coordinates and best estimate (median) of K_s^{app} and k_{max}^{app}

Number of data	Batch vial #	Batch vial #	Coordinate of intersection		Order from the lowest to highest	
			K_s^{app} (μM)	k_{max}^{app} ($\mu mol/mg$ TSS/hr)	K_s^{app} (μM)	k_{max}^{app} ($\mu mol/mg$ TSS/hr)
1	BUDA#7	BUDA#11	14.1	0.22	14.1	0.22
2	BUDA#7	BUDA#15	17.4	0.24	17.4	0.24
3	BUDA#7	BUDA#19	18.2	0.25	18.2	0.25
Median	-	-	-	-	20.4	0.25
4	BUDA#11	BUDA#15	24.2	0.26	22.7	0.25
5	BUDA#11	BUDA#19	23.7	0.26	23.7	0.26
6	BUDA#15	BUDA#19	22.7	0.25	24.2	0.26

Table C2.5. K_s^{app} and k_{max}^{app} values of 1,1-DCA in the presence of butane ($4.9 \pm 0.07 \mu\text{M}$).

- Slope and y intercept of extrapolated linear lines

Batch vial #	Substrate, S_L 1,1-DCA (μM)	Inhibitor, I_L Butane (μM)	$-S_L$ (μM)	Initial degradation rate, v ($\mu\text{mol/mg TSS/hr}$)	Extrapolated line	
					Slope	Y intercept
BUDA#8	15.4	4.895	-15.4	0.062	0.004	0.062
BUDA#12	40.0	4.895	-40.0	0.121	0.003	0.121
BUDA#16	86.3	4.947	-86.3	0.148	0.002	0.148
BUDA#20	132	5.053	-132	0.146	0.001	0.146

- Intersection coordinates and best estimate (median) of K_s^{app} and k_{max}^{app}

Number of data	Batch vial #	Batch vial #	Coordinate of intersection		Order from the lowest to highest	
			K_s^{app} (μM)	k_{max}^{app} ($\mu\text{mol/mg TSS/hr}$)	K_s^{app} (μM)	k_{max}^{app} ($\mu\text{mol/mg TSS/hr}$)
1	BUDA#8	BUDA#12	59.0	0.30	-3.25	0.14
2	BUDA#8	BUDA#16	37.0	0.21	12.9	0.16
3	BUDA#8	BUDA#20	28.6	0.18	20.4	0.18
Median	-	-	-	-	24.5	0.18
4	BUDA#12	BUDA#16	20.4	0.18	28.6	0.18
5	BUDA#12	BUDA#20	12.9	0.16	37.0	0.21
6	BUDA#16	BUDA#20	-3.25	0.142	59.0	0.300

Direct Linear Plot

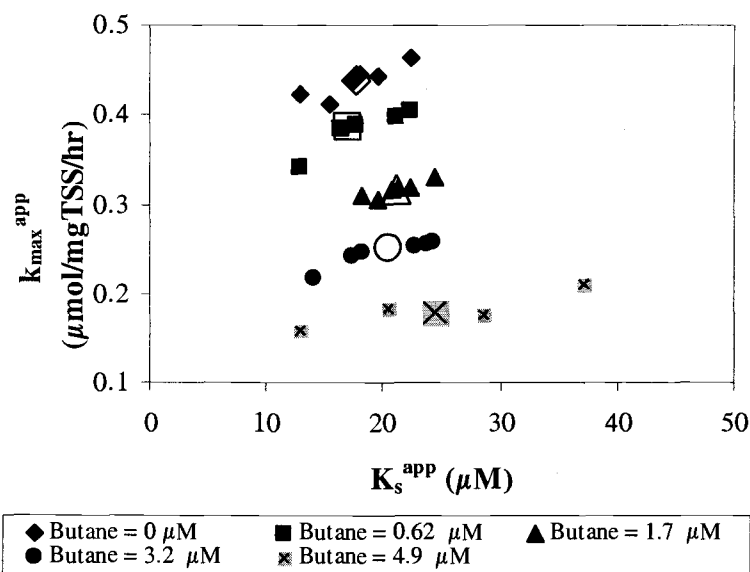


Figure C2.1. Direct linear plot showing mixed inhibition on 1,1-DCA transformation by butane.

Linearized Plot

Table C2.6. Values used for linearized plot in the case of mixed inhibition on 1,1-DCA transformation by butane

Inhibitor (Butane) (μM)	K_s^{app} (μM)	k_{max}^{app} ($\mu\text{mol/ mg TSS/hr}$)	$1/k_{max}^{app}$ ($\text{mg TSS-hr}/\mu\text{mol}$)	K_s^{app}/k_{max}^{app} (mg TSS-hr/L)
0.0	17.7	0.44	2.28	40
0.6	17.1	0.39	2.58	44
1.7	21.1	0.32	3.15	66
3.2	20.4	0.25	3.99	82
4.9	24.5	0.18	5.56	136

Table C2.7. Initial guesses of parameters obtained linearized plot in the case of inhibition on 1,1-DCA transformation by butane

Plot ($1/k_{max}^{app}$ vs. I_L)	Y intercept ($=1/k_{max}$) ($\text{mg TSS-hr}/\mu\text{mol}$)	Slope ($= 1/K_{iu}/k_{max}$) ($\text{mg TSS-hr-L}/\mu\text{mol}^2$)	k_{max} ($\mu\text{mol/ mg TSS/hr}$)	K_{iu} (μM)
	2.1	0.7	0.47	3.30
Plot (K_s^{app}/k_{max}^{app} vs. I_L)	Y intercept ($=K_s/k_{max}$) (mg TSS-hr/L)	Slope ($= K_s/K_{ic}/k_{max}$) ($\text{mg TSS-hr}/\mu\text{mol}$)	K_s ($\mu\text{mol/ mg TSS/hr}$)	K_{ic} (μM)
	34	19	16	1.82

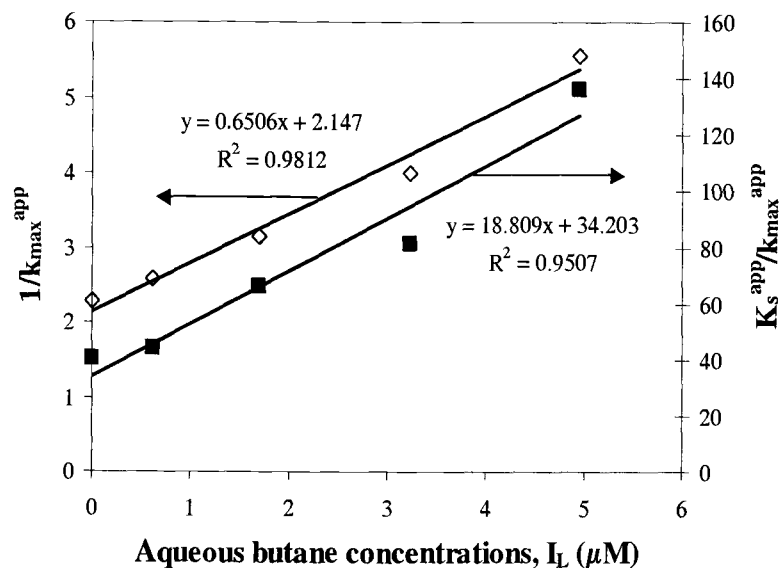


Figure C2.2. Linearized plot in the case of mixed inhibition of 1,1-DCA transformation by butane

NLSR Analysis

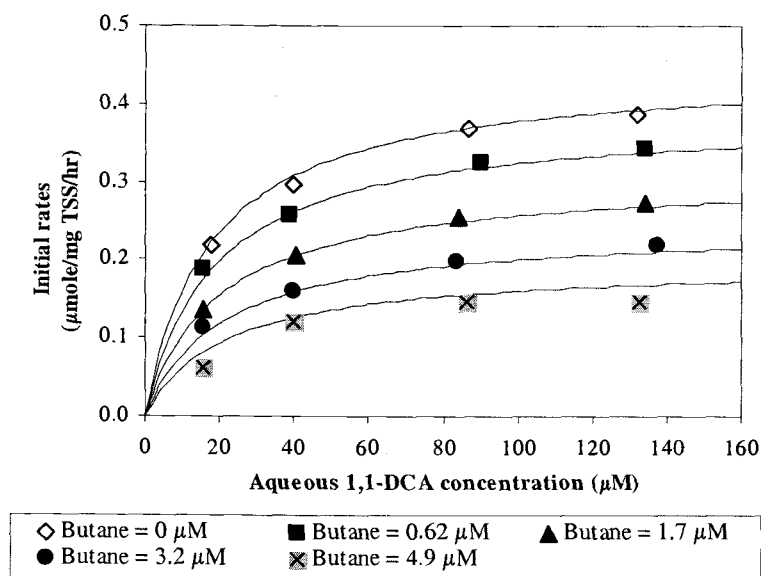


Figure C2.3. Best fit obtained from NLSR analysis using mixed inhibition model. (Residual Standard Error = 0.01, $k_{\text{max}} = 0.45 \pm 0.026 \mu\text{mol/mg TSS/hr}$, $K_s = 17.8 \pm 4.08 \mu\text{M}$, $K_{ic} = 2.8 \pm 1.6$, $K_{iu} = 3.8 \pm 0.88 \mu\text{M}$)

C3. MIXED INHIBITION ON 1,1,1-TCA TRANSFORMATION BY BUTANE

K_s^{app} and k_{max}^{app} Values of 1,1,1-TCA in the Presence of Butane

Table C3.1. K_s^{app} and k_{max}^{app} values of 1,1,1-TCA in the presence of butane (0 μ M).

- Slope and y intercept of extrapolated linear lines

Batch vial #	Substrate, S_L 1,1,1-TCA (μ M)	Inhibitor, I_L Butane (μ M)	$-S_L$ (μ M)	Initial degradation rate, v (μ mol/mg TSS/hr)	Extrapolated line	
					Slope	Y intercept
TA1	2.90	0.00	-2.90	0.039	0.013	0.039
TA2	7.61	0.00	-7.61	0.077	0.010	0.077
TA3	13.1	0.00	-13.1	0.094	0.007	0.094
TA4	19.8	0.00	-19.8	0.120	0.006	0.120
TA5	32.8	0.00	-32.8	0.149	0.005	0.149
TA6	48.5	0.00	-48.5	0.158	0.003	0.158
TA7	65.4	0.00	-65.4	0.163	0.002	0.163
TA8	98.5	0.00	-98.5	0.168	0.002	0.168
TA9	148	0.00	-148	0.181	0.001	0.181
TA10	323	0.00	-323	0.188	0.001	0.188

- Intersection coordinates and best estimate (median) of K_s^{app} and k_{max}^{app}

Number of data	Batch vial #	Batch vial #	Coordinate of intersection		Order from the lowest to highest	
			K_s^{app} (μ M)	k_{max}^{app} (μ mol/mg TSS/hr)	K_s^{app} (μ M)	k_{max}^{app} (μ mol/mg TSS/hr)
1	TA1	TA2	11.7	0.194	5.83	0.135
2	TA1	TA3	8.98	0.157	6.01	0.157
3	TA1	TA4	11.3	0.188	6.36	0.178
4	TA1	TA5	12.6	0.207	6.70	0.179
5	TA1	TA6	11.9	0.197	6.78	0.180
6	TA1	TA7	11.5	0.192	6.81	0.180
7	TA1	TA8	11.2	0.187	7.29	0.180
8	TA1	TA9	11.8	0.195	8.93	0.182
9	TA1	TA10	11.8	0.195	9.52	0.186
10	TA2	TA3	5.83	0.135	9.91	0.187
11	TA2	TA4	10.9	0.186	10.9	0.187
12	TA2	TA5	13.1	0.209	10.9	0.187
13	TA2	TA6	12.0	0.198	11.0	0.188

14	TA2	TA7	11.4	0.192	11.1	0.192
15	TA2	TA8	11.0	0.187	11.2	0.192
16	TA2	TA9	11.8	0.195	11.2	0.192
17	TA2	TA10	11.8	0.195	11.3	0.192
18	TA3	TA4	24.5	0.269	11.4	0.193
19	TA3	TA5	21.3	0.246	11.5	0.194
20	TA3	TA6	16.7	0.213	11.7	0.194
21	TA3	TA7	14.9	0.200	11.8	0.194
22	TA3	TA8	13.7	0.192	11.8	0.195
23 (Median)	TA3	TA9	14.7	0.199	11.8	0.195
24	TA3	TA10	14.4	0.197	11.8	0.195
25	TA4	TA5	19.1	0.236	11.9	0.195
26	TA4	TA6	13.7	0.203	12.0	0.195
27	TA4	TA7	12.0	0.193	12.0	0.195
28	TA4	TA8	11.1	0.187	12.0	0.196
29	TA4	TA9	12.5	0.196	12.5	0.196
30	TA4	TA10	12.5	0.196	12.5	0.196
31	TA5	TA6	7.29	0.182	12.6	0.197
32	TA5	TA7	6.81	0.180	13.2	0.197
33	TA5	TA8	6.78	0.180	13.3	0.198
34	TA5	TA9	9.52	0.192	13.7	0.198
35	TA5	TA10	9.91	0.194	13.7	0.199
36	TA6	TA7	6.01	0.178	13.9	0.199
37	TA6	TA8	6.36	0.179	14.4	0.200
38	TA6	TA9	10.9	0.194	14.7	0.203
39	TA6	TA10	11.2	0.195	14.9	0.207
40	TA7	TA8	6.70	0.180	16.7	0.209
41	TA7	TA9	13.9	0.198	17.8	0.212
42	TA7	TA10	13.3	0.196	19.1	0.213
43	TA8	TA9	25.6	0.212	21.3	0.236
44	TA8	TA10	17.8	0.199	24.5	0.246
45	TA9	TA10	12.0	0.195	25.6	0.269

Table C3.2. K_s^{app} and k_{max}^{app} values of 1,1,1-TCA in the presence of butane ($0.14 \pm 0.04 \mu\text{M}$).

- Slope and y intercept of extrapolated linear lines

Batch vial #	Substrate, S_L 1,1,1-TCA (μM)	Inhibitor, I_L Butane (μM)	$-S_L$ (μM)	Initial degradation rate, v ($\mu\text{mol}/\text{mg TSS}/\text{hr}$)	Extrapolated line	
					Slope	Y intercept
BT#201	32.5	0.136	-32.5	0.099	0.003	0.099
BT#202	68.4	0.141	-68.4	0.116	0.002	0.116
BT#203	101.	0.145	-101	0.135	0.001	0.135
BT#204	135	0.137	-135	0.127	0.001	0.127
BT#205	169	0.141	-169	0.149	0.001	0.149
BT#206	198	0.140	-198	0.139	0.001	0.139
BT#207	3.2	0.149	-3.2	0.022	0.007	0.022

- Intersection coordinates and best estimate (median) of K_s^{app} and k_{max}^{app}

Number of data	Batch vial #	Batch vial #	Coordinate of intersection		Order from the lowest to highest	
			K_s^{app} (μM)	k_{max}^{app} ($\mu\text{mol}/\text{mg TSS}/\text{hr}$)	K_s^{app} (μM)	k_{max}^{app} ($\mu\text{mol}/\text{mg TSS}/\text{hr}$)
1	BT#201	BT#202	12.1	0.136	-21.9	0.100
2	BT#201	BT#203	21.3	0.164	-55.7	0.106
3	BT#201	BT#204	13.1	0.139	6.2	0.136
4	BT#201	BT#205	23.2	0.170	12.1	0.139
5	BT#201	BT#206	17.2	0.151	13.1	0.141
6	BT#201	BT#207	20.1	0.160	14.8	0.143
7	BT#202	BT#203	56.9	0.211	17.2	0.144
8	BT#202	BT#204	14.8	0.141	17.6	0.146
9	BT#202	BT#205	42.0	0.186	18.0	0.151
10	BT#202	BT#206	24.1	0.156	19.0	0.153
11 (Median)	BT#202	BT207	18.0	0.146	20.1	0.156
12	BT#203	BT#204	-21.9	0.106	20.5	0.160
13	BT#203	BT#205	30.7	0.176	21.2	0.163
14	BT#203	BT#206	6.21	0.144	21.3	0.164
15	BT#203	BT207	20.5	0.163	23.2	0.168
16	BT#204	BT#205	394	0.497	24.1	0.170
17	BT#204	BT#206	53.4	0.177	30.7	0.176
18	BT#204	BT207	17.6	0.143	42.0	0.177
19	BT#205	BT#206	-55.8	0.100	53.4	0.186
20	BT#205	BT207	21.3	0.168	56.8	0.211
21	BT#206	BT207	19.0	0.153	394.1	0.497

Table C3.3. K_s^{app} and k_{max}^{app} values of 1,1,1-TCA in the presence of butane ($0.25 \pm 0.004 \mu\text{M}$).

- Slope and y intercept of extrapolated linear lines

Batch Vial #	Substrate, S_L 1,1,1-TCA (μM)	Inhibitor, I_L Butane (μM)	$-S_L$ (μM)	Initial degradation rate, v ($\mu\text{mol}/\text{mg TSS}/\text{hr}$)	Extrapolated line	
					Slope	Y intercept
BUTA301	31.2	0.255	-31.2	0.088	0.0028	0.088
BUTA302	67.3	0.244	-67.3	0.101	0.0015	0.101
BUTA303	150	0.255	-150	0.132	0.0009	0.132
BUTA304	135	0.249	-135	0.112	0.0008	0.112
BUTA305	166	0.254	-166	0.118	0.0007	0.118
BUTA306	202	0.250	-202	0.129	0.0006	0.129

- Intersection coordinates and best estimate (median) of K_s^{app} and k_{max}^{app}

Number of data	Batch vial #	Batch vial #	Coordinate of intersection		Order from the lowest to highest	
			K_s^{app} (μM)	k_{max}^{app} ($\mu\text{mol}/\text{mg}$ TSS/hr)	K_s^{app} (μM)	k_{max}^{app} ($\mu\text{mol}/\text{mg TSS}/\text{hr}$)
1	BUTA301	BUTA302	9.77	0.116	-84.3	-0.231
2	BUTA301	BUTA303	22.7	0.152	-13.9	0.058
3	BUTA301	BUTA304	12.2	0.122	9.88	0.116
4	BUTA301	BUTA305	14.2	0.128	12.2	0.120
5	BUTA301	BUTA306	18.6	0.141	14.2	0.122
6	BUTA302	BUTA303	50.2	0.176	16.9	0.126
7	BUTA302	BUTA304	16.9	0.126	18.6	0.128
8 (Median)	BUTA302	BUTA305	21.6	0.133	21.6	0.133
9	BUTA302	BUTA306	32.2	0.149	22.7	0.141
10	BUTA303	BUTA304	-412	-0.231	32.2	0.149
11	BUTA303	BUTA305	-84.3	0.058	47.9	0.152
12	BUTA303	BUTA306	-13.9	0.120	50.3	0.152
13	BUTA304	BUTA305	47.9	0.152	85.1	0.176
14	BUTA304	BUTA306	85.1	0.183	145	0.183
15	BUTA305	BUTA306	145	0.221	-413	0.221

Table C3.4. K_s^{app} and k_{max}^{app} values of 1,1,1-TCA in the presence of butane ($1.6 \pm 0.08 \mu\text{M}$).

- Slope and y intercept of extrapolated linear lines

Batch vial #	Substrate, S_L 1,1,1-TCA (μM)	Inhibitor, I_L Butane (μM)	$-S_L$ (μM)	Initial degradation rate, v ($\mu\text{mol}/\text{mg TSS}/\text{hr}$)	Extrapolated line	
					Slope	Y intercept
BUTA#9	3.0	1.69	-3.0	0.012	0.004	0.012
BUTA#16	5.5	1.68	-5.5	0.015	0.003	0.015
BUTA#37	19.6	1.61	-19.6	0.021	0.001	0.021
BUTA#44	25.9	1.65	-25.9	0.024	0.001	0.024
BUTA#8	9.8	1.64	-9.8	0.019	0.002	0.019
BUTA#22	35.7	1.65	-35.7	0.033	0.001	0.033
BUTA#29	40.2	1.59	-40.2	0.037	0.001	0.037
BUTA#36	58.4	1.41	-58.4	0.034	0.001	0.034
BUTA#43	127	1.59	-127	0.038	0.0003	0.038

- Intersection coordinates and best estimate (median) of K_s^{app} and k_{max}^{app}

Number of data	Batch vial #	Batch vial #	Coordinate of intersection		Order from the lowest to highest	
			K_s^{app} (μM)	k_{max}^{app} ($\mu\text{mol}/\text{mg TSS}/\text{hr}$)	K_s^{app} (μM)	k_{max}^{app} ($\mu\text{mol}/\text{mg TSS}/\text{hr}$)
1	BUTA#9	BUTA#16	2.06	0.021	-7.92	0.021
2	BUTA#9	BUTA#37	2.97	0.024	2.06	0.024
3	BUTA#9	BUTA#44	3.59	0.027	2.22	0.024
4	BUTA#9	BUTA#8	3.28	0.026	2.97	0.025
5	BUTA#9	BUTA#22	6.44	0.039	3.28	0.026
6	BUTA#9	BUTA#29	7.63	0.043	3.59	0.027
7	BUTA#9	BUTA#36	6.18	0.038	3.70	0.028
8	BUTA#9	BUTA#43	6.89	0.040	3.71	0.028
9	BUTA#16	BUTA#37	3.70	0.025	4.22	0.029
10	BUTA#16	BUTA#44	4.71	0.028	4.71	0.030
11	BUTA#16	BUTA#8	5.35	0.030	5.35	0.036
12	BUTA#16	BUTA#22	9.63	0.042	6.18	0.037
13	BUTA#16	BUTA#29	11.7	0.047	6.44	0.038
14	BUTA#16	BUTA#36	8.71	0.039	6.89	0.039
15	BUTA#16	BUTA#43	9.52	0.041	7.27	0.039
16	BUTA#37	BUTA#44	14.6	0.037	7.63	0.040
17	BUTA#37	BUTA#8	2.22	0.024	8.71	0.040
18	BUTA#37	BUTA#22	68.5	0.095	9.19	0.041
19 (Median)	BUTA#37	BUTA#29	86.8	0.115	9.52	0.041
20	BUTA#37	BUTA#36	25.3	0.049	9.63	0.041

21	BUTA#37	BUTA#43	21.9	0.045	10.6	0.042
22	BUTA#44	BUTA#8	4.22	0.028	11.5	0.042
23	BUTA#44	BUTA#22	-11484	-10.495	11.7	0.043
24	BUTA#44	BUTA#29	1593	1.483	12.3	0.043
25	BUTA#44	BUTA#36	30.6	0.052	12.9	0.043
26	BUTA#44	BUTA#43	23.9	0.046	14.6	0.044
27	BUTA#8	BUTA#22	12.9	0.044	15.8	0.045
28	BUTA#8	BUTA#29	16.4	0.051	16.4	0.046
29	BUTA#8	BUTA#36	10.6	0.040	21.9	0.047
30	BUTA#8	BUTA#43	11.5	0.042	23.9	0.049
31	BUTA#22	BUTA#29	433	0.430	25.3	0.051
32	BUTA#22	BUTA#36	3.71	0.036	30.6	0.052
33	BUTA#22	BUTA#43	9.19	0.041	68.5	0.095
34	BUTA#29	BUTA#36	-7.92	0.029	86.8	0.115
35	BUTA#29	BUTA#43	7.27	0.041	433	0.430
36	BUTA#36	BUTA#43	15.8	0.043	1593	1.483
37	BUTA#9	BUTA#16	2.06	0.021	-11484	-10.495

Table C3.5. K_s^{app} and $k_{\text{max}}^{\text{app}}$ values of 1,1,1-TCA in the presence of butane ($2.7 \pm 0.01 \mu\text{M}$).

- Slope and y intercept of extrapolated linear lines

Batch vial #	Substrate, S_L 1,1,1-TCA (μM)	Inhibitor, I_L Butane (μM)	- S_L (μM)	Initial degradation rate, v ($\mu\text{mol}/\text{mg TSS}/\text{hr}$)	Extrapolated line	
					Slope	Y intercept
BUTA#10	10.3	2.75	-10.3	0.010	0.0010	0.010
BUTA#17	22.6	3.00	-22.6	0.019	0.0008	0.019
BUTA#24	42.0	2.68	-42.0	0.022	0.0005	0.022
BUTA#31	60.8	2.79	-60.8	0.024	0.0004	0.024
BUTA#38	74.8	2.8	-74.8	0.025	0.0003	0.025
BUTA#45	140	2.4	-140	0.026	0.0002	0.026

- Intersection coordinates and best estimate (median) of K_s^{app} and $k_{\text{max}}^{\text{app}}$

Number of data	Batch vial #	Batch vial #	Coordinate of intersection		Order from the lowest to highest	
			K_s^{app} (μM)	$k_{\text{max}}^{\text{app}}$ ($\mu\text{mol}/\text{mg}$ TSS/hr)	K_s^{app} (μM)	$k_{\text{max}}^{\text{app}}$ ($\mu\text{mol}/\text{mg}$ TSS/hr)
1	BUTA#10	BUTA#17	61.4	0.071	6.7	0.027
2	BUTA#10	BUTA#24	25.6	0.035	9.4	0.027
3	BUTA#10	BUTA#31	23.4	0.033	9.6	0.028
4	BUTA#10	BUTA#38	22.8	0.033	10.7	0.028
5	BUTA#10	BUTA#45	19.8	0.030	11.2	0.028
6	BUTA#17	BUTA#24	9.4	0.027	11.8	0.028
7	BUTA#17	BUTA#31	11.2	0.028	11.9	0.029

8 (Median)	BUTA#17	BUTA#38	11.9	0.029	15.8	0.030
9	BUTA#17	BUTA#45	10.7	0.028	16.0	0.030
10	BUTA#24	BUTA#31	15.8	0.030	16.6	0.030
11	BUTA#24	BUTA#38	16.0	0.030	19.8	0.031
12	BUTA#24	BUTA#45	11.9	0.028	22.8	0.033
13	BUTA#31	BUTA#38	16.6	0.031	23.4	0.033
14	BUTA#31	BUTA#45	9.55	0.028	25.6	0.035
15	BUTA#38	BUTA#45	6.71	0.027	61.4	0.071

Table C3.6. K_s^{app} and k_{max}^{app} values of 1,1,1-TCA in the presence of butane ($5.7 \pm 0.22 \mu\text{M}$).

- Slope and y intercept of extrapolated linear lines

Batch vial #	Substrate, S_L 1,1,1-TCA (μM)	Inhibitor, I_L Butane (μM)	$-S_L$ (μM)	Initial degradation rate, v ($\mu\text{mol/mg TSS/hr}$)	Extrapolated line	
					Slope	Y intercept
BUTA#13	8.7	5.48	-8.7	0.006	0.00064	0.0055
BUTA#20	16.6	5.46	-16.6	0.007	0.00044	0.0074
BUTA#27	33.2	6.07	-33.2	0.008	0.00026	0.0085
BUTA#34	44.3	5.76	-44.3	0.011	0.00024	0.0105
BUTA#41	51.8	5.70	-51.8	0.011	0.00021	0.0110
BUTA#48	103	5.63	-103	0.012	0.00011	0.0117

- Intersection coordinates and best estimate (median) of K_s^{app} and k_{max}^{app}

Number of data	Batch vial #	Batch vial #	Coordinate of intersection		Order from the lowest to highest	
			K_s^{app} (μM)	k_{max}^{app} ($\mu\text{mol/mg TSS/hr}$)	K_s^{app} (μM)	k_{max}^{app} ($\mu\text{mol/mg TSS/hr}$)
1	BUTA#13	BUTA#20	9.8	0.012	5.7	0.010
2	BUTA#13	BUTA#27	7.8	0.010	7.0	0.010
3	BUTA#13	BUTA#34	12.6	0.014	7.8	0.012
4	BUTA#13	BUTA#41	13.0	0.014	9.6	0.013
5	BUTA#13	BUTA#48	11.9	0.013	9.8	0.013
6	BUTA#20	BUTA#27	5.7	0.010	11.9	0.013
7	BUTA#20	BUTA#34	15.1	0.014	12.6	0.013
8 (Median)	BUTA#20	BUTA#41	15.7	0.014	13.0	0.014
9	BUTA#20	BUTA#48	13.1	0.013	13.1	0.014
10	BUTA#27	BUTA#34	113	0.037	15.1	0.014
11	BUTA#27	BUTA#41	59.3	0.024	15.7	0.014
12	BUTA#27	BUTA#48	22.8	0.014	20.2	0.014
13	BUTA#34	BUTA#41	20.2	0.015	22.8	0.015
14	BUTA#34	BUTA#48	9.6	0.013	59.3	0.024
15	BUTA#41	BUTA#48	7.0	0.013	112.5	0.037

Direct Linear Plot

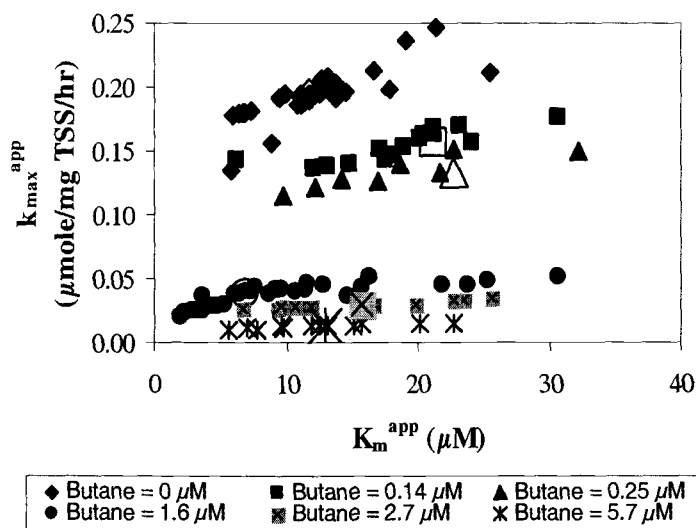


Figure C3.1. Direct linear plot showing mixed inhibition on 1,1,1-TCA transformation by butane.

Linearized Plot

Table C3.7. Values used for linearized plot in the case of mixed inhibition on 1,1,1-TCA transformation by butane

Inhibitor (Butane) (μM)	K_s^{app} (μM)	k_{max}^{app} ($\mu\text{mol/ mg TSS/hr}$)	$1/k_{max}^{app}$ ($\text{mg TSS-hr}/\mu\text{mol}$)	K_s^{app}/k_{max}^{app} (mg TSS-hr/L)
0	11.8	0.20	5.13	60
0.14	20.1	0.16	6.25	126
0.25	21.6	0.13	7.52	162
1.6	9.5	0.041	24.39	232
2.7	15.8	0.030	33.67	532
5.7	13.0	0.014	74.07	963

Table C3.8. Initial guesses of parameters obtained linearized plot in the case of inhibition on 1,1,1-TCA transformation by butane

Plot ($1/k_{max}^{app}$ vs. I_L)	Y intercept ($=1/k_{max}$) ($\text{mg TSS-hr}/\mu\text{mol}$)	Slope ($= 1/K_{iu}/k_{max}$) ($\text{mg TSS-hr-L}/\mu\text{mol}^2$)	k_{max} ($\mu\text{mol/ mg TSS/hr}$)	K_{iu} (μM)
	4.4	12.0	0.23	0.36
Plot (K_s^{app}/k_{max}^{app} vs. I_L)	Y intercept ($=K_s/k_{max}$) (mg TSS-hr/L)	Slope ($= K_s/K_{ic}/k_{max}$) ($\text{mg TSS-hr}/\mu\text{mol}$)	K_s ($\mu\text{mol/ mg TSS/hr}$)	K_{ic} (μM)
	79	154	18	0.52

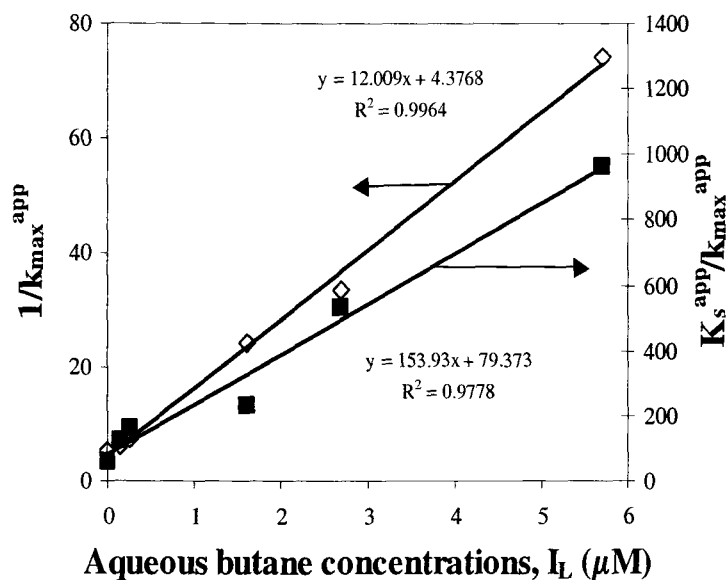


Figure C3.2. Linearized plot in the case of mixed inhibition of 1,1,1-TCA transformation by butane

NLSR Analysis

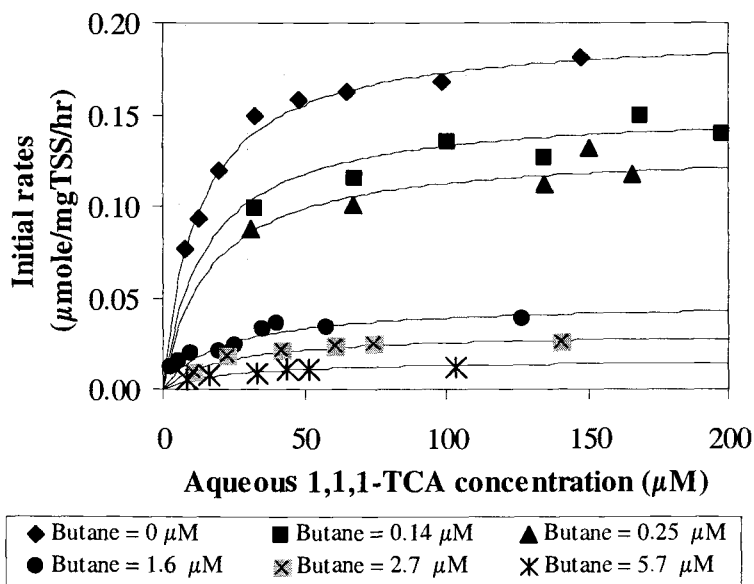


Figure C3.3. Best fit obtained from NLSR analysis using mixed inhibition model. (Residual Standard Error = 0.005, $k_{\text{max}} = 0.20 \pm 0.007 \mu\text{mol/mg TSS/hr}$, $K_s = 12.7 \pm 2.07 \mu\text{M}$, $K_{ic} = 0.28 \pm 0.13 \mu\text{M}$ and $K_{iu} = 0.51 \pm 0.094 \mu\text{M}$)

C4. COMPETITIVE INHIBITION ON BUTANE DEGRADATION BY 1,1-DCE

K_s^{app} and k_{max}^{app} Values of Butane in the Presence of 1,1-DCE

Table C4.1. K_s^{app} and k_{max}^{app} values of butane in the presence of 1,1-DCE (0 μ M).

- Slope and y intercept of extrapolated linear lines

Batch vial #	Substrate, S_L Butane (μ M)	Inhibitor, I_L 1,1-DCE (μ M)	$-S_L$ (μ M)	Initial degradation rate, v (μ mol/mg TSS/hr)	Extrapolated line	
					Slope	Y intercept
DEBU#17	4.32	0	-4.32	0.66	0.15	0.66
DEBU#18	11.79	0	-11.79	1.21	0.10	1.21
DEBU#19	20.03	0	-20.03	1.37	0.07	1.37
DEBU#20	30.60	0	-30.60	1.71	0.06	1.71

- Intersection coordinates and best estimate (median) of K_s^{app} and k_{max}^{app}

Number of data	Batch vial #	Batch vial #	Coordinate of Intersection		Order from the lowest to highest	
			K_s^{app} (μ M)	k_{max}^{app} (μ mol/mg TSS/hr)	K_s^{app} (μ M)	k_{max}^{app} (μ mol/mg TSS/hr)
1	DEBU#17	DEBU#18	10.7	2.30	4.76	1.69
2	DEBU#17	DEBU#19	8.34	1.94	8.34	1.94
3	DEBU#17	DEBU#20	10.8	2.31	10.7	2.30
Median	-	-	-	-	10.8	2.30
4	DEBU#18	DEBU#19	4.76	1.69	10.8	2.31
5	DEBU#18	DEBU#20	10.9	2.32	10.9	2.32
6	DEBU#19	DEBU#20	27.7	3.26	27.7	3.26

Table C4.2. K_s^{app} and k_{max}^{app} values of butane in the presence of 1,1-DCE ($3.3 \pm 0.11 \mu\text{M}$).

- Slope and y intercept of extrapolated linear lines

Batch vial #	Substrate, S_L Butane (μM)	Inhibitor, I_L 1,1-DCE (μM)	$-S_L$ (μM)	Initial degradation rate, v ($\mu\text{mol/mg TSS/hr}$)	Extrapolated line	
					Slope	Y intercept
DEBU#1	4.16	3.12	-4.16	0.59	0.14	0.59
DEBU#2	10.53	3.24	-10.53	1.00	0.09	1.00
DEBU#3	20.00	3.26	-20.00	1.35	0.07	1.35
DEBU#4	30.51	3.38	-30.51	1.54	0.05	1.54

- Intersection coordinates and best estimate (median) of K_s^{app} and k_{max}^{app}

Number of data	Batch vial #	Batch vial #	Coordinate of intersection		Order from the lowest to highest	
			K_s^{app} (μM)	k_{max}^{app} ($\mu\text{mol/mg TSS/hr}$)	K_s^{app} (μM)	k_{max}^{app} ($\mu\text{mol/mg TSS/hr}$)
1	DEBU#1	DEBU#2	8.89	1.84	8.89	1.83
2	DEBU#1	DEBU#3	10.4	2.05	10.4	2.05
3	DEBU#1	DEBU#4	10.7	2.08	10.7	2.08
Median	-	-	-	-	11.2	2.11
4	DEBU#2	DEBU#3	13.0	2.22	11.7	2.14
5	DEBU#2	DEBU#4	12.5	2.18	12.5	2.18
6	DEBU#3	DEBU#4	11.7	2.14	13.0	2.22

Table C4.3. K_s^{app} and k_{max}^{app} values of butane in the presence of 1,1-DCE ($6.5 \pm 0.11 \mu\text{M}$).

- Slope and y intercept of extrapolated linear lines

Batch vial #	Substrate, S_L Butane (μM)	Inhibitor, I_L 1,1-DCE (μM)	$-S_L$ (μM)	Initial degradation rate, v ($\mu\text{mol/mg TSS/hr}$)	Extrapolated line	
					slope	Y intercept
DEBU#5	4.24	6.53	-4.24	0.50	0.118	0.50
DEBU#6	11.16	6.48	-11.16	0.93	0.084	0.93
DEBU#7	19.87	6.40	-19.87	1.22	0.061	1.22
DEBU#8	30.35	6.66	-30.35	1.38	0.046	1.38

- Intersection coordinates and best estimate (median) of K_s^{app} and $k_{\text{max}}^{\text{app}}$

Number of data	Batch vial #	Batch vial #	Coordinate of intersection		Order from the lowest to highest	
			K_s^{app} (μM)	$k_{\text{max}}^{\text{app}}$ ($\mu\text{mol/mg TSS/hr}$)	K_s^{app} (μM)	$k_{\text{max}}^{\text{app}}$ ($\mu\text{mol/mg TSS/hr}$)
1	DEBU#5	DEBU#6	12.7	2.00	10.3	1.85
2	DEBU#5	DEBU#7	12.8	2.00	11.8	1.92
3	DEBU#5	DEBU#8	12.2	1.94	12.2	1.94
Median	-	-	-	-	12.5	1.97
4	DEBU#6	DEBU#7	12.9	2.01	12.7	2.00
5	DEBU#6	DEBU#8	11.8	1.92	12.8	2.00
6	DEBU#7	DEBU#8	10.3	1.85	12.9	2.01

Table C4.4. K_s^{app} and $k_{\text{max}}^{\text{app}}$ values of butane in the presence of 1,1-DCE ($12.6 \pm 0.02 \mu\text{M}$).

- Slope and y intercept of extrapolated linear lines

Batch vial #	Substrate, S_L Butane (μM)	Inhibitor, I_L 1,1-DCE (μM)	$-S_L$ (μM)	Initial degradation rate, v ($\mu\text{mol/mg TSS/hr}$)	Extrapolated line	
					Slope	Y intercept
DEBU#9	4.47	12.7	-4.47	0.39	0.087	0.39
DEBU#10	10.1	12.7	-10.1	0.72	0.072	0.72
DEBU#11	20.6	12.6	-20.6	0.98	0.048	0.98
DEBU#12	29.9	12.6	-29.9	1.20	0.040	1.20

- Intersection coordinates and best estimate (median) of K_s^{app} and $k_{\text{max}}^{\text{app}}$

Number of data	Batch vial #	Batch vial #	Coordinate of intersection		Order from the lowest to highest	
			K_s^{app} (μM)	$k_{\text{max}}^{\text{app}}$ ($\mu\text{mol/mg TSS/hr}$)	K_s^{app} (μM)	$k_{\text{max}}^{\text{app}}$ ($\mu\text{mol/mg TSS/hr}$)
1	DEBU#9	DEBU#10	21.5	2.26	10.7	1.49
2	DEBU#9	DEBU#11	14.9	1.69	14.9	1.69
3	DEBU#9	DEBU#12	17.2	1.89	15.2	1.81
Median	-	-	-	-	16.1	1.85
4	DEBU#10	DEBU#11	10.7	1.49	17.2	1.89
5	DEBU#10	DEBU#12	15.2	1.81	21.5	2.26
6	DEBU#11	DEBU#12	29.6	2.39	29.6	2.39

Table C4.5. K_s^{app} and $k_{\text{max}}^{\text{app}}$ values of butane in the presence of 1,1-DCE ($22.2 \pm 0.10 \mu\text{M}$).

- Slope and y intercept of extrapolated linear lines

Batch vial #	Substrate, S_L Butane (μM)	Inhibitor, I_L 1,1-DCE (μM)	$-S_L$ (μM)	Initial degradation rate, v ($\mu\text{mol}/\text{mg TSS}/\text{hr}$)	Extrapolated line	
					Slope	Y intercept
DEBU#13	4.29	22.1	-4.29	0.28	0.065	0.28
DEBU#14	9.82	22.3	-9.82	0.60	0.061	0.60
DEBU#15	19.6	22.1	-19.6	0.72	0.037	0.72
DEBU#16	29.9	22.2	-29.9	1.12	0.038	1.12

- Intersection coordinates and best estimate (median) of K_s^{app} and $k_{\text{max}}^{\text{app}}$

Number of data	Batch vial #	Batch vial #	Coordinate of intersection		Order from the lowest to highest	
			K_s^{app} (μM)	$k_{\text{max}}^{\text{app}}$ ($\mu\text{mol}/\text{mg TSS}/\text{hr}$)	K_s^{app} (μM)	$k_{\text{max}}^{\text{app}}$ ($\mu\text{mol}/\text{mg TSS}/\text{hr}$)
1	DEBU#13	DEBU#14	77.1	5.31	4.92	0.90
2	DEBU#13	DEBU#15	15.4	1.29	15.4	1.29
3	DEBU#13	DEBU#16	30.3	2.26	22.0	1.95
Median	-	-	-	-	26.2	2.10
4	DEBU#14	DEBU#15	4.92	0.90	30.3	2.26
5	DEBU#14	DEBU#16	22.0	1.95	77.1	5.31
6	DEBU#15	DEBU#16	-499	-17.6	-499	-17.6

Direct Linear Plot

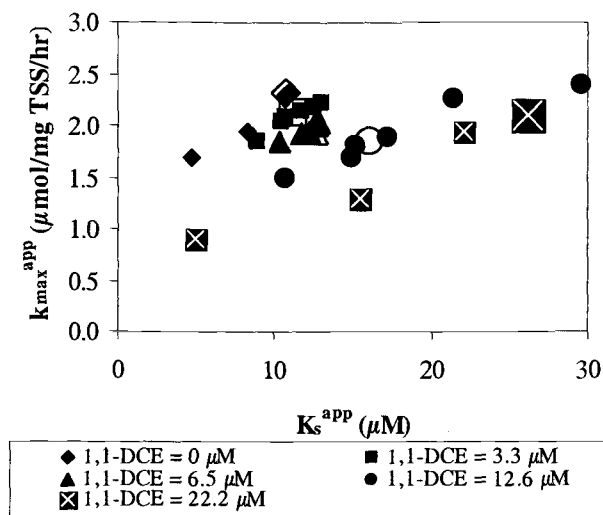


Figure C4.1. Direct linear plot showing competitive inhibition on butane degradation by 1,1-DCE.

Linearized Plot

Table C4.6. Values used for linearized plot in the case of competitive inhibition on butane degradation by 1,1-DCE

Inhibitor (1,1-DCE) (μM)	K_s^{app} (μM)	$k_{\text{max}}^{\text{app}}$ ($\mu\text{mol}/\text{mg TSS/hr}$)
0.0	10.77	2.31
3.3	11.2	2.11
6.5	12.45	1.97
12.6	16.06	1.85
22	26.15	2.101

Table C4.7. Initial guesses of parameters obtained linearized plot in the case of inhibition on butane degradation by 1,1-DCE

Plot (K_s^{app} vs. I_L)	Y intercept ($=K_s$) (μM)	Slope ($=K_s/K_{ic}$) (-)	K_{ic} (μM)	$k_{\text{max}}^{\text{app}}$ ($\mu\text{mol}/\text{mg TSS/hr}$)
	9.0	0.707	12.8	2.07

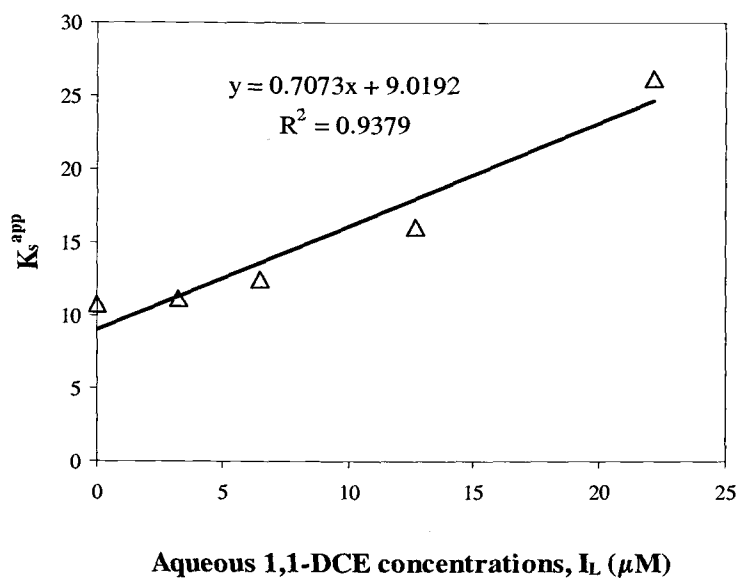


Figure C4.2. Linearized plot in the case of competitive inhibition of butane degradation by 1,1-DCE

NLSR Analysis

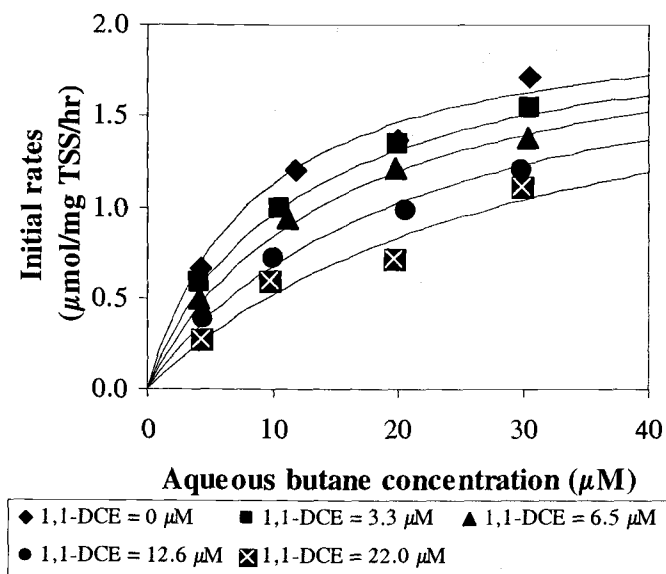


Figure C4.3. Best fit obtained from NLSR analysis using competitive inhibition model. (Residual Standard Error = 0.054, $k_{max} = 2.09 \pm 0.17$ $\mu mol/mg$ TSS/hr, $K_s = 8.5 \pm 2.14$ μM , and $K_{ic} = 8.7 \pm 2.26$ μM)

C5. COMPETITIVE INHIBITION ON 1,1-DCA TRANSFORMATION BY 1,1-DCE

K_s^{app} and k_{max}^{app} Values of 1,1-DCA in the Presence of 1,1-DCE

Table C5.1. K_s^{app} and k_{max}^{app} values of 1,1-DCA in the presence of 1,1-DCE (0 μ M).

- Slope and y intercept of extrapolated linear lines

Batch vial #	Substrate, S_L 1,1-DCA (μ M)	Inhibitor, I_L 1,1-DCE (μ M)	$-S_L$ (μ M)	Initial degradation rate, v (μ mol/mg TSS/hr)	Extrapolated line	
					Slope	y intercept
DEDA#1	10.4	0	-10.4	0.18	0.017	0.18
DEDA#2	45.8	0	-45.8	0.41	0.009	0.41
DEDA#3	81.5	0	-81.5	0.44	0.005	0.44
DEDA#4	161	0	-161	0.52	0.003	0.52

- Intersection coordinates and best estimate (median) of K_s^{app} and k_{max}^{app}

Number of data	Batch vial #	Batch vial #	Coordinate of intersection		Order from the lowest to highest	
			K_s^{app} (μ M)	k_{max}^{app} (μ mol/mg TSS/hr)	K_s^{app} (μ M)	k_{max}^{app} (μ mol/mg TSS/hr)
1	DEDA#1	DEDA#2	28.8	0.668	8.75	0.488
2	DEDA#1	DEDA#3	22.7	0.564	18.4	0.564
3	DEDA#1	DEDA#4	24.5	0.594	22.7	0.575
Median	-	-	-	-	23.6	0.58
4	DEDA#2	DEDA#3	8.75	0.488	24.5	0.594
5	DEDA#2	DEDA#4	18.4	0.575	28.8	0.624
6	DEDA#3	DEDA#4	33.8	0.624	33.8	0.668

Table C5.2. K_s^{app} and k_{max}^{app} values of 1,1-DCA in the presence of 1,1-DCE ($5.4 \pm 0.37 \mu\text{M}$).

- Slope and y intercept of extrapolated linear lines

Batch vial #	Substrate, S_L 1,1-DCA (μM)	Inhibitor, I_L 1,1-DCE (μM)	$-S_L$ (μM)	Initial degradation rate, v ($\mu\text{mol}/\text{mg TSS}/\text{hr}$)	Extrapolated line	
					Slope	Y intercept
DEDA#5	12.5	5.34	-12.5	0.15	0.012	0.15
DEDA#6	48.8	5.89	-48.8	0.33	0.007	0.33
DEDA#7	85.6	5.12	-85.6	0.36	0.004	0.36
DEDA#8	167	5.08	-167	0.47	0.003	0.47

- Intersection coordinates and best estimate (median) of K_s^{app} and k_{max}^{app}

Number of data	Batch vial #	Batch vial #	Coordinate of intersection		Order from the lowest to highest	
			K_s^{app} (μM)	k_{max}^{app} ($\mu\text{mol}/\text{mg TSS}/\text{hr}$)	K_s^{app} (μM)	k_{max}^{app} ($\mu\text{mol}/\text{mg TSS}/\text{hr}$)
1	DEDA#5	DEDA#6	34.7	0.57	9.44	0.40
2	DEDA#5	DEDA#7	26.3	0.47	26.3	0.47
3	DEDA#5	DEDA#8	34.3	0.56	33.8	0.56
Median	-	-	-	-	34.1	0.56
4	DEDA#6	DEDA#7	9.44	0.40	34.3	0.56
5	DEDA#6	DEDA#8	33.8	0.56	34.7	0.53
6	DEDA#7	DEDA#8	80.2	0.69	80.2	0.69

Table C5.3. K_s^{app} and k_{max}^{app} values of 1,1-DCA in the presence of 1,1-DCE ($16 \pm 0.36 \mu\text{M}$).

- Slope and y intercept of extrapolated linear lines

Batch vial #	Substrate, S_L 1,1-DCA (μM)	Inhibitor, I_L 1,1-DCE (μM)	$-S_L$ (μM)	Initial degradation rate, v ($\mu\text{mol}/\text{mg TSS}/\text{hr}$)	Extrapolated line	
					slope	y intercept
DEDA#9	50.5	15.12	-50.5	0.16	0.0032	0.16
DEDA#10	82.8	15.36	-82.8	0.30	0.0037	0.30
DEDA#11	166	15.98	-166	0.37	0.0023	0.37
DEDA#12	230	15.4	-230	0.37	0.0016	0.37

- Intersection coordinates and best estimate (median) of K_s^{app} and k_{max}^{app}

Number of data	Batch vial #	Batch vial #	Coordinate of intersection		Order from the lowest to highest	
			K_s^{app} (μM)	k_{max}^{app} ($\mu mol/mg$ TSS/hr)	K_s^{app} (μM)	k_{max}^{app} ($\mu mol/mg$ TSS/hr)
1	DEDA#9	DEDA#10	-318	-0.86	-10.1	0.35
2	DEDA#9	DEDA#11	221	0.88	31.5	0.42
3	DEDA#9	DEDA#12	127	0.57	51.2	0.49
Median	-	-	-	-	88.9	0.53
4	DEDA#10	DEDA#11	51.2	0.49	127	0.57
5	DEDA#10	DEDA#12	31.5	0.42	221	0.87
6	DEDA#11	DEDA#12	-10.1	0.35	-318	-0.86

Table C5.4. K_s^{app} and k_{max}^{app} values of 1,1-DCA in the presence of 1,1-DCE ($25 \pm 1.03 \mu M$).

- Slope and y intercept of extrapolated linear lines

Batch vial #	Substrate, S_L 1,1-DCA (μM)	Inhibitor, I_L 1,1-DCE (μM)	$-S_L$ (μM)	Initial degradation rate, v ($\mu mol/mg$ TSS/hr)	Extrapolated line	
					Slope	Y intercept
DEDA#13	52.5	25.5	-52.5	0.15	0.0030	0.15
DEDA#14	80.3	24.0	-80.3	0.23	0.0029	0.23
DEDA#15	161	25.0	-161	0.29	0.0018	0.29
DEDA#16	235	26.5	-235	0.35	0.0015	0.35

- Intersection coordinates and best estimate (median) of K_s^{app} and k_{max}^{app}

Number of data	Batch vial #	Batch vial #	Coordinate of intersection		Order from the lowest to highest	
			K_s^{app} (μM)	k_{max}^{app} ($\mu mol/mg$ TSS/hr)	K_s^{app} (μM)	k_{max}^{app} ($\mu mol/mg$ TSS/hr)
1	DEDA#13	DEDA#14	3200	9.60	46.5	0.37
2	DEDA#13	DEDA#15	114	0.49	84.5	0.48
3	DEDA#13	DEDA#16	138	0.56	114	0.49
Median	-	-	-	-	126	0.53
4	DEDA#14	DEDA#15	46.5	0.37	138	0.56
5	DEDA#14	DEDA#16	84.5	0.48	240	0.72
6	DEDA#15	DEDA#16	240	0.72	3200	9.60

Table C5.5. K_s^{app} and k_{max}^{app} values of 1,1-DCA in the presence of 1,1-DCE ($46 \pm 1.00 \mu\text{M}$).

- Slope and y intercept of extrapolated linear lines

Batch vial #	Substrate, S_L 1,1-DCA (μM)	Inhibitor, I_L 1,1-DCE (μM)	$-S_L$ (μM)	Initial degradation rate, v ($\mu\text{mol/mg TSS/hr}$)	Extrapolated line	
					Slope	Y intercept
DEDA#17	80.3	45.3	-80.3	0.13	0.0016	0.13
DEDA#18	161	47.2	-161	0.21	0.0013	0.21
DEDA#19	236	45.0	-235	0.26	0.0011	0.26
DEDA#20	299	45.2	-298	0.33	0.0011	0.09

- Intersection coordinates and best estimate (median) of K_s^{app} and k_{max}^{app}

Number of data	Batch vial #	Batch vial #	Coordinate of intersection		Order from the lowest to highest	
			K_s^{app} (μM)	k_{max}^{app} ($\mu\text{mol/mg TSS/hr}$)	K_s^{app} (μM)	k_{max}^{app} ($\mu\text{mol/mg TSS/hr}$)
1	DEDA#17	DEDA#18	165	0.434	-72.7	0.013
2	DEDA#17	DEDA#19	165	0.433	164	0.432
3	DEDA#17	DEDA#20	-72.7	0.013	165	0.433
Median	-	-	-	-	165	0.43
4	DEDA#18	DEDA#19	164	0.432	165	0.434
5	DEDA#18	DEDA#20	-451	-0.386	-451	-0.386
6	DEDA#19	DEDA#20	-5740	-5.962	-5740	-5.962

Direct Linear Plot

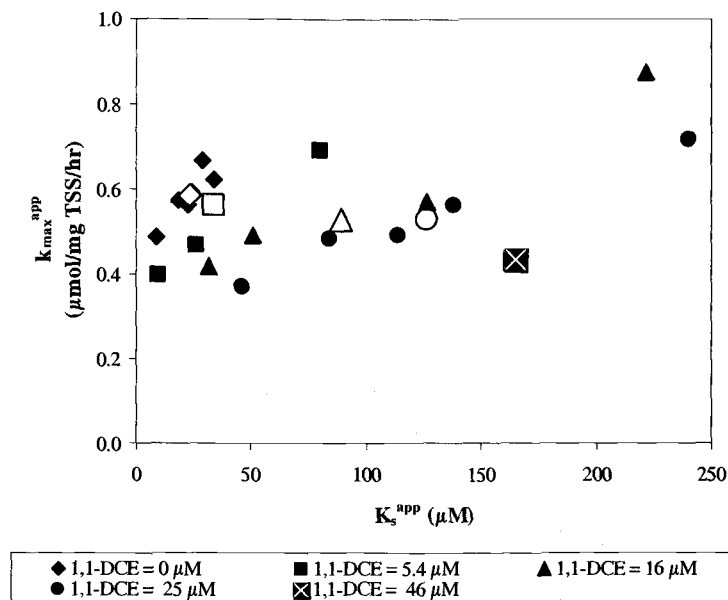


Figure C5.1. Direct linear plot showing competitive inhibition on 1,1-DCA transformation by 1,1-DCE.

Linearized Plot

Table C5.6. Values used for linearized plot in the case of competitive inhibition on 1,1-DCA transformation by 1,1-DCE

Inhibitor (1,1-DCE) (μM)	K_s^{app} (μM)	k_{max}^{app} ($\mu\text{mol/ mg TSS/hr}$)
0.0	23.6	0.58
5.4	34.1	0.56
16	88.9	0.53
25	126	0.53
46	165	0.43

Table C5.7. Initial guesses of parameters obtained linearized plot in the case of inhibition on 1,1-DCA transformation by 1,1-DCE

Plot (K_s^{app} vs. I_L)	Y intercept ($=K_s$) (μM)	Slope ($=K_s/K_{ic}$) (-)	K_{ic} (μM)	k_{max}^{app} ($\mu\text{mol/ mg TSS/hr}$)
	28.0	3.247	8.6	0.53

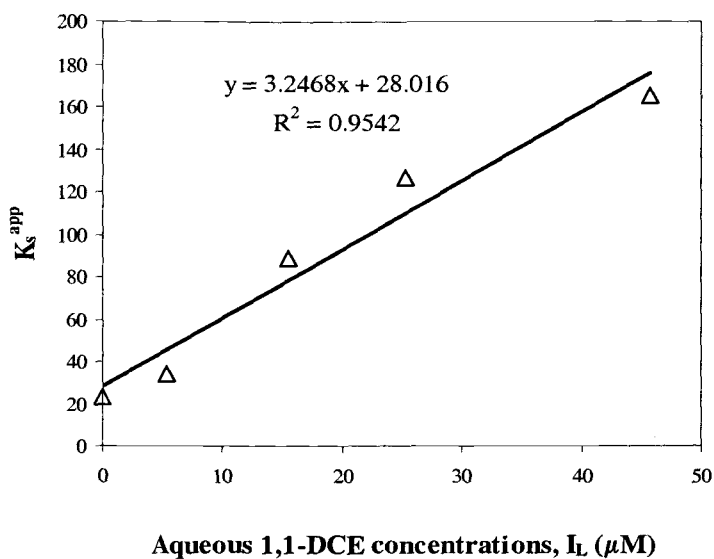


Figure C5.2. Linearized plot in the case of competitive inhibition of 1,1-DCA transformation by 1,1-DCE

NLSR Analysis

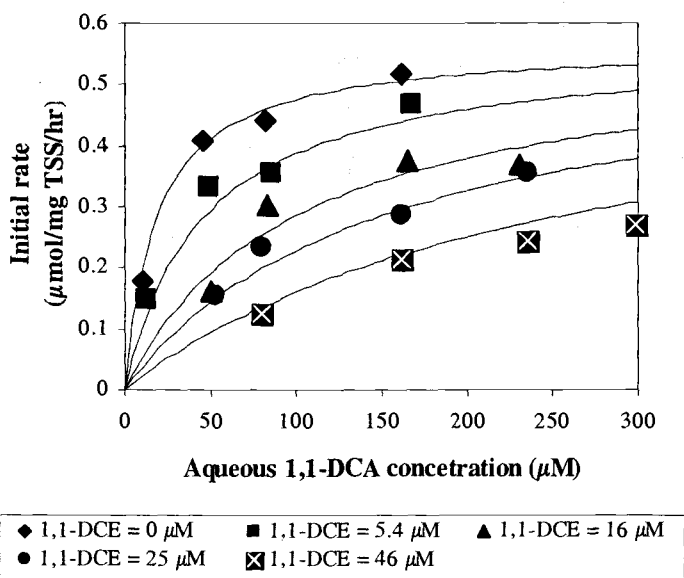


Figure C5.3. Best fit obtained from NLSR analysis using competitive inhibition model. (Residual Standard Error = 0.028, $k_{max} = 0.56 \pm 0.06 \mu\text{mol/mg TSS/hr}$, $K_s = 18.4 \pm 8.5 \mu\text{M}$, and $K_{ic} = 3.64 \pm 1.46 \mu\text{M}$)

C6. COMPETITIVE INHIBITION ON 1,1,1-TCA TRANSFORMATION BY 1,1-DCE

K_s^{app} and k_{max}^{app} Values of 1,1,1-TCA in the Presence of 1,1-DCE

Table C6.1. K_s^{app} and k_{max}^{app} values of 1,1,1-TCA in the presence of 1,1-DCE (0 μ M).

- Slope and y intercept of extrapolated linear lines

Batch vial #	Substrate, S_L 1,1,1-TCA (μ M)	Inhibitor, I_L 1,1-DCE (μ M)	- S_L (μ M)	Initial degradation rate, v (μ mol/mg TSS/hr)	Extrapolated line	
					slope	Y intercept
DETA#1	9.36	0	-9.36	0.085	0.0091	0.09
DETA#2	36.6	0	-36.6	0.135	0.0037	0.14
DETA#3	75.9	0	-75.9	0.168	0.0022	0.17
DETA#4	158	0	-158	0.196	0.0012	0.20

- Intersection coordinates and best estimate (median) of K_s^{app} and k_{max}^{app}

Number Of data	Batch vial #	Batch vial #	Coordinate of intersection		Order from the lowest to highest	
			K_s^{app} (μ M)	k_{max}^{app} (μ mol/mg TSS/hr)	K_s^{app} (μ M)	k_{max}^{app} (μ mol/mg TSS/hr)
1	DETA#1	DETA#2	9.27	0.169	9.27	0.169
2	DETA#1	DETA#3	12.1	0.195	12.1	0.195
3	DETA#1	DETA#4	14.1	0.213	14.1	0.213
Median	-	-	-	-	18.2	0.215
4	DETA#2	DETA#3	22.3	0.217	22.3	0.217
5	DETA#2	DETA#4	24.6	0.226	24.6	0.226
6	DETA#3	DETA#4	28.2	0.230	28.2	0.230

Table C6.2. K_s^{app} and k_{max}^{app} values of 1,1,1-TCA in the presence of 1,1-DCE ($1.4 \pm 0.14 \mu\text{M}$).

- Slope and y intercept of extrapolated linear lines

Batch vial #	Substrate, S_L 1,1,1-TCA (μM)	Inhibitor, I_L 1,1-DCE (μM)	$-S_L$ (μM)	Initial degradation rate, v ($\mu\text{mol}/\text{mg TSS}/\text{hr}$)	Extrapolated line	
					Slope	Y intercept
DETA#5	32.6	1.33	-32.6	0.08	0.0024	0.08
DETA#6	75.9	1.43	-75.9	0.13	0.0018	0.13
DETA#7	156	1.57	-156	0.16	0.0010	0.16
DETA#8	290	1.24	-290	0.18	0.0006	0.18

- Intersection coordinates and best estimate (median) of K_s^{app} and k_{max}^{app}

Number Of data	Batch vial #	Batch vial #	Coordinate of intersection		Order from the lowest to highest	
			K_s^{app} (μM)	k_{max}^{app} ($\mu\text{mol}/\text{mg}$ TSS/hr)	K_s^{app} (μM)	k_{max}^{app} ($\mu\text{mol}/\text{mg}$ TSS/hr)
1	DETA#5	DETA#6	85.9	0.287	33.5	0.194
2	DETA#5	DETA#7	57.8	0.219	38.3	0.203
3	DETA#5	DETA#8	55.4	0.213	47.1	0.208
Median	-	-	-	-	51.3	0.21
4	DETA#6	DETA#7	33.5	0.194	55.4	0.213
5	DETA#6	DETA#8	38.3	0.203	57.8	0.219
6	DETA#7	DETA#8	47.1	0.208	85.9	0.287

Table C6.3. K_s^{app} and k_{max}^{app} values of 1,1,1-TCA in the presence of 1,1-DCE ($4.3 \pm 0.16 \mu\text{M}$).

- Slope and y intercept of extrapolated linear lines

Batch vial #	Substrate, S_L 1,1,1-TCA (μM)	Inhibitor, I_L 1,1-DCE (μM)	$-S_L$ (μM)	Initial degradation rate, v ($\mu\text{mol}/\text{mg TSS}/\text{hr}$)	Extrapolated line	
					Slope	Y intercept
DETA#9	32.6	4.52	-32.6	0.08	0.0025	0.08
DETA#10	75.9	4.23	-75.9	0.10	0.0013	0.10
DETA#11	156	4.15	-156	0.13	0.0008	0.13
DETA#12	291	4.33	-291	0.16	0.0005	0.16

- Intersection coordinates and best estimate (median) of K_s^{app} and k_{max}^{app}

Number of data	Batch vial #	Batch vial #	Coordinate of intersection		Order from the lowest to highest	
			K_s^{app} (μM)	k_{max}^{app} ($\mu mol/mg$ TSS/hr)	K_s^{app} (μM)	k_{max}^{app} ($\mu mol/mg$ TSS/hr)
1	DETA#9	DETA#10	11.6	0.11	11.6	0.11
2	DETA#9	DETA#11	30.1	0.16	30.1	0.16
3	DETA#9	DETA#12	39.2	0.18	39.2	0.18
Median	-	-	-	-	62.0	0.19
4	DETA#10	DETA#11	84.8	0.20	84.8	0.20
5	DETA#10	DETA#12	86.9	0.21	86.9	0.21
6	DETA#11	DETA#12	89.9	0.21	89.9	0.21

Table C6.4. K_s^{app} and k_{max}^{app} values of 1,1,1-TCA in the presence of 1,1-DCE ($7.3 \pm 0.15 \mu M$).

- Slope and y intercept of extrapolated linear lines

Batch vial #	Substrate, S_L 1,1,1-TCA (μM)	Inhibitor, I_L 1,1-DCE (μM)	$-S_L$ (μM)	Initial degradation rate, v ($\mu mol/mg$ TSS/hr)	Extrapolated line	
					Slope	Y intercept
DETA#13	75.9	7.26	-75.9	0.080	0.0011	0.080
DETA#14	151	7.49	-151	0.125	0.0008	0.125
DETA#15	231	7.12	-231	0.127	0.0005	0.127
DETA#16	299	7.35	-299	0.135	0.0005	0.135

- Intersection coordinates and best estimate (median) of K_s^{app} and k_{max}^{app}

Number of data	Batch vial #	Batch vial #	Coordinate of intersection		Order from the lowest to highest	
			K_s^{app} (μM)	k_{max}^{app} ($\mu mol/mg$ TSS/hr)	K_s^{app} (μM)	k_{max}^{app} ($\mu mol/mg$ TSS/hr)
1	DETA#13	DETA#14	200	0.291	6.1	0.130
2	DETA#13	DETA#15	92.5	0.177	26.5	0.147
3	DETA#13	DETA#16	91.3	0.176	85.3	0.174
Median	-	-	-	-	88.3	0.18
4	DETA#14	DETA#15	6.1	0.130	91.3	0.176
5	DETA#14	DETA#16	26.5	0.147	92.5	0.177
6	DETA#15	DETA#16	85.3	0.174	200	0.291

Table C6.5. K_s^{app} and $k_{\text{max}}^{\text{app}}$ values of 1,1,1-TCA in the presence of 1,1-DCE ($12.6 \pm 0.15 \mu\text{M}$).

- Slope and y intercept of extrapolated linear lines

Batch vial #	Substrate, S_L 1,1,1-TCA (μM)	Inhibitor, I_L 1,1-DCE (μM)	$-S_L$ (μM)	Initial degradation rate, v ($\mu\text{mol/mg TSS/hr}$)	Extrapolated line	
					Slope	Y intercept
DETA#17	75.9	12.46	-75.9	0.049	0.00064	0.049
DETA#18	151	12.58	-151	0.086	0.00057	0.086
DETA#19	231	12.80	-231	0.100	0.00043	0.100
DETA#20	299	12.70	-299	0.120	0.00040	0.090

- Intersection coordinates and best estimate (median) of K_s^{app} and $k_{\text{max}}^{\text{app}}$

Number of data	Batch vial #	Batch vial #	Coordinate of intersection		Order from the lowest to highest	
			K_s^{app} (μM)	$k_{\text{max}}^{\text{app}}$ ($\mu\text{mol/mg}$ TSS/hr)	K_s^{app} (μM)	$k_{\text{max}}^{\text{app}}$ ($\mu\text{mol/mg}$ TSS/hr)
1	DETA#17	DETA#18	547	0.398	23.7	0.100
2	DETA#17	DETA#19	250	0.209	102	0.144
3	DETA#17	DETA#20	175	0.160	175	0.160
Median	-	-	-	-	212	0.18
4	DETA#18	DETA#19	102	0.144	250	0.209
5	DETA#18	DETA#20	23.7	0.100	547	0.398
6	DETA#19	DETA#20	-315	-0.036	-315	-0.036

Direct Linear Plot

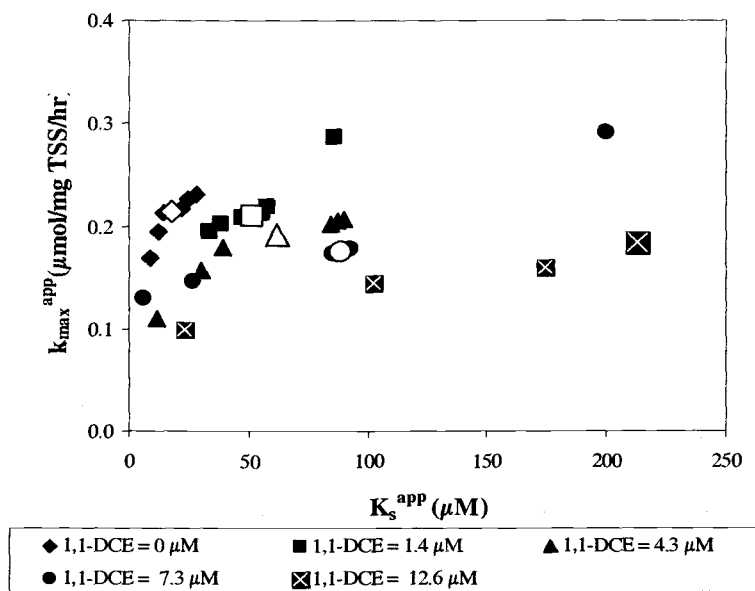


Figure C6.1. Direct linear plot showing competitive inhibition on 1,1,1-TCA transformation by 1,1-DCE.

Linearized Plot

Table C6.6. Values used for linearized plot in the case of competitive inhibition on 1,1,1-TCA transformation by 1,1-DCE

Inhibitor (1,1-DCE) (μM)	K_s^{app} (μM)	k_{\max}^{app} (μmol/ mg TSS/hr)
0.0	18.2	0.22
1.4	51.3	0.21
4.3	62.0	0.19
7.3	88.3	0.18
12.6	212	0.18

Table C6.7. Initial guesses of parameters obtained linearized plot in the case of inhibition on 1,1,1-TCA transformation by 1,1-DCE

Plot (K_s^{app} vs. I_L)	Y intercept (= K_s) (μM)	Slope (= K_s/K_{ic}) (-)	K_{ic} (μM)	k_{\max}^{app} (μmol/ mg TSS/hr)
	13.5	14.238	0.9	0.20

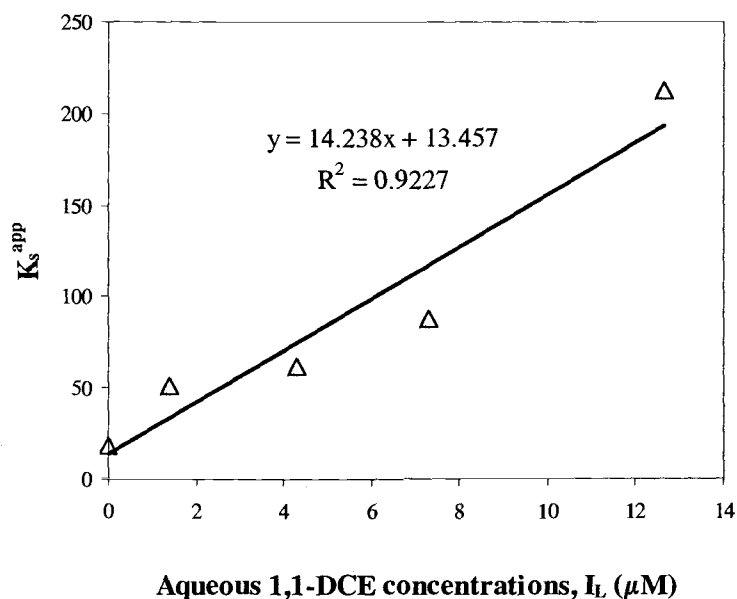


Figure C6.2. Linearized plot in the case of competitive inhibition of 1,1,1-TCA transformation by 1,1-DCE

NLSR Analysis

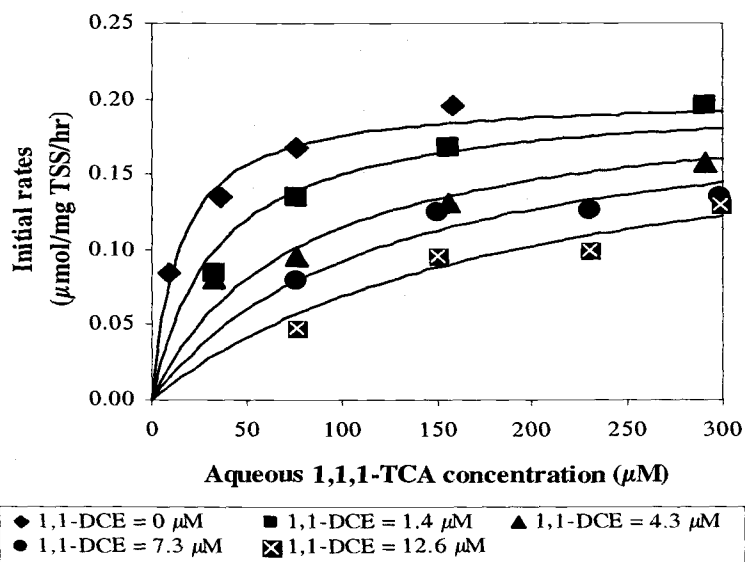


Figure C6.3. Best fit obtained from NLSR analysis using competitive inhibition model. (Residual Standard Error = 0.01, $k_{max} = 0.20 \pm 0.015 \mu\text{mol/mg TSS/hr}$, $K_s = 14.3 \pm 4.8 \mu\text{M}$, and $K_{ic} = 1.02 \pm 0.304 \mu\text{M}$)

C7. COMPETITIVE INHIBITION ON BUTANE DEGRADATION BY 1,1-DCA

K_s^{app} and k_{max}^{app} Values of butane in the Presence of 1,1-DCA

Table C7.1. K_s^{app} and k_{max}^{app} values of butane in the presence of 1,1-DCA (0 μ M).

- Slope and y intercept of extrapolated linear lines

Batch vial #	Substrate, S_L Butane (μ M)	Inhibitor, I_L 1,1-DCA (μ M)	- S_L (μ M)	Initial degradation rate, v (μ mol/mg TSS/hr)	Extrapolated line	
					slope	Y intercept
DABU#45	1.71	0	-1.71	0.29	0.171	0.29
DABU#46	4.97	0	-4.97	0.68	0.138	0.68
DABU#47	8.21	0	-8.21	0.87	0.106	0.87
DABU#48	13.4	0	-13.4	1.18	0.088	1.18

- Intersection coordinates and best estimate (median) of K_s^{app} and k_{max}^{app}

Number of data	Batch vial #	Batch vial #	Coordinate of intersection		Order from the lowest to highest	
			K_s^{pp} (μ M)	k_{max}^{app} (μ mol/mg TSS/hr)	K_s^{app} (μ M)	k_{max}^{app} (μ mol/mg TSS/hr)
1	DABU#45	DABU#46	11.5	2.27	6.12	1.53
2	DABU#45	DABU#47	9.0	1.83	9.0	1.83
3	DABU#45	DABU#48	10.7	2.13	10.1	2.08
Median	-	-	-	-	10.4	2.1
4	DABU#46	DABU#47	6.12	1.53	10.7	2.13
5	DABU#46	DABU#48	10.1	2.08	11.5	2.27
6	DABU#47	DABU#48	17.0	2.68	16.9	2.68

Table C7.2 K_s^{app} and k_{max}^{app} values of butane in the presence of 1,1-DCA ($238 \pm 4.8 \mu\text{M}$).

- Slope and y intercept of extrapolated linear lines

Batch vial #	Substrate, S_L Butane (μM)	Inhibitor, I_L 1,1-DCA (μM)	$-S_L$ (μM)	Initial degradation rate, v ($\mu\text{mol/mg TSS/hr}$)	Extrapolated line	
					slope	Y intercept
DABU#29	1.71	234	-1.71	0.20	0.116	0.20
DABU#33	4.84	243	-4.84	0.47	0.097	0.47
DABU#37	8.39	236	-8.39	0.66	0.078	0.66
DABU#41	13.1	241	-13.1	0.91	0.069	0.91

- Intersection coordinates and best estimate (median) of K_s^{app} and k_{max}^{app}

Number of data	Batch vial #	Batch vial #	Coordinate of intersection		Order from the lowest to highest	
			K_s^{app} (μM)	k_{max}^{app} ($\mu\text{mol/mg TSS/hr}$)	K_s^{app} (μM)	k_{max}^{app} ($\mu\text{mol/mg TSS/hr}$)
1	DABU#29	DABU#33	14.5	1.88	9.83	1.43
2	DABU#29	DABU#37	12.1	1.61	12.1	1.61
3	DABU#29	DABU#41	15.2	1.96	14.5	1.88
Median	-	-	-	-	14.8	1.92
4	DABU#33	DABU#37	9.83	1.43	15.2	1.96
5	DABU#33	DABU#41	15.7	2.00	15.7	2.00
6	DABU#37	DABU#41	28.1	2.86	28.1	2.86

Table C7.3 K_s^{app} and k_{max}^{app} values of butane in the presence of 1,1-DCA ($464 \pm 8.0 \mu\text{M}$).

- Slope and y intercept of extrapolated linear lines

Batch vial #	Substrate, S_L Butane (μM)	Inhibitor, I_L 1,1-DCA (μM)	$-S_L$ (μM)	Initial degradation rate, v ($\mu\text{mol/mg TSS/hr}$)	Extrapolated line	
					slope	Y intercept
DABU#30	1.65	467	-1.65	0.16	0.096	0.16
DABU#34	4.92	453	-4.92	0.38	0.076	0.38
DABU#38	8.50	462	-8.50	0.58	0.068	0.58
DABU#42	13.1	472	-13.1	0.79	0.060	0.79

- Intersection coordinates and best estimate (median) of K_s^{app} and k_{max}^{app}

Number of data	Batch vial #	Batch vial #	Coordinate of intersection		Order from the lowest to highest	
			K_s^{app} (μM)	k_{max}^{app} ($\mu mol/mg$ TSS/hr)	K_s^{app} (μM)	k_{max}^{app} ($\mu mol/mg$ TSS/hr)
1	DABU#30	DABU#34	11.0	1.21	11.0	1.21
2	DABU#30	DABU#38	14.9	1.59	14.9	1.59
3	DABU#30	DABU#42	17.7	1.85	17.7	1.85
Median	-	-	-	-	21.0	2.04
4	DABU#34	DABU#38	24.3	2.23	24.3	2.23
5	DABU#34	DABU#42	26.0	2.35	26.0	2.35
6	DABU#38	DABU#42	27.8	2.46	27.8	2.46

Table C7.4 K_s^{app} and k_{max}^{app} values of butane in the presence of 1,1-DCA ($693 \pm 5.4 \mu M$).

- Slope and y intercept of extrapolated linear lines

Batch vial #	Substrate, S_L Butane (μM)	Inhibitor, I_L 1,1-DCA (μM)	$-S_L$ (μM)	Initial degradation rate, v ($\mu mol/mg$ TSS/hr)	Extrapolated line	
					slope	Y intercept
DABU#31	1.62	689	-1.62	0.11	0.065	0.11
DABU#35	4.92	689	-4.92	0.31	0.063	0.31
DABU#39	8.29	695	-8.29	0.48	0.057	0.48
DABU#43	13.1	700	-13.1	0.62	0.047	0.62

- Intersection coordinates and best estimate (median) of K_s^{app} and k_{max}^{app}

Number of data	Batch vial #	Batch vial #	Coordinate of intersection		Order from the lowest to highest	
			K_s^{app} (μM)	k_{max}^{app} ($\mu mol/mg$ TSS/hr)	K_s^{app} (μM)	k_{max}^{app} ($\mu mol/mg$ TSS/hr)
1	DABU#31	DABU#35	76.7	5.13	13.7	1.26
2	DABU#31	DABU#39	45.6	3.09	19.5	1.53
3	DABU#31	DABU#43	27.7	1.92	27.7	1.92
Median	-	-	-	-	29.1	2.07
4	DABU#35	DABU#39	30.4	2.22	30.4	2.22
5	DABU#35	DABU#43	19.5	1.53	45.6	3.09
6	DABU#39	DABU#43	13.7	1.26	76.8	5.13

Table C7.5 K_s^{app} and k_{max}^{app} values of butane in the presence of 1,1-DCA ($908 \pm 13.0 \mu\text{M}$).

- Slope and y intercept of extrapolated linear lines

Batch vial #	Substrate, S_L Butane (μM)	Inhibitor, I_L 1,1-DCA (μM)	$-S_L$ (μM)	Initial degradation rate, v ($\mu\text{mol/mg TSS/hr}$)	Extrapolated line	
					slope	Y intercept
DABU#32	1.65	919	-1.65	0.09	0.057	0.09
DABU#36	4.87	896	-4.87	0.23	0.048	0.23
DABU#40	8.18	919	-8.18	0.38	0.047	0.38
DABU#44	13.3	896	-13.3	0.59	0.044	0.59

- Intersection coordinates and best estimate (median) of K_s^{app} and k_{max}^{app}

Number of data	Batch vial #	Batch vial #	Coordinate of intersection		Order from the lowest to highest	
			K_s^{app} (μM)	k_{max}^{app} ($\mu\text{mol/mg TSS/hr}$)	K_s^{app} (μM)	k_{max}^{app} ($\mu\text{mol/mg TSS/hr}$)
1	DABU#32	DABU#36	15.6	0.98	15.6	0.98
2	DABU#32	DABU#40	29.3	1.75	29.3	1.75
3	DABU#32	DABU#44	34.1	2.03	34.1	2.03
Median	-	-	-	-	40.1	2.28
4	DABU#36	DABU#40	151	7.43	46.1	2.54
5	DABU#36	DABU#44	66.8	3.42	66.8	3.42
6	DABU#40	DABU#44	46.1	2.54	151	7.43

Direct Linear Plot

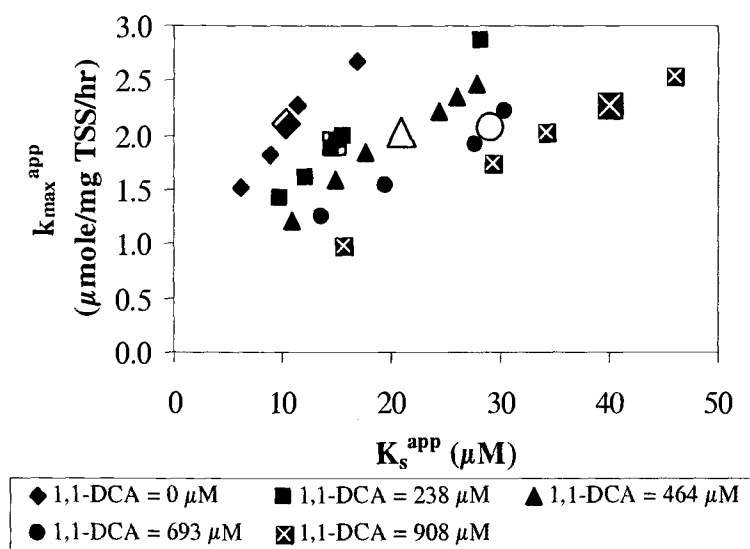


Figure C7.1. Direct linear plot showing competitive inhibition on butane degradation by 1,1-DCA.

Linearized Plot

Table C7.6. Values used for linearized plot in the case of competitive inhibition on butane degradation by 1,1-DCA.

Inhibitor (1,1-DCA) (μM)	K_s^{app} (μM)	k_{max}^{app} ($\mu\text{mol/ mg TSS/hr}$)
0	10.4	2.10
239	14.8	1.92
464	21.0	2.04
693	29.1	2.07
908	40.1	2.28

Table C7.7. Initial guesses of parameters obtained linearized plot in the case of inhibition on butane degradation by 1,1-DCA.

Plot (K_s^{app} vs. I_L)	Y intercept ($=K_s$) (μM)	Slope ($=K_s/K_{ic}$) (-)	K_{ic} (μM)	k_{max}^{app} ($\mu\text{mol/ mg TSS/hr}$)
	8.2	0.032	253	2.08

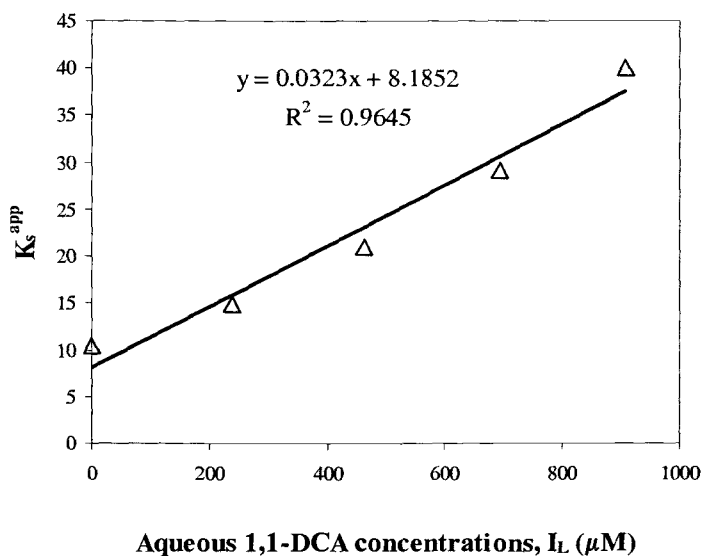


Figure C7.2. Linearized plot in the case of competitive inhibition of butane degradation by 1,1-DCA.

NLSR Analysis

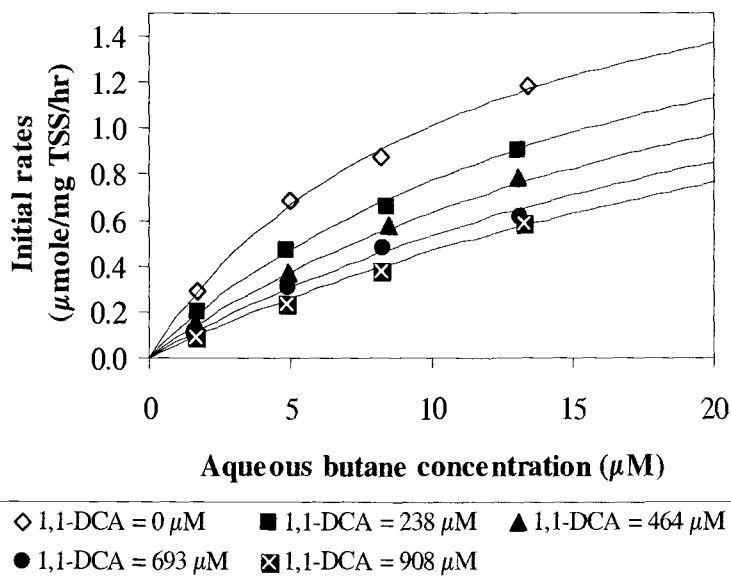


Figure C7.3. Best fit obtained from NLSR analysis using competitive inhibition model. (Residual Standard Error = 0.020, $k_{max} = 2.12 \pm 0.23 \mu\text{mol/mg TSS/hr}$, $K_s = 10.9 \pm 2.22 \mu\text{M}$, and $K_{ic} = 403 \pm 51 \mu\text{M}$)

C8. COMPETITIVE INHIBITION ON 1,1-DCE TRANSFORMATION BY 1,1-DCA

K_s^{app} and k_{max}^{app} Values of 1,1-DCE in the Presence of 1,1-DCA

Table C8.1. K_s^{app} and k_{max}^{app} values of 1,1-DCE in the presence of 1,1-DCA (0 μ M).

- Slope and y intercept of extrapolated linear lines

Batch vial #	Substrate, S_L 1,1-DCE (μ M)	Inhibitor, I_L 1,1-DCA (μ M)	$-S_L$ (μ M)	Initial degradation rate, v (μ mol/mg TSS/hr)	Extrapolated line	
					slope	Y intercept
DADE#17	1.64	0	-1.64	0.53	0.319	0.53
DADE#18	6.26	0	-6.26	0.99	0.158	0.99
DADE#19	12.7	0	-12.7	1.05	0.083	1.05
DADE#20	27.2	0	-27.2	1.05	0.039	1.05

- Intersection coordinates and best estimate (median) of K_s^{app} and k_{max}^{app}

Number of data	Batch vial #	Batch vial #	Coordinate of intersection		Order from the lowest to highest	
			K_s^{app} (μ M)	k_{max}^{app} (μ mol/mg TSS/hr)	K_s^{app} (μ M)	k_{max}^{app} (μ mol/mg TSS/hr)
1	DADE#17	DADE#18	2.87	1.44	0.16	1.06
2	DADE#17	DADE#19	2.20	1.23	0.54	1.07
3	DADE#17	DADE#20	1.88	1.13	0.77	1.11
Median	-	-	-	-	1.32	1.12
4	DADE#18	DADE#19	0.77	1.11	1.88	1.13
5	DADE#18	DADE#20	0.54	1.07	2.20	1.23
6	DADE#19	DADE#20	0.16	1.06	2.87	1.44

Table C8.2 K_s^{app} and k_{max}^{app} values of 1,1-DCE in the presence of 1,1-DCA ($154 \pm 3.9 \mu\text{M}$).

- Slope and y intercept of extrapolated linear lines

Batch vial #	Substrate, S_L 1,1-DCE (μM)	Inhibitor, I_L 1,1-DCA (μM)	$-S_L$ (μM)	Initial degradation rate, v ($\mu\text{mol/mg TSS/hr}$)	Extrapolated line	
					slope	Y intercept
DADE#1	1.52	152	-1.52	0.11	0.074	0.11
DADE#2	6.14	157	-6.14	0.39	0.064	0.39
DADE#3	12.4	156	-12.4	0.52	0.042	0.52
DADE#4	27.2	148	-27.2	0.70	0.026	0.70

- Intersection coordinates and best estimate (median) of K_s^{app} and k_{max}^{app}

Number of data	Batch vial #	Batch vial #	Coordinate of intersection		Order from the lowest to highest	
			K_s^{app} (μM)	k_{max}^{app} ($\mu\text{mol/mg TSS/hr}$)	K_s^{app} (μM)	k_{max}^{app} ($\mu\text{mol/mg TSS/hr}$)
1	DADE#1	DADE#2	27.3	2.13	5.72	0.76
2	DADE#1	DADE#3	12.6	1.04	8.22	0.92
3	DADE#1	DADE#4	12.3	1.02	11.7	1.01
Median	-	-	-	-	12.0	1.01
4	DADE#2	DADE#3	5.72	0.76	12.3	1.02
5	DADE#2	DADE#4	8.22	0.92	12.6	1.04
6	DADE#3	DADE#4	11.7	1.01	27.3	2.13

Table C8.3 K_s^{app} and k_{max}^{app} values of 1,1-DCE in the presence of 1,1-DCA ($387 \pm 24.3 \mu\text{M}$).

- Slope and y intercept of extrapolated linear lines

Batch vial #	Substrate, S_L 1,1-DCE (μM)	Inhibitor, I_L 1,1-DCA (μM)	$-S_L$ (μM)	Initial degradation rate, v ($\mu\text{mol/mg TSS/hr}$)	Extrapolated line	
					slope	Y intercept
DADE#5	1.5	375	-1.5	0.05	0.033	0.05
DADE#6	6.1	423	-6.1	0.16	0.027	0.16
DADE#7	12.4	376	-12.4	0.28	0.023	0.28
DADE#8	27.1	372	-27.1	0.46	0.017	0.46

- Intersection coordinates and best estimate (median) of K_s^{app} and k_{max}^{app}

Number of data	Batch vial #	Batch vial #	Coordinate of intersection		Order from the lowest to highest	
			K_s^{app} (μM)	k_{max}^{app} ($\mu mol/mg$ TSS/hr)	K_s^{app} (μM)	k_{max}^{app} ($\mu mol/mg$ TSS/hr)
1	DADE#5	DADE#6	18.1	0.65	18.1	0.65
2	DADE#5	DADE#7	22.7	0.80	22.7	0.80
3	DADE#5	DADE#8	25.0	0.88	25.0	0.88
Median	-	-	-	-	27.1	0.91
4	DADE#6	DADE#7	29.8	0.96	29.1	0.95
5	DADE#6	DADE#8	29.4	0.95	29.4	0.95
6	DADE#7	DADE#8	29.1	0.95	29.8	0.96

Table C8.4 K_s^{app} and k_{max}^{app} values of 1,1-DCE in the presence of 1,1-DCA ($608 \pm 14.8 \mu M$).

- Slope and y intercept of extrapolated linear lines

Batch vial #	Substrate, S_L 1,1-DCE (μM)	Inhibitor, I_L 1,1-DCA (μM)	$-S_L$ (μM)	Initial degradation rate, v ($\mu mol/mg$ TSS/hr)	Extrapolated line	
					slope	Y intercept
DADE#9	1.7	627	-1.7	0.03	0.018	0.03
DADE#10	6.1	611	-6.1	0.12	0.020	0.12
DADE#11	12.0	599	-12.0	0.21	0.018	0.21
DADE#12	27.0	594	-27.0	0.35	0.013	0.35

- Intersection coordinates and best estimate (median) of K_s^{app} and k_{max}^{app}

Number of data	Batch vial #	Batch vial #	Coordinate of intersection		Order from the lowest to highest	
			K_s^{app} (μM)	k_{max}^{app} ($\mu mol/mg$ TSS/hr)	K_s^{app} (μM)	k_{max}^{app} ($\mu mol/mg$ TSS/hr)
1	DADE#9	DADE#10	-36.7	-0.61	29.7	0.73
2	DADE#9	DADE#11	-5699	-100	31.5	0.75
3	DADE#9	DADE#12	68.8	1.24	34.8	0.82
Median	-	-	-	-	51.8	1.03
4	DADE#10	DADE#11	34.8	0.82	68.8	1.24
5	DADE#10	DADE#12	31.5	0.75	-36.7	-0.61
6	DADE#11	DADE#12	29.7	0.73	-5699	-100

Table C8.5 K_s^{app} and k_{max}^{app} values of 1,1-DCE in the presence of 1,1-DCA ($887 \pm 15.4 \mu\text{M}$).

- Slope and y intercept of extrapolated linear lines

Batch vial #	Substrate, S_L 1,1-DCE (μM)	Inhibitor, I_L 1,1-DCA (μM)	$-S_L$ (μM)	Initial degradation rate, v ($\mu\text{mol}/\text{mg TSS}/\text{hr}$)	Extrapolated line	
					slope	Y intercept
DADE#13	1.6	880	-1.6	0.02	0.014	0.02
DADE#14	5.9	868	-5.9	0.08	0.013	0.08
DADE#15	12.1	896	-12.1	0.15	0.012	0.15
DADE#16	27.1	902	-27.1	0.29	0.011	0.29

- Intersection coordinates and best estimate (median) of K_s^{app} and k_{max}^{app}

Number of data	Batch vial #	Batch vial #	Coordinate of intersection		Order from the lowest to highest	
			K_s^{app} (μM)	k_{max}^{app} ($\mu\text{mol}/\text{mg TSS}/\text{hr}$)	K_s^{app} (μM)	k_{max}^{app} ($\mu\text{mol}/\text{mg TSS}/\text{hr}$)
1	DADE#13	DADE#14	75.1	1.08	52.9	0.78
2	DADE#13	DADE#15	61.2	0.88	61.2	0.88
3	DADE#13	DADE#16	80.1	1.15	75.1	1.08
Median	-	-	-	-	77.6	1.12
4	DADE#14	DADE#15	52.9	0.78	80.1	1.15
5	DADE#14	DADE#16	81.5	1.17	81.5	1.17
6	DADE#15	DADE#16	109	1.46	109	1.46

Direct Linear Plot

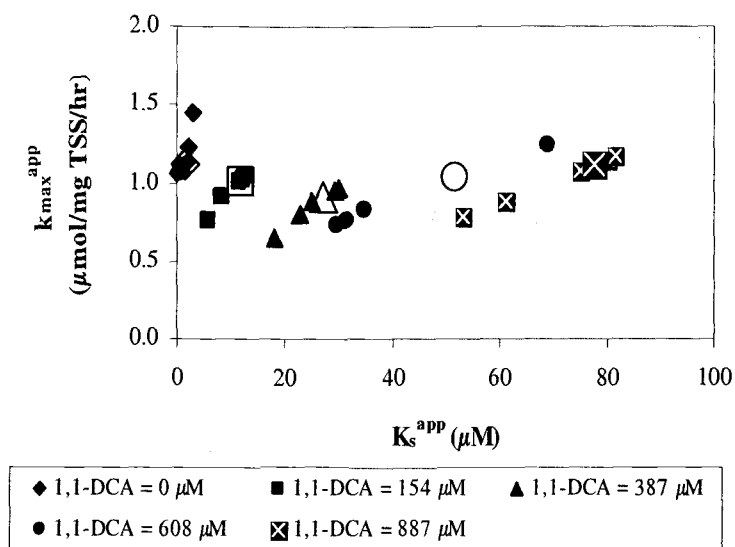


Figure C8.1. Direct linear plot showing competitive inhibition on 1,1-DCE transformation by 1,1-DCA.

Linearized Plot

Table C8.6. Values used for linearized plot in the case of competitive inhibition on 1,1-DCE transformation by 1,1-DCA.

Inhibitor (1,1-DCA) (μM)	K_s^{app} (μM)	k_{max}^{app} ($\mu\text{mol/mg TSS/hr}$)
0	1.32	1.12
154	12.0	1.01
387	27.1	0.91
608	51.8	1.03
887	77.6	1.12

Table C8.7. Initial guesses of parameters obtained linearized plot in the case of inhibition on 1,1-DCE transformation by 1,1-DCA.

Plot (K_s^{app} vs. I_L)	Y intercept ($=K_s$) (μM)	slope ($=$ K_s/K_{ic}) (-)	K_{ic} (μM)	k_{max}^{app} ($\mu\text{mol/mg TSS/hr}$)
	-1.4	0.087	-16	1.04

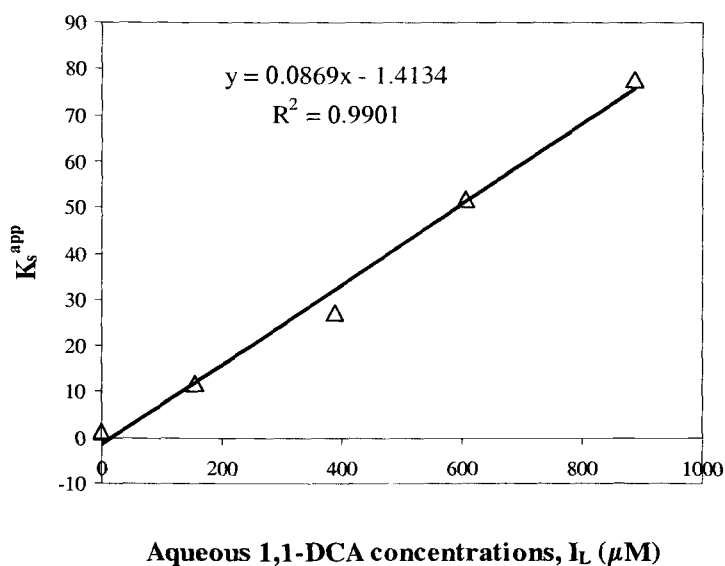


Figure C8.2. Linearized plot in the case of competitive inhibition of 1,1-DCE transformation by 1,1-DCA.

NLSR Analysis

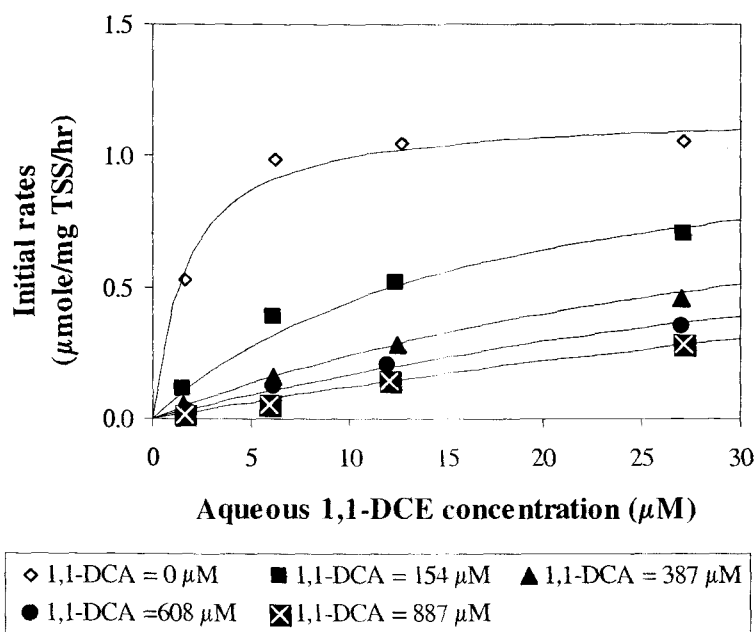


Figure C8.3. Best fit obtained from NLSR analysis using competitive inhibition model. (Residual Standard Error = 0.035, $k_{max} = 1.16 \pm 0.07 \mu\text{mol/mg TSS/hr}$, $K_s = 1.67 \pm 0.51 \mu\text{M}$, and $K_{ic} = 17.8 \pm 4.87 \mu\text{M}$)

C9. COMPETITIVE INHIBITION ON 1,1,1-TCA TRANSFORMATION BY 1,1-DCA

K_s^{app} and k_{max}^{app} Values of 1,1,1-TCA in the Presence of 1,1-DCA

Table C9.1. K_s^{app} and k_{max}^{app} values of 1,1,1-TCA in the presence of 1,1-DCA (0 μ M).

- Slope and y intercept of extrapolated linear lines

Batch vial #	Substrate, S_L 1,1,1-TCA (μ M)	Inhibitor, I_L 1,1-DCA (μ M)	$-S_L$ (μ M)	Initial degradation rate, v (μ mol/mg TSS/hr)	Extrapolated line	
					slope	Y intercept
DATA#17	9.4	0	-9.4	0.08	0.009	0.08
DATA#18	19.4	0	-19.4	0.12	0.006	0.12
DATA#19	35.0	0	-35.0	0.14	0.004	0.14
DATA#20	55.4	0	-55.4	0.16	0.003	0.16

- Intersection coordinates and best estimate (median) of K_s^{app} and k_{max}^{app}

Number of data	Batch vial #	Batch vial #	Coordinate of intersection		Order from the lowest to highest	
			K_s^{app} (μ M)	k_{max}^{app} (μ mol/mg TSS/hr)	K_s^{app} (μ M)	k_{max}^{app} (μ mol/mg TSS/hr)
1	DATA#17	DATA#18	14.4	0.20	8.57	0.17
2	DATA#17	DATA#19	11.7	0.18	11.7	0.18
3	DATA#17	DATA#20	13.8	0.20	13.3	0.20
Median	-	-	-	-	13.5	0.20
4	DATA#18	DATA#19	8.57	0.17	13.8	0.20
5	DATA#18	DATA#20	13.3	0.20	14.4	0.20
6	DATA#19	DATA#20	23.4	0.23	23.4	0.23

Table C9.2. K_s^{app} and k_{max}^{app} values of 1,1,1-TCA in the presence of 1,1-DCA ($5.8 \pm 0.53 \mu\text{M}$).

- Slope and y intercept of extrapolated linear lines

Batch vial #	Substrate, S_L 1,1,1-TCA (μM)	Inhibitor, I_L 1,1-DCA (μM)	$-S_L$ (μM)	Initial degradation rate, v ($\mu\text{mol}/\text{mg TSS}/\text{hr}$)	Extrapolated line	
					slope	Y intercept
DATA#1	10.5	5.1	-10.5	0.07	0.0062	0.07
DATA#2	23.1	5.8	-23.2	0.11	0.0049	0.11
DATA#3	38.3	6.3	-38.3	0.13	0.0034	0.13
DATA#4	56.3	6.1	-56.3	0.15	0.0026	0.15

- Intersection coordinates and best estimate (median) of K_s^{app} and k_{max}^{app}

Number of data	Batch vial #	Batch vial #	Coordinate of intersection		Order from the lowest to highest	
			K_s^{app} (μM)	k_{max}^{app} ($\mu\text{mol}/\text{mg TSS}/\text{hr}$)	K_s^{app} (μM)	k_{max}^{app} ($\mu\text{mol}/\text{mg TSS}/\text{hr}$)
1	DATA#1	DATA#2	36.5	0.29	9.58	0.16
2	DATA#1	DATA#3	21.9	0.20	14.8	0.19
3	DATA#1	DATA#4	22.7	0.21	21.9	0.20
Median	-	-	-	-	22.3	0.21
4	DATA#2	DATA#3	9.58	0.16	22.7	0.21
5	DATA#2	DATA#4	14.8	0.19	25.7	0.22
6	DATA#3	DATA#4	25.7	0.22	36.5	0.29

Table C9.3. K_s^{app} and k_{max}^{app} values of 1,1,1-TCA in the presence of 1,1-DCA ($9.8 \pm 1.12 \mu\text{M}$).

- Slope and y intercept of extrapolated linear lines

Batch vial #	Substrate, S_L 1,1,1-TCA (μM)	Inhibitor, I_L 1,1-DCA (μM)	$-S_L$ (μM)	Initial degradation rate, v ($\mu\text{mol}/\text{mg TSS}/\text{hr}$)	Extrapolated line	
					slope	Y intercept
DATA#5	11.0	11.0	-11.0	0.061	0.0055	0.061
DATA#6	20.8	10.1	-20.8	0.094	0.0045	0.094
DATA#7	56.1	9.8	-56.1	0.138	0.0025	0.138
DATA#8	34.8	8.3	-34.8	0.124	0.0036	0.124

- Intersection coordinates and best estimate (median) of K_s^{app} and $k_{\text{max}}^{\text{app}}$

Number of data	Batch vial #	Batch vial #	Coordinate of intersection		Order from the lowest to highest	
			K_s^{app} (μM)	$k_{\text{max}}^{\text{app}}$ ($\mu\text{mol/mg TSS/hr}$)	K_s^{app} (μM)	$k_{\text{max}}^{\text{app}}$ ($\mu\text{mol/mg TSS/hr}$)
1	DATA#5	DATA#6	32.9	0.24	12.5	0.17
2	DATA#5	DATA#7	25.1	0.20	21.4	0.19
3	DATA#5	DATA#8	32.2	0.24	25.12	0.20
Median	-	-	-	-	28.4	0.22
4	DATA#6	DATA#7	21.4	0.19	31.6	0.24
5	DATA#6	DATA#8	31.6	0.24	32.2	0.24
6	DATA#7	DATA#8	12.5	0.17	32.9	0.24

Table C9.4. K_s^{app} and $k_{\text{max}}^{\text{app}}$ values of 1,1,1-TCA in the presence of 1,1-DCA ($21 \pm 1.8 \mu\text{M}$).

- Slope and y intercept of extrapolated linear lines

Batch vial #	Substrate, S_L 1,1,1-TCA (μM)	Inhibitor, I_L 1,1-DCA (μM)	$-S_L$ (μM)	Initial degradation rate, v ($\mu\text{mol/mg TSS/hr}$)	Extrapolated line	
					slope	Y intercept
DATA#9	10.7	22.2	-10.7	0.05	0.0043	0.05
DATA#10	18.4	19.6	-18.4	0.08	0.0045	0.08
DATA#11	35.2	19.6	-35.2	0.10	0.0029	0.10
DATA#12	53.6	23.0	-53.6	0.13	0.0024	0.13

- Intersection coordinates and best estimate (median) of K_s^{app} and $k_{\text{max}}^{\text{app}}$

Number of data	Batch vial #	Batch vial #	Coordinate of intersection		Order from the lowest to highest	
			K_s^{app} (μM)	$k_{\text{max}}^{\text{app}}$ ($\mu\text{mol/mg TSS/hr}$)	K_s^{app} (μM)	$k_{\text{max}}^{\text{app}}$ ($\mu\text{mol/mg TSS/hr}$)
1	DATA#9	DATA#10	-175	-0.71	11.0	0.13
2	DATA#9	DATA#11	38.6	0.21	22.5	0.19
3	DATA#9	DATA#12	44.8	0.24	38.6	0.21
Median	-	-	-	-	41.5	0.23
4	DATA#10	DATA#11	11.0	0.13	44.8	0.24
5	DATA#10	DATA#12	22.5	0.19	64.7	0.29
6	DATA#11	DATA#12	64.7	0.29	-175	-0.71

Table C9.5. K_s^{app} and k_{max}^{app} values of 1,1,1-TCA in the presence of 1,1-DCA ($29 \pm 2.15 \mu\text{M}$).

- Slope and y intercept of extrapolated linear lines

Batch vial #	Substrate, S_L 1,1,1-TCA (μM)	Inhibitor, I_L 1,1-DCA (μM)	$-S_L$ (μM)	Initial degradation rate, v ($\mu\text{mol}/\text{mg TSS}/\text{hr}$)	Extrapolated line	
					Y slope	intercept
DATA#13	9.7	31.7	-9.7	0.03	0.0033	0.03
DATA#14	20.6	29.2	-20.6	0.07	0.0035	0.07
DATA#15	42.3	26.4	-42.3	0.10	0.0023	0.10
DATA#16	54.7	28.5	-54.7	0.11	0.0020	0.11

- Intersection coordinates and best estimate (median) of K_s^{app} and k_{max}^{app}

Number of data	Batch vial #	Batch vial #	Coordinate of intersection		Order from the lowest to highest	
			K_s^{app} (μM)	k_{max}^{app} ($\mu\text{mol}/\text{mg}$ TSS/hr)	K_s^{app} (μM)	k_{max}^{app} ($\mu\text{mol}/\text{mg}$ TSS/hr)
1	DATA#13	DATA#14	-155	-0.48	21.3	0.15
2	DATA#13	DATA#15	71.0	0.26	26.2	0.17
3	DATA#13	DATA#16	65.5	0.25	47.3	0.21
Median	-	-	-	-	56.4	0.23
4	DATA#14	DATA#15	21.3	0.15	65.5	0.25
5	DATA#14	DATA#16	26.2	0.17	70.9	0.26
6	DATA#15	DATA#16	47.3	0.21	-155	-0.48

Direct Linear Plot

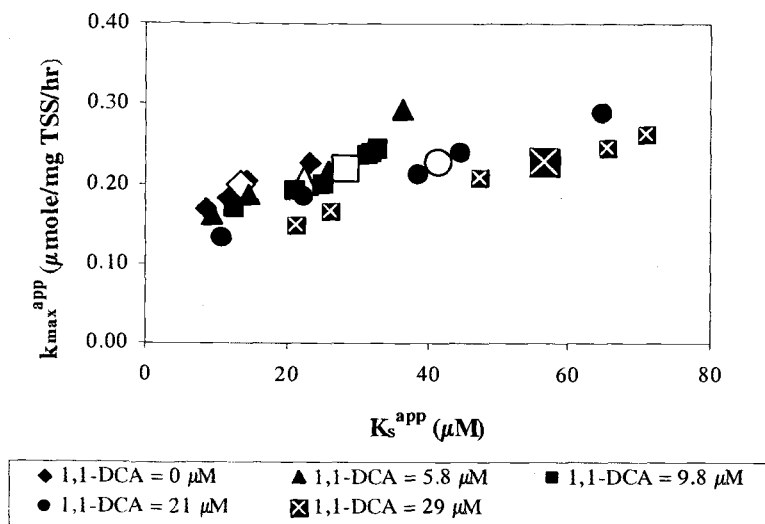


Figure C9.1. Direct linear plot showing competitive inhibition on 1,1,1-TCA transformation by 1,1-DCA.

Linearized Plot

Table C9.6. Values used for linearized plot in the case of competitive inhibition on 1,1,1-TCA transformation by 1,1-DCA.

Inhibitor (1,1-DCA) (μM)	K_s^{app} (μM)	k_{\max}^{app} ($\mu\text{mol/ mg TSS/hr}$)
0	13.5	0.20
5.8	22.3	0.21
9.8	28.4	0.22
21	41.5	0.23
29	56.4	0.23

Table C9.7. Initial guesses of parameters obtained linearized plot in the case of inhibition on 1,1,1-TCA transformation by 1,1-DCA.

Plot (K_s^{app} vs. I_L)	Y intercept ($=K_s$) (μM)	slope ($=K_s/K_{ic}$) (-)	K_{ic} (μM)	k_{\max}^{app} ($\mu\text{mol/ mg TSS/hr}$)
	13.7	1.43	10	0.22

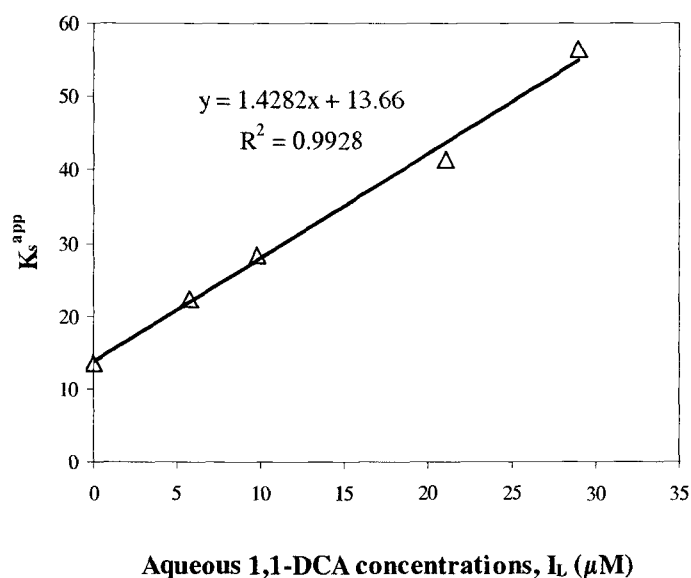


Figure C9.2. Linearized plot in the case of competitive inhibition of 1,1,1-TCA transformation by 1,1-DCA.

NLSR Analysis

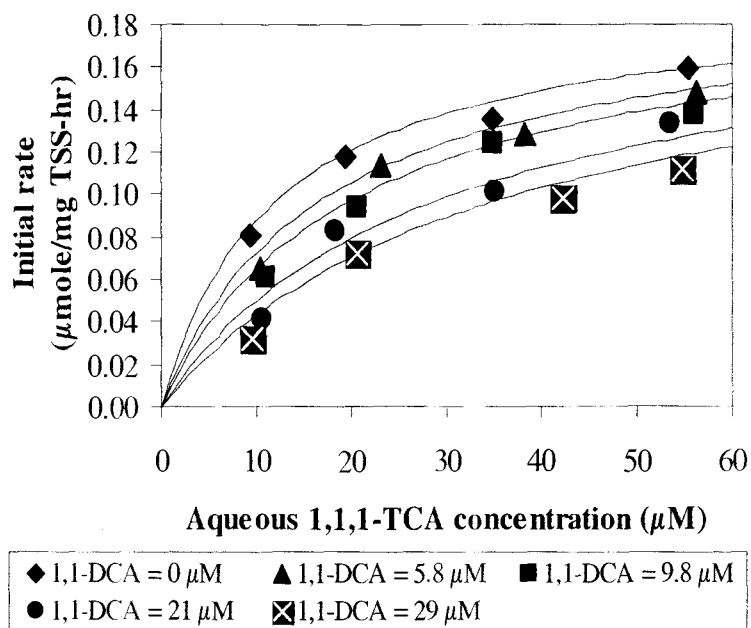


Figure C9.3. Best fit obtained from NLSR analysis using competitive inhibition model. (Residual Standard Error = 0.006, $k_{max} = 0.20 \pm 0.016 \mu\text{mol/mg TSS/hr}$, $K_s = 14.3 \pm 3.69 \mu\text{M}$, and $K_{ic} = 16.24 \pm 4.77 \mu\text{M}$)

C10. COMPETITIVE INHIBITION ON BUTANE DEGRADATION BY 1,1,1-TCA

K_s^{app} and k_{max}^{app} Values of butane in the Presence of 1,1,1-TCA

Table C10.1. K_s^{app} and k_{max}^{app} values of butane in the presence of 1,1,1-TCA (0 μ M).

- Slope and y intercept of extrapolated linear lines

Batch vial #	Substrate, S_L Butane (μ M)	Inhibitor, I_L 1,1,1-TCA (μ M)	$-S_L$ (μ M)	Initial degradation rate, v (μ mol/mg TSS/hr)	Extrapolated line	
					slope	Y intercept
TABU#417	3.24	0	-3.24	0.60	0.184	0.60
TABU#418	11.6	0	-11.6	1.13	0.098	1.13
TABU#419	22.6	0	-22.6	1.66	0.074	1.66
TABU#420	40.2	0	-40.2	1.97	0.049	1.97

- Intersection coordinates and best estimate (median) of K_s^{app} and k_{max}^{app}

Number of data	Batch vial #	Batch vial #	Coordinate of intersection		Order from the lowest to highest	
			K_s^{app} (μ M)	k_{max}^{app} (μ mol/mg TSS/hr)	K_s^{app} (μ M)	k_{max}^{app} (μ mol/mg TSS/hr)
1	TABU#417	TABU#418	6.18	1.73	6.18	1.73
2	TABU#417	TABU#419	9.65	2.37	9.65	2.37
3	TABU#417	TABU#420	10.2	2.47	10.2	2.47
Median	-	-	-	-	11.4	2.52
4	TABU#418	TABU#419	22.2	3.29	12.5	2.59
5	TABU#418	TABU#420	17.3	2.82	17.3	2.82
6	TABU#419	TABU#420	12.5	2.59	22.2	3.29

Table C10.2. K_s^{app} and k_{max}^{app} values of butane in the presence of 1,1,1-TCA ($184 \pm 4.84 \mu\text{M}$).

- Slope and y intercept of extrapolated linear lines

Batch vial #	Substrate, S_L Butane (μM)	Inhibitor, I_L 1,1,1-TCA (μM)	$-S_L$ (μM)	Initial degradation rate, v ($\mu\text{mol/mg TSS/hr}$)	Extrapolated line	
					slope	Y intercept
TABU#401	3.24	178	-3.24	0.38	0.116	0.38
TABU#405	11.6	182	-11.6	0.85	0.073	0.85
TABU#409	22.9	188	-22.9	1.17	0.051	1.17
TABU#413	40.0	188	-40.0	1.60	0.040	1.60

- Intersection coordinates and best estimate (median) of K_s^{app} and k_{max}^{app}

Number of data	Batch vial #	Batch vial #	Coordinate of intersection		Order from the lowest to highest	
			K_s^{app} (μM)	k_{max}^{app} ($\mu\text{mol/mg TSS/hr}$)	K_s^{app} (μM)	k_{max}^{app} ($\mu\text{mol/mg TSS/hr}$)
1	TABU#401	TABU#405	10.8	1.63	10.8	1.63
2	TABU#401	TABU#409	12.2	1.80	12.2	1.80
3	TABU#401	TABU#413	16.0	2.24	15.2	1.96
Median	-	-	-	-	15.6	2.10
4	TABU#405	TABU#409	15.2	1.96	16.0	2.24
5	TABU#405	TABU#413	23.0	2.52	23.0	2.52
6	TABU#409	TABU#413	38.1	3.13	38.1	3.13

Table C10.3. K_s^{app} and k_{max}^{app} values of butane in the presence of 1,1,1-TCA ($548 \pm 7.2 \mu\text{M}$).

- Slope and y intercept of extrapolated linear lines

Batch vial #	Substrate, S_L Butane (μM)	Inhibitor, I_L 1,1,1-TCA (μM)	$-S_L$ (μM)	Initial degradation rate, v ($\mu\text{mol/mg TSS/hr}$)	Extrapolated line	
					slope	Y intercept
TABU#402	3.24	554	-3.24	0.26	0.081	0.26
TABU#406	11.6	554	-11.6	0.57	0.049	0.57
TABU#410	23.5	545	-23.5	0.99	0.042	0.99
TABU#414	39.9	539	-39.9	1.39	0.035	1.39

- Intersection coordinates and best estimate (median) of K_s^{app} and k_{max}^{app}

Number of data	Batch vial #	Batch vial #	Coordinate of intersection		Order from the lowest to highest	
			K_s^{app} (μM)	k_{max}^{app} ($\mu mol/mg$ TSS/hr)	K_s^{app} (μM)	k_{max}^{app} ($\mu mol/mg$ TSS/hr)
1	TABU#402	TABU#406	9.92	1.06	9.92	1.06
2	TABU#402	TABU#410	18.9	1.79	18.9	1.79
3	TABU#402	TABU#414	24.7	2.25	24.7	2.25
Median	-	-	-	-	39.8	2.78
4	TABU#406	TABU#410	59.1	3.48	54.8	3.30
5	TABU#406	TABU#414	56.9	3.38	56.9	3.38
6	TABU#410	TABU#414	54.8	3.30	59.1	3.48

Table C10.4. K_s^{app} and k_{max}^{app} values of butane in the presence of 1,1,1-TCA ($902 \pm 5.0 \mu M$).

- Slope and y intercept of extrapolated linear lines

Batch vial #	Substrate, S_L Butane (μM)	Inhibitor, I_L 1,1,1-TCA (μM)	$-S_L$ (μM)	Initial degradation rate, v ($\mu mol/mg$ TSS/hr)	Extrapolated line	
					slope	Y intercept
TABU#403	3.21	908	-3.21	0.19	0.059	0.19
TABU#407	11.6	904	-11.6	0.50	0.043	0.50
TABU#411	23.4	897	-23.4	0.96	0.041	0.96
TABU#415	40.4	898	-40.4	1.13	0.028	1.13

- Intersection coordinates and best estimate (median) of K_s^{app} and k_{max}^{app}

Number of data	Batch vial #	Batch vial #	Coordinate of intersection		Order from the lowest to highest	
			K_s^{app} (μM)	k_{max}^{app} ($\mu mol/mg$ TSS/hr)	K_s^{app} (μM)	k_{max}^{app} ($\mu mol/mg$ TSS/hr)
1	TABU#403	TABU#407	18.5	1.29	13.8	1.29
2	TABU#403	TABU#411	41.0	2.62	18.5	1.52
3	TABU#403	TABU#415	29.9	1.97	29.9	1.97
Median	-	-	-	-	35.4	2.15
4	TABU#407	TABU#411	222	10.0	41.0	2.33
5	TABU#407	TABU#415	42.7	2.33	42.7	2.62
6	TABU#411	TABU#415	13.8	1.52	222	10.0

Table C10.5. K_s^{app} and k_{max}^{app} values of butane in the presence of 1,1,1-TCA ($1228 \pm 31 \mu\text{M}$).

- Slope and y intercept of extrapolated linear lines

Batch vial #	Substrate, S_L Butane (μM)	Inhibitor, I_L 1,1,1-TCA (μM)	$-S_L$ (μM)	Initial degradation rate, v ($\mu\text{mol/mg TSS/hr}$)	Extrapolated line	
					slope	Y intercept
TABU#404	3.20	1270	-3.20	0.11	0.036	0.11
TABU#408	11.6	1232	-11.6	0.42	0.036	0.42
TABU#412	23.1	1210	-23.1	0.65	0.028	0.65
TABU#416	39.4	1201	-39.4	0.90	0.023	0.90

- Intersection coordinates and best estimate (median) of K_s^{app} and k_{max}^{app}

Number of data	Batch vial #	Batch vial #	Coordinate of intersection		Order from the lowest to highest	
			K_s^{app} (μM)	k_{max}^{app} ($\mu\text{mol/mg TSS/hr}$)	K_s^{app} (μM)	k_{max}^{app} ($\mu\text{mol/mg TSS/hr}$)
1	TABU#404	TABU#408	-2819	-100	30.3	1.50
2	TABU#404	TABU#412	70.7	2.64	38.2	1.78
3	TABU#404	TABU#416	62.3	2.33	50.0	2.05
Median	-	-	-	-	56.1	2.19
4	TABU#408	TABU#412	30.3	1.50	62.3	2.33
5	TABU#408	TABU#416	38.2	1.78	70.7	2.64
6	TABU#412	TABU#416	49.9	2.05	-2819	-100

Direct Linear Plot

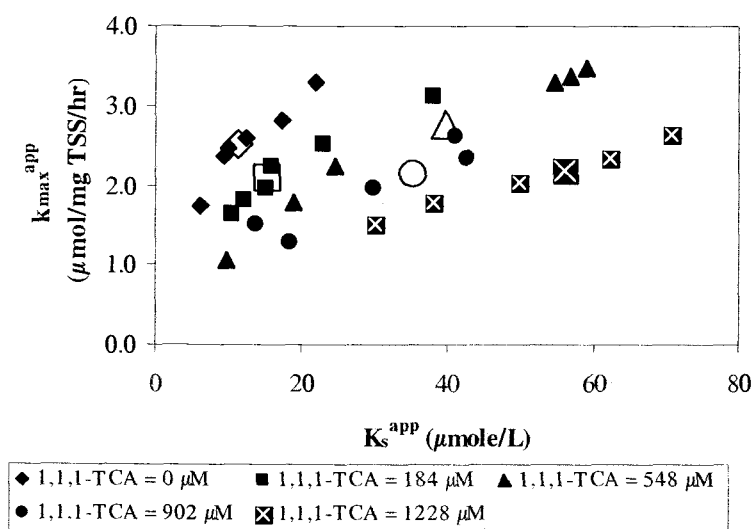


Figure C10.1. Direct linear plot showing competitive inhibition on butane degradation by 1,1,1-TCA.

Linearized Plot

Table C10.6. Values used for linearized plot in the case of competitive inhibition on butane degradation 1,1,1-TCA.

Inhibitor (1,1,1-TCA) (μM)	K_s^{app} (μM)	k_{max}^{app} ($\mu\text{mol/ mg TSS/hr}$)
0	11.4	2.53
184	15.6	2.10
548	39.8	2.78
902	35.4	2.15
1228	56.1	2.19

Table C10.7. Initial guesses of parameters obtained linearized plot in the case of inhibition on butane degradation by 1,1,1-TCA.

Plot (K_s^{app} vs. I_L)	Y intercept ($=K_s$) (μM)	Slope ($=K_s/K_{ic}$) (-)	K_{ic} (μM)	k_{max}^{app} ($\mu\text{mol/ mg TSS/hr}$)
	12.0	0.034	350	2.35

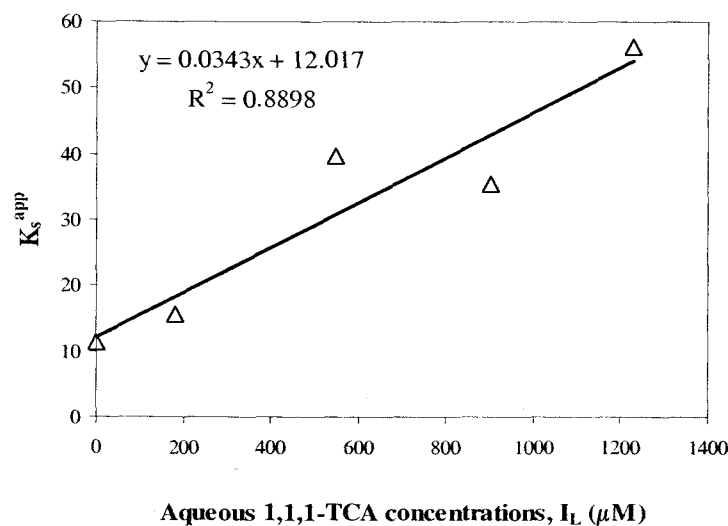


Figure C10.2. Linearized plot in the case of competitive inhibition of butane degradation by 1,1,1-TCA.

NLSR Analysis

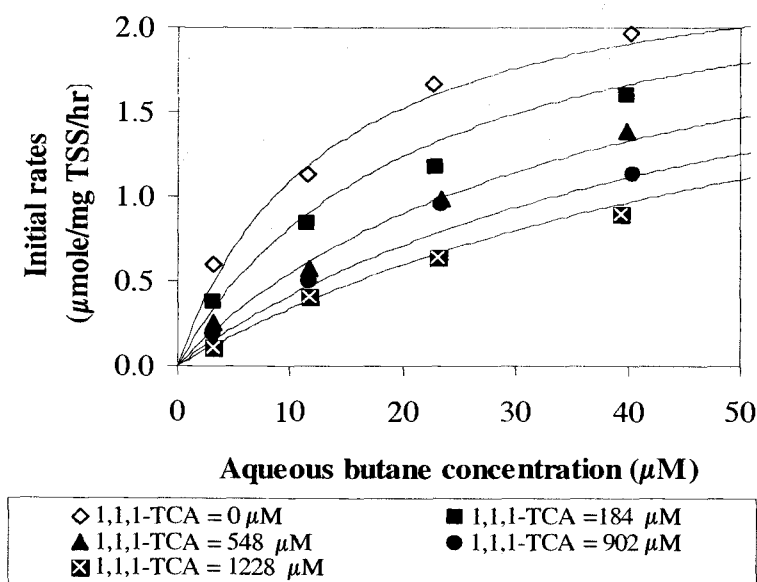


Figure C10.3. Best fit obtained from NLSR analysis using competitive inhibition model. (Residual Standard Error = 0.073, $k_{max} = 2.53 \pm 0.312 \mu\text{mol/mg TSS/hr}$, $K_s = 13.1 \pm 4.4 \mu\text{M}$, and $K_{ic} = 313 \pm 88 \mu\text{M}$)

C11. COMPETITIVE INHIBITION ON 1,1-DCE TRANSFORMATION BY 1,1,1-TCA

K_s^{app} and k_{max}^{app} Values of 1,1-DCE in the Presence of 1,1,1-TCA

Table C11.1. K_s^{app} and k_{max}^{app} values of 1,1-DCE in the presence of 1,1,1-TCA (0 μ M).

- Slope and y intercept of extrapolated linear lines

Batch vial #	Substrate, S_L 1,1-DCE (μ M)	Inhibitor, I_L 1,1,1-TCA (μ M)	$-S_L$ (μ M)	Initial degradation rate, v (μ mol/mg TSS/hr)	Extrapolated line	
					slope	Y intercept
TADE#17	1.50	0	-1.50	0.49	0.328	0.49
TADE#18	5.82	0	-5.82	0.84	0.145	0.84
TADE#19	11.9	0	-11.9	1.07	0.090	1.07
TADE#20	20.4	0	-20.4	1.04	0.051	1.04

- Intersection coordinates and best estimate (median) of K_s^{app} and k_{max}^{app}

Number of data	Batch vial #	Batch vial #	Coordinate of intersection		Order from the lowest to highest	
			K_s^{app} (μ M)	k_{max}^{app} (μ mol/mg TSS/hr)	K_s^{app} (μ M)	k_{max}^{app} (μ mol/mg TSS/hr)
1	TADE#17	TADE#18	1.89	1.12	-0.88	0.99
2	TADE#17	TADE#19	2.43	1.29	1.89	1.12
3	TADE#17	TADE#20	1.96	1.14	1.96	1.14
Median	-	-	-	-	2.03	1.14
4	TADE#18	TADE#19	4.25	1.46	2.09	1.14
5	TADE#18	TADE#20	2.09	1.14	2.43	1.29
6	TADE#19	TADE#20	-0.88	0.99	4.25	1.46

Table C11.2. K_s^{app} and k_{max}^{app} values of 1,1-DCE in the presence of 1,1,1-TCA ($66 \pm 2.6 \mu\text{M}$).

- Slope and y intercept of extrapolated linear lines

Batch vial #	Substrate, S_L 1,1-DCE (μM)	Inhibitor, I_L 1,1,1-TCA (μM)	$-S_L$ (μM)	Initial degradation rate, v ($\mu\text{mol/mg TSS/hr}$)	Extrapolated line	
					slope	Y intercept
TADE#1	1.55	63.2	-1.55	0.17	0.108	0.17
TADE#2	5.87	69.3	-5.87	0.43	0.074	0.43
TADE#3	11.5	65.2	-11.5	0.58	0.051	0.58
TADE#4	19.9	64.5	-19.9	0.79	0.040	0.79

- Intersection coordinates and best estimate (median) of K_s^{app} and k_{max}^{app}

Number of data	Batch vial #	Batch vial #	Coordinate of intersection		Order from the lowest to highest	
			K_s^{app} (μM)	k_{max}^{app} ($\mu\text{mol/mg TSS/hr}$)	K_s^{app} (μM)	k_{max}^{app} ($\mu\text{mol/mg TSS/hr}$)
1	TADE#1	TADE#2	7.89	1.01	7.89	1.02
2	TADE#1	TADE#3	7.27	0.95	6.38	0.90
3	TADE#1	TADE#4	9.21	1.16	7.27	0.95
Median	-	-	-	-	8.6	1.09
4	TADE#2	TADE#3	6.38	0.90	9.21	1.16
5	TADE#2	TADE#4	10.5	1.21	10.5	1.21
6	TADE#3	TADE#4	19.3	1.56	19.3	1.56

Table C11.3. K_s^{app} and k_{max}^{app} values of 1,1-DCE in the presence of 1,1,1-TCA ($133 \pm 3.3 \mu\text{M}$).

- Slope and y intercept of extrapolated linear lines

Batch vial #	Substrate, S_L 1,1-DCE (μM)	Inhibitor, I_L 1,1,1-TCA (μM)	$-S_L$ (μM)	Initial degradation rate, v ($\mu\text{mol/mg TSS/hr}$)	Extrapolated line	
					slope	Y intercept
TADE#5	1.6	132	-1.6	0.09	0.053	0.09
TADE#6	5.6	129	-5.6	0.31	0.056	0.31
TADE#7	11.7	136	-11.7	0.45	0.038	0.45
TADE#8	20.4	136	-20.4	0.64	0.032	0.64

- Intersection coordinates and best estimate (median) of K_s^{app} and k_{max}^{app}

Number of data	Batch vial #	Batch vial #	Coordinate of intersection		Order from the lowest to highest	
			K_s^{app} (μM)	k_{max}^{app} ($\mu mol/mg$ TSS/hr)	K_s^{app} (μM)	k_{max}^{app} ($\mu mol/mg$ TSS/hr)
1	TADE#5	TADE#6	-68.9	-3.54	7.79	0.75
2	TADE#5	TADE#7	25.6	1.43	13.6	1.08
3	TADE#5	TADE#8	26.7	1.49	25.6	1.43
Median	-	-	-	-	26.1	1.46
4	TADE#6	TADE#7	7.79	0.75	26.7	1.49
5	TADE#6	TADE#8	13.6	1.08	29.0	1.56
6	TADE#7	TADE#8	29.0	1.56	-68.9	-3.53

Table C11.4. K_s^{app} and k_{max}^{app} values of 1,1-DCE in the presence of 1,1,1-TCA ($278 \pm 6.6 \mu M$).

- Slope and y intercept of extrapolated linear lines

Batch vial #	Substrate, S_L 1,1-DCE (μM)	Inhibitor, I_L 1,1,1-TCA (μM)	$-S_L$ (μM)	Initial degradation rate, v ($\mu mol/mg$ TSS/hr)	Extrapolated line	
					slope	Y intercept
TADE#9	1.8	281	-1.8	0.08	0.038	0.08
TADE#10	6.1	283	-6.1	0.21	0.034	0.21
TADE#11	11.5	268	-11.5	0.31	0.027	0.31
TADE#12	20.7	279	-20.7	0.42	0.020	0.42

- Intersection coordinates and best estimate (median) of K_s^{app} and k_{max}^{app}

Number of data	Batch vial #	Batch vial #	Coordinate of intersection		Order from the lowest to highest	
			K_s^{app} (μM)	k_{max}^{app} ($\mu mol/mg$ TSS/hr)	K_s^{app} (μM)	k_{max}^{app} ($\mu mol/mg$ TSS/hr)
1	TADE#9	TADE#10	33.9	1.35	13.9	0.68
2	TADE#9	TADE#11	21.1	0.87	16.2	0.75
3	TADE#9	TADE#12	20.4	0.84	18.9	0.81
Median	-	-	-	-	19.6	0.82
4	TADE#10	TADE#11	13.9	0.68	20.4	0.84
5	TADE#10	TADE#12	16.2	0.75	21.1	0.87
6	TADE#11	TADE#12	18.9	0.81	33.9	1.35

Table C11.5. K_s^{app} and k_{max}^{app} values of 1,1-DCE in the presence of 1,1,1-TCA ($409 \pm 1.8 \mu\text{M}$).

- Slope and y intercept of extrapolated linear lines

Batch vial #	Substrate, S_L 1,1-DCE (μM)	Inhibitor, I_L 1,1,1-TCA (μM)	$-S_L$ (μM)	Initial degradation rate, v ($\mu\text{mol/mg TSS/hr}$)	Extrapolated line	
					slope	Y intercept
TADE#13	1.83	410	-1.83	0.04	0.023	0.04
TADE#14	5.95	410	-5.95	0.13	0.021	0.13
TADE#15	11.9	410	-11.9	0.22	0.019	0.22
TADE#16	20.2	406	-20.2	0.29	0.014	0.29

- Intersection coordinates and best estimate (median) of K_s^{app} and k_{max}^{app}

Number Of data	Batch vial #	Batch vial #	Coordinate of intersection		Order from the lowest to highest	
			K_s^{app} (μM)	k_{max}^{app} ($\mu\text{mol/mg TSS/hr}$)	K_s^{app} (μM)	k_{max}^{app} ($\mu\text{mol/mg TSS/hr}$)
1	TADE#13	TADE#14	50.7	1.19	13.9	0.49
2	TADE#13	TADE#15	46.1	1.09	23.6	0.62
3	TADE#13	TADE#16	28.9	0.70	28.8	0.70
Median	-	-	-	-	35.8	0.86
4	TADE#14	TADE#15	42.8	1.03	42.8	1.03
5	TADE#14	TADE#16	23.6	0.62	46.1	1.09
6	TADE#15	TADE#16	13.9	0.49	50.7	1.19

Direct Linear Plot

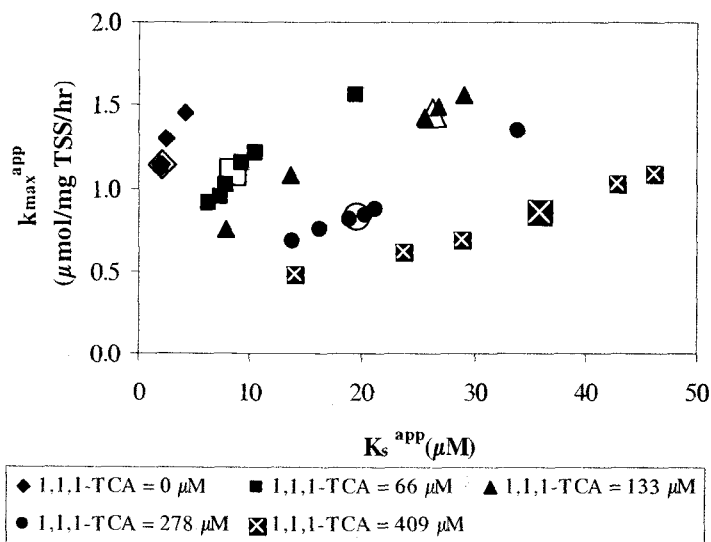


Figure C11.1. Direct linear plot showing competitive inhibition on 1,1-DCE transformation by 1,1,1-TCA.

Linearized Plot

Table C11.6. Values used for linearized plot in the case of competitive inhibition on 1,1-DCE transformation 1,1,1-TCA.

Inhibitor (1,1,1-TCA) (μM)	K_s^{app} (μM)	k_{\max}^{app} ($\mu\text{mol/ mg TSS/hr}$)
0	2.03	1.14
66	8.6	1.09
133	26.1	1.46
278	19.6	0.82
409	35.8	0.86

Table C11.7. Initial guesses of parameters obtained linearized plot in the case of inhibition on 1,1-DCE transformation by 1,1,1-TCA.

Plot (K_s^{app} vs. I_L)	Y intercept ($=K_s$) (μM)	Slope ($=K_s/K_{ic}$) (-)	K_{ic} (μM)	k_{\max}^{app} ($\mu\text{mol/ mg TSS/hr}$)
	5.8	0.071	81	1.07

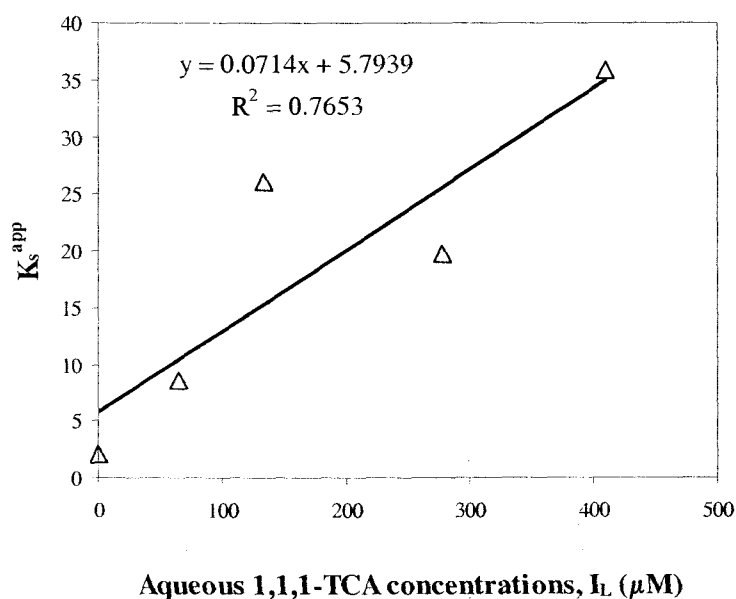


Figure C11.2. Linearized plot in the case of competitive inhibition of 1,1-DCE transformation by 1,1,1-TCA.

NLSR Analysis

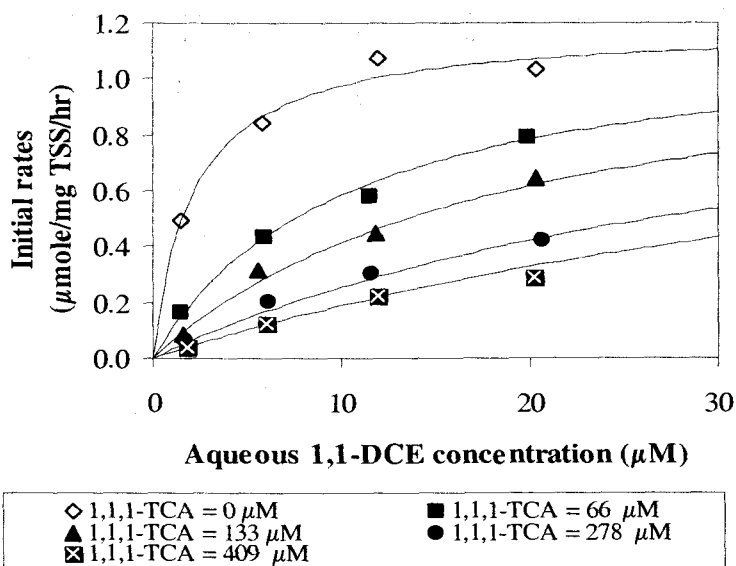


Figure C11.3. Best fit obtained from NLSR analysis using competitive inhibition model. (Residual Standard Error = 0.029, $k_{max} = 1.18 \pm 0.068 \mu\text{mol/mg TSS/hr}$, $K_s = 2.11 \pm 0.542 \mu\text{M}$, and $K_{ic} = 17.3 \pm 3.91 \mu\text{M}$)

C12. COMPETITIVE INHIBITION ON 1,1-DCA TRANSFORMATION BY 1,1,1-TCA

K_s^{app} and k_{max}^{app} Values of 1,1-DCA in the Presence of 1,1,1-TCA

Table C12.1. K_s^{app} and k_{max}^{app} values of 1,1-DCA in the presence of 1,1,1-TCA (0 μ M).

- Slope and y intercept of extrapolated linear lines

Batch vial #	Substrate, S_L 1,1-DCA (μ M)	Inhibitor, I_L 1,1,1-TCA (μ M)	$-S_L$ (μ M)	Initial degradation rate, v (μ mol/mg TSS/hr)	Extrapolated line	
					slope	Y intercept
TADA#21	14.9	0	-14.9	0.26	0.018	0.26
TADA#22	38.7	0	-38.7	0.33	0.009	0.33
TADA#23	86.3	0	-86.3	0.40	0.005	0.40
TADA#24	160	0	-160	0.45	0.003	0.45

- Intersection coordinates and best estimate (median) of K_s^{app} and k_{max}^{app}

Number of data	Batch vial #	Batch vial #	Coordinate of intersection		Order from the lowest to highest	
			K_s^{app} (μ M)	k_{max}^{app} (μ mol/mg TSS/hr)	K_s^{app} (μ M)	k_{max}^{app} (μ mol/mg TSS/hr)
1	TADA#21	TADA#22	7.62	0.40	7.62	0.40
2	TADA#21	TADA#23	10.3	0.45	10.3	0.45
3	TADA#21	TADA#24	12.7	0.49	12.7	0.48
Median	-	-	-	-	14.6	0.48
4	TADA#22	TADA#23	16.5	0.48	16.5	0.49
5	TADA#22	TADA#24	20.7	0.51	20.7	0.51
6	TADA#23	TADA#24	30.1	0.54	30.1	0.54

Table C12.2. K_s^{app} and k_{max}^{app} values of 1,1-DCA in the presence of 1,1,1-TCA ($16 \pm 0.32 \mu\text{M}$).

- Slope and y intercept of extrapolated linear lines

Batch vial #	Substrate, S_L 1,1-DCA (μM)	Inhibitor, I_L 1,1,1-TCA (μM)	$-S_L$ (μM)	Initial degradation rate, v ($\mu\text{mol}/\text{mg TSS}/\text{hr}$)	Extrapolated line	
					slope	Y intercept
TADA#5	38.2	15.5	-38.2	0.23	0.006	0.23
TADA#9	84.0	16.2	-84.0	0.31	0.004	0.31
TADA#13	173	15.5	-173	0.39	0.002	0.39
TADA#17	16.1	15.5	-16.1	0.15	0.009	0.15

- Intersection coordinates and best estimate (median) of K_s^{app} and k_{max}^{app}

Number of data	Batch vial #	Batch vial #	Coordinate of intersection		Order from the lowest to highest	
			K_s^{app} (μM)	k_{max}^{app} ($\mu\text{mol}/\text{mg TSS}/\text{hr}$)	K_s^{app} (μM)	k_{max}^{app} ($\mu\text{mol}/\text{mg TSS}/\text{hr}$)
1	TADA#5	TADA#9	34.6	0.44	22.8	0.37
2	TADA#5	TADA#13	41.6	0.48	27.6	0.41
3	TADA#5	TADA#17	22.8	0.37	32.7	0.44
Median	-	-	-	-	33.6	0.45
4	TADA#9	TADA#13	52.8	0.51	34.6	0.46
5	TADA#9	TADA#17	27.6	0.41	41.6	0.48
6	TADA#13	TADA#17	32.7	0.46	52.8	0.51

Table C12.3. K_s^{app} and k_{max}^{app} values of 1,1-DCA in the presence of 1,1,1-TCA ($41 \pm 0.86 \mu\text{M}$).

- Slope and y intercept of extrapolated linear lines

Batch vial #	Substrate, S_L 1,1-DCA (μM)	Inhibitor, I_L 1,1,1-TCA (μM)	$-S_L$ (μM)	Initial degradation rate, v ($\mu\text{mol}/\text{mg TSS}/\text{hr}$)	Extrapolated line	
					slope	Y intercept
TADA#6	38.9	39.6	-38.9	0.17	0.005	0.17
TADA#10	82.4	41.5	-82.4	0.25	0.003	0.25
TADA#14	156	41.1	-156	0.34	0.002	0.34
TADA#18	15.4	40.1	-15.4	0.08	0.005	0.08

- Intersection coordinates and best estimate (median) of K_s^{app} and k_{max}^{app}

Number of data	Batch vial #	Batch vial #	Coordinate of intersection		Order from the lowest to highest	
			K_s^{app} (μM)	k_{max}^{app} ($\mu mol/mg$ TSS/hr)	K_s^{app} (μM)	k_{max}^{app} ($\mu mol/mg$ TSS/hr)
1	TADA#6	TADA#10	53.5	0.41	53.5	0.41
2	TADA#6	TADA#14	73.4	0.50	73.4	0.50
3	TADA#6	TADA#18	175	0.96	87.5	0.52
Median	-	-	-	-	90.4	0.53
4	TADA#10	TADA#14	107	0.58	93.2	0.55
5	TADA#10	TADA#18	87.5	0.52	106	0.58
6	TADA#14	TADA#18	93.2	0.55	175	0.96

Table C12.4. K_s^{app} and k_{max}^{app} values of 1,1-DCA in the presence of 1,1,1-TCA ($83 \pm 0.5 \mu M$).

- Slope and y intercept of extrapolated linear lines

Batch vial #	Substrate, S_L 1,1-DCA (μM)	Inhibitor, I_L 1,1,1-TCA (μM)	$-S_L$ (μM)	Initial degradation rate, v ($\mu mol/mg$ TSS/hr)	Extrapolated line	
					slope	Y intercept
TADA#7	38.5	82.7	-38.5	0.11	0.003	0.11
TADA#11	81.2	82.8	-81.2	0.18	0.002	0.18
TADA#15	156	82.6	-156	0.27	0.002	0.27
TADA#19	15.9	83.7	-15.9	0.06	0.004	0.06

- Intersection coordinates and best estimate (median) of K_s^{app} and k_{max}^{app}

Number of data	Batch vial #	Batch vial #	Coordinate of intersection		Order from the lowest to highest	
			K_s^{app} (μM)	k_{max}^{app} ($\mu mol/mg$ TSS/hr)	K_s^{app} (μM)	k_{max}^{app} ($\mu mol/mg$ TSS/hr)
1	TADA#7	TADA#11	81.1	0.36	76.6	0.34
2	TADA#7	TADA#15	123	0.48	78.9	0.35
3	TADA#7	TADA#19	76.6	0.34	81.1	0.36
Median	-	-	-	-	93.5	0.40
4	TADA#11	TADA#15	192	0.60	106	0.45
5	TADA#11	TADA#19	78.9	0.35	123	0.48
6	TADA#15	TADA#19	106	0.45	192	0.60

Table C12.5. K_s^{app} and k_{max}^{app} values of 1,1-DCA in the presence of 1,1,1-TCA ($202 \pm 5.7 \mu\text{M}$).

- Slope and y intercept of extrapolated linear lines

Batch vial #	Substrate, S_L 1,1-DCA (μM)	Inhibitor, I_L 1,1,1-TCA (μM)	$-S_L$ (μM)	Initial degradation rate, v ($\mu\text{mol/mg TSS/hr}$)	Extrapolated line	
					slope	Y intercept
TADA#8	38.7	204	-38.7	0.07	0.0017	0.07
TADA#12	77.3	194	-77.3	0.10	0.0013	0.10
TADA#16	161	205	-161	0.16	0.0010	0.16
TADA#20	15.2	206	-15.2	0.02	0.0013	0.02

- Intersection coordinates and best estimate (median) of K_s^{app} and k_{max}^{app}

Number of data	Batch vial #	Batch vial #	Coordinate of intersection		Order from the lowest to highest	
			K_s^{app} (μM)	k_{max}^{app} ($\mu\text{mol/mg TSS/hr}$)	K_s^{app} (μM)	k_{max}^{app} ($\mu\text{mol/mg TSS/hr}$)
1	TADA#8	TADA#12	83.1	0.21	83.1	0.21
2	TADA#8	TADA#16	126	0.28	126	0.28
3	TADA#8	TADA#20	-124	-0.15	181	0.33
Median	-	-	-	-	280	0.43
4	TADA#12	TADA#16	181	0.33	380	0.53
5	TADA#12	TADA#20	1814	2.43	1814	2.43
6	TADA#16	TADA#20	380	0.53	-124	-0.15

Direct Linear Plot

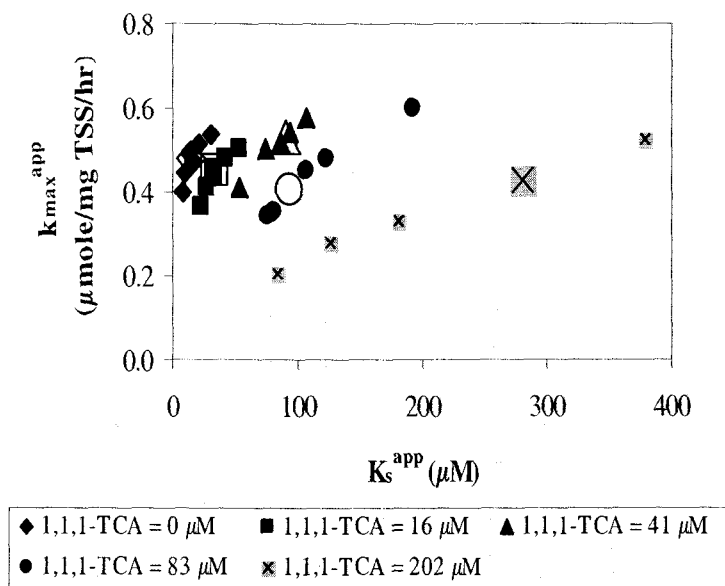


Figure C12.1. Direct linear plot showing competitive inhibition on 1,1-DCA transformation by 1,1,1-TCA.

Linearized Plot

Table C12.6. Values used for linearized plot in the case of competitive inhibition on 1,1-DCA transformation 1,1,1-TCA.

Inhibitor (1,1,1-TCA) (μM)	K_s^{app} (μM)	$k_{\text{max}}^{\text{app}}$ ($\mu\text{mol}/\text{mg TSS/hr}$)
0.0	14.6	0.48
16	33.6	0.45
41	90.4	0.53
83	93.5	0.40
202	280	0.43

Table C12.7. Initial guesses of parameters obtained linearized plot in the case of inhibition on 1,1-DCA transformation by 1,1,1-TCA.

Plot (K_s^{app} vs. I_L)	Y intercept (= K_s) (μM)	slope (= K_s/K_{ic}) (-)	K_{ic} (μM)	$k_{\text{max}}^{\text{app}}$ ($\mu\text{mol}/\text{mg TSS/hr}$)
	15.29	1.28	12.0	0.46

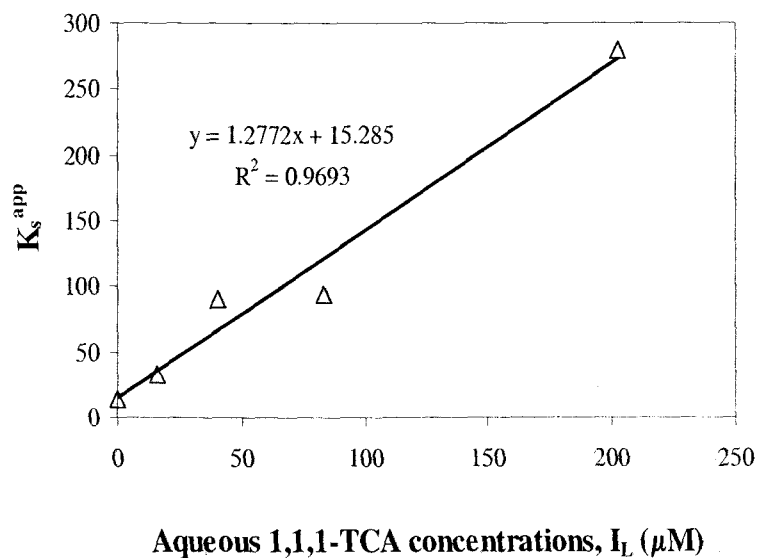


Figure C12.2. Linearized plot in the case of competitive inhibition of 1,1-DCA transformation by 1,1,1-TCA.

NLSR Analysis

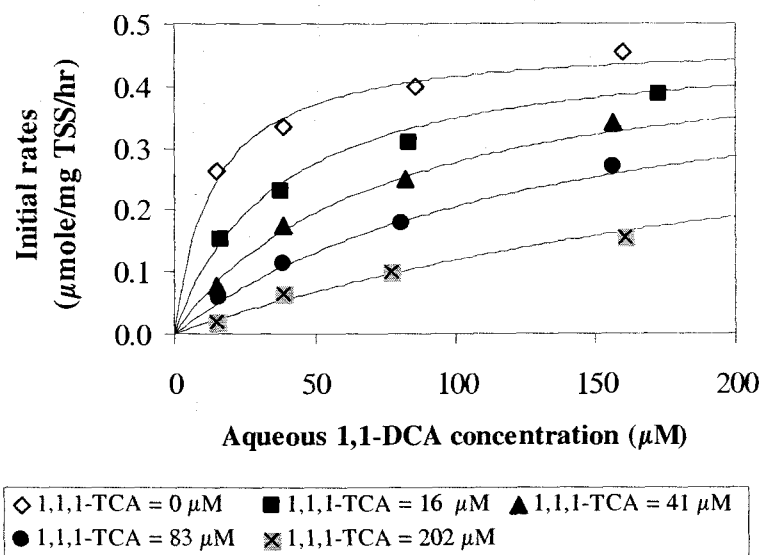


Figure C12.3. Best fit obtained from NLSR analysis using competitive inhibition model. (Residual Standard Error = 0.012, $k_{max} = 0.47 \pm 0.023$ $\mu\text{mol/mg TSS/hr}$, $K_s = 13.7 \pm 3.2$ μM , and $K_{ic} = 9.8 \pm 2.21$ μM)

C13. SUMMARY OF KINETIC PARAMETERS AND COMPARISON OF THOSE OBTAINED FROM DIFFERENT METHODS

Comparison of k_{\max} and K_s Obtained with Different Methods

Table C13.1. Comparison of k_{\max} and K_s values of butane obtained from different methods

	k_{\max} ($\mu\text{mol/mg TSS/hr}$)			K_s (μM)		
	Single Compound ^a	Linearized equation ^b	NLSR ^c	Single compound	Linearized equation	NLSR
1 ^d	2.6	2.1	2.1	19	9.0	8.5
2 ^e		2.1	2.1		8.2	10.9
3 ^f		2.4	2.5		12	13.1
Average	2.6	2.2	2.2	19	9.7	10.8
Standard error	0.07	0.16	0.25	1.6	2.0	2.3
95% confidence interval	0.14	0.18	0.28	3.3	2.3	2.6

a: The k_{\max} and K_s were estimated in single compound kinetic studies using NLSR. **b:** The parameters were estimated in inhibition studies using linearized plot and linear least squares regression. **c:** The parameters were estimated in the inhibition studies using NLSR with all kinetic parameters varying. **d:** 1,1-DCE inhibition. **e:** 1,1-DCA inhibition. **f:** 1,1,1-TCA inhibition

Table C13.2. Comparison of k_{\max} and K_s values of 1,1-DCE obtained from different methods

	k_{\max} ($\mu\text{mol/mg TSS/hr}$)			K_s (μM)		
	Single Compound ^a	Linearized equation ^b	NLSR ^c	Single compound	Linearized equation	NLSR
1 ^d	1.3	1.37	1.19	1.5	0.83	1.05
2 ^e		1.04	1.16		-1.40	1.67
3 ^f		1.07	1.18		5.80	2.11
Average	1.3	1.16	1.18	1.5	1.74	1.61
Standard error	0.04	0.18	0.02	0.19	3.69	0.53
95% confidence interval	0.09	0.21	0.02	0.39	4.17	0.60

a: The k_{\max} and K_s were estimated in single compound kinetic studies using NLSR. **b:** The parameters were estimated in inhibition studies using linearized plot and linear least squares regression. **c:** The parameters were estimated in the inhibition studies using NLSR with all kinetic parameters varying. **d:** butane inhibition. **e:** 1,1-DCA inhibition. **f:** 1,1,1-TCA inhibition

Table C13.3. Comparison of k_{\max} and K_s values of 1,1-DCA obtained from different methods

	k_{\max} ($\mu\text{mol}/\text{mg TSS}/\text{hr}$)			K_s (μM)		
	Single Compound ^a	Linearized equation ^b	NLSR ^c	Single compound	Linearized equation	NLSR
1 ^d	0.49	0.47	0.45	19	15.9	19.0
2 ^e		0.53	0.56		28.0	18.4
3 ^f		0.46	0.47		15.3	13.7
Average	0.49	0.49	0.50	19	19.7	17.0
Standard error	0.02	0.04	0.06	2.4	7.2	2.9
95% confidence interval	0.03	0.04	0.07	5.0	8.1	3.2

a: The k_{\max} and K_s were estimated in single compound kinetic studies using NLSR. **b:** The parameters were estimated in inhibition studies using linearized plot and linear least squares regression. **c:** The parameters were estimated in the inhibition studies using NLSR with all kinetic parameters varying. **d:** butane inhibition. **e:** 1,1-DCE inhibition. **f:** 1,1,1-TCA inhibition

Table C13.4. Comparison of k_{\max} and K_s values of 1,1,1-TCA obtained from different methods

	k_{\max} ($\mu\text{mol}/\text{mg TSS}/\text{hr}$)			K_s (μM)		
	Single Compound ^a	Linearized equation ^b	NLSR ^c	Single compound	Linearized equation	NLSR
1 ^d	0.19	0.23	0.20	12	18.2	19.1
2 ^e		0.20	0.20		13.5	14.3
3 ^f		0.22	0.20		13.7	14.3
Average	0.19	0.22	0.20	12	15.1	15.9
Standard error	0.005	0.015	0.001	1.4	2.7	2.8
95% confidence interval	0.010	0.017	0.001	2.8	3.0	3.2

a: The k_{\max} and K_s were estimated in single compound kinetic studies using NLSR. **b:** The parameters were estimated in inhibition studies using linearized plot and linear least squares regression. **c:** The parameters were estimated in the inhibition studies using NLSR with all kinetic parameters varying. **d:** butane inhibition. **e:** 1,1-DCE inhibition. **f:** 1,1-DCA inhibition

Comparison of K_{ic} and K_{iu} Obtained with Different Methods

Table C13.5. Comparison of K_{ic} and K_{iu} obtained with different methods

Substrate	Method	Inhibitor ^f				
		Butane K_{ic} (μ M)	Butane K_{iu} (μ M)	1,1-DCE K_{ic} (μ M)	1,1-DCA K_{ic} (μ M)	1,1,1-TCA K_{ic} (μ M)
Butane	Linearized ^a	-	-	12.8	253	350
	NLSR ^b	-	-	8.71 \pm 2.26	403 \pm 51	313 \pm 88
	NLSR $Gk_{max}K_s$ ^c	-	-	14.5 \pm 3.03	514 \pm 43	419 \pm 65
	NLSR Gk_{max} ^d	-	-	11.1 \pm 3.32	457 \pm 53	318 \pm 72
	NLSR GK_s ^e	-	-	13.1 \pm 3.8	475 \pm 52	356 \pm 64
1,1-DCE	Linearized	0.23	4.64	-	-16.3	81
	NLSR	0.33 \pm 0.07	6.9 \pm 1.6	-	18 \pm 4.9	17 \pm 3.9
	NLSR $Gk_{max}K_s$	0.43 \pm 0.1	5.6 \pm 1.8	-	13 \pm 2.5	9.8 \pm 1.9
	NLSR Gk_{max}	0.44 \pm 0.13	5.6 \pm 1.9	-	23 \pm 6.1	21 \pm 4.3
	NLSR GK_s	0.45 \pm 0.09	6.1 \pm 1.8	-	16 \pm 2.0	13 \pm 1.6
1,1-DCA	Linearized	1.82	3.3	8.6	-	12
	NLSR	2.8 \pm 1.6	3.8 \pm 0.8	3.6 \pm 1.5	-	9.8 \pm 2.2
	NLSR $Gk_{max}K_s$	2.6 \pm 1.8	3.0 \pm 0.8	5.6 \pm 1.4	-	14 \pm 1.4
	NLSR Gk_{max}	4.9 \pm 3.9	3.0 \pm 0.6	3.0 \pm 1.5	-	11 \pm 2.1
	NLSR GK_s	3.1 \pm 1.3	3.7 \pm 0.6	3.8 \pm 0.8	-	12 \pm 1.8
1,1,1-TCA	Linearized	0.52	0.36	0.95	9.6	-
	NLSR	0.28 \pm 0.1	0.51 \pm 0.1	1.02 \pm 0.3	16 \pm 4.8	-
	NLSR $Gk_{max}K_s$	0.25 \pm 0.1	0.56 \pm 0.1	0.94 \pm 0.14	13 \pm 1.7	-
	NLSR Gk_{max}	0.24 \pm 0.1	0.56 \pm 0.1	0.98 \pm 0.29	16 \pm 4.2	-
	NLSR GK_s	0.25 \pm 0.1	0.53 \pm 0.1	0.92 \pm 0.18	14 \pm 3.0	-

a: The parameters were estimated using linearized plot and linear least squares regression. b: NLSR indicates NLSR with all 4 kinetic parameters varying (k_{max} , K_s , K_{ic} , and/or K_{iu}). c: NLSR $Gk_{max}K_s$ indicates NLSR with constant k_{max} and K_s and with 2 inhibition coefficients varying. d: NLSR Gk_{max} indicates NLSR with constant k_{max} and with K_s and inhibition coefficients varying. e: NLSR GK_s indicates NLSR with constant K_s , and with k_{max} and inhibition coefficients varying. f: kinetic parameter are presented with 95% confidence interval.

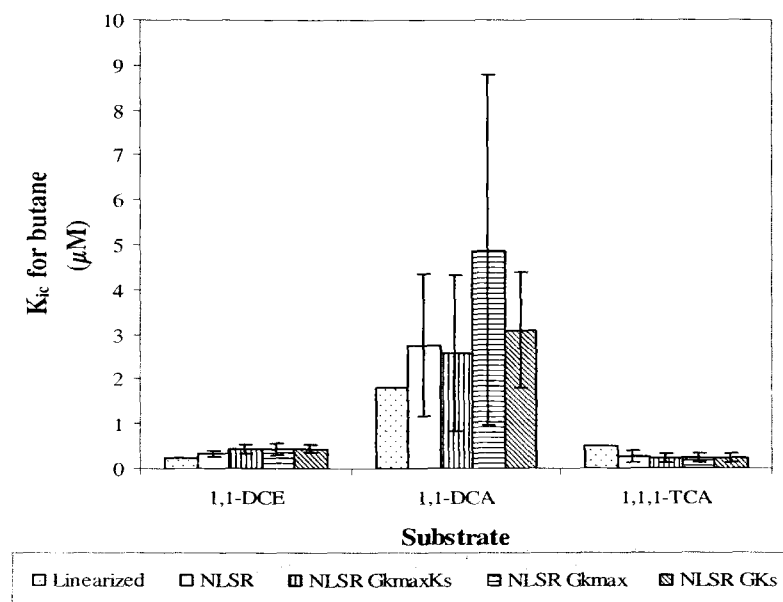


Figure C13.1. Comparison of K_{ic} values for butane determined different methods.

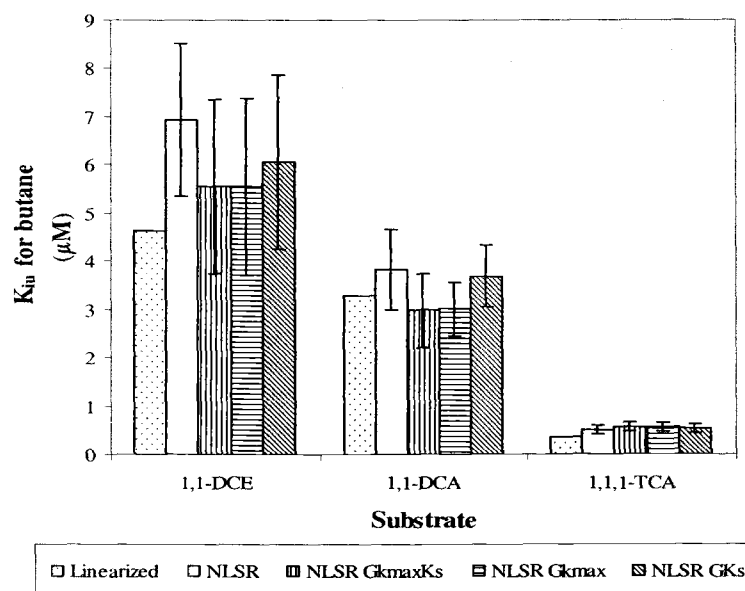


Figure C13.2. Comparison of K_{iu} values for butane determined different methods.

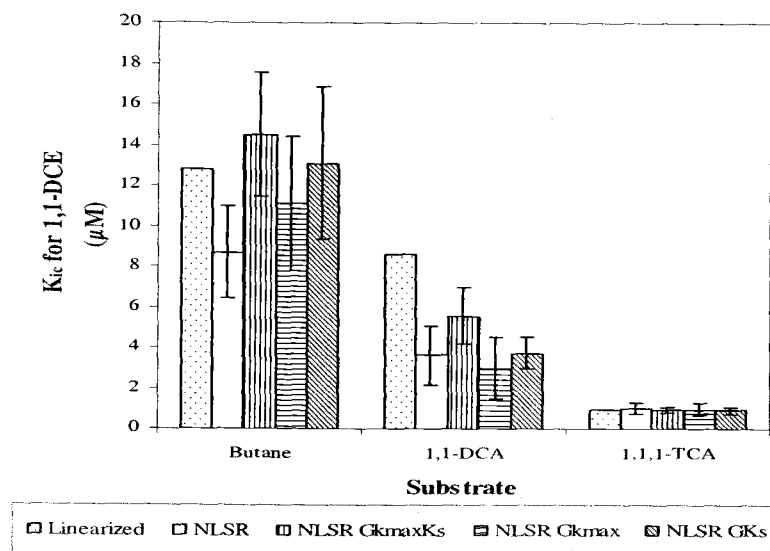


Figure C13.3. Comparison of K_{ic} values for 1,1-DCE determined different methods.

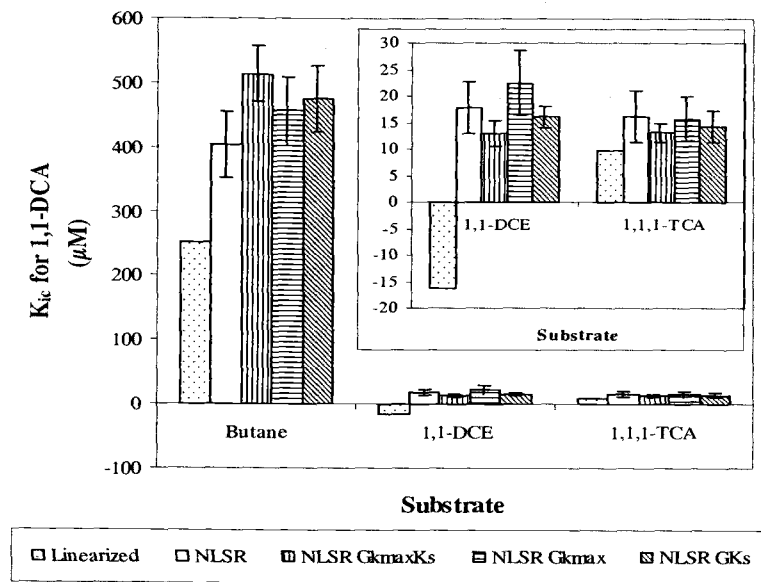


Figure C13.4. Comparison of K_{ic} values for 1,1-DCA determined different methods.

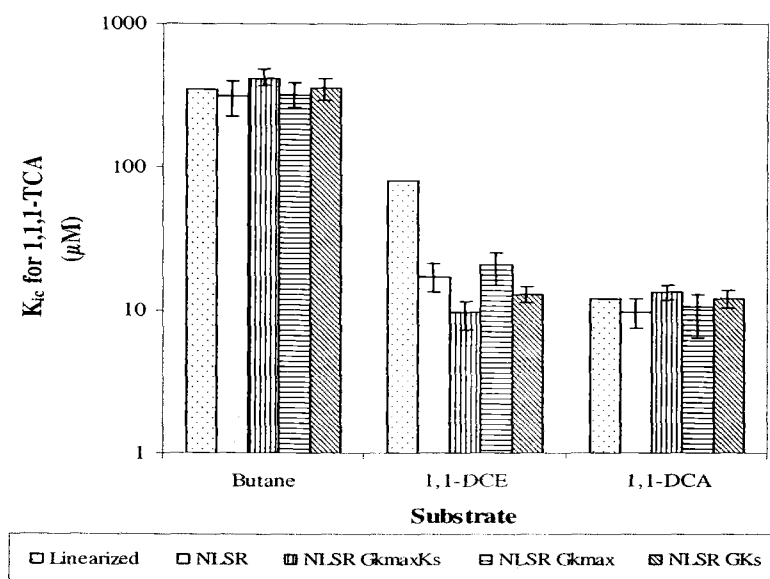


Figure C13.5. Comparison of K_{ic} values for 1,1,1-TCA determined different methods.

APPENCIX D

Kinetic Parameters Obtained by Performing NLSR Analysis Using the Different Inhibition Models and Fit of Data to the Models

D1. BUTANE INHIBITION ON 1,1-DCE TRANSFORMATION

Table D1.1. Kinetic parameters (k_{\max} and K_s) for 1,1-DCE and inhibition coefficients for butane obtained from NLSR analysis by fitting competitive and noncompetitive inhibition models to data identified as mixed inhibition of butane on 1,1-DCE transformation.

	Inhibition Type	k_{\max} ($\mu\text{mol}/\text{mgTSS}/\text{hr}$)	K_s (μM)	K_{ic} (μM)	K_{iu} (μM)	Residual Stand Error
NLSR	NC	1.41 ± 0.17	3.45 ± 1.55	-	2.63 ± 0.58	0.064
NLSR $Gk_{\max}K_s$		Given	Given	-	2.16 ± 0.48	0.085
NLSR Gk_{\max}		Given	2.71 ± 0.86	-	2.72 ± 0.62	0.067
NLSR GK_s		1.23 ± 0.12	Given	-	2.38 ± 0.67	0.083
NLSR	C	1.15 ± 0.11	0.78 ± 0.87	0.15 ± 0.16	-	0.048
NLSR $Gk_{\max}K_s$		Given	Given	0.24 ± 0.04	-	0.058
NLSR Gk_{\max}		Given	1.87 ± 0.69	0.31 ± 0.13	-	0.056
NLSR GK_s		1.22 ± 0.07	Given	0.27 ± 0.05	-	0.050

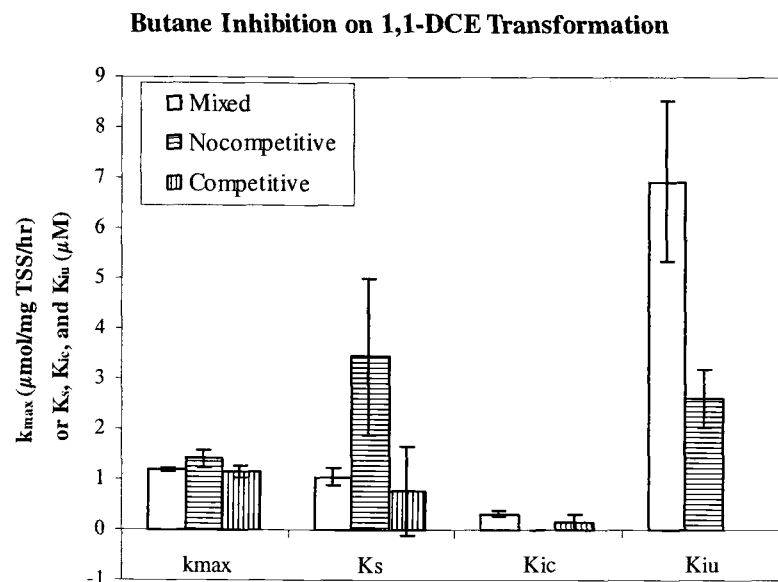


Figure D1.1. Comparison of parameters obtained from NLSR analysis fitting all inhibition models to data identified as mixed inhibition on 1,1-DCE transformation by butane

Fit with Different Inhibition Models

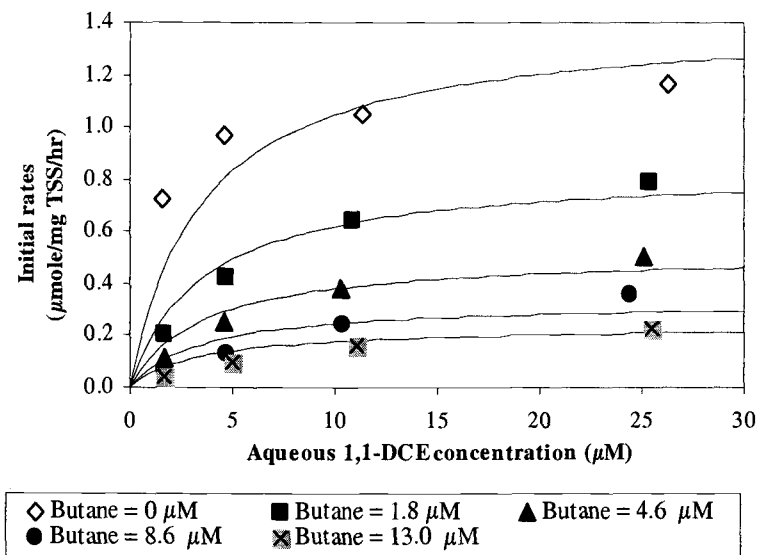


Figure D1.2. Noncompetitive inhibition model fit to data identified as mixed inhibition of butane on 1,1-DCE transformation.

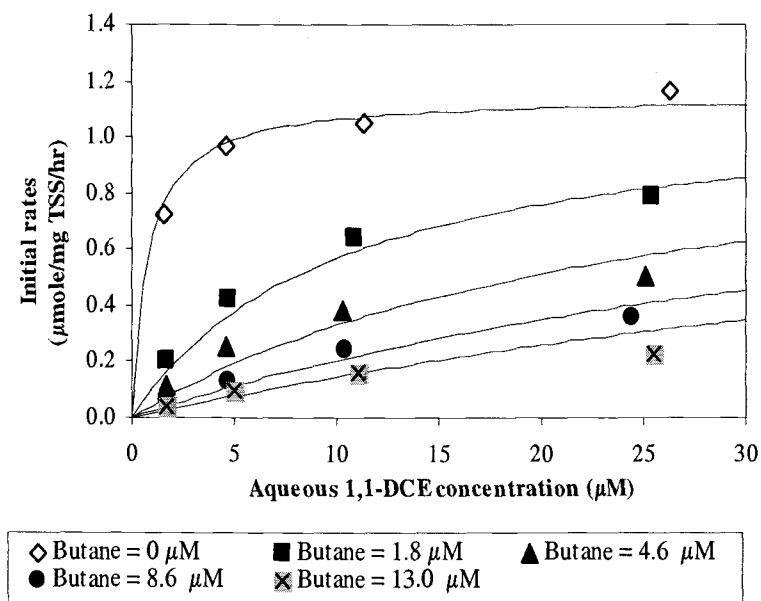


Figure D1.3. Competitive inhibition model fit to data identified as mixed inhibition of butane on 1,1-DCE transformation.

D2. BUTANE INHIBITION ON 1,1-DCA TRANSFORMATION

Table D2.1. Kinetic parameters (k_{\max} and K_s) for 1,1-DCA and inhibition coefficients for butane obtained from NLSR analysis by fitting competitive and noncompetitive inhibition models to data identified as mixed inhibition of butane on 1,1-DCA transformation.

	Inhibition Type	k_{\max} ($\mu\text{mol}/\text{mgTSS}/\text{hr}$)	K_s (μM)	K_{ic} (μM)	K_{iu} (μM)	Residual Stand Error
NLSR	NC	0.45 ± 0.02	19 ± 3.0	-	3.53 ± 2.99	0.010
NLSR $Gk_{\max}K_s$		Given	Given	-	2.89 ± 0.34	0.017
NLSR Gk_{\max}		Given	24 ± 2.7	-	3.29 ± 0.40	0.013
NLSR GK_s		0.45 ± 0.01	Given	-	3.53 ± 0.36	0.010
NLSR	C	0.39 ± 0.05	9.8 ± 7.7	0.49 ± 0.37	-	0.030
NLSR $Gk_{\max}K_s$		Given	Given	0.58 ± 0.15	-	0.037
NLSR Gk_{\max}		Given	23.8 ± 8.5	0.78 ± 0.44	-	0.037
NLSR GK_s		0.44 ± 0.04	Given	0.80 ± 0.29	-	0.032

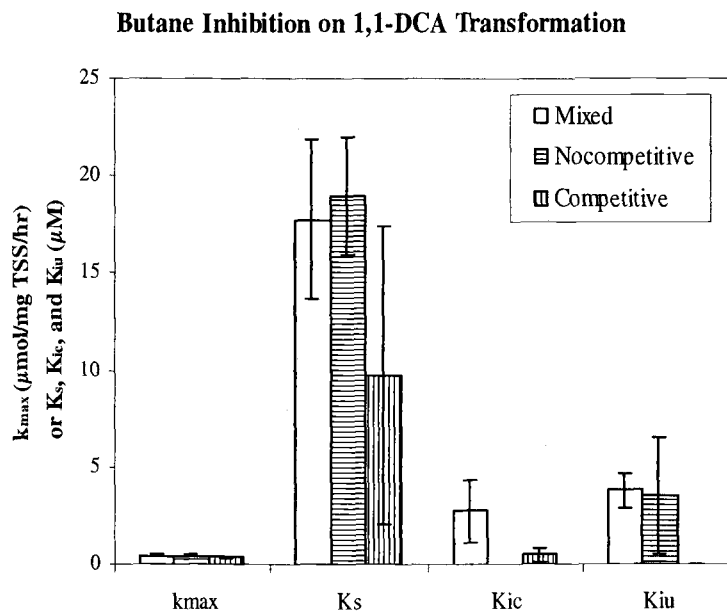


Figure D2.1. Comparison of parameters obtained from NLSR analysis fitting all inhibition models to data identified as mixed inhibition of butane on 1,1-DCA transformation

Fit with Different Inhibition Models

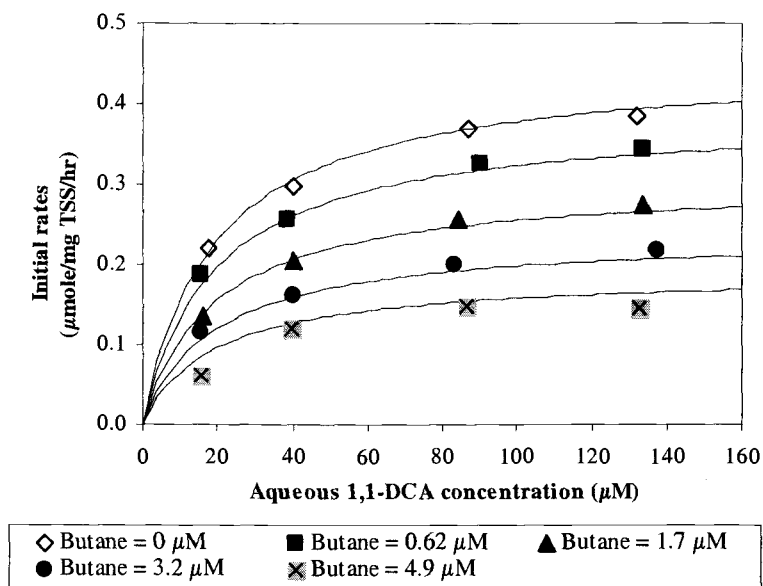


Figure D2.2. Noncompetitive inhibition model fit to data identified as mixed inhibition of butane on 1,1-DCA transformation.

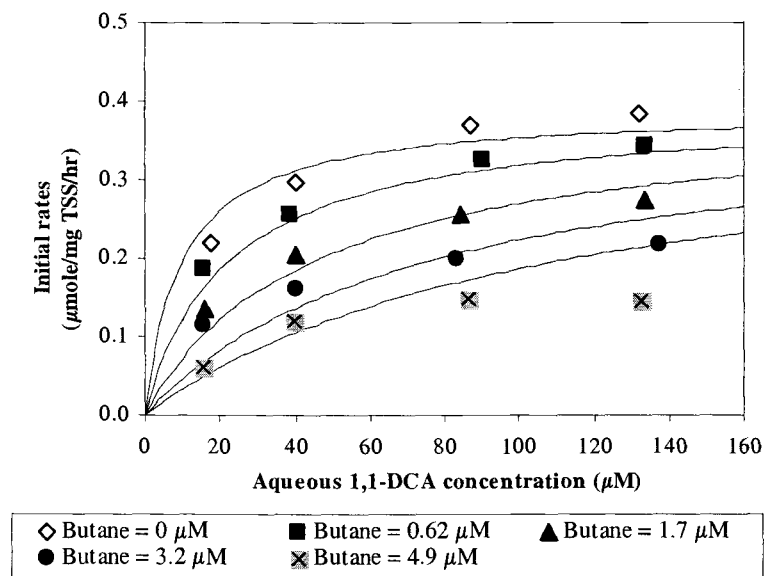


Figure D2.3. Competitive inhibition model fit to data identified as mixed inhibition of butane on 1,1-DCA transformation.

D3. BUTANE INHIBITION ON 1,1,1-TCA TRANSFORMATION

Table D3.1. Kinetic parameters (k_{\max} and K_s) for 1,1-DCA and inhibition coefficients for butane obtained from NLSR analysis by fitting competitive and noncompetitive inhibition models to data identified as mixed inhibition of butane on 1,1,1-TCA transformation.

	Inhibition Type	k_{\max} ($\mu\text{mol}/\text{mgTSS}/\text{hr}$)	K_s (μM)	K_{ic} (μM)	K_{iu} (μM)	Residual Stand Error
NLSR	NC	0.20 ± 0.01	19.1 ± 4.3	-	0.50 ± 0.08	0.005
NLSR $Gk_{\max}K_s$		Given	Given	-	0.45 ± 0.04	0.006
NLSR Gk_{\max}		Given	18.1 ± 4.1	-	0.54 ± 0.07	0.005
NLSR GK_s		0.19 ± 0.01	Given	-	0.47 ± 0.10	0.006
NLSR	C	0.18 ± 0.01	9.4 ± 3.3	0.05 ± 0.02	-	0.011
NLSR $Gk_{\max}K_s$		Given	Given	0.06 ± 0.01	-	0.011
NLSR Gk_{\max}		Given	11.4 ± 2.5	0.05 ± 0.02	-	0.011
NLSR GK_s		0.19 ± 0.01	Given	0.06 ± 0.01	-	0.011

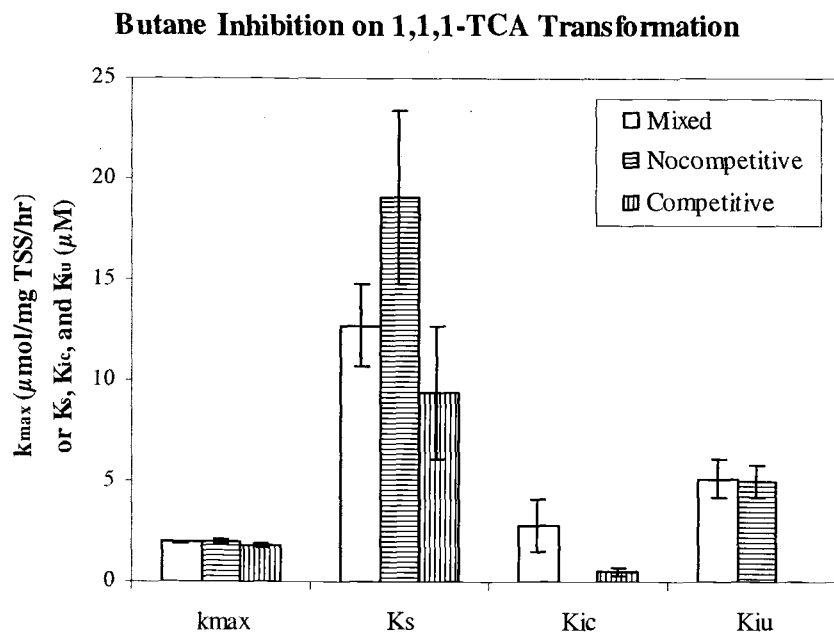


Figure D3.1. Comparison of parameters obtained from NLSR analysis fitting all inhibition models to data identified as mixed inhibition of butane on 1,1,1-TCA transformation. The values for k_{\max} , K_{ic} and K_{iu} were multiplied by a factor of 10.

Fit with Different Inhibition Models

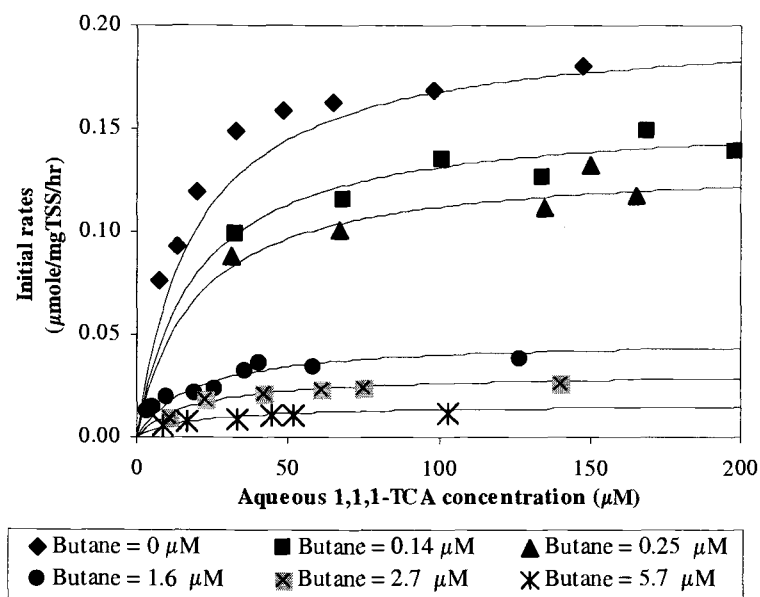


Figure D3.2. Noncompetitive inhibition model fit to data identified as mixed inhibition of butane on 1,1,1-TCA transformation.

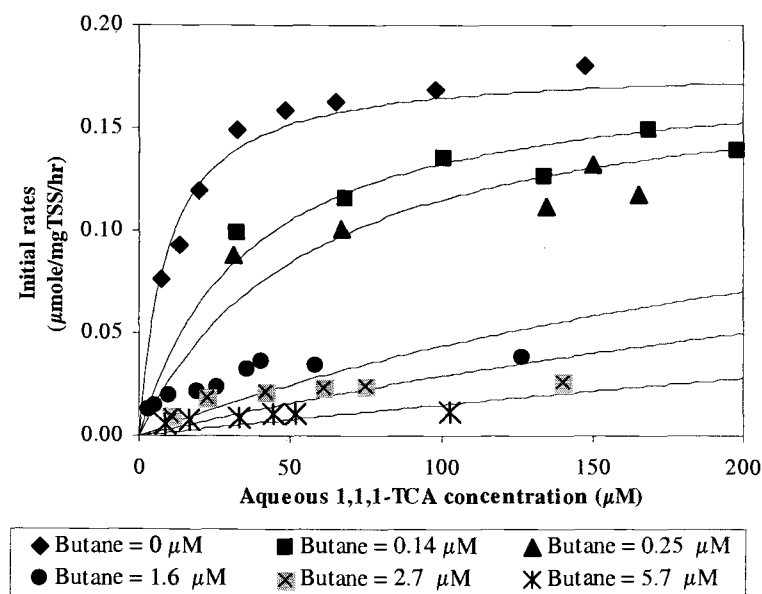


Figure D3.3. Competitive inhibition model fit to data identified as mixed inhibition of butane on 1,1,1-TCA transformation.

D4. 1,1-DCE INHIBITION ON BUTANE DEGRADATION

Table D4.1. Kinetic parameters (k_{\max} and K_s) for butane and inhibition coefficients for 1,1-DCE obtained from NLSR analysis by fitting mixed and noncompetitive inhibition models to data identified as competitive inhibition of 1,1-DCE on butane degradation.

	Inhibition Type	k_{\max} ($\mu\text{mol}/\text{mgTSS}/\text{hr}$)	K_s (μM)	K_{ic} (μM)	K_{iu} (μM)	Residual Stand Error
NLSR	Mix	2.19 ± 0.244	9.8 ± 3.0	12.73 ± 7.4	91 ± 146	0.055
NLSR $Gk_{\max}K_s$		Given	Given	30 ± 2235	33 ± 21.7	0.069
NLSR Gk_{\max}		Given	14.9 ± 1.5	24.1 ± 16.7	33 ± 20.5	0.066
NLSR GK_s		2.65 ± 0.012	Given	28.7 ± 21.3	31 ± 20	0.070
NLSR	NC	2.43 ± 0.249	13.0 ± 3.0	-	30 ± 6.2	0.064
NLSR $Gk_{\max}K_s$		Given	Given	-	32 ± 5.0	0.067
NLSR Gk_{\max}		Given	15.0 ± 1.4	-	29 ± 5.8	0.065
NLSR GK_s		2.65 ± 0.118	Given	-	30 ± 6.7	0.068

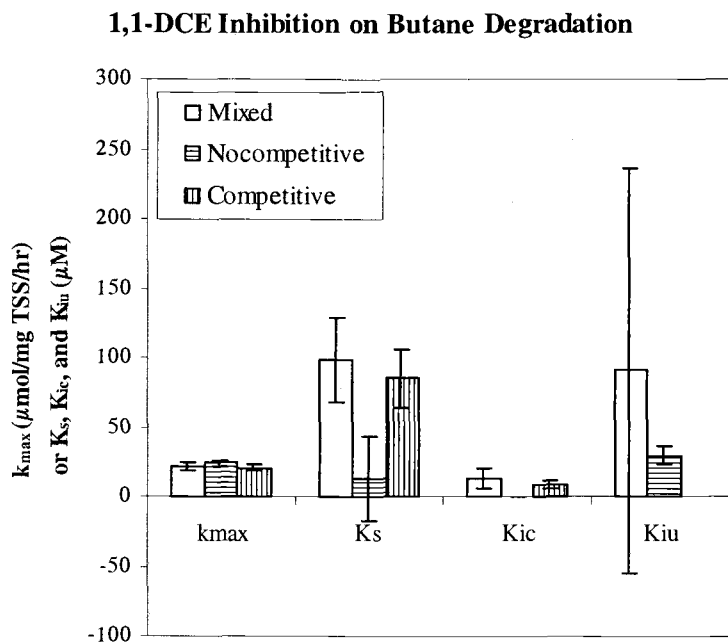


Figure D4.1. Comparison of parameters obtained from NLSR analysis fitting all inhibition models to data identified as competitive inhibition of 1,1-DCE on butane degradation. The values for k_{\max} , and K_s were multiplied by a factor of 10.

Fit with Different Inhibition Models

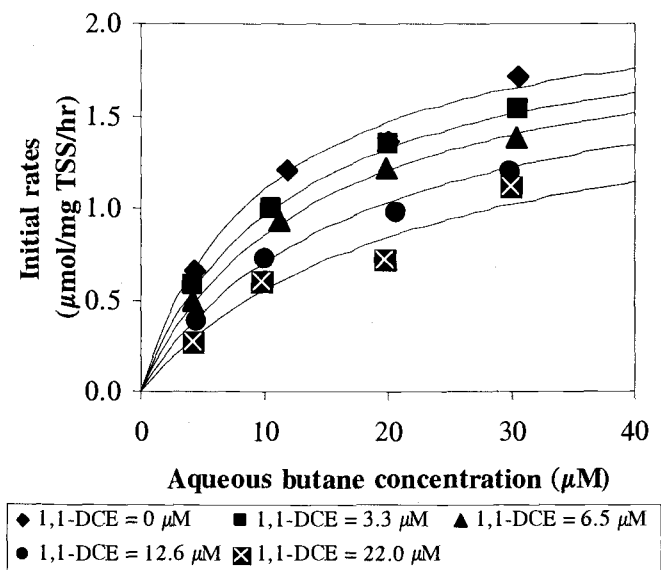


Figure D4.2. Mixed inhibition model fit to data identified as competitive inhibition of 1,1-DCE on butane degradation.

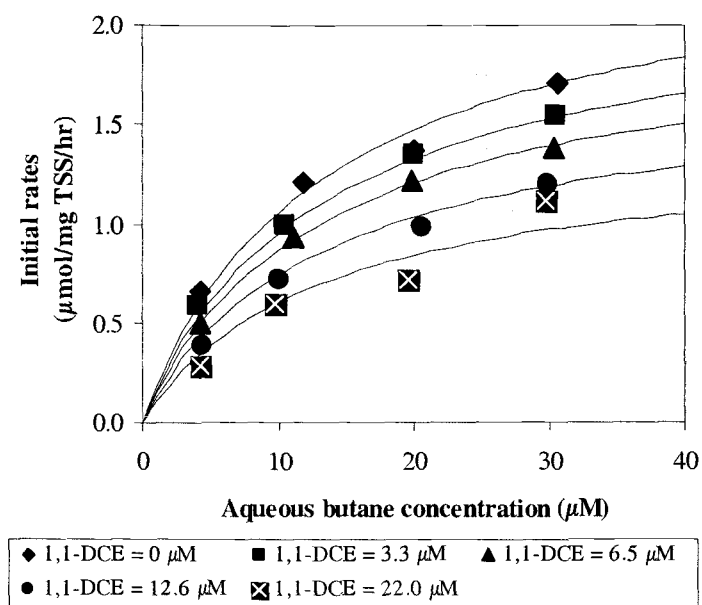


Figure D4.3. Noncompetitive inhibition model fit to data identified as competitive inhibition of 1,1-DCE on butane degradation.

D5. 1,1-DCE INHIBITION ON 1,1-DCA TRANSFORMATION

Table D5.1. Kinetic parameters (k_{\max} and K_s) for 1,1-DCA and inhibition coefficients for 1,1-DCE obtained from NLSR analysis by fitting mixed and noncompetitive inhibition models to data identified as competitive inhibition of 1,1-DCE on 1,1-DCA transformation.

	Inhibition Type	k_{\max} ($\mu\text{mol}/\text{mgTSS}/\text{hr}$)	K_s (μM)	K_{ic} (μM)	K_{iu} (μM)	Residual Stand Error
NLSR	Mix	0.59 ± 0.062	22.1 ± 9.5	5.58 ± 3.1	101 ± 98	0.024
NLSR $Gk_{\max}K_s$		Given	Given	6.84 ± 4.1	213 ± 485	0.040
NLSR Gk_{\max}		Given	11.59 ± 5.0	3.45 ± 2.4	317 ± 911	0.034
NLSR GK_s		0.57 ± 0.031	Given	4.82 ± 1.6	119 ± 111	0.024
NLSR	NC	0.69 ± 0.12	42.5 ± 19.8	-	29 ± 8.4	0.038
NLSR $Gk_{\max}K_s$		Given	Given	-	46 ± 14.8	0.052
NLSR Gk_{\max}		Given	17.8 ± 8.5	-	45 ± 16.9	0.053
NLSR GK_s		0.55 ± 0.057	Given	-	33 ± 11.8	0.046

1,1-DCE Inhibition on 1,1-DCA Transformation

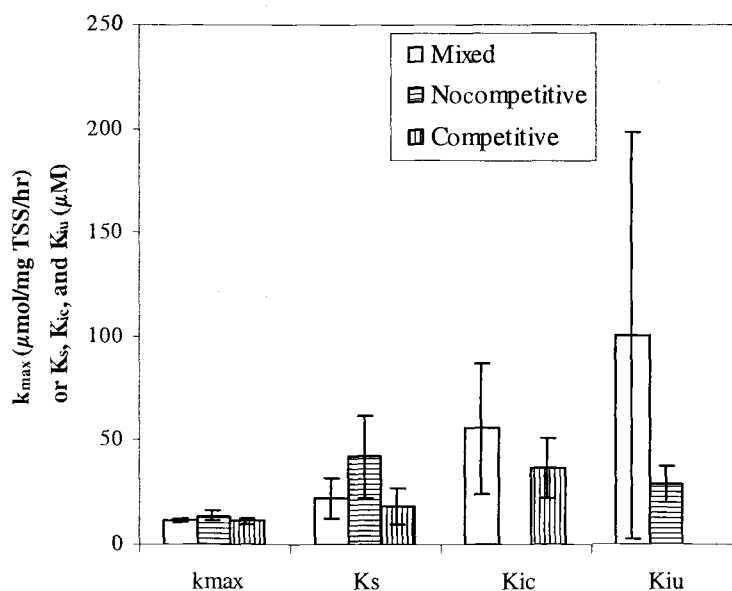


Figure D5.1. Comparison of parameters obtained from NLSR analysis fitting all inhibition models to data identified as competitive inhibition of 1,1-DCE on 1,1-DCA transformation. The k_{\max} and K_{ic} values were multiplied by a factor of 10 and 20, respectively.

Fit with Different Inhibition Models

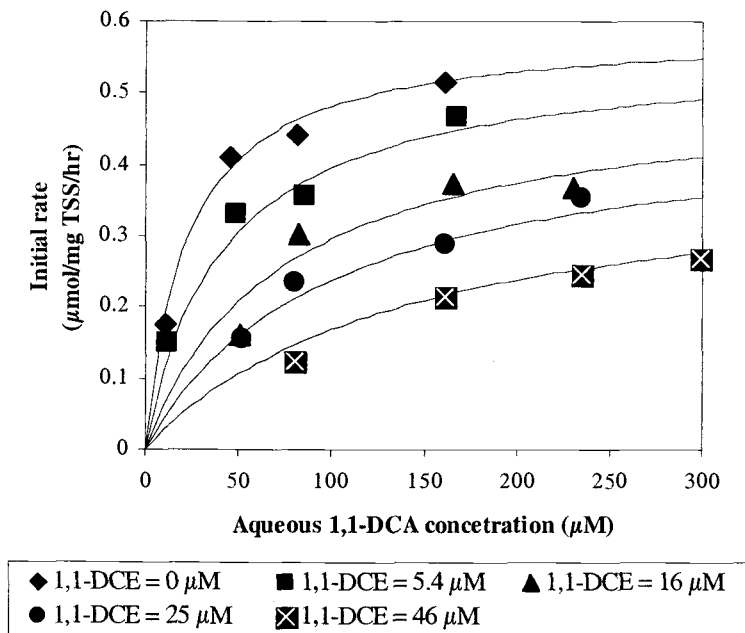


Figure D5.2 Mixed inhibition model fit to data identified as competitive inhibition of 1,1-DCE on 1,1-DCA transformation.

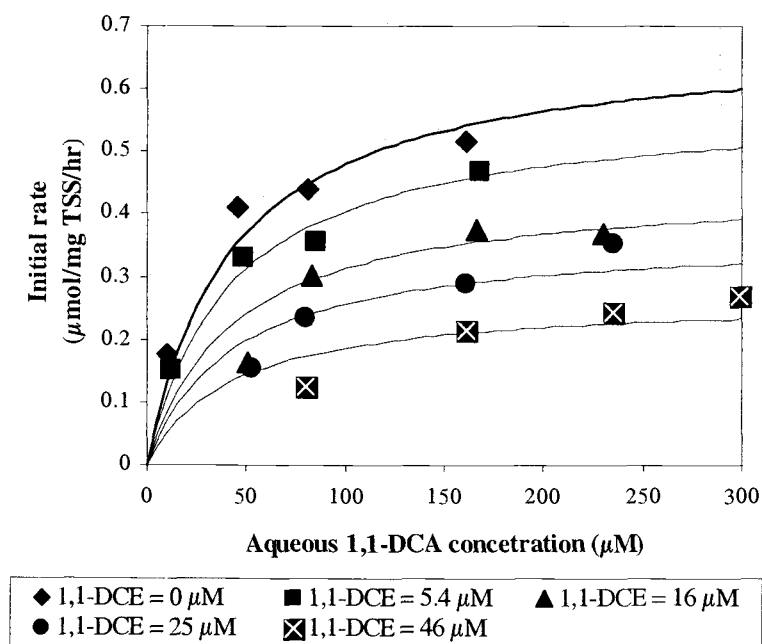


Figure D5.3. Noncompetitive inhibition model fit to data identified as competitive inhibition of 1,1-DCE on 1,1-DCA transformation.

D6. 1,1-DCE INHIBITION ON 1,1,1-TCA TRANSFORMATION

Table D6.1. Kinetic parameters (k_{\max} and K_s) for 1,1,1-TCA and inhibition coefficients for 1,1-DCE obtained from NLSR analysis by fitting mixed and noncompetitive inhibition models to data identified as competitive inhibition of 1,1-DCE on 1,1,1-TCA transformation.

	Inhibition Type	k_{\max} ($\mu\text{mol}/\text{mgTSS}/\text{hr}$)	K_s (μM)	K_{ic} (μM)	K_{iu} (μM)	Residual Stand Error
NLSR	Mix	0.21 ± 0.02	17.8 ± 7.95	1.27 ± 0.75	103 ± 310	0.010
NLSR $Gk_{\max}K_s$		Given	Given	0.93 ± 0.32	-285 ± 1987	0.011
NLSR Gk_{\max}		Given	11.8 ± 4.32	0.91 ± 0.54	-271 ± 1871	0.012
NLSR GK_s		0.20 ± 0.012	Given	0.85 ± 0.30	-2458 ± 1541	0.011
NLSR	NC	0.25 ± 0.042	39.6 ± 19.1	-	11 ± 3.8	0.017
NLSR $Gk_{\max}K_s$		Given	Given	-	14 ± 4.5	0.022
NLSR Gk_{\max}		Given	19.0 ± 9.0	-	16 ± 6.5	0.021
NLSR GK_s		0.19 ± 0.023	Given	-	13 ± 6.9	0.022

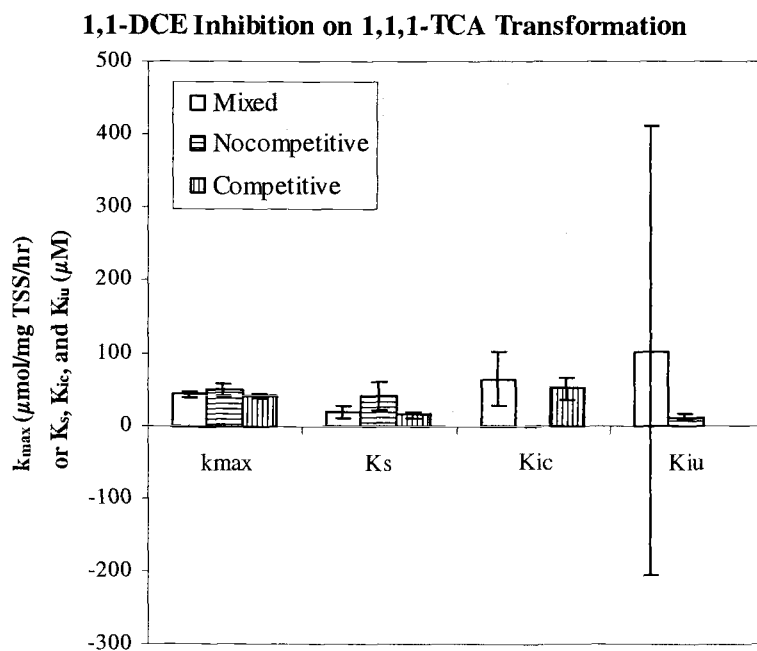


Figure D6.1. Comparison of parameters obtained from NLSR analysis fitting all inhibition models to data identified as competitive inhibition of 1,1-DCE on 1,1,1-TCA transformation. The k_{\max} , and K_{ic} values were multiplied by a factor of 200 and 50, respectively.

Fit with Different Inhibition Models

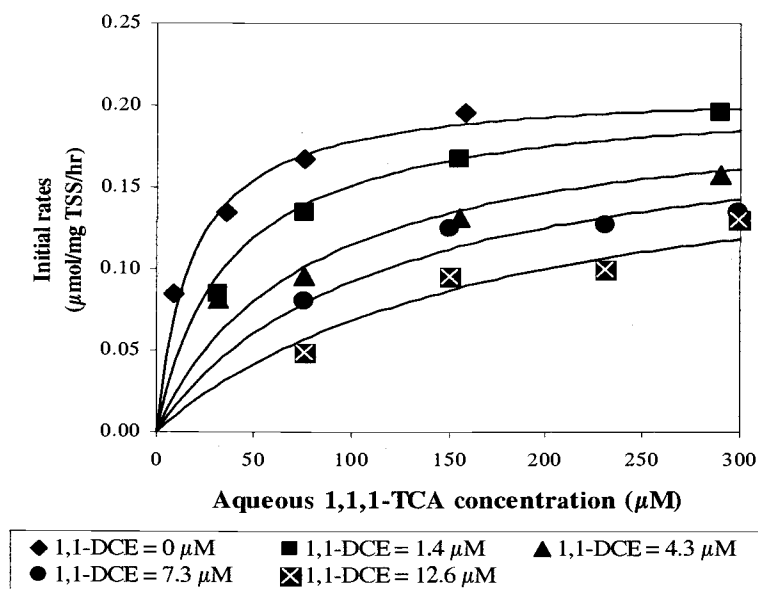


Figure D6.2 Mixed inhibition model fit to data identified as competitive inhibition of 1,1-DCE on 1,1,1-TCA transformation.

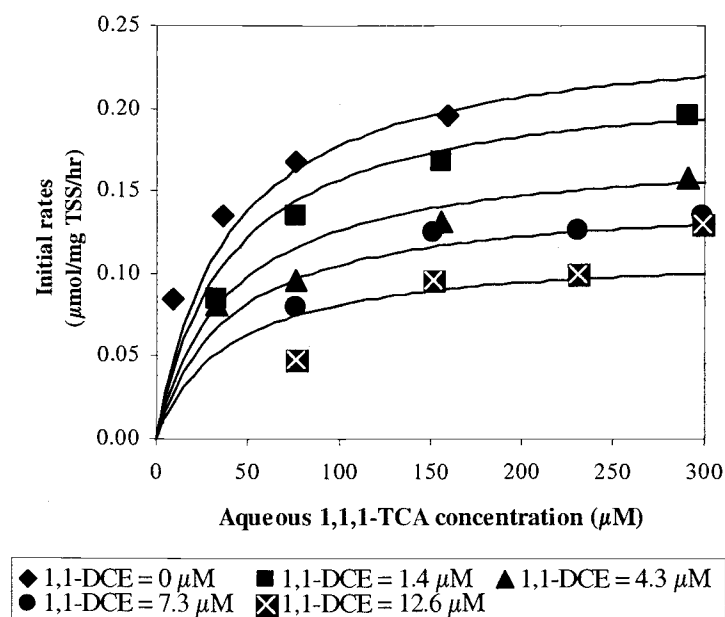


Figure D6.3. Noncompetitive inhibition model fit to data identified as competitive inhibition of 1,1-DCE on 1,1,1-TCA transformation.

D7. 1,1-DCA INHIBITION ON BUTANE DEGRADATION

Table D7.1. Kinetic parameters (k_{\max} and K_s) for butane and inhibition coefficients for 1,1-DCA obtained from NLSR analysis by fitting mixed and noncompetitive inhibition models to data identified as competitive inhibition of 1,1-DCA on butane degradation.

	Inhibition Type	k_{\max} ($\mu\text{mol}/\text{mgTSS}/\text{hr}$)	K_s (μM)	K_{ic} (μM)	K_{iu} (μM)	RSE
NLSR	Mix	0.01 ± 0.53	-13.3 ± 6.0	5421 ± 88703	129 ± 1361	0.559
NLSR $Gk_{\max}K_s$		Given	Given	567 ± 144	2346 ± 3788	0.026
NLSR Gk_{\max}		Given	15.5 ± 0.76	528 ± 138	2369 ± 3779	0.025
NLSR GK_s		2.64 ± 0.082	Given	549 ± 143	2175 ± 3331	0.026
NLSR	NC	2.67 ± 0.476	16.3 ± 4.6	-	768 ± 96	0.031
NLSR $Gk_{\max}K_s$		Given	Given	-	798 ± 67	0.030
NLSR Gk_{\max}		Given	15.6 ± 0.89	-	770 ± 93	0.030
NLSR GK_s		2.64 ± 0.095	Given	-	768 ± 93	0.030

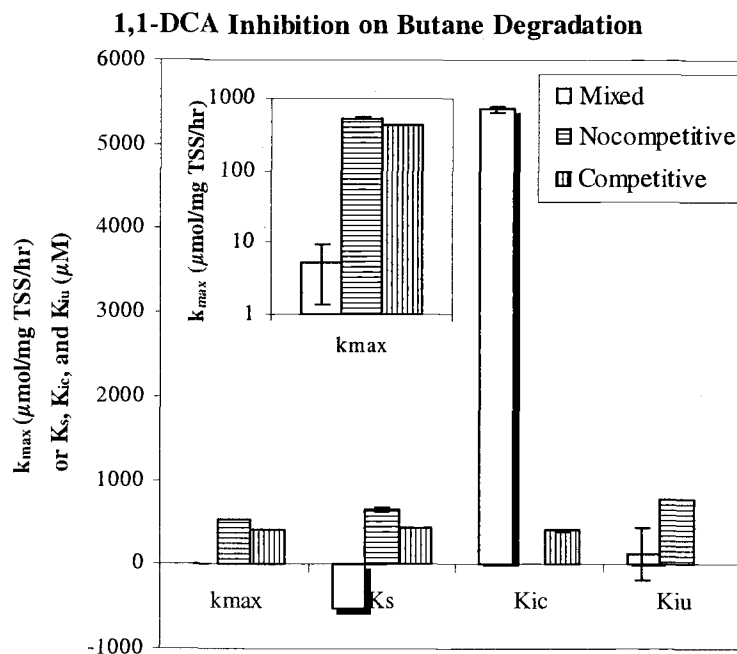


Figure D7.1. Comparison of parameters obtained from NLSR analysis fitting all inhibition models to data identified as competitive inhibition of 1,1-DCA on butane degradation. The k_{\max} , and K_s values were multiplied by a factor of 200 and 40, respectively. Inset shows k_{\max} values in logarithmic scale

Fit with Different Inhibition Models

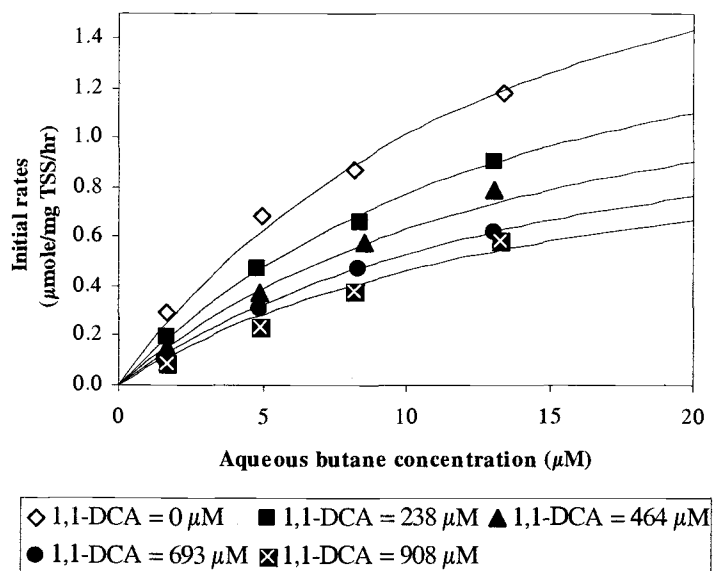


Figure D7.2. Noncompetitive inhibition model fit to data identified as competitive inhibition of 1,1-DCA on butane degradation.

D8. 1,1-DCA INHIBITION ON 1,1-DCE TRANSFORMATION

Table D8.1. Kinetic parameters (k_{\max} and K_s) for 1,1-DCE and inhibition coefficients for 1,1-DCA obtained from NLSR analysis by fitting mixed and noncompetitive inhibition models to data identified as competitive inhibition of 1,1-DCA on 1,1-DCE transformation.

	Inhibition Type	k_{\max} ($\mu\text{mol}/\text{mgTSS}/\text{hr}$)	K_s (μM)	K_{ic} (μM)	K_{iu} (μM)	Residual Stand Error
NLSR	Mix	1.17 ± 0.063	1.73 ± 0.46	23.32 ± 7.9	856 ± 719	0.030
NLSR $Gk_{\max}K_s$		Given	Given	17.69 ± 8.9	600 ± 842	0.066
NLSR Gk_{\max}		Given	2.53 ± 0.49	31.44 ± 12.6	593 ± 523	0.042
NLSR GK_s		1.15 ± 0.039	Given	20.43 ± 4.9	938 ± 831	0.031
NLSR	NC	1.31 ± 0.2	3.13 ± 1.8	-	164 ± 47	0.083
NLSR $Gk_{\max}K_s$		Given	Given	-	128 ± 38	0.109
NLSR Gk_{\max}		Given	3.10 ± 1.03	-	165 ± 43	0.081
NLSR GK_s		1.15 ± 0.123	Given	-	156 ± 52	0.096

1,1-DCA Inhibition on 1,1-DCE Transformation

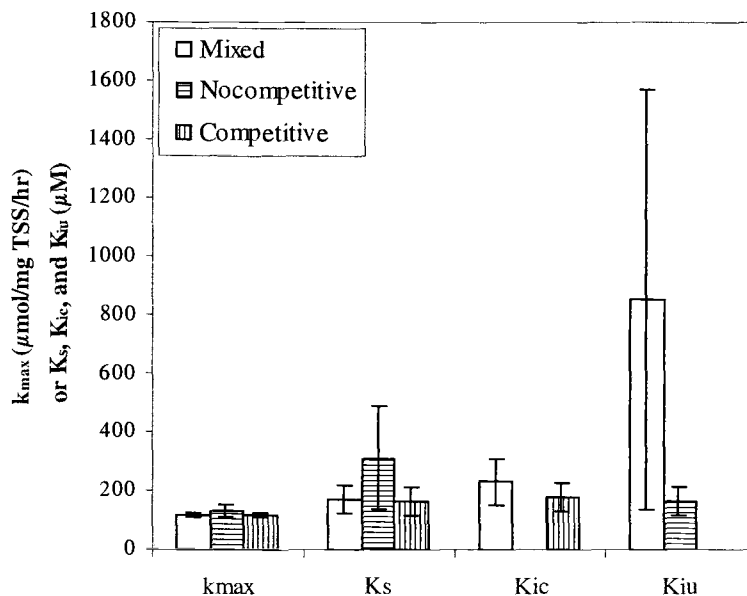


Figure D8.1. Comparison of parameters obtained from NLSR analysis fitting all inhibition models to data identified as competitive inhibition of 1,1-DCA on 1,1-DCE transformation. The k_{\max} , K_s and K_{ic} values were multiplied by a factor of 100, 100 and 10, respectively.

Fit with Different Inhibition Models

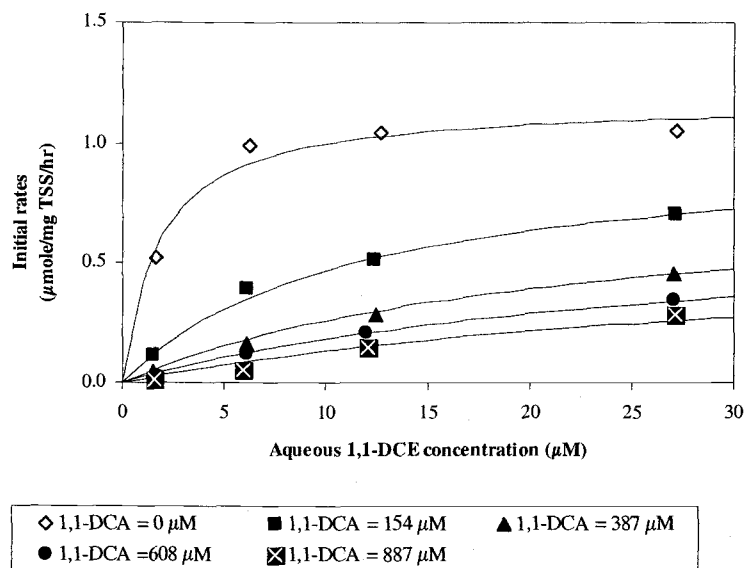


Figure D8.2. Mixed inhibition model fit to data identified as competitive inhibition of 1,1-DCA on 1,1-DCE transformation.

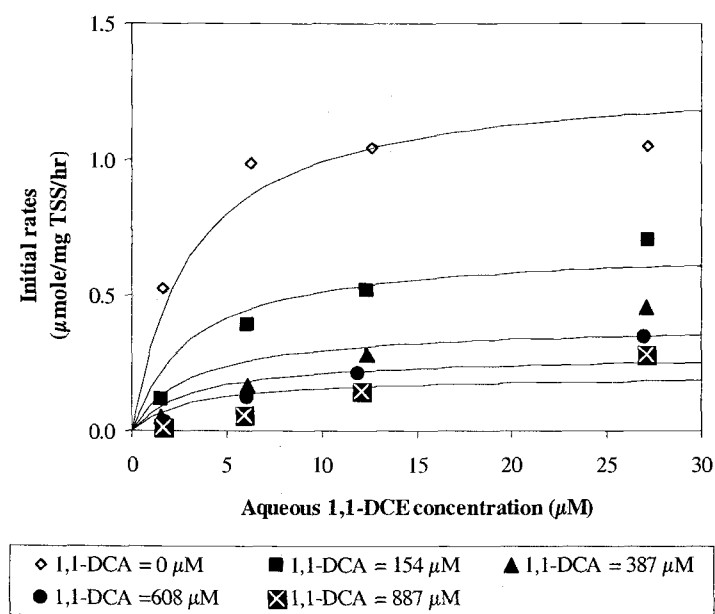


Figure D8.3. Noncompetitive inhibition model fit to data identified as competitive inhibition of 1,1-DCA on 1,1-DCE transformation.

D9. 1,1-DCA INHIBITION ON 1,1,1-TCA TRANSFORMATION

Table D9.1. Kinetic parameters (k_{\max} and K_s) for 1,1,1-TCA and inhibition coefficients for 1,1-DCA obtained from NLSR analysis by fitting mixed and noncompetitive inhibition models to data identified as competitive inhibition of 1,1-DCA on 1,1,1-TCA transformation.

	Inhibition Type	k_{\max} ($\mu\text{mol}/\text{mgTSS}/\text{hr}$)	K_s (μM)	K_{ic} (μM)	K_{iu} (μM)	Residual Stand Error
NLSR	Mix	0.20 ± 0.021	13.7 ± 4.6	14.76 ± 8.1	-516 ± 25424	0.006
NLSR $Gk_{\max}K_s$		Given	Given	12.25 ± 3.3	-264 ± 490	0.006
NLSR Gk_{\max}		Given	12.5 ± 1.6	13.19 ± 5.0	-277 ± 553	0.006
NLSR GK_s		0.19 ± 0.007	Given	12.42 ± 3.7	-249 ± 454	0.006
NLSR	NC	0.23 ± 0.029	22 ± 6.4	-	57 ± 17.3	0.008
NLSR $Gk_{\max}K_s$		Given	Given	-	53 ± 13.9	0.011
NLSR Gk_{\max}		Given	14.5 ± 2.8	-	69 ± 28.7	0.010
NLSR GK_s		0.19 ± 0.014	Given	-	55 ± 23.5	0.011

1,1-DCA Inhibition on 1,1,1-TCA Transformation

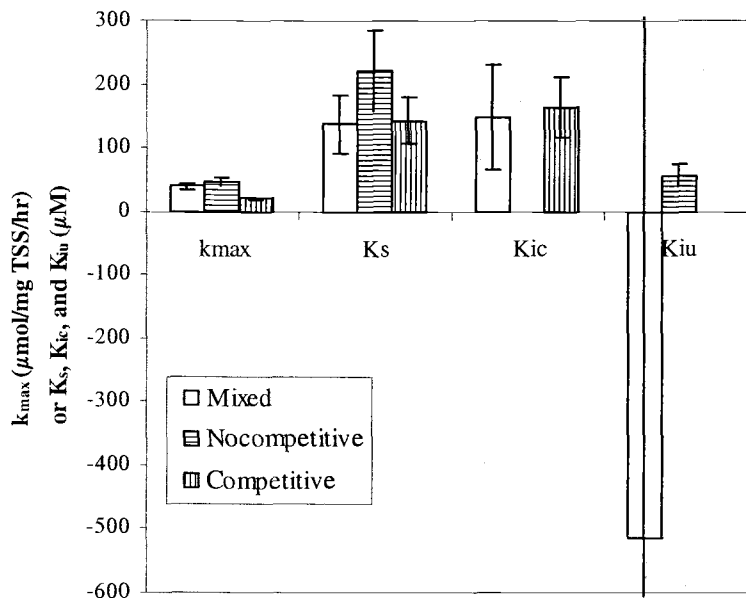


Figure D9.1. Comparison of parameters obtained from NLSR analysis fitting all inhibition models to data identified as competitive inhibition of 1,1-DCA on 1,1,1-TCA transformation. The k_{\max} , K_s and K_{ic} values were multiplied by a factor of 100, 10 and 10, respectively.

Fit with Different Inhibition Models

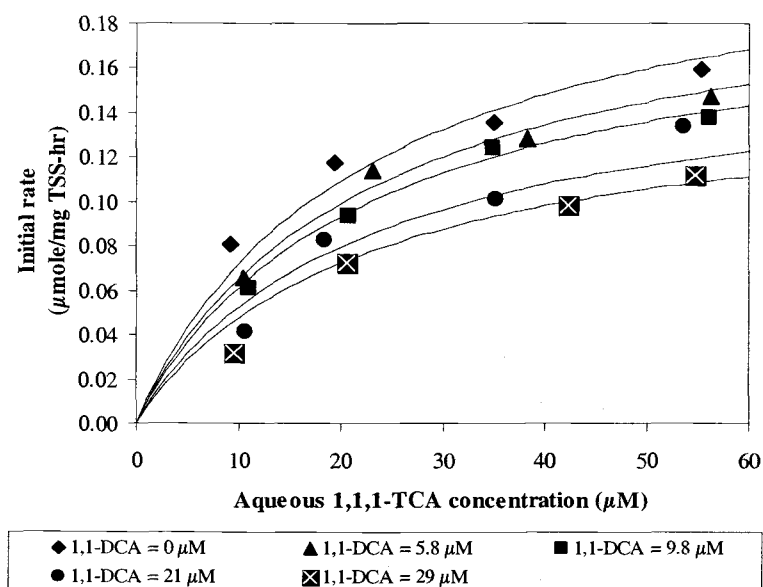


Figure D9.2. Noncompetitive inhibition model fit to data identified as competitive inhibition of 1,1-DCA on 1,1,1-TCA transformation.

D10. 1,1,1-TCA INHIBITION ON BUTANE DEGRADATION

Table D10.1. Kinetic parameters (k_{\max} and K_s) for butane and inhibition coefficients for 1,1,1-TCA obtained from NLSR analysis by fitting mixed and noncompetitive inhibition models to data identified as competitive inhibition of 1,1,1-TCA on butane degradation.

	Inhibition Type	k_{\max} ($\mu\text{mol}/\text{mgTSS}/\text{hr}$)	K_s (μM)	K_{ic} (μM)	K_{iu} (μM)	Residual Stand Error
NLSR	Mix	2.6 ± 0.38	13.6 ± 5.3	346 ± 189	8915 ± 42184	0.075
NLSR $Gk_{\max}K_s$		Given	Given	453 ± 183	5959 ± 17186	0.079
NLSR Gk_{\max}		Given	14.1 ± 1.8	358 ± 146	7276 ± 23968	0.072
NLSR GK_s		2.7 ± 0.13	Given	412 ± 156	4409 ± 9465	0.074
NLSR	NC	3.1 ± 0.53	21.6 ± 7.7	-	964 ± 215	0.093
NLSR $Gk_{\max}K_s$		Given	Given	-	1072 ± 193	0.101
NLSR Gk_{\max}		Given	15.4 ± 2.5	-	1027 ± 250	0.103
NLSR GK_s		2.7 ± 0.18	Given	-	955 ± 225	0.098

1,1,1-TCA Inhibition on Butane Degradation

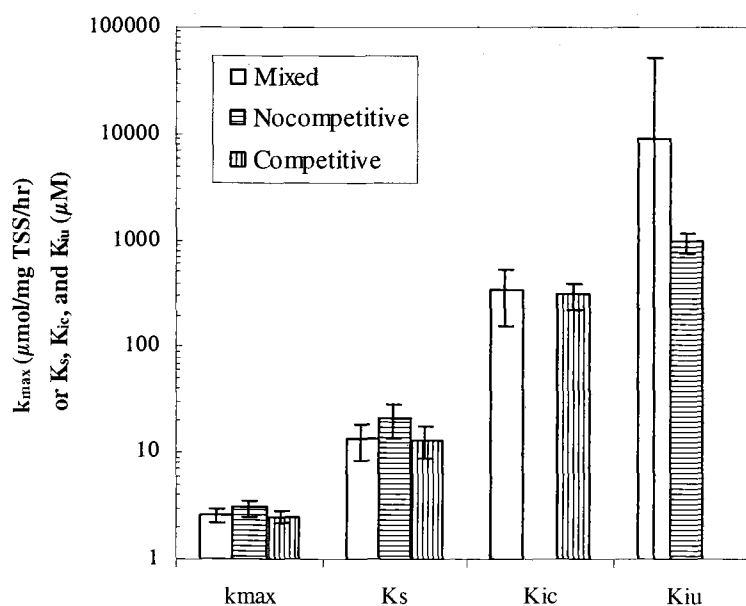


Figure D10.1. Comparison of parameters obtained from NLSR analysis fitting all inhibition models to data identified as competitive inhibition of 1,1,1-TCA on butane degradation. A y-axis is in logarithmic scale.

Fit with Different Inhibition Models

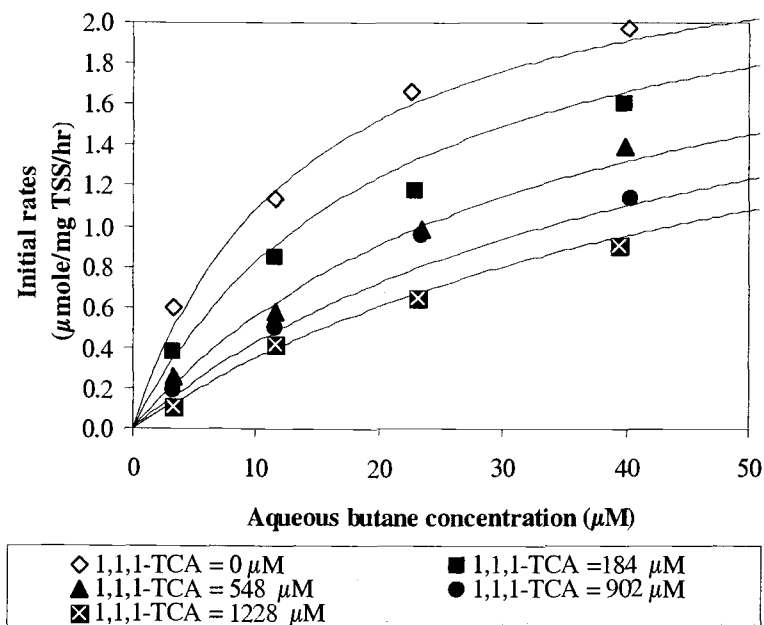


Figure D10.2 Mixed inhibition model fit to data identified as competitive inhibition of 1,1,1-TCA on butane degradation.

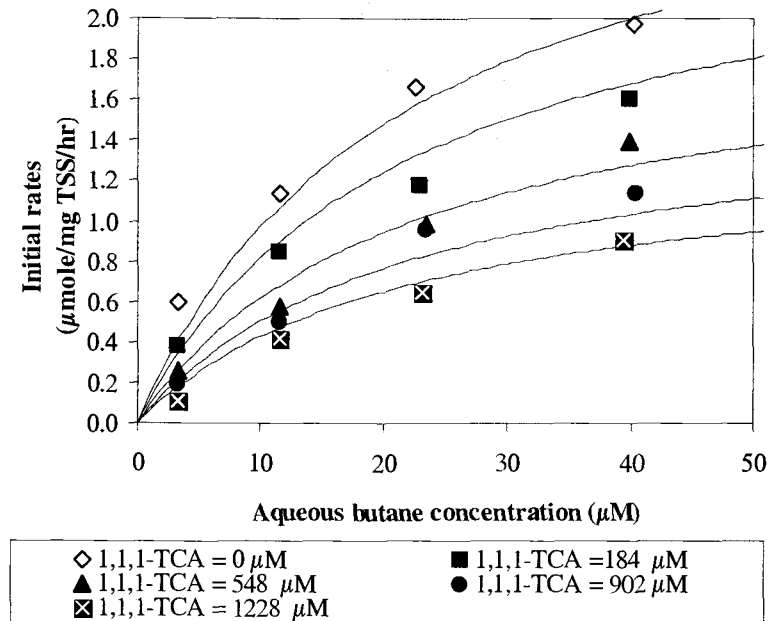


Figure D10.3. Noncompetitive inhibition model fit to data identified as competitive inhibition of 1,1,1-TCA on butane degradation.

D11. 1,1,1-TCA INHIBITION ON 1,1-DCE TRANSFORMATION

Table D11.1. Kinetic parameters (k_{\max} and K_s) for 1,1-DCE and inhibition coefficients for 1,1,1-TCA obtained from NLSR analysis by fitting mixed and noncompetitive inhibition models to data identified as competitive inhibition of 1,1,1-TCA on 1,1-DCE transformation.

	Inhibition Type	k_{\max} ($\mu\text{mol}/\text{mgTSS}/\text{hr}$)	K_s (μM)	K_{ic} (μM)	K_{iu} (μM)	Residual Stand Error
NLSR	Mix	1.19 ± 0.07	2.16 ± 0.57	19.1 ± 6.3	1352 ± 3129	0.030
NLSR $Gk_{\max}K_s$		Given	Given	11.0 ± 5.7	894 ± 3887	0.078
NLSR Gk_{\max}		Given	2.96 ± 0.46	24.8 ± 8.2	694 ± 1059	0.036
NLSR GK_s		1.12 ± 0.004	Given	13.6 ± 3.4	3792 ± 26379	0.035
NLSR	NC	1.40 ± 0.24	4.53 ± 2.28	-	116 ± 31	0.075
NLSR $Gk_{\max}K_s$		Given	Given	-	81 ± 25	0.125
NLSR Gk_{\max}		Given	3.69 ± 1.05	-	119 ± 30	0.075
NLSR GK_s		1.11 ± 0.14	Given	-	108 ± 40	0.106

1,1,1-TCA Inhibition on 1,1-DCE Transformation

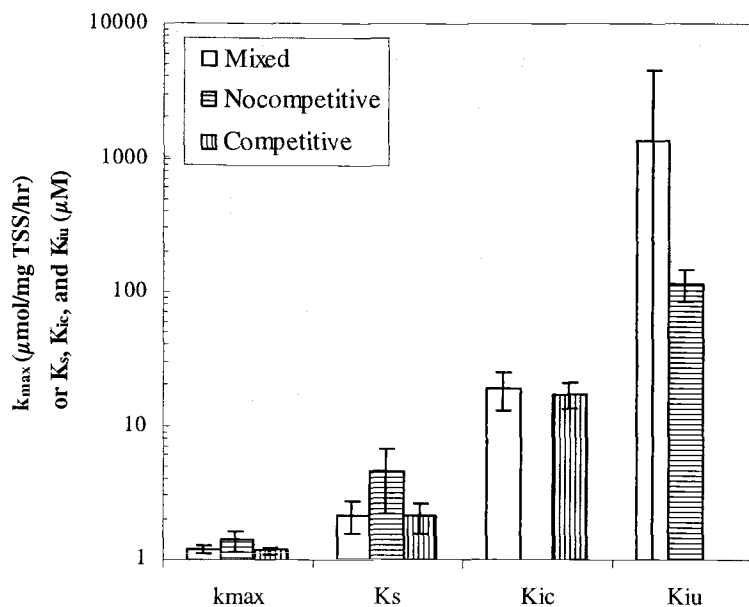


Figure D11.1. Comparison of parameters obtained from NLSR analysis fitting all inhibition models to data identified as competitive inhibition of 1,1,1-TCA on 1,1-DCE transformation. A y-axis is in logarithmic scale.

Fit with Different Inhibition Models

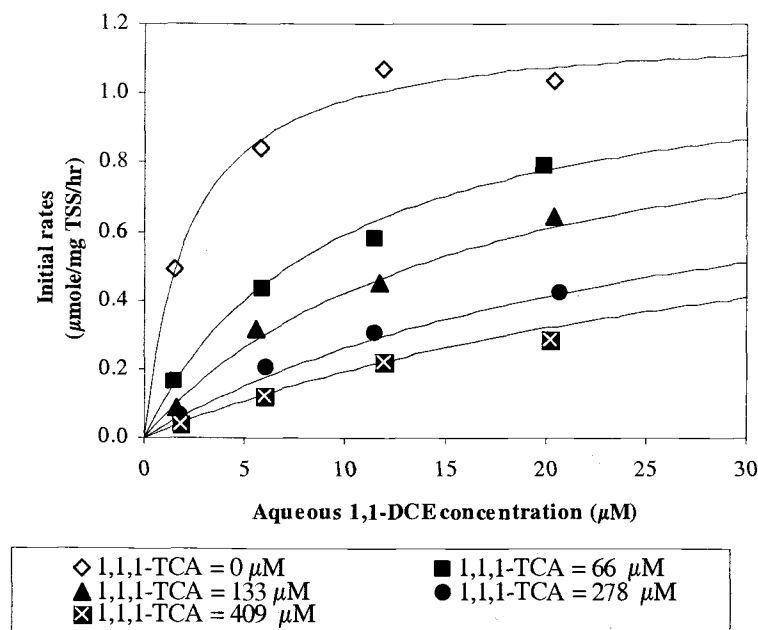


Figure D11.2. Mixed inhibition model fit to data identified as competitive inhibition of 1,1,1-TCA on 1,1-DCE transformation.

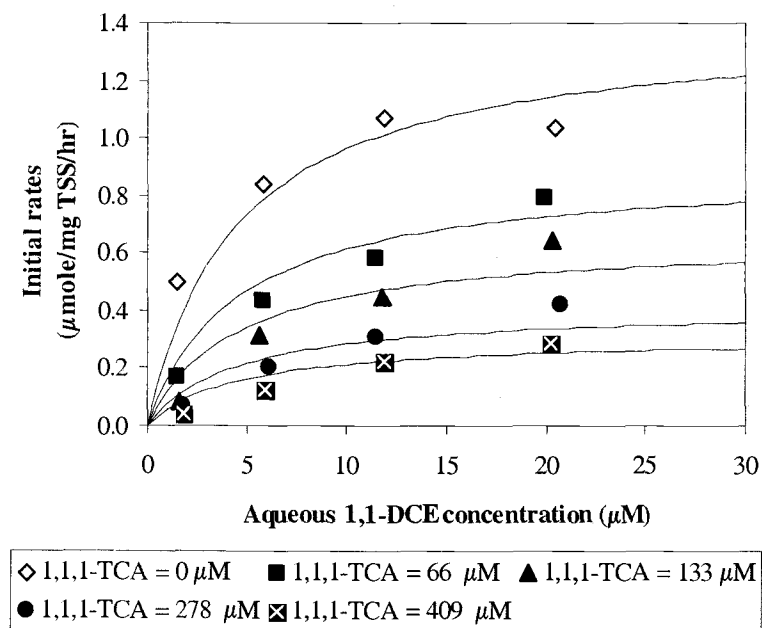


Figure D11.3. Noncompetitive inhibition model fit to data identified as competitive inhibition of 1,1,1-TCA on 1,1-DCE transformation.

D12. 1,1,1-TCA INHIBITION ON 1,1-DCA TRANSFORMATION

Table D12.1. Kinetic parameters (k_{\max} and K_s) for 1,1-DCA and inhibition coefficients for 1,1,1-TCA obtained from NLSR analysis by fitting mixed and noncompetitive inhibition models to data identified as competitive inhibition of 1,1,1-TCA on 1,1-DCA transformation.

	Inhibition Type	k_{\max} ($\mu\text{mol}/\text{mgTSS}/\text{hr}$)	K_s (μM)	K_{ic} (μM)	K_{iu} (μM)	Residual Stand Error
NLSR	Mix	0.47 ± 0.03	13.4 ± 3.53	9.3 ± 3.01	-1768 ± 7755	0.012
NLSR $Gk_{\max}K_s$		Given	Given	14.0 ± 3.10	1778 ± 9025	0.029
NLSR Gk_{\max}		Given	15.9 ± 2.31	10.8 ± 2.91	5766 ± 84528	0.013
NLSR GK_s		0.50 ± 0.02	Given	13.4 ± 3.06	1254 ± 4673	0.015
NLSR	Non	0.57 ± 0.09	33.1 ± 14.8	-	72 ± 24	0.034
NLSR $Gk_{\max}K_s$		Given	Given	-	71 ± 19	0.038
NLSR Gk_{\max}		Given	22.9 ± 7.4	-	80 ± 28	0.037
NLSR GK_s		0.50 ± 0.05	Given	-	68 ± 25	0.039

1,1,1-TCA Inhibition on 1,1-DCA Transformation

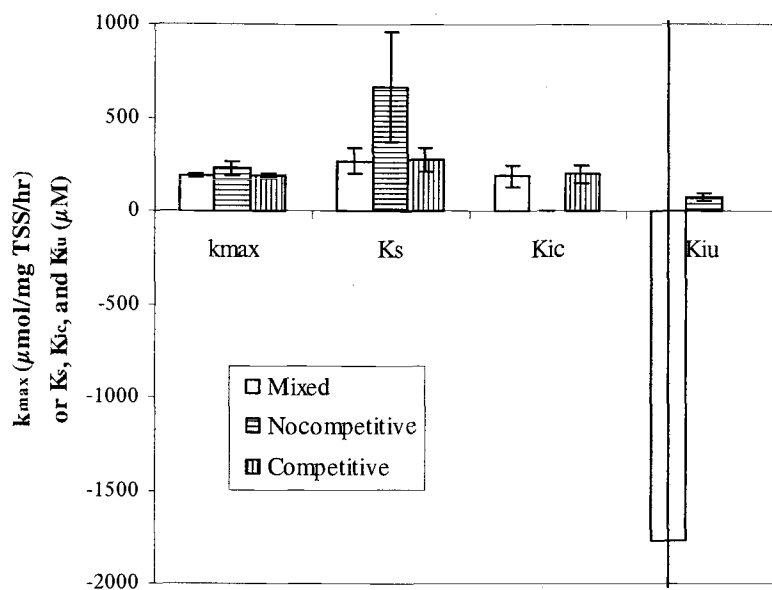


Figure D12.1. Comparison of parameters obtained from NLSR analysis fitting all inhibition models to data identified as competitive inhibition of 1,1,1-TCA on 1,1-DCA transformation. A y-axis is in logarithmic scale.

Fit with Different Inhibition Models

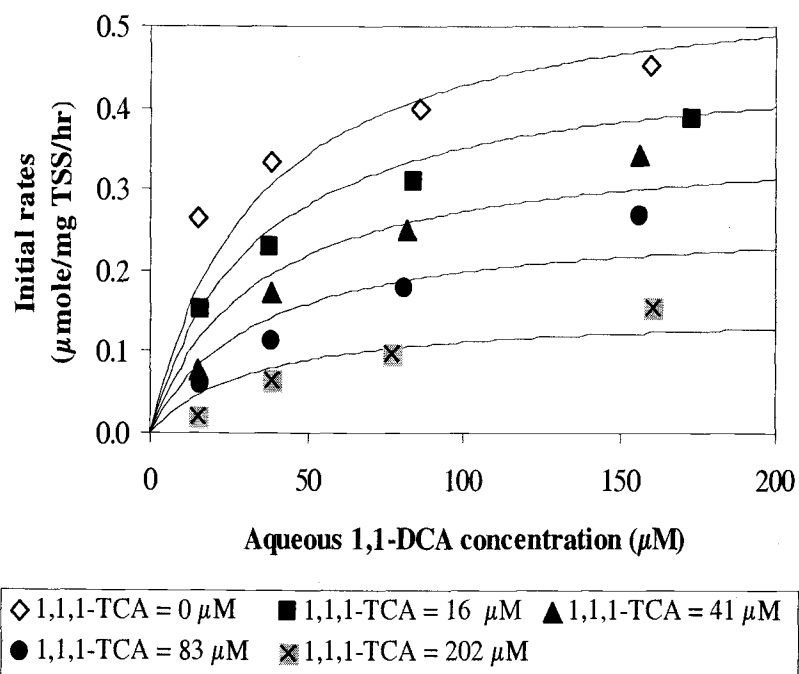


Figure D12.2. Noncompetitive inhibition model fit to data identified as competitive inhibition of 1,1,1-TCA on 1,1-DCA transformation.

APPENDIX E

Kinetic Parameters Obtained from Linear Plots Using the Linearized Equations for Different Inhibition Models

E1. COMPETITIVE INHIBITION LINEAR PLOTS USING THE DATA SHOWING MIXED INHIBITION OF BUTANE ON THE CAHs

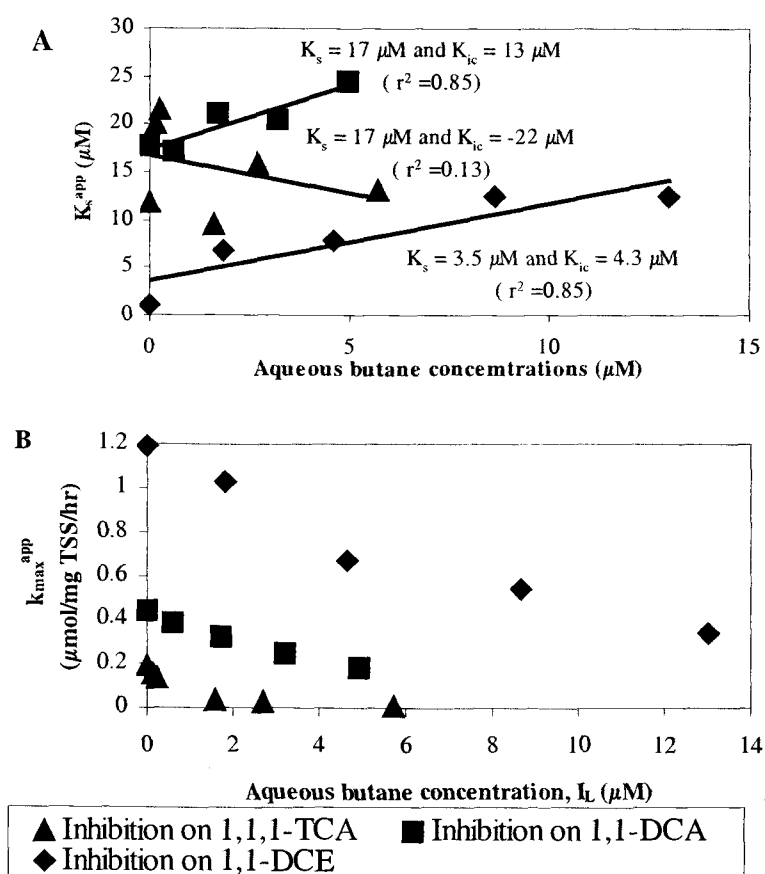


Figure E1.1. Linear plots using the linearized equation for competitive inhibition and the data showing mixed inhibition of butane on CAHs transformation (A) and a plot of k_{max}^{app} versus inhibitor (butane) concentrations (B).

Table E1.1. Kinetic parameters (K_s) for the CAHs and inhibition coefficients for butane obtained from the linear plots using the linearized equation for competitive inhibition model and the data identified as mixed inhibition of butane on CAHs transformation.

Plot (K_s^{app} vs. I_L)	y intercept ($=K_s$) (μM)	slope ($=K_s/K_{ic}$) (-)	K_{ic} (μM)	r^2
Butane inhibition on 1,1-DCE	3.5	0.82	4.3	0.82
Butane inhibition on 1,1-DCA	17.3	1	12.72	0.85
Butane inhibition on 1,1,1-TCA	17	-0.77	-22	0.13

E2. MIXED INHIBITION LINEAR PLOTS USING THE DATA SHOWING COMPETITIVE INHIBITION

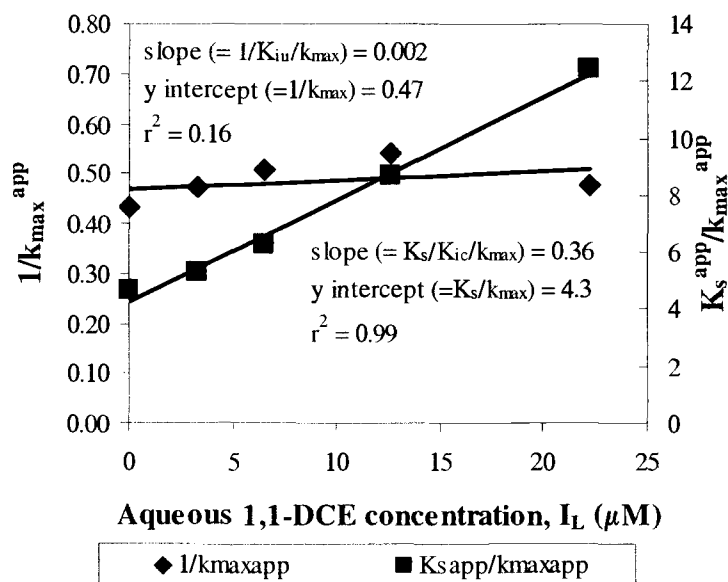


Figure E2.1. Two linear plots using data showing competitive inhibition of 1,1-DCE on butane degradation.

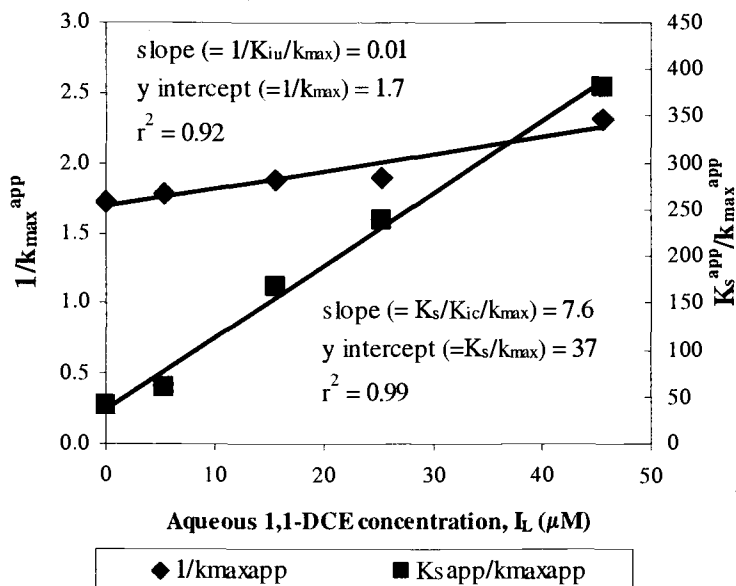


Figure E2.2. Two linear plots using data showing competitive inhibition of 1,1-DCE on 1,1-DCA transformation.

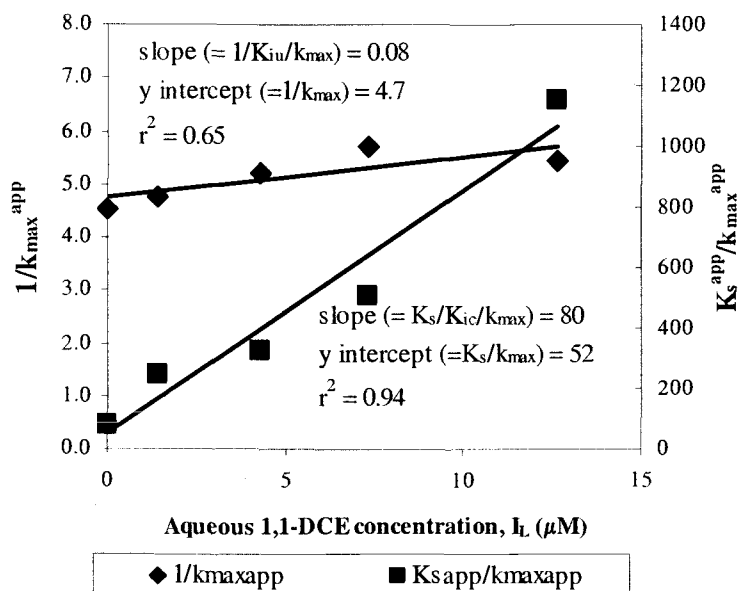


Figure E2.3. Two linear plots using data showing competitive inhibition of 1,1-DCE on 1,1,1-TCA transformation.

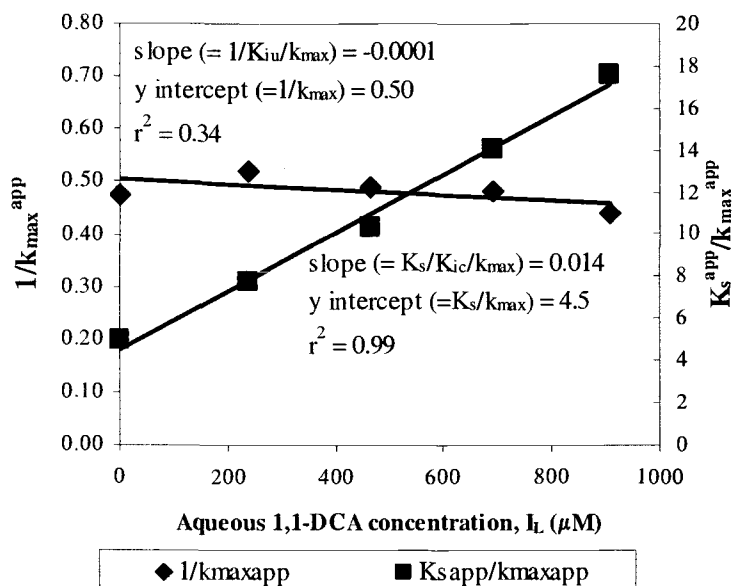


Figure E2.4. Two linear plots using data showing competitive inhibition of 1,1-DCA on butane degradation.

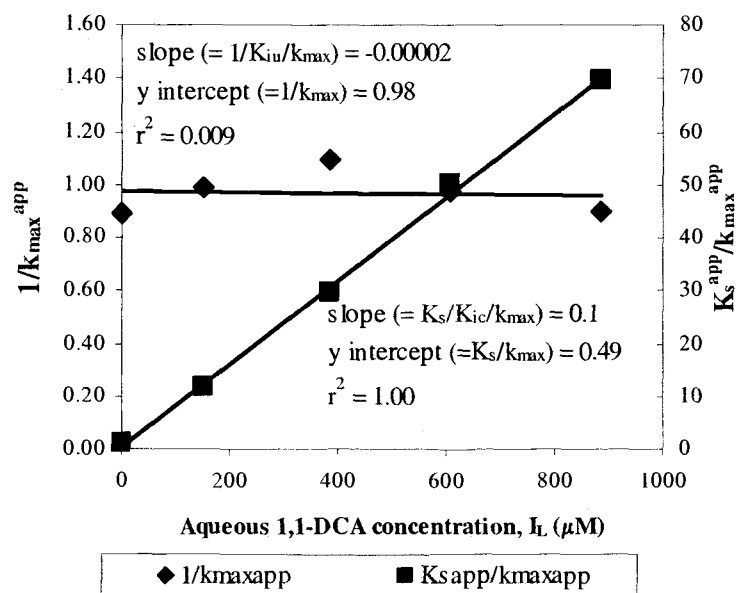


Figure E2.5. Two linear plots using data showing competitive inhibition of 1,1-DCA on 1,1-DCE transformation.

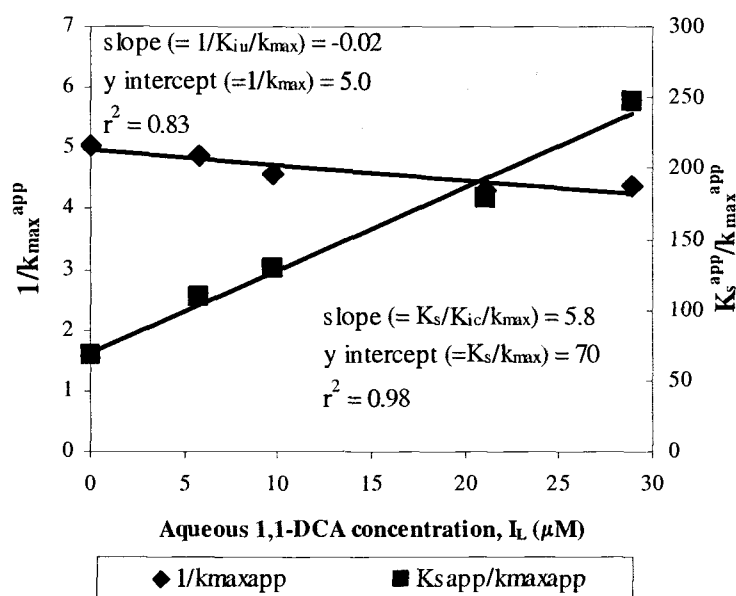


Figure E2.6. Two linear plots using data showing competitive inhibition of 1,1-DCA on 1,1,1-TCA transformation.

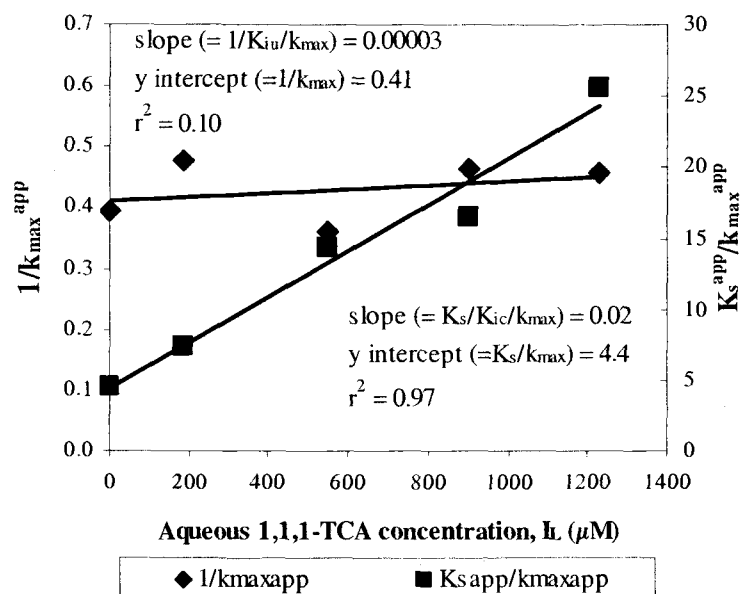


Figure E2.7. Two linear plots using data showing competitive inhibition of 1,1,1-TCA on butane degradation.

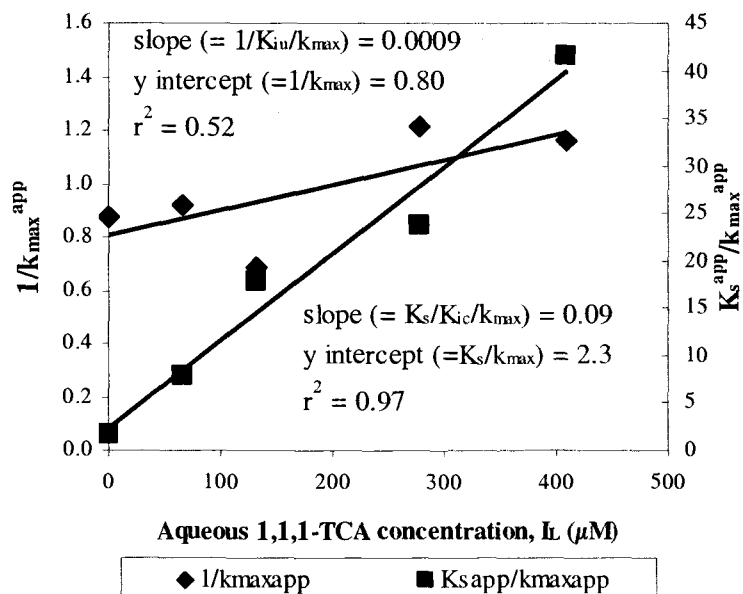


Figure E2.8. Two linear plots using data showing competitive inhibition of 1,1,1-TCA on 1,1-DCE transformation.

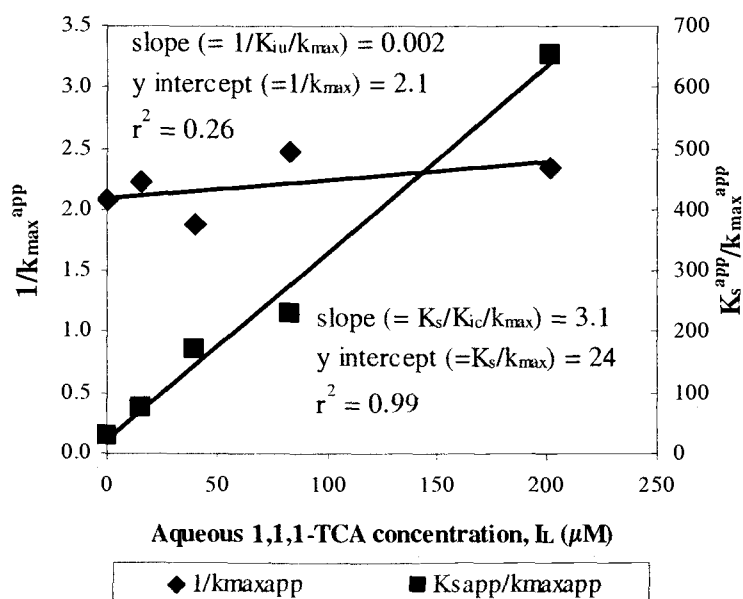


Figure E2.9. Two linear plots using data showing competitive inhibition of 1,1,1-TCA on 1,1-DCA transformation.

Table E2.1. Kinetic parameters (k_{max} and K_s) for the substrates and inhibition coefficients (K_{ic} and K_{iu}) for the inhibitions obtained from two linear plots for mixed inhibition model and the data identified as competitive inhibition

Inhibitor	Substrate	k_{max} ($\mu\text{mol}/\text{mg TSS}/\text{hr}$)	K_s (μM)	K_{ic} (μM)	K_{iu} (μM)
1,1-DCE	Butane	2.1	9.1	12	261
1,1-DCE	1,1-DCA	0.59	22	4.9	140
1,1-DCE	1,1,1-TCA	0.21	11	0.64	62
1,1-DCA	Butane	2.0	9.0	325	-10080
1,1-DCA	1,1-DCE	1.0	0.50	6.2	-48915
1,1-DCA	1,1,1-TCA	0.20	14	12	-203
1,1,1-TCA	Butane	2.4	0.04	0.004	13760
1,1,1-TCA	1,1-DCE	1.2	2.9	25	894
1,1,1-TCA	1,1-DCA	0.5	11	7.9	1401

APPENDIX F

Criteria to be Classified as Mechanism-Based Inactivator

Silverman (1985) reported 7 criteria in order to truly characterize an inactivator as falling into the mechanism-based inactivator. The criteria are discussed in more detail below. First, the loss of enzyme activity is time dependent. The loss of enzyme activity is a function of time (equations 2.1, 2.2, 2.3, and 2.4 in Chapter 2). If k_2 is rate-determining step, the time dependence would be a measure of the rate of this inactivation step. A plot of the log percent of enzyme activity remaining vs. time can be constructed (as shown in Figure F.1) as evidence for time-dependent inactivation. The plots often show pseudo first-order kinetics, but this is not universal as shown in equation 2.2 (Chapter 2). Several problems can arise in obtaining the plot shown in Figure F.1. One of the important problem arise from the inactivator with a high partition ratio, thus I_L is a function of time and may be decreased below its K_I . This results in nonpseudo first order kinetics of inactivation, because those conditions do not met the assumptions that satisfying pseudo first order kinetic of inactivation as described above (equations 2.2 and 2.3 in Chapter 2). To overcome this problem, the inhibitor concentration needs to be kept nearly constant. This condition can be obtained by using a much greater inactivator concentration than the amount of enzyme.

The second criterion is that inactivation shows saturation kinetics (equation 2.2 in Chapter 2), that is, the rate of inactivation is proportional at low concentrations of inhibitor, but independent at high concentrations. The third criterion is that addition of substrate decreases inactivation rates (Figure F.2). Since a mechanism-based inactivator is a substrate for the enzyme, it must be competitive with the normal substrate for the active site. Consequently, when substrate is added concomitant with

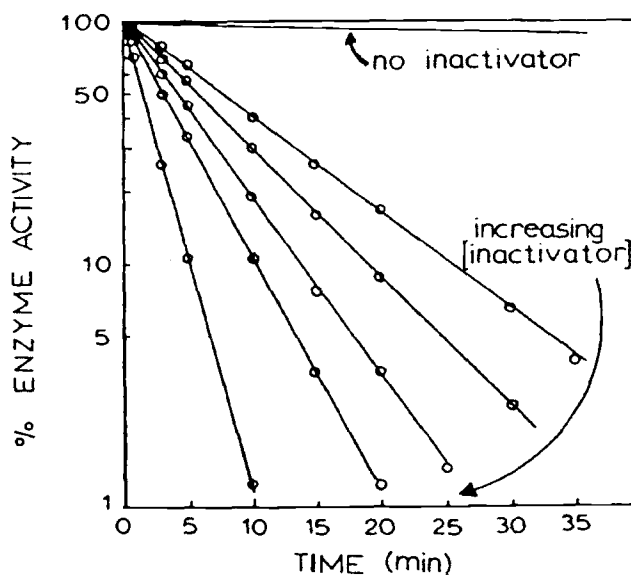


Figure F.1. Time-dependent inactivation of enzymes by mechanism-based enzyme inactivators (Silverman 1988).

the inactivator, the competition for binding at the active site prevents $E \cdot I$ formation and, therefore, decreases the rate of inactivation. The irreversibility of the inhibitor is the fourth criteria to be classified as a mechanism-based inactivator, because the inactivation results in covalent attachment of the inactivator to the enzyme. Therefore, removal of excess inactivator will not affect the inactivated enzyme.

The fifth criterion is the stoichiometry of inactivation. Since mechanism-based inactivation requires that the enzyme catalyze a reaction on the inactivator, active-site attachment is most likely. This, in general, prevents further reactions from taking place since the active site is blocked. Therefore, if a radioactively labeled inactivator and a homogeneous enzyme were mixed, a 1:1 stoichiometry of inactivation to active

site would be expected. Frequently, 100% inactivation occurs when only half of the active sites are labeled. This is believed to be the result of negative cooperativity upon binding to one active site.

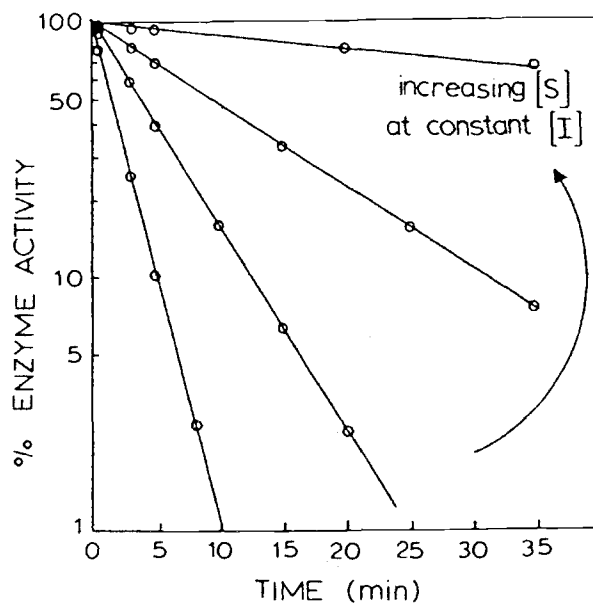


Figure F.2. Substrate protection during mechanism-based inactivation (Silverman 1988).

The first five criteria would also define other inactivator such as covalent or tightly bound inactivators. The last two criteria (discussed below) characterize the inactivator as a mechanism-based inactivator. Involvement of a catalytic step is the sixth criterion. By definition, a mechanism-based inactivator is converted by the enzyme into the actual inactivating species. Therefore, some catalytic step must be demonstrated as a requirement for inactivation.

The last criterion is that inactivation occurs prior to release of the activated species. If the inactivator is converted into an activated form that escapes the active site, and then returns to inactivate the enzyme, the inactivator is considered to be metabolically inactivated, not mechanism-based. Thus, the partition ratio is an important factor in determining how much of the activated species are released from the enzyme, because partition ratio is k_3/k_4 (equation 2.1 in Chapter 2). If the inactivator is mechanism-based inactivator, it would be 0. Ideally, all of these criteria should be satisfied before one can be confident that the inactivator is mechanism-based.